

AD-A087 280

GENERAL DYNAMICS CORP FORT WORTH TX FORT WORTH DIV
FATIGUE BEHAVIOR OF ADHESIVELY BONDED JOINTS. VOLUME I.(U)
APR 80 J ROMANKO, W G KNAUSS

F/G 11/1

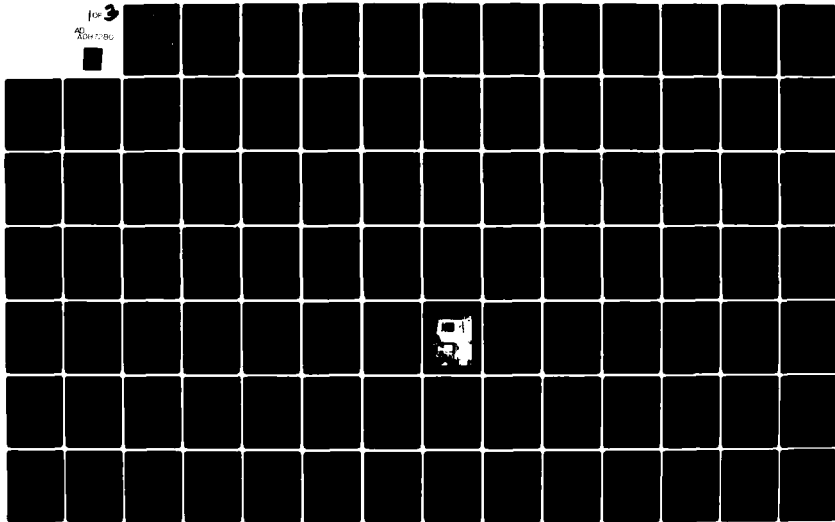
F33615-76-C-5220

UNCLASSIFIED

AFWAL-TR-80-4037-VOL-1

NL

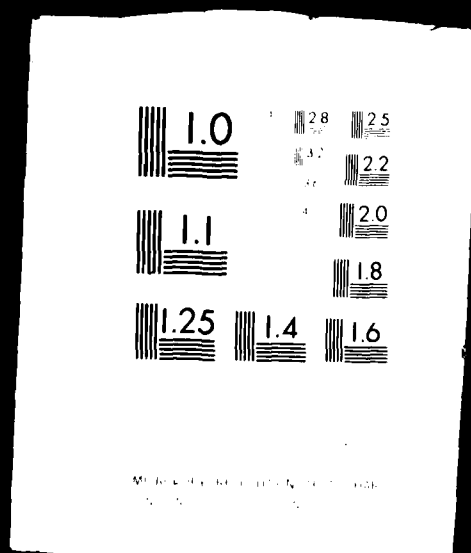
for 3
AD-A087 280



1 OF 3

AD
A087280

5
ADA 087280



DDC FILE COPY

AFWAL-TR-80-4037
Volume I

LEVEL II

2

ADA 087280

FATIGUE BEHAVIOR OF ADHESIVELY BONDED JOINTS

JOHN ROMANKO
W. G. KNAUSS

GENERAL DYNAMICS, FORT WORTH DIVISION
PASADENA, CALIFORNIA

APRIL 1980

DTIC
ECTE
JUL 29 1980

TECHNICAL REPORT AFWAL-TR-80-4037, Volume I
Final Report for period July 1976 — December 1979

Approved for public release; distribution unlimited.

MATERIALS LABORATORY
AIR FORCE WRIGHT AERONAUTICAL LABORATORIES
AIR FORCE SYSTEMS COMMAND
WRIGHT-PATTERSON AIR FORCE BASE, OHIO 45433

DDC FILE COPY


80 7 28 053


NOTICE

When Government drawings, specifications, or other data are used for any purpose other than in connection with a definitely related Government procurement operations, the United States Government thereby incurs no responsibility nor any obligation whatsoever; and the fact that the government may have formulated, furnished, or in any way supplied the said drawings, specifications, or other data, is not to be regarded by implication or otherwise as in any manner licensing the holder or any other person or corporation, or conveying any rights or permission to manufacture, use, or sell any patented invention that may in any way be related thereto.

This report has been reviewed by the Office of Public Affairs (ASD/PA) and is releasable to the National Technical Information Service (NTIS). At NTIS, it will be available to the general public, including foreign nations.

This technical report has been reviewed and is approved for publication.


WILLIAM B. JONES, JR., Ph.D., Matls Rsch Engr.
Composites, Adhesives & Fibrous Matls Br
Nonmetallic Materials Division


THEODORE J. REINHART, JR., Chief
Composites, Adhesives & Fibrous Matls Br
Nonmetallic Materials Division

FOR THE COMMANDER


FRANKLIN D. CHERRY, Chief
Nonmetallic Materials Division

"If your address has changed, if you wish to be removed from our mailing list, or if the addressee is no longer employed by your organization please notify AFWAL/MLBC, W-PAFB, OH 45433 to help us maintain a current mailing list".

Copies of this report should not be returned unless return is required by security considerations, contractual obligations, or notice on a specific document.

Unclassified

SECURITY CLASSIFICATION OF THIS PAGE (When Data Entered)

Final Technical rpt.
Jul 76 - Apr 80

19 REPORT DOCUMENTATION PAGE		READ INSTRUCTIONS BEFORE COMPLETING FORM	
1. REPORT NUMBER	2. GOVT ACCESSION NO.	3. RECIPIENT'S CATALOG NUMBER	
18 AFWAL TR-80-4037-Vol-1	AD-A087280		
4. TITLE (and Subtitle)	5. TYPE OF REPORT & PERIOD COVERED		
6 Fatigue Behavior of Adhesively Bonded Joints, Volume I.	Technical - Final July 1976 - April 1980		
	6. PERFORMING ORG. REPORT NUMBER		
7. AUTHOR(s)	8. CONTRACT OR GRANT NUMBER(s)		
10 John Romanko W. G. Knauss	15 F33615-76-C-5220		
9. PERFORMING ORGANIZATION NAME AND ADDRESS	10. PROGRAM ELEMENT, PROJECT, TASK AREA & WORK UNIT NUMBERS		
General Dynamics Corp. Fort Worth Division Pasadena, CA	16 73400226 17 221		
11. CONTROLLING OFFICE NAME AND ADDRESS	12. REPORT DATE		
Materials Laboratory Air Force Wright Aeronautical Laboratories AFSC, WP AFB, Ohio 45433	11 Apr 1980		
14. MONITORING AGENCY NAME & ADDRESS (if different from Controlling Office)	13. NUMBER OF PAGES		
	12 193		
		15. SECURITY CLASS. (of this report)	
		Unclassified	
		15a. DECLASSIFICATION/DOWNGRADING SCHEDULE	
16. DISTRIBUTION STATEMENT (of this Report)			
Approved for public release; distribution unlimited.			
17. DISTRIBUTION STATEMENT (of the abstract entered in Block 20, if different from Report)			
18. SUPPLEMENTARY NOTES			
19. KEY WORDS (Continue on reverse side if necessary and identify by block number)			
Adhesive Bonding, Structural Adhesives, Adhesive Material Characterization, Instrumented Fatigue Testing, Neat Materials, Bonded Joints, Stress Analysis, Finite Elements.			
20. ABSTRACT (Continue on reverse side if necessary and identify by block number)			
2 The fatigue behavior of adhesively bonded aluminum joints was investigated analytically and experimentally. Stress distributions in the adhesive interlayer were calculated to guide planning of the joint tests and the interpretation of the test results. Finite element stress analyses were conducted using a linear elastic, and a three-element linear viscoelastic model for (continued)			

DD FORM 1 JAN 75 1473 EDITION OF 1 NOV 65 IS OBSOLETE

Unclassified

SECURITY CLASSIFICATION OF THIS PAGE (When Data Entered)

40-701-1

cont

SECURITY CLASSIFICATION OF THIS PAGE(When Data Entered)

the adhesive behavior. Thick adherend lap-shear specimens of the model joint configuration were fabricated and tested. These specimens were instrumented and subjected to sinusoidal fatigue tests at several frequencies, humidities and temperatures. Certain tests were interrupted at various stages and the specimens examined for fatigue damage. Damage was found to initiate in the (calculated) high stress regions, and to propagate with further load cycling. Observations and recommendations resulting from the investigation are included in this final report.

SECURITY CLASSIFICATION OF THIS PAGE(When Data Entered)

FOREWORD

This technical report describes the research conducted for the Air Force Wright Aeronautical Laboratory, Air Force Systems Command, Wright-Patterson Air Force Base, OH 45433, under Contract F33615-76-C-5220, with Dr. W. B. Jones, Jr., MLBC, as Project Engineer.

Dr. John Romanko, GD/FWD Program Manager, acknowledges the interest and guidance of Dr. Jones and consultant Dr. W. G. Knauss of California Institute of Technology in this program. Many scientists of Materials and Structures Technology, General Dynamics' Fort Worth Division, contributed to the efforts reported herein: Messrs. R. S. Chambers and L. R. Collins conducted the stress analysis task; Drs. P. L. Flynn and J. Romanko, and Messrs. R. H. McDaniel, F. C. Nordquist, M. A. Flanders and J. D. Reynolds were responsible for the materials characterization; Messrs. R. L. Jones and F. C. Nordquist conducted the cyclic fatigue testing; Ms. C. L. Amerson and Mr. M. E. Tohlen performed data evaluation, and Messrs. B. O. McCauley and E. W. Turns prepared the model joints and neat adhesive coupons, with assistance from Mr. W. L. Toothaker of the Quality Assurance Group.

This report is written in two volumes. Volume I contains the essential details of the program with Volume II contributing the supportive data and derivations in Appendix form.

Accession For	
NIS General	<input checked="checked" type="checkbox"/>
DDC TAB	<input type="checkbox"/>
Unannounced	<input type="checkbox"/>
Justification	
By _____	
Date _____	
All the following codes	
Dist	Available and/or special
A	

TABLE OF CONTENTS

SECTION		PAGE
I	INTRODUCTION	1
	1.1 Introduction	1
	1.2 Program Objectives	2
	1.3 Background	3
II	SPECIMEN FABRICATION AND CONDITIONING	7
	2.1 Model Joint Specimens	7
	2.1.1 NDE Ultrasonic Inspection	9
	2.1.2 Measurement of Bondline Thickness	9
	2.2 Adhesive Characterization Specimens	10
	2.3 Fracture-Energy Coupons	10
	2.4 Moisture Control Specimens	13
	2.5 Specimen Conditioning	13
	2.6 Moisture Diffusion in Bonded Joints	13
III	MATERIALS CHARACTERIZATION	16
	3.1 Introduction	16
	3.2 Response Property Measurements	17
	3.2.1 Static Tensile Tests	18
	3.2.2 Moisture Expansion	19
	3.2.3 "Anomalous" Moisture Uptake in FM-73M	23
	3.2.4 Thermomechanical Tests	23
	3.2.5 Creep Compliance Measurements	25
	3.2.6 Poisson's Ratio Measurements	28
	3.2.7 Material Characterization of FM-400	32

TABLE OF CONTENTS (Continued)

SECTION	PAGE
3.3 Material Characterization of Other 350°F-Cure Adhesives	34
3.3.1 Moisture Uptake Effects	35
3.3.2 "Cyclic" Tg Measurements	35
3.3.3 Tensile Creep Compliance Measurements	40
3.3.4 Smith Plot Measurements	44
3.4 Fracture Properties	48
3.4.1 Specimen Design and Precracking	48
3.4.2 Stress Intensity Measurements	49
3.4.3 Cyclic Crack Growth Rate Meas- urements	52
3.5 Fatigue Testing of Neat Adhesives	62
IV STRESS ANALYSIS	64
4.1 Finite Element Technique	64
4.2 Elastic Analysis	65
4.2.1 Corner Singularity	65
4.2.2 Moisture Absorption Stresses	67
4.2.3 Cure Shrinkage	74
4.2.4 Combination of Moisture Absorp- tion with Cure Shrinkage Stresses	78
4.2.5 Prediction of Joint Stiffness	80
4.3 Viscoelastic Analysis	85
4.3.1 Viscoelastic Characterization of FM-73M	85
4.3.2 Viscoelastic Analysis of Model Joint	91
4.3.3 Rigid Versus Non-Rigid Adherends	101
4.3.4 Effects of Material Nonlinear- ities	104

TABLE OF CONTENTS (Continued)

SECTION	PAGE
V CYCLIC TESTING OF BONDED JOINTS	105
5.1 Fatigue Testing Equipment	105
5.2 Monitoring of Loads and Deformation Measurement	107
5.3 Fatigue Testing Matrix	108
5.4 Fatigue Testing Results	112
5.4.1 Data Reduction and Deductions	119
5.4.1.2 Joint Stiffness Ratios, K_N/K_i	119
5.4.1.2 Hysteresis Energy Dis- sipation Ratios, A_N/A_i	132
5.4.1.3 Creep Ratio Measurements, δ_N/δ_i	132
5.4.1.4 Effect of Stress Level on Creep Rate	134
5.4.2 Material Shakedown	134
VI POST-TEST EXAMINATION	137
6.1 Optical and SEM Analysis of Failed Joints	137
6.2 Direct Measurement of Crack Growth	141
6.3 Optical Analysis of Adhesive Inter- layers After Adherend Removal by Etching	141
6.4 Effects of Cycling Duration and Humidity	144
6.5 Discussion/Deduction	145
6.6 Stiffness of Center-Cracked Test Specimen	148

TABLE OF CONTENTS (Continued)

SECTION		PAGE
	6.7 XPS Surface Analysis of Failed Joints	152
	6.8 Chemical Aging in Moisture-Conditioned FM-73M Adhesive Interlayers	153
VII	MODEL DEVELOPMENT	158
	7.1 Bulk Effects	158
	7.2 Interfacial Effects	159
	7.3 Fatigue Degradation Mechanisms	161
	7.3.1 Dry FM-73M Joint, Room Temperature Case	162
	7.3.2 Wet FM-73M Joint, and High Temperature Case	162
VIII	CONCLUSIONS AND RECOMMENDATIONS	165
	REFERENCES	173

LIST OF ILLUSTRATIONS

Figure		Page
1	Model Thick-Adherend Single Lap Shear Specimen	8
2	Adhesive Characterization Tensile Specimen	11
3	FM-73M Neat Adhesive Fracture Energy Coupon	12
4	Moisture Distribution in FM-73M Adhesive Exposed to 100% RH at 60°C (Calculated Values)	15
5	Strength-Temperature Histories for Neat FM-73M	20
6	Tensile Stress-Strain Histories for Dry and Wet FM-73M	21
7	Moisture Expansion Curve for Neat FM-73M	22
8	Anomalous Moisture Absorption in FM-73M	24
9	Expansion Temperature Curve for FM-73M Dry and Wet	26
10	Point-to-Point Derivative of Thermal Expansion Data for Neat FM-73M	27
11	Tensile Creep Compliance for FM-73M Dry at Various Temperatures	29
12	Tensile Creep Compliance for Wet FM-73M at Various Temperatures	30
13	Tensile Creep Compliance Master Curves for FM-73M (Reduced to Reference Temperature 0°C)	32
14	Comparison of Time Dependence in Creep Compliance at 25°C with Time Invariance of Poisson's Ratio for Neat FM-73M	33
15	Weight Gain of 350°F Adhesives in Water Vapor at 150°F	36
16	Comparison of Weight Gain in 350°F-Cure Adhesives	37
17	Comparison of Equilibrium Moisture Expansion in 350°F-Cure Adhesives	37
18	Thermal Expansion of Dry PL-729-3 Adhesive	38

LIST OF ILLUSTRATIONS (Continued)

Figure		Page
19	Thermal Expansion Coefficient of Dry PL-729-3 Adhesive	39
20	Tensile Creep Compliance of AF-147, Dry and Wet, (Reduced to 104°F)	41
21	Tensile Creep Compliance of Dry 350°F-Cure Adhesives (Reduced to 104°F)	42
22	Tensile Creep Compliance of Wet 350°F-Cure Adhesives (Reduced to 104°F)	43
23	Experimental Set Up for Fracture Energy & Smith Plot Measurements	46
24	Smith Plot Envelopes for 350°F-Cure Adhesives	47
25	Crack Growth in Dry FM-73M at 140°F	51
26	Crack Growth Rate vs. Stress Intensity, FM-73M, Series I	53
27	Crack Growth Rate vs. Stress Intensity, FM-73M, Series II	54
28	Crack Growth Rate vs. Stress Intensity, FM-73M, Series III	55
29	Crack Growth Rate vs. Stress Intensity, FM-73M, Various Environmental Conditions (Shifted in da/dt)	56
30	Cyclic Crack Growth Rate Dependence on Stress Intensity for Dry FM-73M at 75°F	57
31	Cyclic Crack Growth Rate Dependence on Stress Intensity for Dry FM-73M at 140°F	58
32	Cyclic Crack Growth Rate Dependence on Stress Intensity for Wet FM-73M at 75°F	59
33	Cyclic Crack Growth Rate Dependence on Stress Intensity for Wet FM-73M at 104°F	60
34	Cyclic Crack Growth Rate vs. Stress Intensity (Shifted Master Curves)	61
35	Load-Deflection History of Dry FM-73M Coupon, First Two Cycles of Loading and Unloading, Low Frequency	63
36	Peel Stress in Center of Adhesive: Poisson's Ratio Sensitivity	68

LIST OF ILLUSTRATIONS (Continued)

Figure		Page
37	Shear Stress in Center of Adhesive: Poisson's Ratio Sensitivity	69
38	MARC Calculated Peel Stress Distribution in FM-73M Interlayer	70
39	MARC Calculated Shear Stress Distribution in FM-73M Interlayer	71
40	Moisture Uptake by FM-73M at 60°C and 100% RH	73
41	Moisture Expansion Coefficient vs. Time for FM-73M	73
42	Bond Normal Stresses in Adhesive Overlap of Bonded Joint Resulting From Moisture Infusion	75
43	Adhesive Shear Stresses in Adhesive Overlap of Bonded Joint Resulting from Moisture Infusion	76
44	Bond Normal Stresses at Edge of Adhesive Overlap Corresponding to 3 Days of Moisture Conditioning	77
45	Shear Stress Variation at Edge of Adhesive Overlap Corresponding to 3 Days of Moisture Conditioning	77
46	Bond Normal Stress Variation at Edge of Adhesive Overlap Created by Cure Shrinkage	79
47	Shear Stress Variation at Edge of Adhesive Overlap Created by Cure Shrinkage	79
48	Bond Normal Stresses Corresponding to 1 and 3 Days of Moisture Conditioning and Cure Shrinkage	81
49	Adhesive Shear Stresses Corresponding to 1 and 3 Days of Moisture Conditioning and Cure Shrinkage	81
50	Dependence of Model Joint Stiffness on Interfacial Crack Length and Adhesive Modulus	83
51	Effect of Interfacial Cracks on Adhesive Peel Stress	84
52	Effect of Interfacial Cracks on Adhesive Shear Stress	84
53	FM-73M Tensile Creep Compliance Data Fit	87
54	Comparison of Analytical and Experimental FM-73M Neat Load-Deflection Responses	87

LIST OF ILLUSTRATIONS (Continued)

Figure		Page
55	Comparison of Analytical and Experimental Load-Deflection Responses (Cycle 1)	88
56	Comparison of Analytical and Experimental Load-Deflection Responses (Cycle 2)	88
57	Comparison of Analytical and Experimental Load-Deflection Responses (Cycle 3)	88
58	Comparison of FM-73M Analytical and Experimental Creep Compliance (Cycle 1)	90
59	Comparison of FM-73M Analytical and Experimental Creep Compliance (Cycle 2)	90
60	Comparison of FM-73M Analytical and Experimental Creep Compliance (Cycle 3)	90
61	Comparison of Experimental and Predicted Response of Bonded Joint 40A5	92
62	Comparison of Experimental and Predicted Response of Bonded Joint 52A11	92
63	Comparison of Experimental Creep Compliance Data and Predicted Creep Compliance Based on Model Joint Data	93
64	Poisson's Ratio Sensitivity: Peel Stress Contours	95
65	Poisson's Ratio Sensitivity: Shear Stress Contours	96
66	Peel Stress Distributions Along Adhesive-Adherend Interface (Sinusoidal Load)	97
67	Shear Stress Distributions Along Adhesive-Adherend Interface (Sinusoidal Load)	98
68	Peel Stress Distributions Along Adhesive-Adherend Interface (Constant Load)	99
69	Shear Stress Distributions Along Adhesive-Adherend Interface (Constant Load)	100
70	Effect of Adherend Stiffness on Bond Normal Stress Distribution	103
71	Effect of Adherend Stiffness on Adhesive Shear Stress Distribution	103

LIST OF ILLUSTRATIONS (Continued)

Figure		Page
72	High Temperature Chamber for Fatigue Testing of Model Joints	106
73	Instrumented Model Joint	109
74	Comparison of Measured and MARC Predicted Joint Displacements	110
75	Load-Deflection History of Wet FM-73M Model Joint (Sine Wave Loading)	115
76	Load-Deflection History of Dry FM-73M Model Joint (Sine Wave Loading)	116
77	Load-Deflection History of Dry FM-73M Model Joint (Square Wave Loading)	117
78	Load-Deflection Hysteresis Loop Elements	118
79	Joint Stiffness Ratio vs. Number of Cycles for Dry and Wet FM-73M Model Joints	121
80	Joint Stiffness Ratio vs. Number of Cycles for Wet FM-73M Model Joints	123
81	Joint Stiffness Ratio vs. Number of Cycles for Wet FM-73M Model Joints (2)	124
82	Joint Stiffness Ratio vs. Number of Cycles for Wet FM-73M Model Joints (3)	125
83	Joint Stiffness Ratios vs. Number of Cycles for Various Temperatures and Moisture Conditions	126
84	Joint Stiffness Ratios vs. Number of Cycles for Different Moisture Conditions	127
85	Joint Stiffness Ratio vs. Number of Cycles for Wet FM-73M Model Joints (4)	129
86	Joint Stiffness Ratio vs. Number of Cycles for Dry FM-73M Model Joint	130
87	Load vs. Inferred Crack Length for Various Test Conditions	131
88	Deflection vs. Number of Cycles for Adherend Etched Joints	133
89	Effects of Stress Level on Joint Compliance	135

LIST OF ILLUSTRATIONS (Continued)

Figure		Page
90	Master Curve Shifting of Joint Compliance with Stress Level	136
91	Appearance of Fracture Surfaces of Fatigue-Failed FM-73M Model Joints, Different Testing Conditions	139
92	Crack and Craze Loci in FM-73M Model Joint Interlayer	140
93	Failure Mode Characteristics of Model Joints	140
94	Scanning Electron Micrographs of Fatigue-Failed FM-73M Model Joint 3C-10,1	142
95	SEM Photomicrographs of Failed Surface of FM-73M Model Joint	143
96	Dependence of Debond Length on Number of Cycles for Sacrificial Dry and Wet Model Joints	146
97	Load-Deflection History, Wet Model Joint, 3C5	146
98	MARC Predicted and Experimental Joint Stiffness Ratios vs. Debond Length	149
99	Load-Deflection History of Dry FM-73M Fracture-Energy Specimen	150
100	Comparison of Experimental and Analytical Stiffness Ratios for Fracture Energy Specimen	151
101	XPS Spectra of Dry Neat FM-73M and FM-400 Adhesive	154
102	Adhesive Interlayer Between Glass Plates Conditioned for 24 Months at 150°F/100% Condensing Humidity	155
103	High Resolution XPS Spectra: O _{1s} Peak for Different FM-73M Adhesive Conditions	157

LIST OF TABLES

Table		Page
1	Model Joint Constant-Amplitude Fatigue Cycling Matrix	111
2	Test Histories of Dry FM-73M Model Joints Under Cyclic Loading	113
3	Test Histories of Wet FM-73M Model Joints Under Cyclic Loading	114
4	Time Under Load Data For Selected FM-73M Model Joints	120
5	Summary of Delamination Length & Joint Stiffness Ratio Measurements	147
6	Summary of Severity of Environmental Conditions on Model Joints	164

SECTION I

1.1 Introduction

Adhesive bonding offers many advantages for joining metal aircraft structures. The advantages are primarily economic, with initial costs being reduced through design simplicity and reduced part count, and with additional savings potential being offered through increased fatigue and corrosion resistance and through reduced maintainance costs.

Until recently, adhesive bonding had been used in secondary structures and rarely for joining primary structural elements, due to poor reproducibility and, consequently, low confidence on the part of the designer. In recent years rapid and substantial improvements in materials and in processing and in bonded joint structural analyses have been made that contribute to improved bonded joint reliability and design confidence.

These improvements facilitated the transition of adhesive bonding into aircraft primary structural applications in the PABST (Contract F33615-75-C03016) advanced development program. This program has clearly established the initial cost savings potential for adhesive bonding and is exploring fatigue endurance through accelerated laboratory and structural verification tests. While this approach addresses the adequacy of joints early in service, there is no basis for extrapolating the test results to long term service. Further, there is little information or data generated that can be used to diagnose the causes of fatigue degradation and to suggest approaches to improve the fatigue life of adhesively bonded joints.

In order to achieve the full potential offered by adhesive bonding, a thorough understanding is required of the fundamental mechanisms of fatigue damage operative during service. In particular, it is important to inquire into the behavior of the polymeric adhesive interlayer of the metal/adhesive/metal bonded joint in terms of service environmental regimes, recognizing the time, temperature, and moisture sensitivity of polymers.

Knowledge of the time/temperature/moisture behavior of the adhesive interlayer in itself is an important part of understanding the behavior of the total metal/adhesive/metal joint. To use this material response advantageously in order to analyze overall joint behavior requires an adequate representation of the stress/strain distribution within the adhesive interlayer on a point-to-point basis. This requires a sophisticated stress analysis.

Stresses in bonded joints, and especially in the adhesive interlayer, can be calculated using structural mechanics methods. Due consideration should be given to all stress-generating stimuli including cure and thermal shrinkage, as well as externally applied mechanical loads. However, such analyses, taking into account the time-dependent behavior of the adhesive layer, are beyond the state of the art. While other investigations are underway, discussions in this report will address the more simplified case of an elastic joint under static load, and one three-element viscoelastic model of the adhesive behavior. These simplified analyses can effectively serve to guide experiments and to organize the resulting data.

For the coordinated analytical/experimental investigation, a "model" joint has been selected. The joint selected is the Bell thick-adherend specimen that has the advantages of being conveniently processable using normal production processing methods, and upon loading, has a relatively low "peel" or normal component in the stress distribution.

1.2 Program Objectives

The objectives of this program are to elucidate the fundamental mechanisms of fatigue degradation in structural adhesive joints and to identify the dominant fatigue mechanisms with aircraft service environmental regimes.

The scope involves an in-depth assessment of fatigue degradation mechanisms and failure modes in adhesively bonded joints subjected to a range of cyclic mechanical loads, temperatures, and moisture environments representative of service conditions for modern high performance aircraft. It defines the constitutive relations for the adhesive interlayer to establish and describe the physical and mechanical property changes and rate of changes that occur during instrumented fatigue testing, to provide a correlative framework from which to describe and to predict degradation mechanisms and failure modes in adhesively bonded joints exposed to service environments.

The program involves a model adhesive joint, a thick-adherend single lap shear test specimen, with Al 7075-T651 adherends and FM-73M adhesive, and selected "neat" adhesive specimens to characterize the physico-chemical behavior of the adhesives.

The program was conducted in six interrelated experimental and analytical parts:

- o Specimen Preparation - Fabrication and environmental conditioning of model shear test specimens, neat adhesive specimens, and moisture control specimens
- o Adhesive Characterization - Measurement of mechanical adhesive property data necessary to define the constitutive relations for the adhesive interlayer over a range of temperatures and moisture contents
- o Stress Analysis - Use of finite element techniques to describe the stress-strain distributions within the adhesive interlayer
- o Model Joint Testing - Measurement of static and dynamic mechanical response of lap shear specimens as a function of temperature, moisture content, load level, load rate, load duration, and frequency
- o Post-Test Examination - Use of NDE techniques, such as ultrasonics, neutron radiography, adherend etching and optical and scanning electron microscopy (SEM), and X-ray photoelectron spectroscopy (XPS) techniques to characterize the physical, topographical, and chemical characteristics of neat specimens and failed surfaces
- o Prediction of Fatigue Degradation Mechanisms - Delineation and assessment of the observed degradation mechanisms and failure modes in terms of the individual and combined effects of environment, and prediction of service-induced degradation.

1.3 Background

The AFWAL/ML W-P AFB, has sponsored a number of separate programs, each designed to provide solutions to various segments of the puzzle of the structural behavior of adhesively bonded systems. They fall under the general topics of analysis, failure mechanisms, design/failure criteria, test methods, and design data. Some of these include: Characterization of Surfaces Prior to Adhesive Bonding (F33615-75-R-5143), Fracture Mechanics Meth-

odology for Structural Adhesive Bonds (F33615-75-R-5224); Structural Properties of Adhesives (F33615-75-R-5205), Cure Monitoring Techniques for Adhesive Bonding Processes (F33615-76-R-5170) and Improved Adhesive Bond Flaw Measurement Methods (F33615-75-R-5079), and the aforementioned PABST program.

Among these, the program on Fatigue Behavior of Adhesively Bonded Joints (F33615-76-5220), conducted by General Dynamics/Fort Worth Division and the subject of this final report, is one of the more ambitious technology programs contributing towards the development of accurate methods for predicting the service life of adhesively bonded joints (Ref. 1).

This program, initiated in mid 1976, has generated important environmental behavior data on advanced adhesives FM-73M (and FM-400) and on model joints fabricated therewith and conditioned to a range of fatigue loads, temperature, and moisture environments representative of service conditions for modern high performance aircraft. In an iterative procedure, this data is coupled with a finite element stress analysis computer program developed at General Dynamics using a sophisticated (MARC) viscoelastic procedure to define and accurately predict the behavior of the bonded joints for in-service environmental conditions.

Some of the questions this formulation intends to answer include: why low cycle fatigue failure is detected in what appears to be a relatively short period of time; what is the relation between load intensity and fatigue life; and whether data generated on environmental testing under "accelerated" testing conditions are valid, and, if so, to what extent?

A precursor program on "Structural Properties of Adhesives", recently completed by Vought Corporation, Advanced Technology Center Inc., Dallas, Texas (Ref. 2) was to have laid some of the groundwork for the program on "Fatigue Behavior of Adhesively Bonded Joints", but the timing of the two programs, which commenced within a few months of each other, precluded the use of a number of test procedures eventually developed in the former for generating rigorous engineering structural property data on adhesives. For example, use of the creep compliance strain gage device in instrumented fatigue testing of the model thick-adherend single lap shear bonded joint specimen in the "Fatigue Behavior program" was a matter of going ahead with an instrument which was a workable device and available at the time. It was only after much of the instrumented fatigue testing had been completed in the fatigue behavior program that another type of gage, viz., the capacitance gage was recommended and subsequently checked out in the structural properties program (Ref. 3).

It would be remiss not to mention other researchers who have conducted some limited cyclic fatigue testing of bonded joints of the thick adherend design. Schjelderup of Douglas Aircraft Co. (Ref. 4) has conducted a series of such tests sponsored by the USAF as part of the PABST program (Ref. 5) to obtain mechanical property data for FM-73M and to determine if a correlation between neat (cast) tension tests and thick adherend shear tests could be established. A compilation of the mechanical property data, including load-deflection curves are summarized in Ref. 4 without analysis of the data. A more complete compilation is found in Ref. 6.

In yet another USAF-sponsored program, Marceau and McMillan of the Boeing Commercial Airplane Co. (Ref. 7) have conducted cyclic load testing of thick adherend lap shear specimens, among others, and have reported results on the effects of cyclic rate, stress level, environmental exposure, and loading mode, on fracture path and specimen life. The latter program, with its orientation on fracture mechanics, however, does not delve into the basic understanding of the operative fatigue mechanisms per se, which was not the intent of the program anyway.

Althof of DFVLR in Braunschweig (West Germany) has done extensive research into the viscoelastic behavior of FM-73M (and other adhesive systems) and on bonded joints therewith. (See, for example, Ref. 8).

The Fatigue Behavior program, however, is probably the only program investigating mechanisms information systematically on the adhesive interlayer of a bonded joint under fatigue cycling. It takes an innovative approach; analytical and experimental stress analysis techniques are applied to the entire bonded joint; experimental results of instrumented fatigue testing thereof (the measurement of the complete load-deflection histories for combinations of environmental exposure and testing parameters) and subsequent post-test examination of the adhesive interlayer, before, during and fatigue failure using sophisticated analysis techniques are combined with the stress analysis to elucidate on the basic fatigue degradation mechanisms characterizing the joint failure.

This program was concerned with a specific bonded joint geometry, viz., the single lap shear geometry with normal adhesive interlayer thickness in the range 6-10 mils, but with thick (1/4 inch) adherend of the Bell Helicopter design (Ref. 9).

The primary interest of this program centers around the fatigue properties of such a joint as a function of various environmental exposure and testing parameters. The term "fatigue" as used herein refers to cyclic mechanical loading and unloading in a broad sense, and includes a range of combinations of duration of load applied and load removed, as well as a range of loading rates or strain rates. Both sinusoidal and square wave tension-tension loading is considered.

In the interest of preserving the natural sequence of events, this document will discuss each of the six main topic areas in turn.

SECTION II

SPECIMEN PREPARATION

2. SPECIMEN FABRICATION AND CONDITIONING

Details regarding the specimen fabrication of three basic types, including materials, processes, and inspection, are provided in the following sections. They are the model joint specimens for the fatigue testing program, the "neat" adhesive material specimens for the material characterization studies, and the fracture energy specimens for the stress intensity measurements and crack propagation rate versus stress intensity measurements.

2.1 Model Joint Specimens

The model joint specimen used for all fatigue testing is the thick-adherend single lap shear test specimen shown in Figure 1 (Ref. 10). The adherend material is bare aluminum alloy 7075-T651. The aluminum is alkaline cleaned, acid etched, and phosphoric-acid anodized using the BAC-5555 process (Ref. 11). After oven drying following rinse, the anodized parts are coated with Bloomingdale BR-127 primer and cured for 30 minutes at RT and 60 minutes at 250°F (Ref. 12). The processed parts are not contacted in any manner from the beginning of the anodize process cycle to the completion of the primer oven dry cycle to avoid such contamination as is possible from hands, gloves, and paper.

Test tabs from the aluminum panels are measured for contaminants, both after anodize and after primer application, with wet-ability measurements and spot check Auger electron spectroscopy (AES) and/or XPS scans.

The adhesive used is FM-73M, a 250°F-cure tape from American Cyanamid of Havre de Grace, MD. This adhesive has a matte Dacron^R carrier. PABST testing results (Ref. 13) have shown this carrier to be superior to the woven type.

One-quarter inch panels, approximately 7" x 16" are assembled with the primed aluminum and single layer adhesive film, and bonded as per recommended cure procedures for each adhesive. (Ref. 14). The panels are saw cut on each side to form the ½" overlap, and 7" and 1" model joint specimens are cut from the panels, slotted, drilled and individually identified.

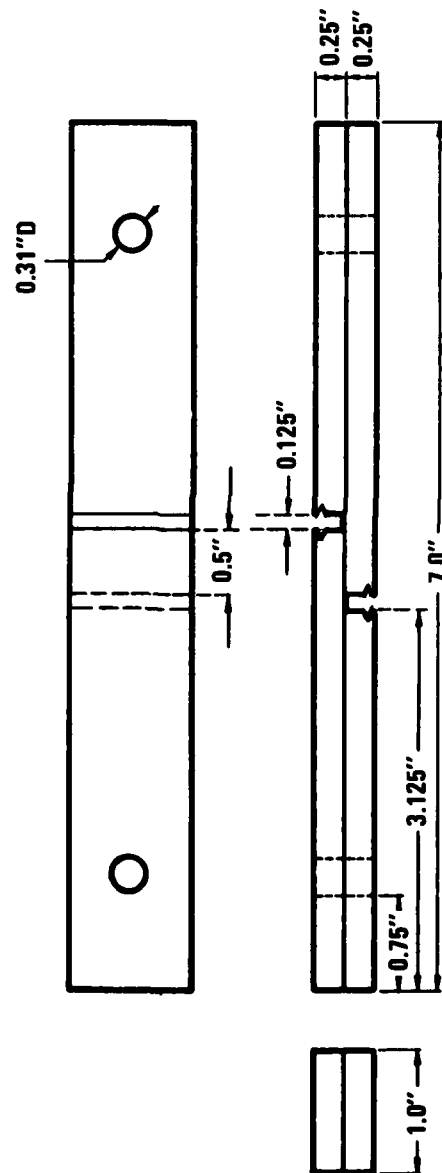


Figure 1 Model Thick-Adherend Single Lap Shear Specimen

2.1.1 NDE Ultrasonic Inspection

Since the fatigue behavior or failure mechanisms of the test specimens are strongly dependent on the initial quality of the adhesively bonded specimens, the test specimens are prepared under carefully controlled laboratory conditions. In addition, each finished test specimen (test area) is ultrasonically inspected for debonds, voids, bondline thickness, porosities, and saw cut edge damage. The inspection is accomplished using one of two computer automated ultrasonic inspection systems. The inspection records of each acceptable specimen are kept in a computer disk or tape for future correlation and clarification of mechanical test results.

2.1.2 Measurement of Bondline Thickness

Two techniques were used to measure bondline thickness in the lap area of the model joint specimens. One technique involved the use of a Scherr Tumico Optical Comparator (projection microscope) with 20X optics. The other technique involved the use of a computer-automated ultrasonic inspection system in the pulse-echo mode using Fourier transform analysis (Ref. 15).

The former technique permits measurement of bondline thickness along the exposed edges of individual model test specimens and an averaging procedure of a number of measurements is used to obtain an effective bondline thickness measurement over the lap area. The latter technique can be carried out on an uncut 8" x 16" bonded sandwich plate and measurements can be made over the lap area locations of the yet-to-be-cut and milled model specimens.

The optical technique also permits direct visual inspection of each model specimen along the edges for voids, porosity and other bondline anomalies, which information can be correlated with the ultrasonic through transmission C-scan data obtained on the parent uncut sandwich plate.

The ultrasonic Fourier analysis technique of bondline thickness measurement is a more sophisticated technique and involves pulse-echo signal convolution of the resonance frequency, Δf , using an analytical Fourier transform coded for a PDP11/45 digital computer. In addition, the velocity of sound, v , must be known in the adhesive interlayer of thickness, t , the latter being determined from the well-known relation $t = v/2 \Delta f$.

A comparison of bondline thickness measurements obtained using the aforementioned optical and ultrasonic techniques shows good agreement.

2.2 Adhesive Characterization Specimens

Two specimen thicknesses are used for adhesive characterization tests. Two and four-ply laminates of each of the adhesive films are made by bonding the layers of tape as per the recommended adhesive cure cycle. Laminating and bonding is accomplished between $\frac{1}{4}$ " aluminum plates, coated with release agent, so that these adhesive specimens are subjected to the same bonding environment as the adhesive in the model joint specimens.

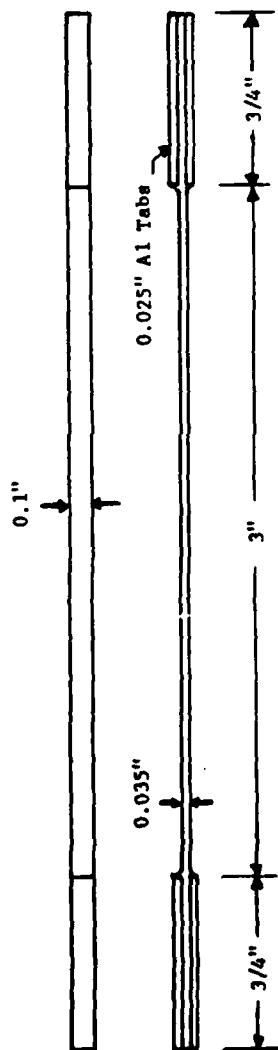
After cure, the laminated adhesive panels are cut with a wafering saw to provide: specimens for tensile creep and cyclic load-deflection (F vs δ) tests at temperatures between -65°F and $+140^{\circ}\text{F}$, and specimens for Poisson ratio, ν , thermal expansion, α_T , and glass transition temperature T_g measurements to be described later.

Experimentation with these neat adhesive materials, available with and without scrim carrier material, has yielded a very satisfactory specimen design for the creep compliance measurements, as shown in Figure 2. It is composed of three or four adhesive film layers with integrally-bonded aluminum end tabs. The specimen has an aspect ratio of 30 and has dimensions that allow moisture conditioning in a reasonable length of time. The end tabs are bonded during cure and provide positive gripping and a sharply defined gage length. The specimen dimensions also are designed to provide dead-weight loading to high stress levels with modest weights and the length of the specimen gives an easily measurable response without exceeding the linear capabilities of the LVDT instrumentation used.

This design also allows the production of the specimens in sheet form as seen in Figure A1. The curved adhesive sheet with integrally bonded end tabs is then sliced carefully with a wafering saw to produce the individual tensile specimens of the dimension shown. This concept has been proven to work experimentally and provides consistent specimens in large quantities.

2.3 Fracture-Energy Coupons

Two-inch wide center-notched tensile coupons of the design shown in Figure 3 were fabricated for the energy release rate



Scale 2:1

Figure 2 Adhesive Characterization Tensile Specimen

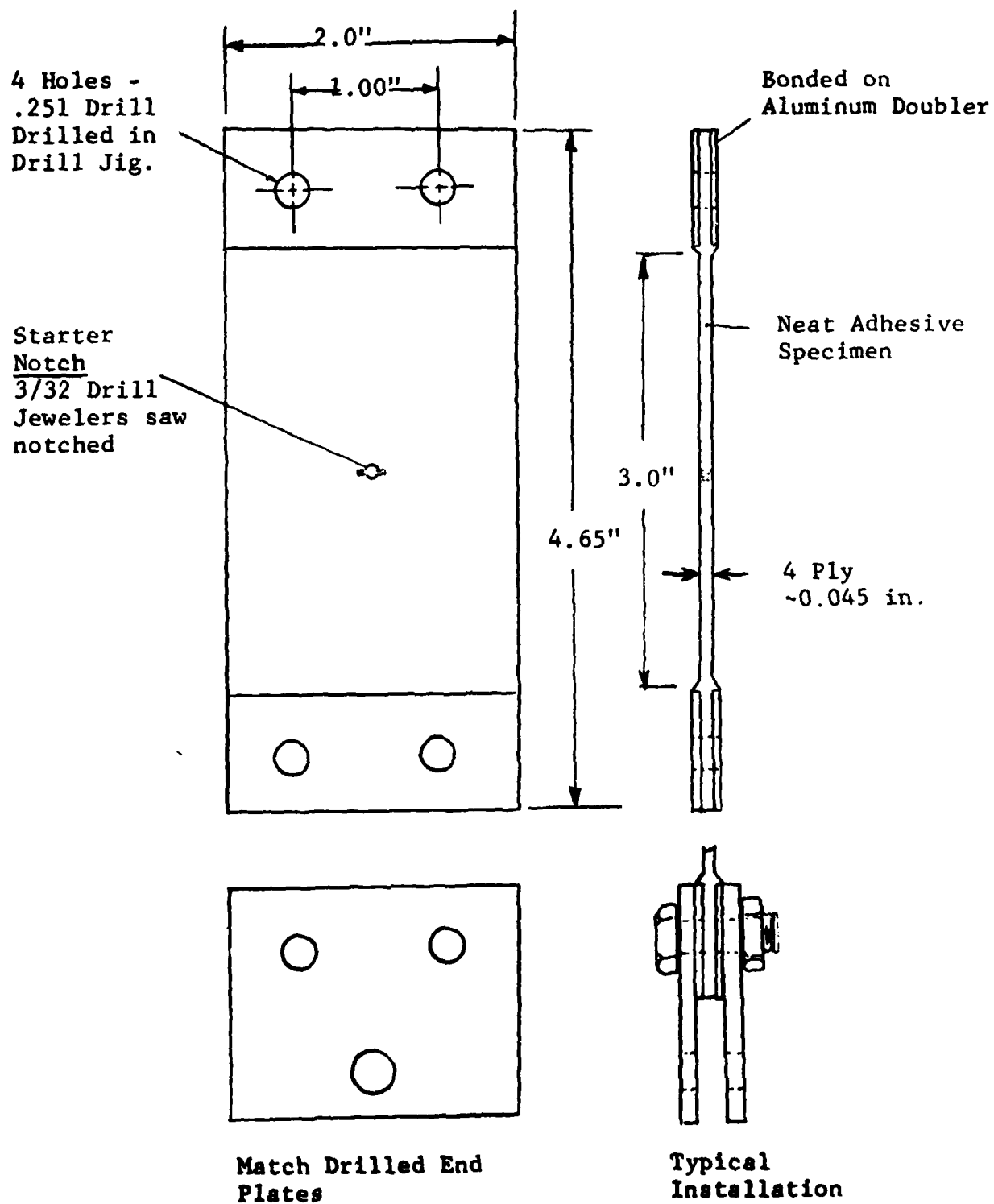


Figure 3 FM-73M Neat Adhesive Fracture Energy Coupon

and crack growth rate versus stress intensity measurements (reported in another section). The specimens were layed up with four-ply FM-73M tape, with Al end tabs integrally bonded thereto during cure. A double-hole pattern at the end tabs with adaptors to a single pin load was selected to provide a more uniform stress field in the specimens during loading.

Details of pre-cracking of these specimens (before conditioning) is described in another section.

2.4 Moisture Control Specimens

Two types of moisture control specimens are fabricated: individually-made, joint-type specimens with glass adherends and moisture control specimens consisting of single films of adhesive bonded with 0.002" Al foil skins. Specimens of various sizes from 0.5" x 1.0" (to simulate the model joint lap area) to about 3" x 4" are used. During specimen conditioning, small slices are cut from the edges to measure moisture content. These specimens are also used during fatigue testing to monitor moisture desorption.

2.5 Specimen Conditioning

All resins absorb moisture to various extents. The saturation level attained is directly related to the relative humidity of the exposure environment, and to the rate of absorption, i.e., the approach to saturation, is controlled by the exposure temperature. Extensive experimental and analytical investigations of the moisture absorption process have been conducted by various researchers. Although the diffusion process varies quantitatively with resin, the qualitative behavior is relatively well understood.

A moisture absorption model using a finite difference solution to Fick's Law of Diffusion has been developed to predict the concentration and distribution of moisture in resin systems. A comparison of predictions of this model with laboratory test results shows good agreement.

2.6 Moisture Diffusion in Bonded Joints

The diffusion coefficients were determined for neat FM-73M and FM-400 and used to calculate the moisture distribution in the overlap region of the bonded joints. The moisture diffusion parameters

for this adhesive was determined to be: $P_e = 2.17\%$ in 100% RH, and $D_{H_2O} = 1.84 \times 10^{-4} \text{ in}^2/\text{day}$.

The one dimensional solution for moisture distribution as a function of time and position in a body exposed on both sides is given by the following relation:

$$\frac{P(x,t)}{P_e} = 1 - \frac{4}{\pi} \sum_{j=1}^{\infty} \left[\frac{(-1)^{j-1}}{2j-1} \right] \exp \left[-(2j-1)^2 Kt \right] \cos \left[(2j-1) \frac{\pi X}{2\delta} \right] \quad (1)$$

where P_e = Equilibrium Moisture Content (Saturation level)

δ = 1/2 Total Thickness

$k = \pi^2 D / (2\delta)^2$ with D = Diffusion Constant.

The bondline in the bonded joint specimens measures 1.0" x 0.5". If the moisture ingress from the 1.0" dimension can be neglected along the centerline, the bondline can be modeled as a wide plate with a thickness of 0.5".

Equation (1) was programmed on a 9820 desk computer and the results for FM-73M are shown in Figure 4. The small peaks near the center of the overlap are attributed to poor series convergence of Equation (1) at very low concentrations. After one year, the FM-73M specimens will be nearly saturated.

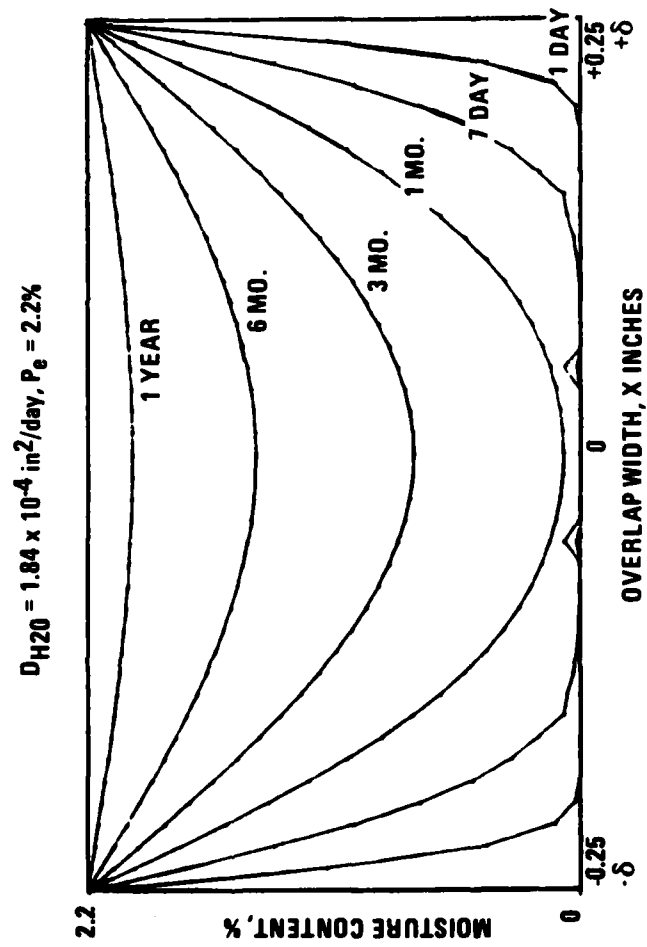


Figure 4 Moisture Distribution in FM-73M Adhesive Exposed to 100% RH at 60°C (Calculated Values)

SECTION III

MATERIALS CHARACTERIZATION

3.1 Introduction

The fatigue behavior of an adhesively bonded joint will be greatly influenced by the constituent material properties, especially those of the adhesive, which define the deformational characteristics.

The physical and mechanical properties of the adhesive interlayer of a bonded joint or structure can be divided into two categories in this respect: these are "response" properties on the one hand, dealing with the deformational characteristics (up to material failure), and the "fracture" or "failure" properties on the other hand, dealing with the fracture properties, e.g., crack growth. The "response" properties are inputs primarily for the stress analysis, and the "fracture" properties are inputs primarily for the determination of failure criteria and failure analysis.

Response properties, such as the creep compliance, thermal coefficient of linear expansion, and moisture coefficient of absorption (and desorption), among others, are measured over a wide temperature range, regardless of what the end use environmental temperature limits may be. This is due to the general use of time-temperature equivalence (superposition) principles, which are commonly employed in viscoelastic stress analysis. This principle has been poorly understood in the past by those who have tended to specify the determination of the properties only at the expected environmental temperatures, without taking into account the time dependence of adhesive properties.

After cyclic loading of the environmentally conditioned (temperature and humidity) bonded joints in environments representative of an aircraft mission, the "fracture" or "failure" properties of the adhesive will control the residual strength capabilities of the structure. Typical "fracture" properties of the adhesive (joint) include the stress intensity factor, K , the energy release rate, G , and the crack growth rate with cyclic frequency, viz., $\frac{da}{dN}$. These are discussed elsewhere.

Thus, the physical and mechanical behaviors considered include constitutive relations under monotonic and cyclic loading conditions, dilatation during cure, cooling and moisture infusion, aging, mechanisms of damage accumulation, fracture toughness and ultimate strength spectra, among others.

3.2 Response Property Measurements

One of the basic prerequisites of the stress analysis and for understanding of bonded joints is the development of an accurate analytical representation of the stress/strain (constitutive) relation for the adhesive interlayer over the range of loads/environments expected during service. We have taken the view that the physical and mechanical properties of the adhesive interlayer will be the same* in neat form or when sandwiched between metal adherends.

In this study, we consider the adhesive layer to be homogeneous and isotropic; and with mechanical response to be definable by the tensile creep compliance, $D(t)$, and Poisson's ratio, $\nu(t)$. These are the constitutive relations of the material (Ref. 16), and may be time, temperature, and moisture dependent in general.

Other material properties that influence the determination of the stress-strain state of the adhesive include moisture absorption (expansion) and moisture desorption (contraction) characteristics; thermal expansion coefficient, α_T , glass transition temperature, T_g , among others, and these have been measured for FM-73M. (Ref. 17).

The adhesive material of interest is commercially available FM-73M, a 250°F-cure adhesive available as a tape or film containing a matte Dacron^R carrier. Moreover FM-73M is a rubber-

* Given the same state of cure, etc., it is recognized that a number of reports draw conclusions to the contrary. Some of these investigations may have encountered the plasticizing effect of retained solvents entrapped in sandwich specimens, as we did. In some other investigations, the conclusion that the mechanical response of the adhesive interlayer in neat form differs from response in joints was based on the erroneous assumption that the joint shear stress was uniform. That assumption is no longer necessary.

modified epoxy and the material is, strictly speaking, not homogeneous nor isotropic. However, because the matte carrier is a random matte, we assume that specimens laminated from these films are sufficiently isotropic so that characterization techniques developed for isotropic solids are sufficiently accurate. Results on time-dependence (or independence) are not violated by this assumption.

A more important consideration in the materials properties will be an assessment regarding the linear or non-linear viscoelasticity representation of the adhesive interlayer. In the first approximation, the linear viscoelastic representation will be used, as this situation is decidedly simpler to handle analytically.

Some response properties have also been measured in the other aforementioned USAF programs, by the Firestone Laboratories at California Institute of Technology (Ref. 31), and by Althof et al. (Ref. 8), among others. These were also available to this proposed program as input data to the stress analysis.

The entire procedure for adhesively bonded joint design analysis may be extended for purposes of service life prediction if a valid means is made available for accelerating the deterioration of the adhesive system. Since the adhesive is the most significant age-sensitive component in the bonded structure and since catastrophic failures occur due to cracks or debonds, it is particularly appropriate that accelerated aging techniques be established for each specific formulation. Valid relationships between results of accelerated aging tests and results from actual long-term tests will be developed in another AFML/MBC-sponsored program to be initiated in late 1980.

3.2.1 Static Tensile Tests

In order to establish the maximum load carrying capacity of the creep compliance specimens, constant strain rate tensile tests were conducted over a broad temperature range. The tests were conducted at a strain rate of 5×10^{-4} 1/sec on an Instron machine with a Missimer environmental chamber.

Two duplicates were tested for each condition with FM-73M wet and dry adhesives. Grip failures were not a problem with the tough adhesives as reflected in the small scatter in the duplicate specimens.

The data obtained from the tensile tests are shown in Figure 5. FM-73M was very strong at low temperatures and its strength decreased monotonically with increasing temperature. For low and ambient temperatures, the strength of the wet FM-73M was slightly lower than that of dry FM-73M, but at 140°F (60°C) the strength of the wet adhesive started falling off more rapidly.

Stress-strain histories for dry and wet FM-73M adhesive coupons at room temperature are shown in Figure 6.

3.2.2 Moisture Expansion

When an adhesive material absorbs moisture a volumetric expansion takes place and when it loses moisture a shrinkage occurs. These dimensional changes can be of the order of a percent when going from the dry to the moisture saturated condition. Such dimensional changes can be a very important influence on the stress state in the adhesive layer of a bonded joint.

In order to characterize the moisture expansion characteristics of FM-73M, small coupons (1.0" x 0.5" x 0.035") were cut from laminated adhesive sheets. Two coupons of each adhesive were exposed to 140°F water immersion, 140°F 100% RH and 140°F dry air. The coupons were periodically weighed and measured in micrometer jigs. It is recognized that the data obtained represent the expansion induced by moisture gradients and that the true moisture expansion can only be determined from specimens under equilibrium conditions. However, it was felt that this error would be small with the thin coupons.

The moisture expansion data for FM-73M are presented in Figure 7.

The coupons exposed to the dry atmosphere lost appreciable moisture from the as-cured state. The FM-73M lost 0.6% by weight.

The adhesive gained weight faster when immersed in H₂O than in the 100% RH atmosphere. The two moist environments also resulted in different saturation values. The 100% RH conditioned FM-73M saturated at 2.1% after 500 hours and the water immersion coupons saturated at 3.0% after 1000 hours. Both conditions resulted in the same moisture expansion rate of 0.22"/"gm/gm.

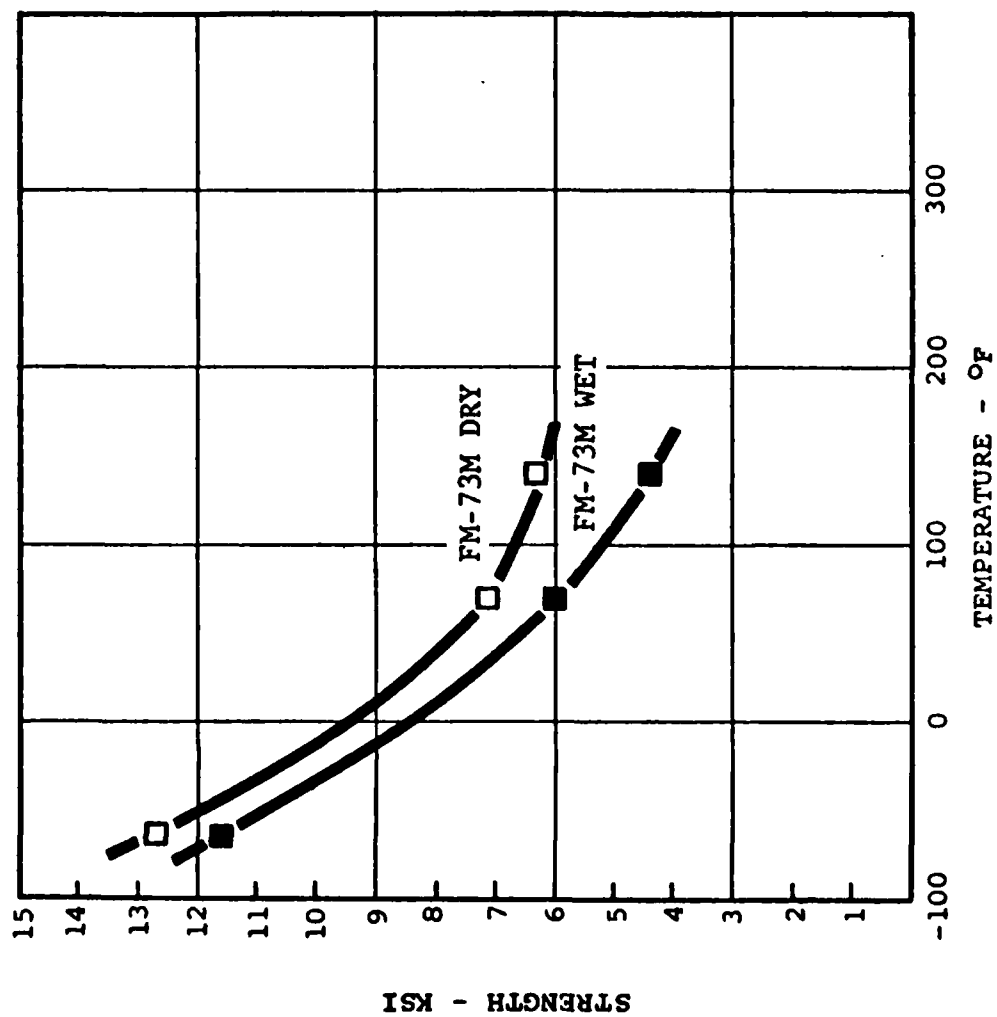


Figure 5 Strength-Temperature Histories for Neat FM-73M

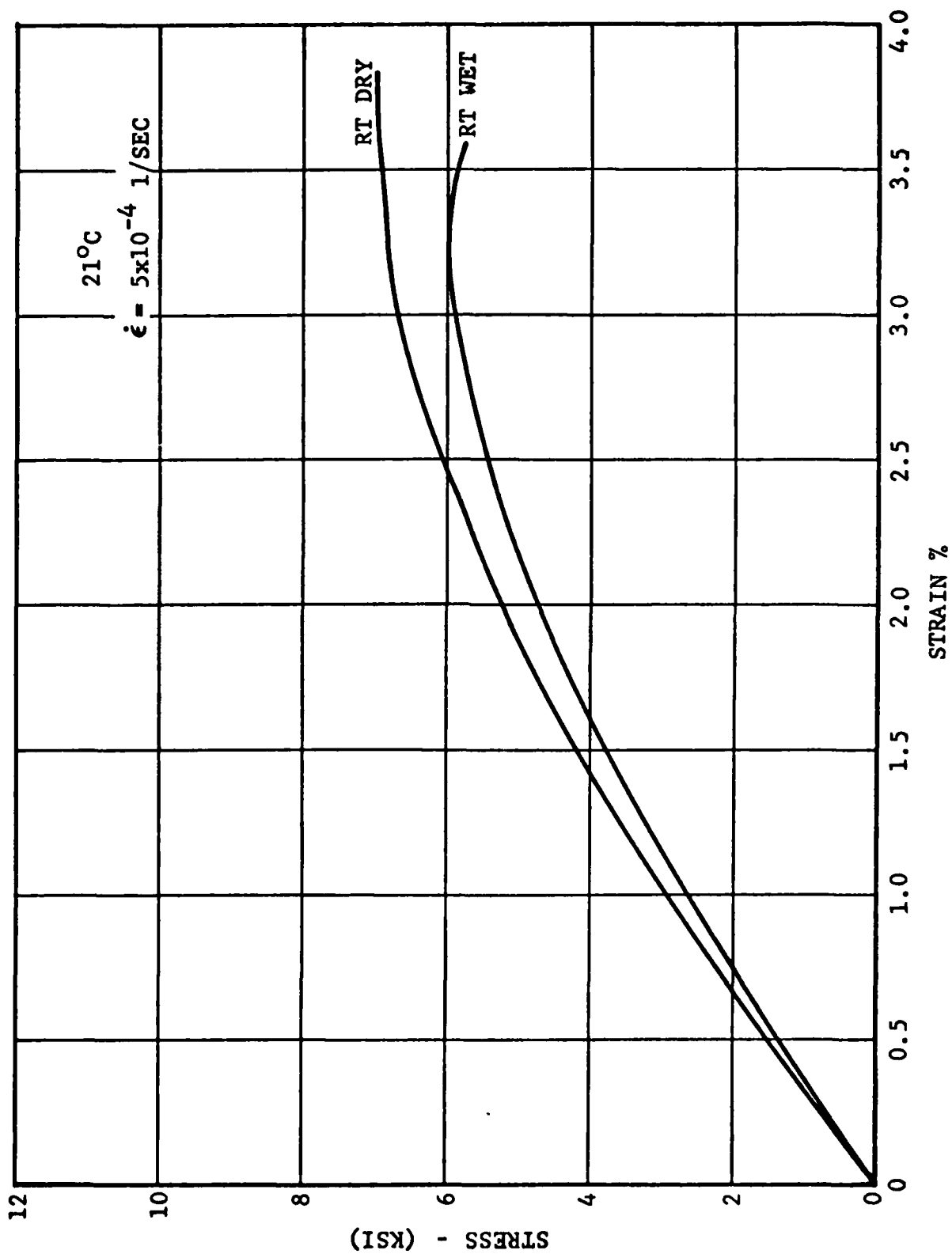


Figure 6 Tensile Stress-Strain Histories for Dry and Wet FM-73M

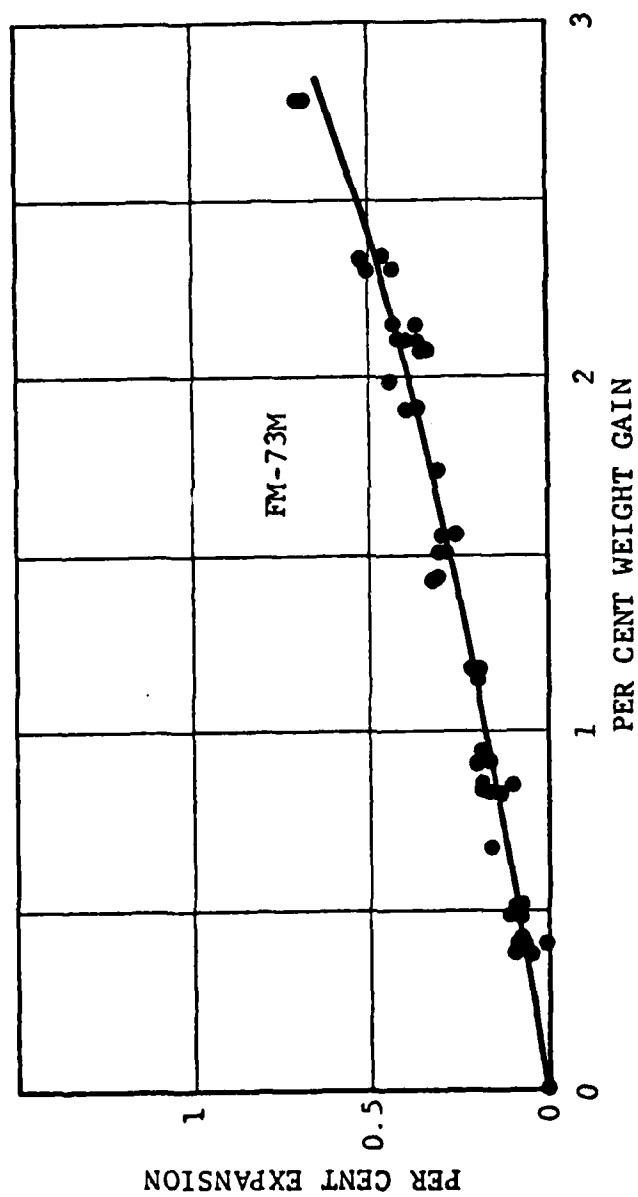


Figure 7 Moisture Expansion Curve for Neat FM-73M

Because the weight gain after 1000 hours was small, all mechanical test specimens were exposed to 1000 hours in 100% RH at 140°F. This yields nearly saturated specimens with consistent moisture contents.

3.2.3 "Anomalous" Moisture Uptake in FM-73M

We refer to moisture uptake as being anomalous when it deviates from Fickian diffusion (Ref. 18). We associate such an anomaly primarily with the effect of water on the free volume. Actually, two effects are likely to be present: one arises through the dilatational stresses associated with the advance of the moisture front; the other is associated with the decrease of molecule-to-molecule interaction due to water infusion. One must bear in mind that volume increase, per se, is a time-dependent process which may be sped up or retarded depending on the moisture content. Thus it becomes possible that water infusion decreases the glass transition temperature, T_g , to the point where the molecular structure can be more readily dilated as a result of the water-polymer interaction. This would register on a trace of weight gain vs. time as an increase in the water absorption rate. If one performs such experiments at different temperatures, exceeding temperatures beyond T_g should accelerate this process significantly.

We believe that these phenomena are reflected in the case of our experimental data on moisture uptake at various temperatures by FM-73M, as shown in Figure 8.

Approximately 10°C below the T_g of FM-73M, (viz., 60°C) diffusion appears to be Fickian. We conclude that a moisture uptake of 1.5% is not sufficient to suppress the T_g down to 50°C. However, as moisture uptake is facilitated by a thermally dilated structure at 60 to 70°C, a significantly higher moisture absorption suppresses the T_g sufficiently low to allow more rapid volume dilatations. The combined effect of moisture- and temperature-induced dilatation produces the more rapid volume growth rate with the shorter hold times in the range of 2-4% water content, possibly being associated with the process to plasticize the material down to the new T_g .

3.2.4 Thermomechanical Tests

Tests to determine thermal expansion coefficient, α_T , and glass transition temperature, T_g , were conducted on wet and dry FM-73M adhesives. This work was done in a Perkin-Elmer TMA

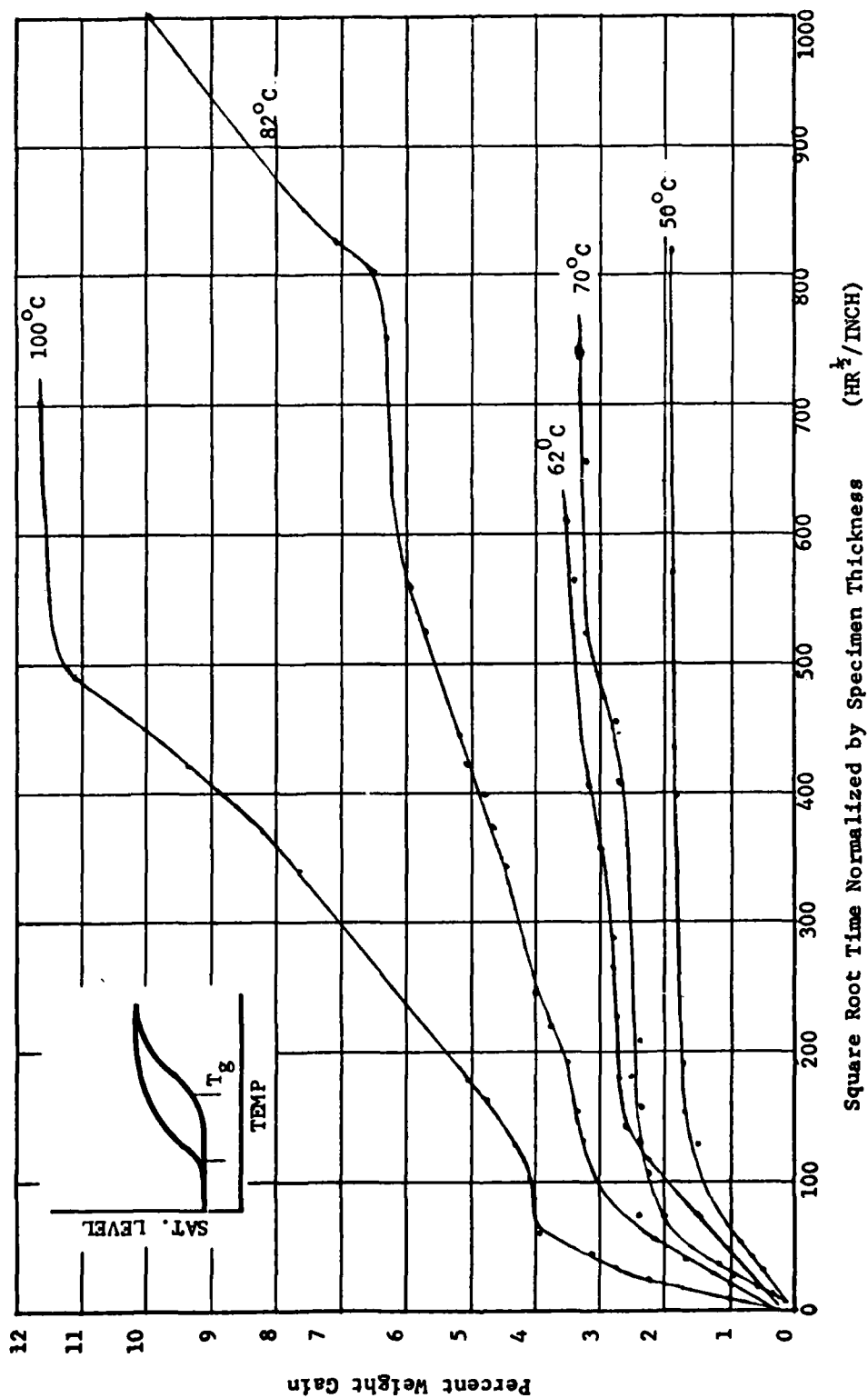


Figure 8 Anomalous Moisture Absorption in FM-73M

apparatus (Fig. A2). The dimensions of the adhesive samples were 0.5" x 0.25" x 0.035". They were loaded and measured as upright columns. The measurement device consisted of a flat quartz probe connected to an LVDT. The probe was balanced and loaded to 10 gm. This load corresponds to a compressive stress of 3 psi. The temperature was scanned over a preset range of 20°C per minute. This high scan rate was used to keep moisture losses to a minimum.

The data obtained in this test was plotted as strain versus temperature. The local slope of the curve gives the thermal expansion coefficient as a function of temperature. The local thermal expansion coefficient can also be plotted to observe transition temperatures. This latter plot can then be statistically analyzed for the second order glass transition temperature, T_2 , or the expansion curve can be observed directly for the compressive strain caused by a rapid change in compliance as this transition is crossed. However, this dynamic transition is affected by load, temperature, scan rate, and creep compliance behavior. While the second order transition is closely related to T_g , the dynamic transition, T_D , is related to a heat distortion temperature.

The expansion-temperature plot and the expansion coefficient-temperature plot for wet FM-73M are shown in Figures 9 and 10 respectively. Figure 9 reveals a dynamic transition at 220°F, while a correlation analysis of the expansion coefficient data in Figure 10 gives T_2 at 150°F. The expansion coefficient-temperature plot for wet FM-73M is shown in Figure 10. The dynamic transition has been lowered to 195°F. The second order glass transition temperature, T_2 , has been lowered to 120°F.

3.2.5 Creep Compliance Measurements

A dead-weight-loading creep frame was used for specific use in the creep compliance measurements of the variously-conditioned neat adhesive specimens. The apparatus, shown in Figure A3, has an LVDT elongation measurement system and loads can be applied from either top or bottom of the frame.

The creep compliance measurements at a constant stress of 2000 psi have been obtained for FM-73M in the dry and moisture-saturated conditions. The creep data for FM-73M was taken from -54°C to +60°C. The purpose of this data is to construct creep compliance master curves from which the viscoelastic response of the materials to other load histories can be calculated. Specifically, the creep compliance master curves can be used to predict

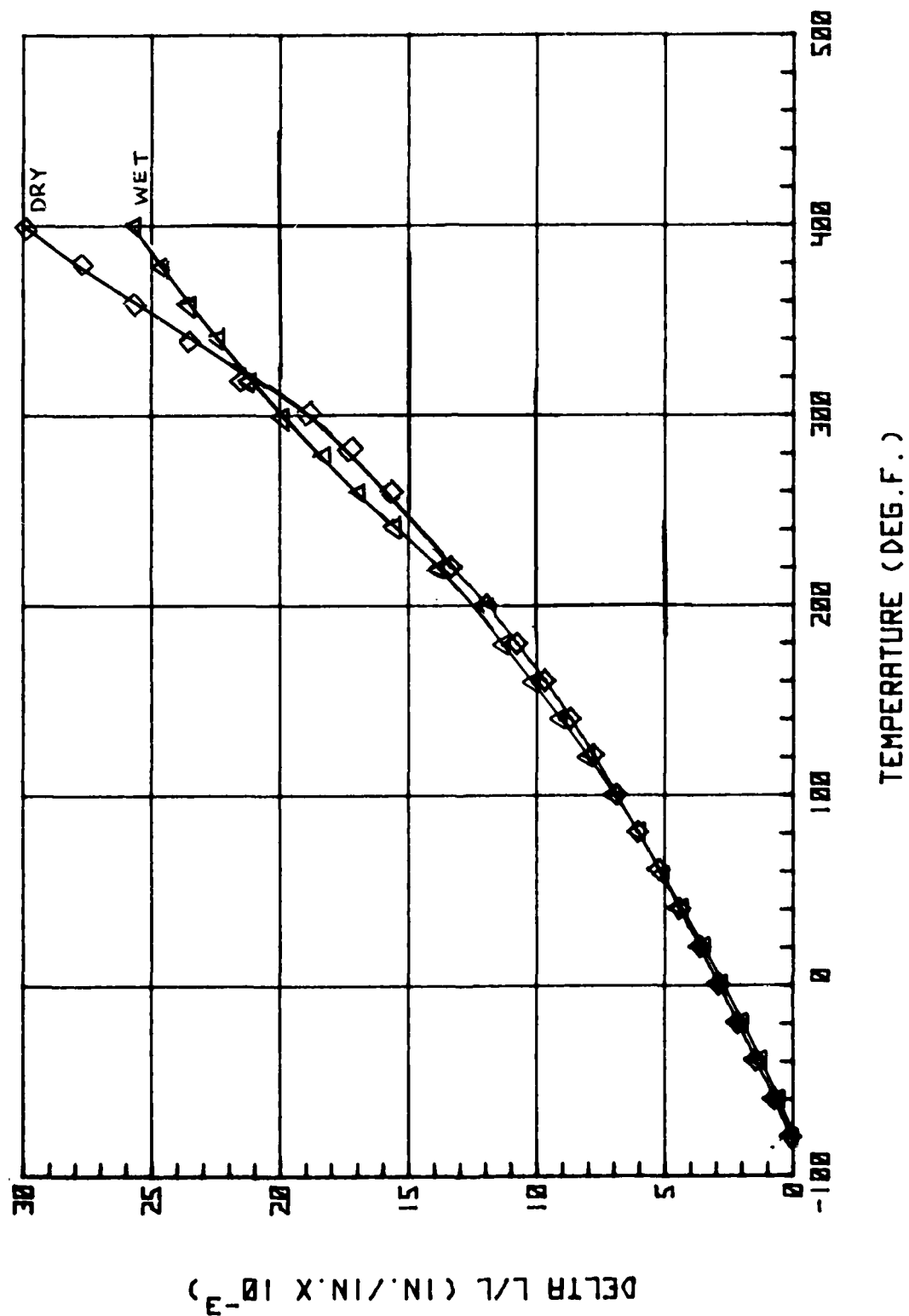


Figure 9 Expansion Temperature Curve for FM-73M Dry and Wet

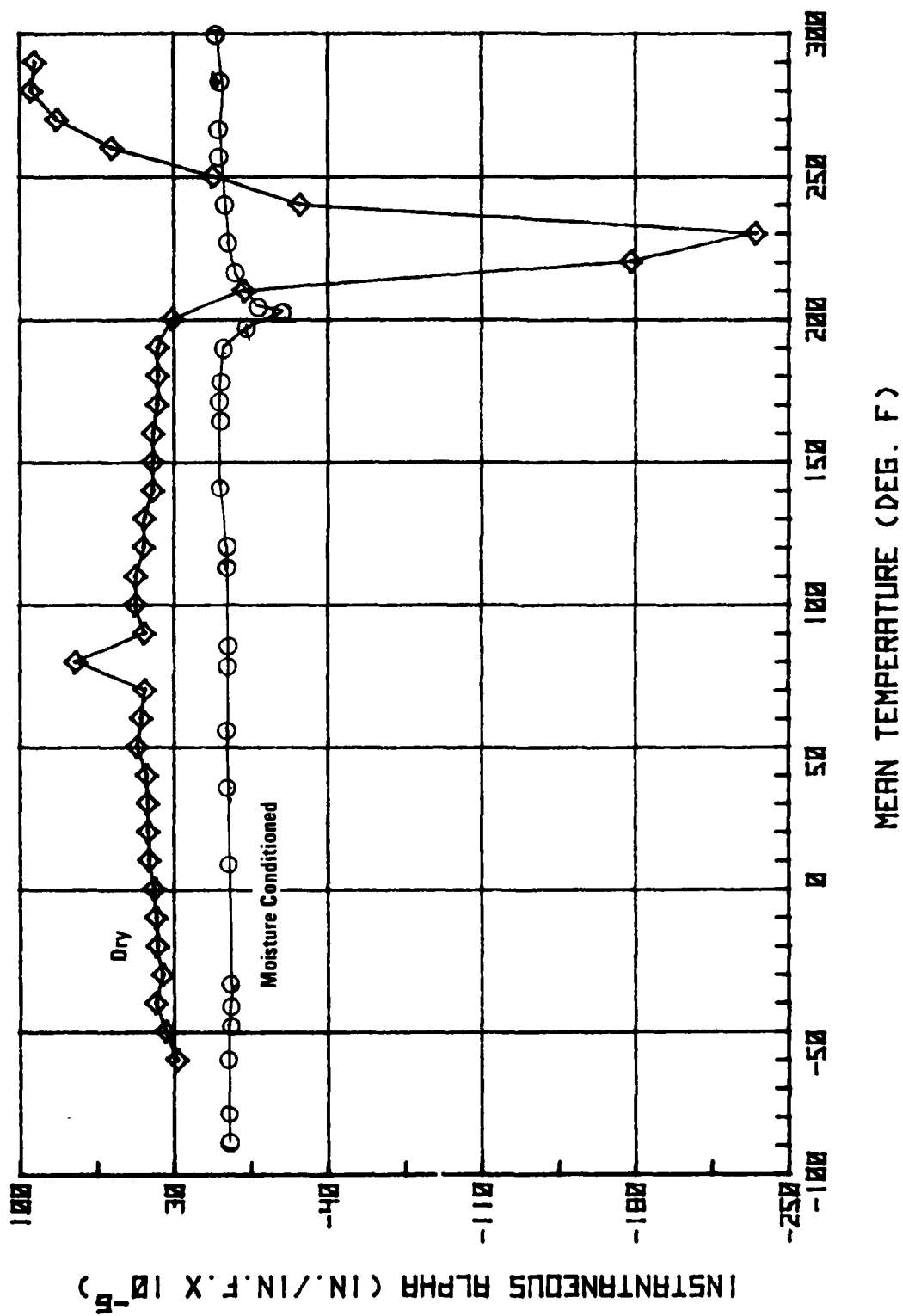


Figure 10 Point-to-Point Derivative of Thermal Expansion Data for Neat FM-73M

relaxation and dynamic behavior of the adhesive specimens and eventually the same behavior for the bonded joint specimens.

The series of creep curves for master curve development on dry and wet FM-73M are presented in Figures 11 and 12. Each series of measurements covers a temperature range from -54°C through the glass transition temperature of the material. The creep data on dry FM-73M indicate a radical change in creep behavior between 60 and 72°C (140 and 162°F). This is consistent with the placement of a second order glass transition temperature at 65°C (150°F) from the TMA tests. The creep data on wet FM-73M, presented in Figure 13, indicate the presence of T_2 between 43 and 57°C . This range is consistent with the value of T_g obtained from TMA testing at 49°C .

The creep curves at various temperatures were shifted in compliance and time to form a creep compliance master curve. First, the curves were shifted along the ordinate (creep compliance) to reduce the initial compliance to the value at 0°C . This operation removes the temperature dependence of the elastic contribution. After the vertical shift, the curves were shifted along the time axis until they matched in slope and height over the largest part of their length. The resulting master creep compliance is shown in Figure 13.

3.2.6 Poisson's Ratio Measurements

If any two of seven characteristic functions describing the mechanical properties of (isotropic) adhesive materials are known from experiment, the others can be determined analytically (Ref. 16). In the current program the two characteristic functions measured are $D(t)$ and $\nu(t)$. Thus it is important to establish the time dependence, if any, of $\nu(t)$ for the adhesive material of interest, viz., FM-73M, for various environmental conditions, including temperature, and moisture content, among others.

Combining some of the good ideas of Heflinger et al. (Ref. 19) and those of Jones (Refs. 20, 21), with additional innovative modifications, including the use of retro-reflective paint (Ref. 22), a laser/optical technique has been developed in this program (Ref. 23) to measure ν of compliant materials.

The laser/optical configuration optimized for compliant materials is shown schematically in Figure A4. L is a low power laser, a 15 mw HeNe laser, BEC is a beam expander collimator, BSC is a 50/50 beam splitting cube, M is a plane front surface

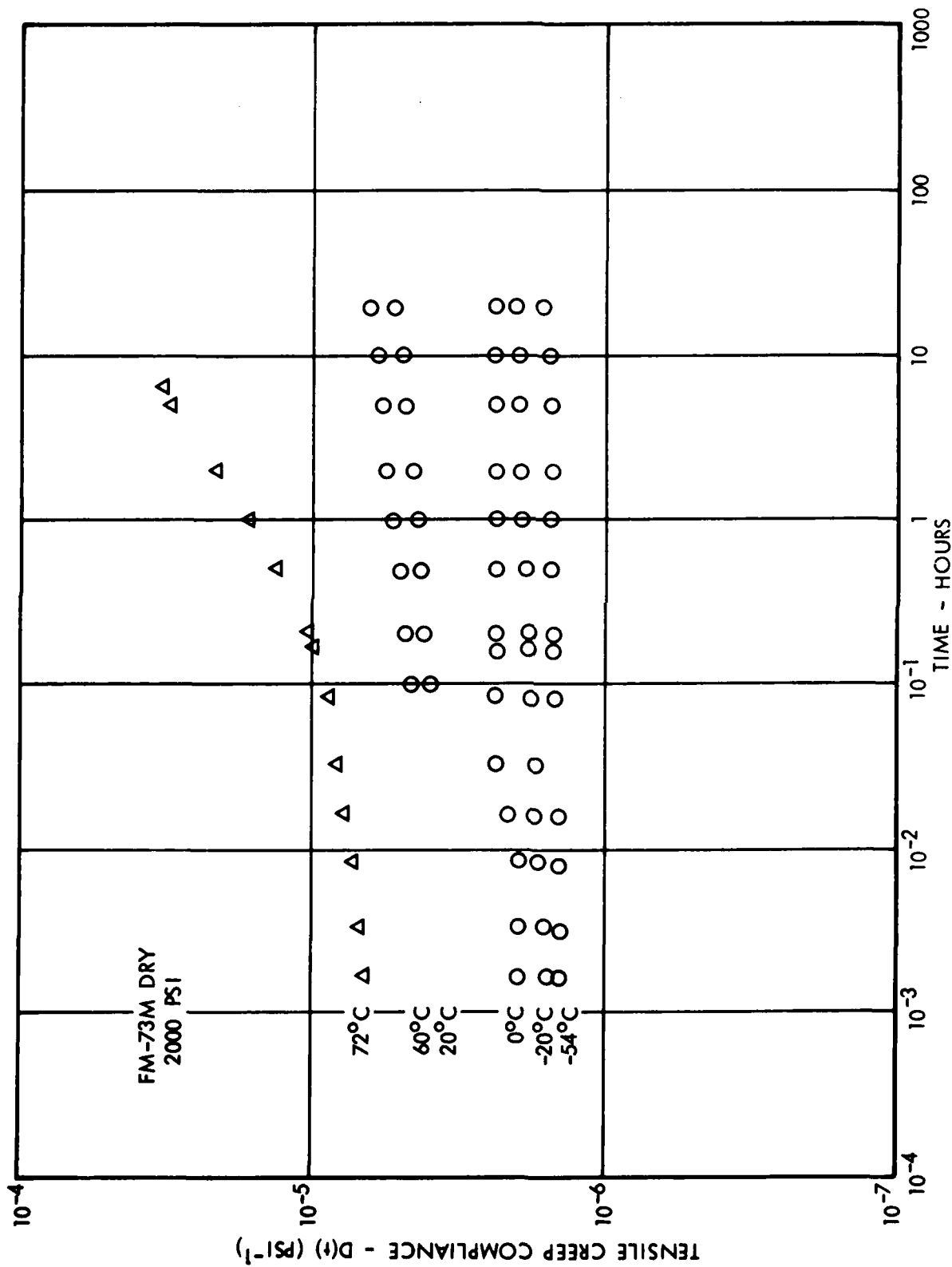


Figure 11 Tensile Creep Compliance for FM-73M Dry at Various Temperatures

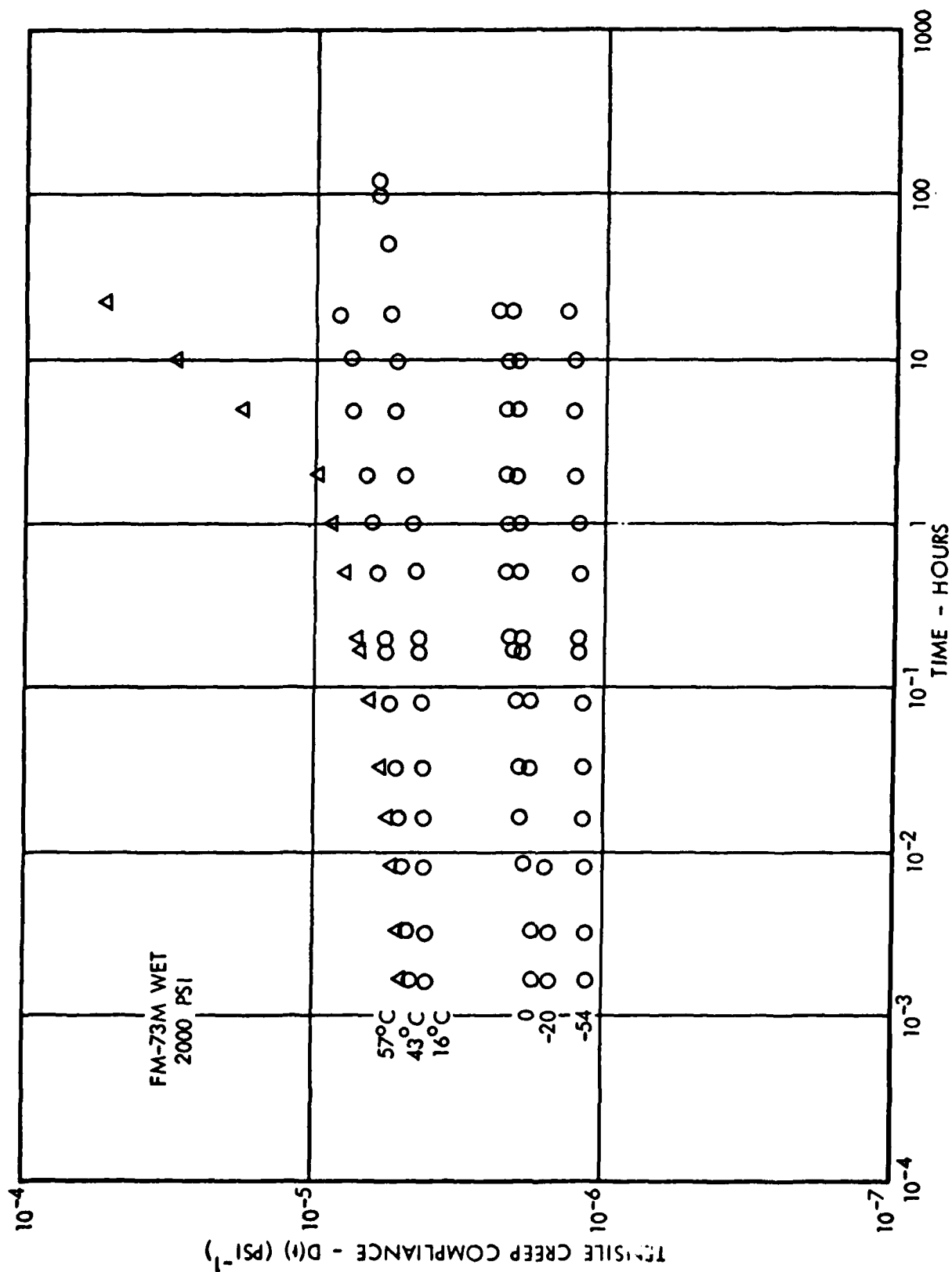


Figure 12 Tensile Creep Compliance for Wet FM-73M at Various Temperature

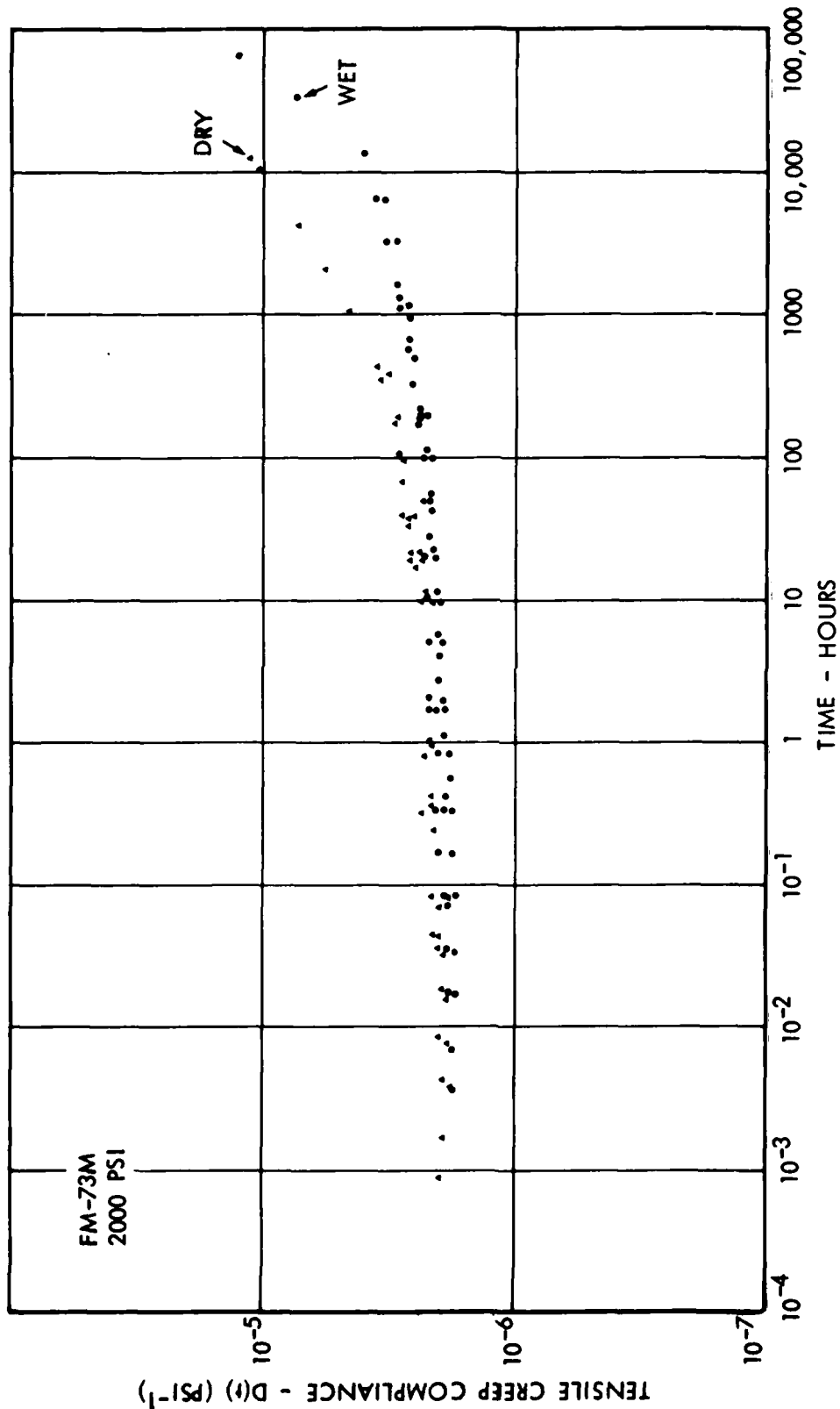


Figure 13 Tensile Creep Compliance Master Curves for FM-73M (Reduced to Reference Temperature 0°C)

mirror, F is a filter and H is the holographic recording plane. The retro-reflective painted adhesive strip specimen, of dimensions 3 1/8" x 3/4" x 1/16", is loaded in a modified fourpoint bending configuration (Fig. A5).

The technique consists of interferometrically observing the deformation of the central region of the specimen between two loads, L and L + ΔL , where $\Delta L \ll L$. When the deformation produced by four-point bending is interferometrically observed under these conditions, the fringes represent contours of constant out-of-plane displacement (Ref. 24 and 25). The strip deforms into a state of anticlastic (saddle-shape) curvature and the fringes produced are two conjugate sets of hyperbolas with the Poisson's ratio, ν , of the material related to the smaller asymptotic angle, α , between the hyperbolas by the equation.

$$\nu = \tan^2 \frac{1}{2} \alpha$$

Within experimental error of measuring the angle α (about 2%), the respective ν values determined for the dry adhesive assumes a constant value over a period of 29 days. This is true whether the differential load ΔL is applied externally to the specimen, or whether the natural creep in the material is allowed to provide the differential motion in the specimen between the double exposures.

The Poisson ratio values obtained at room temperature for approximately 1 mm thick strips of aluminum and FM-73M dry are 0.333 and 0.320, respectively. (Figure A6).

Figure 14 summarizes the measured time dependence of the uniaxial tensile creep compliance and Poisson ratio functions for dry FM-73M at room temperature.

Reference 26, a published paper in the Journal of Adhesion, describes in detail the experimental procedure for measuring $\nu(t)$ of FM-73M.

3.2.7 Material Characterization of FM-400

In the early stages of the Fatigue Behavior program, viz., during the first year thereof, a second adhesive system, a 350°F-cure commercial tape, FM-400, was selected for parallel studies with the 250°F-cure FM-73M system. In fact, the same complement of neat coupons and bonded joints were fabricated with FM-400 as

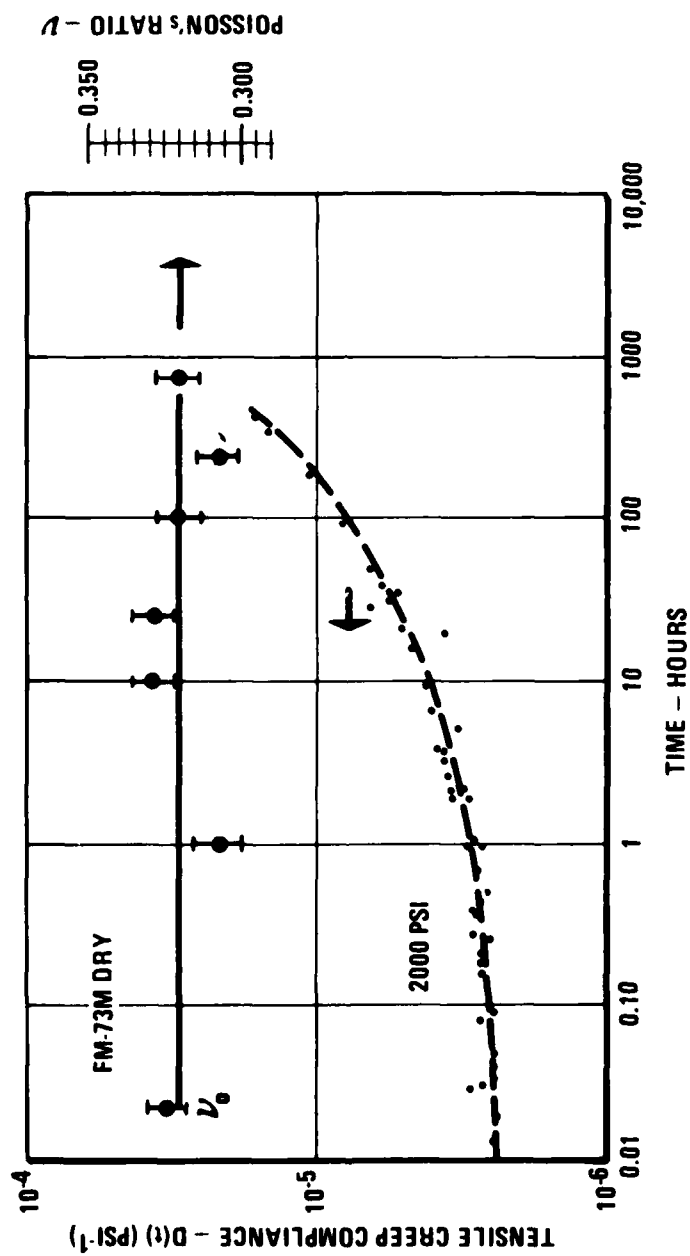


Figure 14 Comparison of Time Dependence in Creep Compliance at 25°C with Time Invariance of Poisson's Ratio for Neat FM-73M

with FM-73M and most of the material characterization (and some model joint testing) were conducted. Figures A7 through A13 of the Appendix summarize the material characterization of FM-400. In these tests, an upper temperature limit of 310°F was used for FM-400, instead of +140°F as for FM-73M). These tests, especially those under hot, wet conditions, revealed that the FM-400 adhesive system was especially sensitive to water. Moisture plasticizes FM-400 (lowers the $T_g \sim 80^\circ\text{F}$) degrading the neat strength ($\sim 64\%$) at room temperature, with a corresponding large strength reduction of the bonded joints. Because of the poor hot-wet characteristics of this 350°F-cure adhesive system (see, for example Figures A7 and A11), it was decided to abort further tests with FM-400 in this program as a suitable 350°F-cure adhesive system for high performance military aircraft.

Accordingly, some additional material characterization was conducted on four other representative commercially-available 350°F-cure adhesive systems in the quest for a possible replacement for FM-400.

3.3 Material Characterization of Other 350°F-Cure Adhesives

A series of screening tests were developed to assist in the selection of a 350°F-cure adhesive material for use in place of FM-400. The tapes considered were AF-147, PL-729-3, N-329-7, and Rb-398, as commercially available representative, state of the art 350°F-cure adhesive systems. The "screening" tests on the wet and dry materials consisted of:

1. Change in volume and weight gain during moisture uptake.
2. "Cyclic" T_g measurements using TMA techniques between -80°F and $+350^\circ\text{F}$.
3. Tensile creep compliance measurements at 40°C , 70°C , and 121°C .
4. Smith plots (σ_f vs. ϵ_f) at different strain rates for three temperatures (RT, 160°F and 200°F (wet/ 300°F (dry))).
5. Examination of the deformed materials and fracture surfaces by optical microscopy and/or SEM techniques.

The results of these tests are summarized below:

3.3.1 Moisture Uptake Effects

Moisture uptake characteristics were measured on small coupons (1.0" x 0.5" x 0.045") cut from 4-ply laminated sheets of the four candidate 350°F-cure adhesives. Three coupons of each adhesive were exposed to 150°F water immersion, 140°F 100% (condensing) relative humidity, and 140°F dry air. The coupons were periodically weighed and length and width measurements made in micrometer jigs. The results are shown plotted (by computer) in Figures 15 and A14 through A18, respectively. From these data are plotted the % weight gain (Figure 16) and equilibrium expansion in water (Figure 17) for the four candidate 350°F-cure adhesives, FM-400 and FM-73M.

From these data it is observed that:

- No specific evaluation of diffusion data was made. All specimens were 0.045" thick and attained apparent saturation after approximately 25 days.
- Moisture uptake was 4% for all 350°F-cure (Figure 16) as compared to 2.2% for FM-73M.
- For a stress analysis and failure analysis viewpoint, it is more important to consider dimensional rather than weight changes. In this regard, significant differences appear as illustrated in Figure 17.

3.3.2 "Cyclic" Tg Measurements

Dry specimens of the four adhesive systems were run on the Perkin-Elmer TMS-1 Thermomechanical Analyzer (TMA) (Figure A2) to determine thermal expansion coefficient, α_T , and glass transition temperature, T_g .

Determinations were made from -80°F to 350°F at a scan rate of 10°C/minute. Several temperature cycles were applied to each specimen to observe hysteresis. A probe loading of 10 grams was used on a specimen 0.5" x 0.25" x .045" in the long axis.

Data obtained are presented in Figures A19 through A24 for three of the adhesives as $\Delta L/L$ vs. temperature and α vs. temperature. Data on the fourth adhesive PL-729-3 are presented herein in Figures 18 and 19, respectively.

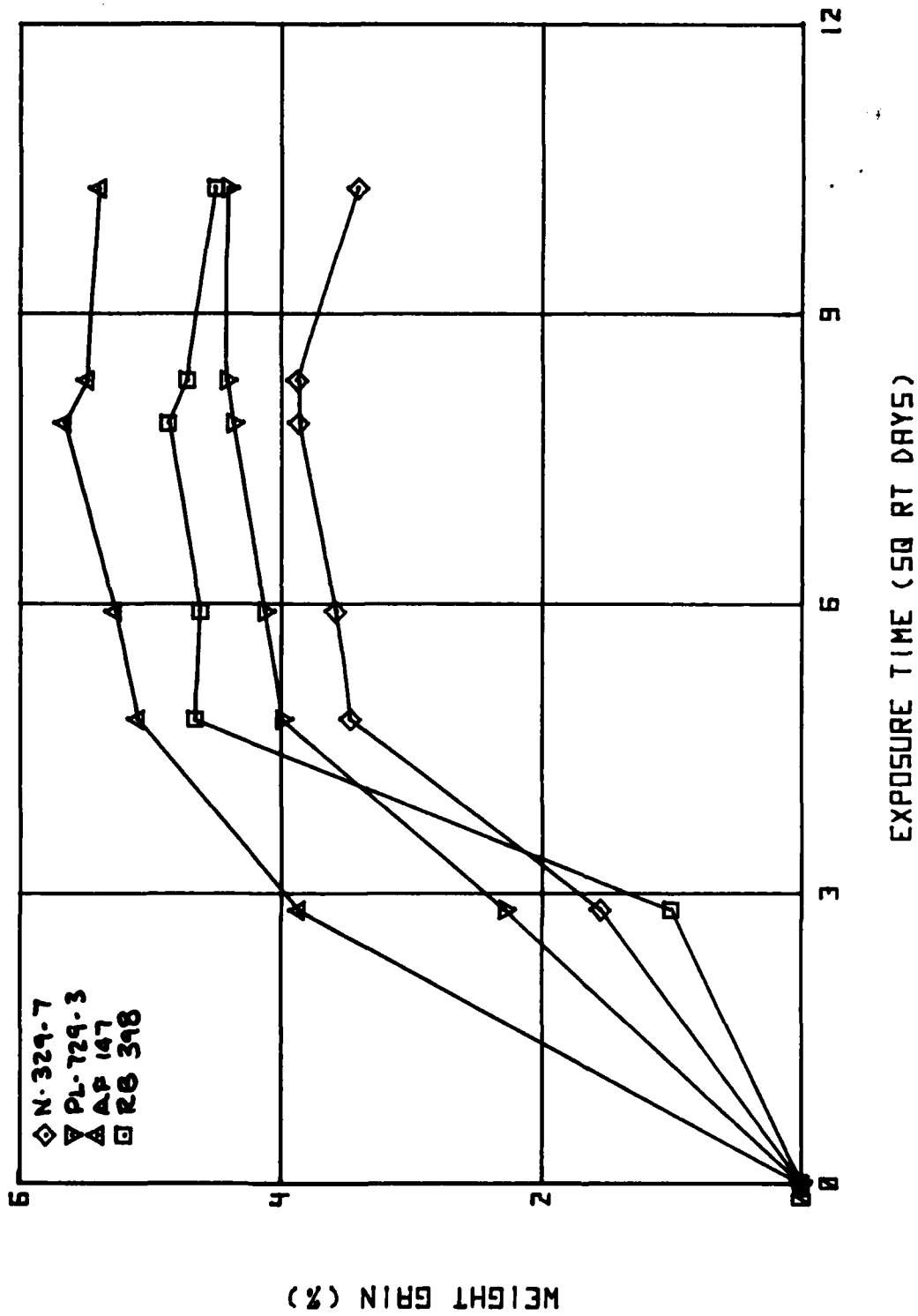


Figure 15 Weight Gain of 350°F Adhesives in Water Vapor at 150°F

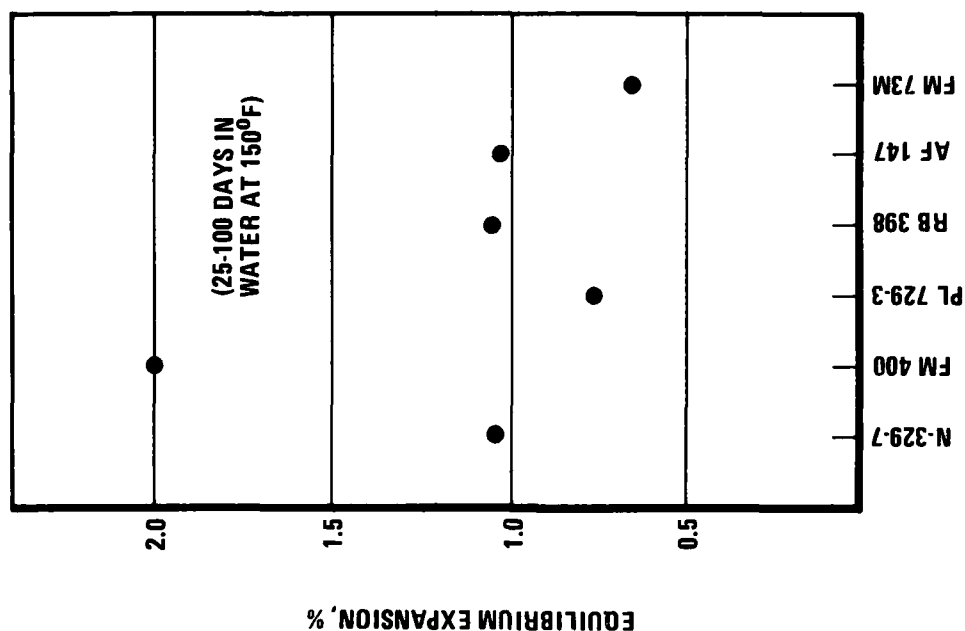


Figure 17 Comparison of Equilibrium Moisture Expansion in 350°F - Cure Adhesives

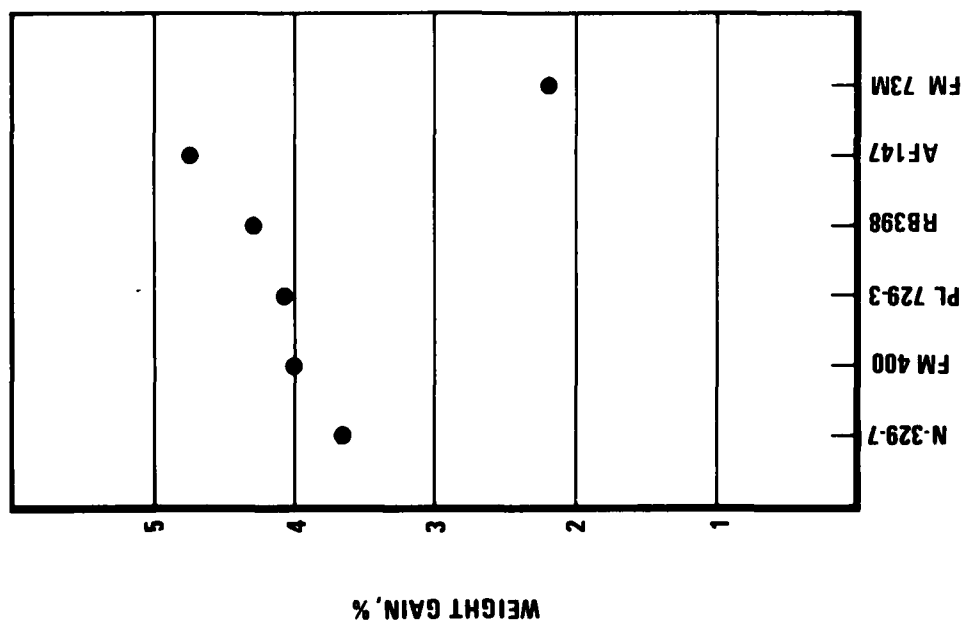


Figure 16 Comparison of Weight Gain in 350°F - Cure Adhesives

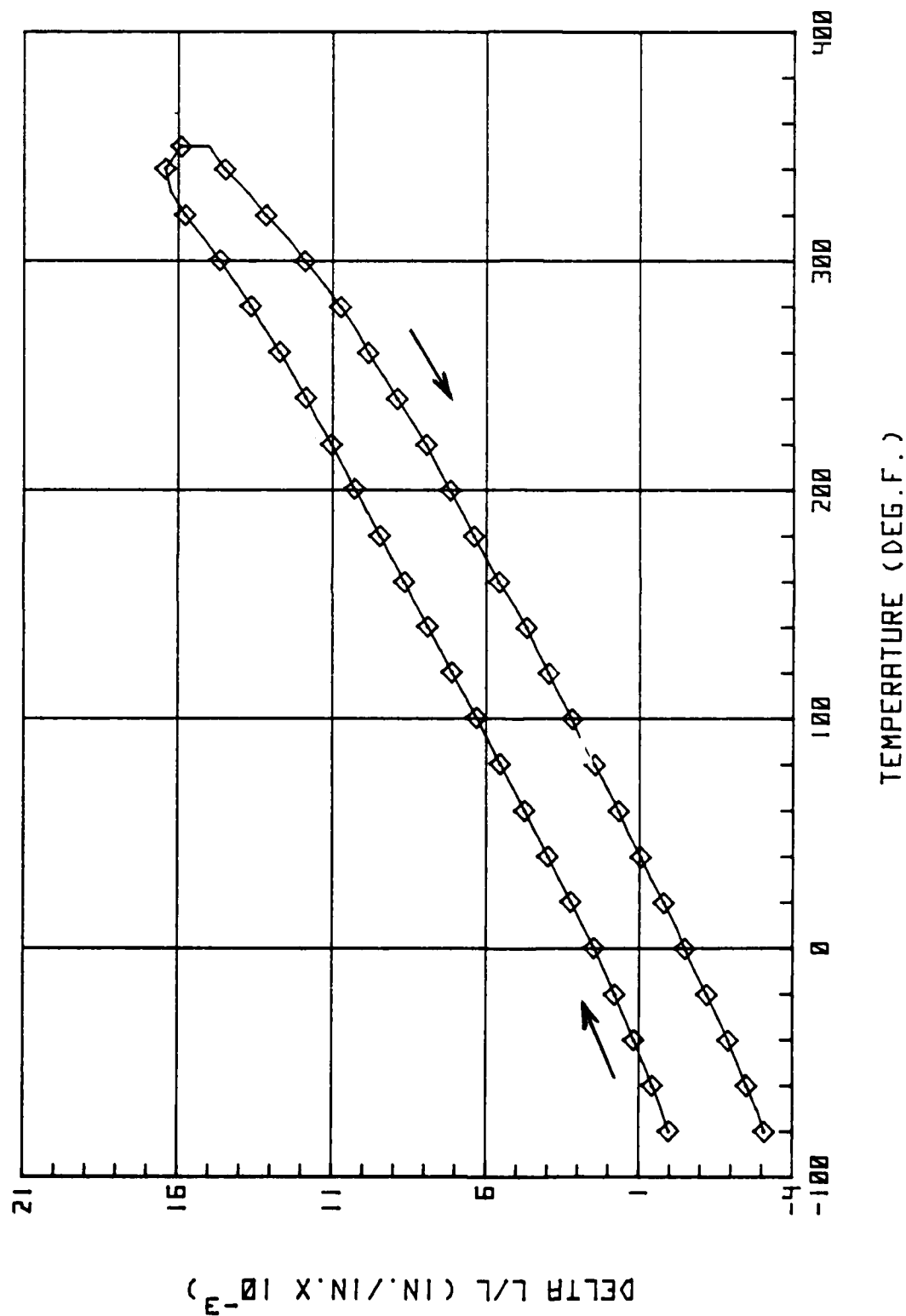


Figure 18 Thermal Expansion of Dry PL 729-3 Adhesive

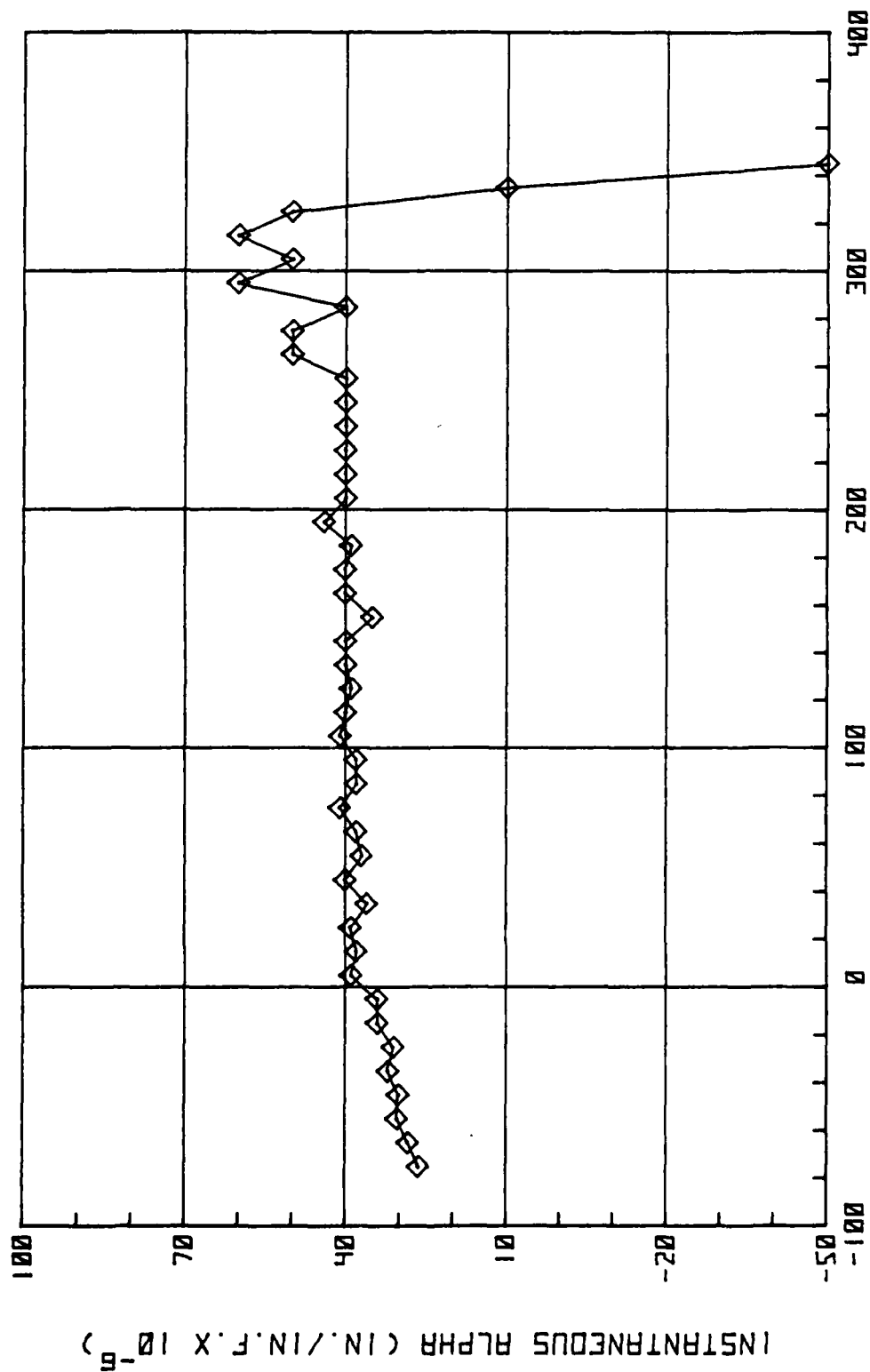


Figure 19 Thermal Expansion Coefficient of Dry PL 729-3 Adhesive

The hysteresis in the initial loops are attributed to "shakedown" or physical aging effects as discussed in Section 5.4.2.

3.3.3 Tensile Creep Compliance Measurements

The experimental apparatus shown in Figure A25 was used to measure the creep compliance of the 350°F-cure neat adhesive wet and dry specimens at various temperatures. This creep apparatus is a modified version of that used earlier in measuring the creep compliance of FM-73M (and FM-400). A Hewlett-Packard DC input, output displacement transducer Mod. #7DCDT-500 with a linear range of 0.50 inches was used to measure the rate of elongation of the specimen. The transducer is calibrated by depressing the rod a known displacement, e.g., with calipers, and adjusting the output voltage with a voltage potentiometer as registered by a convenient displacement on the strip chart. A neat adhesive specimen is then clamped in the extensometer and heated to the desired temperature.

The cross sectional area of each neat adhesive specimen is measured in order to precisely determine the weight needed to achieve a stress of 2000 psi. After the weight is attached to the specimen, the strip chart records the calibrated displacement as a function of time and the creep compliance is then calculated for the particular adhesive at the desired temperature.

The wet tensile coupons were encased in a glass chamber filled with moist gauze (Figure A25) which was kept wet at all times to ensure that the wet specimens did not lose moisture during the course of creep measurement especially at high temperatures.

Figures A26 through A31 of the Appendix show plots of the creep compliance data obtained for the dry and wet candidate four 350°F-cure adhesive systems. For comparison, Figures A32 and A33 show the corresponding results obtained for FM-400 earlier in this program. (Ref. 17).

Figures 20, A34, A35 and A36 show creep compliance master curves of the original data reduced to 104°F. These are then presented as two sets of smooth curves, Figure 21 and 22, one for dry and one for wet, for intercomparison of the four candidate 350°F-cure adhesive systems, and FM-400.

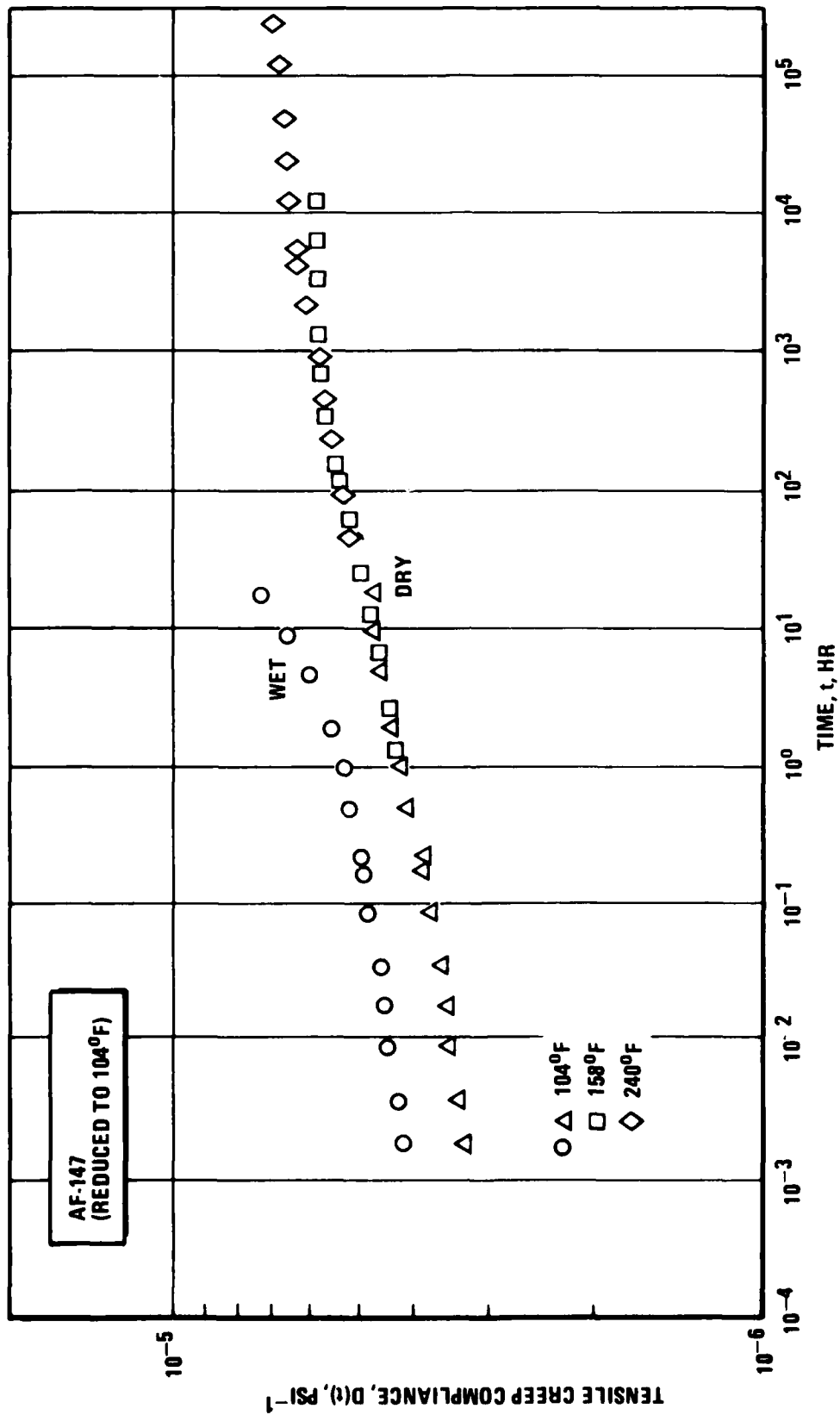


Figure 20 Tensile Creep Compliance of AF-147, Dry and Wet, (Reduced to 104°F)

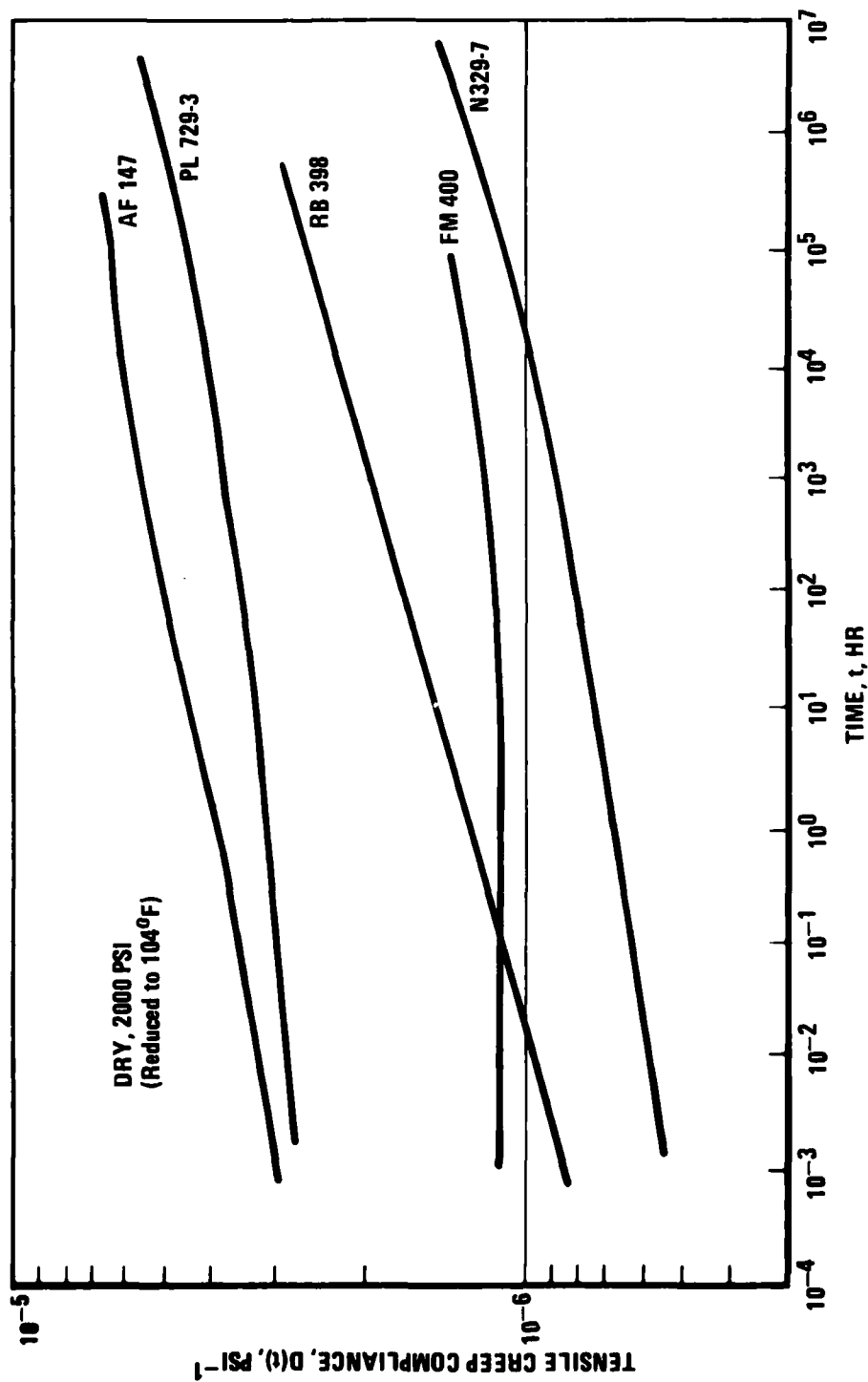


Figure 21 Tensile Creep Compliance of Dry 350°F – Cure Adhesives (Reduced to 104°F)

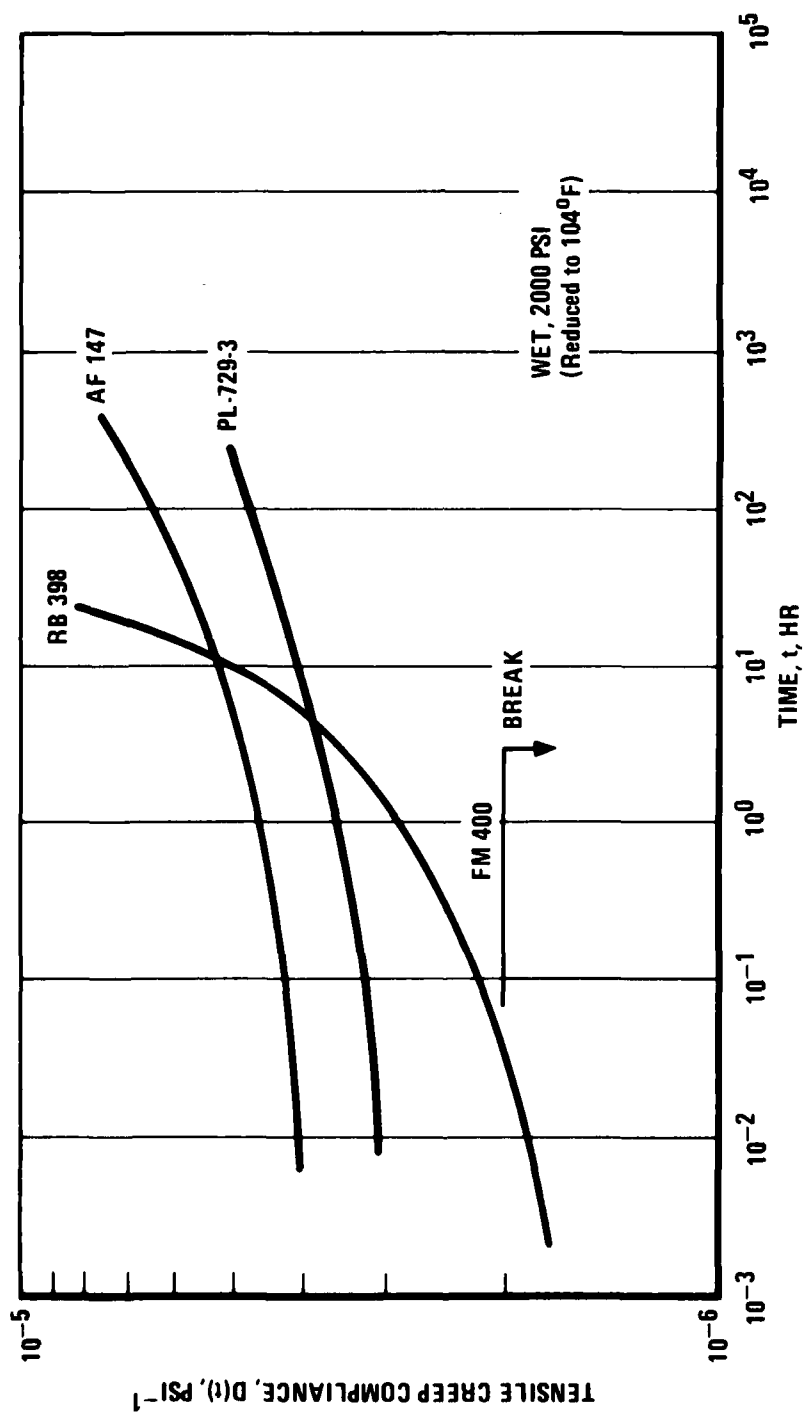


Figure 22 Tensile Creep Compliance of Wet 350°F – Cure Adhesives (Reduced to 104°F)

The dry materials tested represent a range of compliance magnitudes (and modulus) of a factor of ten as shown in Figure 21. With the exception of FM-400 dry, the materials have comparable log-log slopes in the temperature-reduced time range tested. It is of interest to note that the low compliance materials, N329-7 and Rb-398, appear on the Smith plots (see Section 3.3.4) with relatively low elongation, while the more compliant materials, PL-729-3 and AF-147, seem to exhibit some measure of ductile-like behavior leading to a tougher failure characteristic. In addition, it may be tentatively deduced that from this observation the less compliant materials might also achieve high elongations provided they are tested under higher temperatures and/or for longer periods of time.

Moisture introduction increases the compliance by virtue of accelerating the time scale as shown in Figure 22. Some materials distinguish themselves by a particularly strong acceleration, e.g., RB-398 (Fig. 22). It is expected that the failure process is accelerated in a similar fashion. In fact, in FM-400, the failure process is accelerated so much that the creep test terminated unexpectedly by fracture as shown in Figure 22. (See also Figure A32).

3.3.4 Smith Plot Measurements

The stress-at failure and strain-at-failure data points determined from constant strain rate testing (using the area corrected stress at failure) plotted after the manner suggested by Smith (Ref. 27) constitute the so-called Smith plots. These graphs are especially useful for organizing and conveying the range of stresses and strains at failure. Failure data taken at high strain rates and low temperatures appear in the upper left-hand region of the graphs. Data from low strain rates and high temperatures appear at the lower right.

Neat tensile coupons of AF 147, PL-729-3, RB 398 and N-329-7 were tested in both the as-cured and moisture-conditioned conditions. The as-cured specimens were tested at -65°F , $R T$, 160°F , 200°F , and 300°F . A minimum of three specimens were tested at each test temperature. The moisture conditioned specimens were tested at the same temperature as the dry specimens except the 300°F test point was deleted because of experimental difficulties therewith.

The configuration of the tensile coupons is described in Section II. Testing was conducted in the table model Instron test machine shown in Figure 23. A cross head movement of 0.02 inches per minute was used. With the 3.0 inch gage length of the specimen, this gave a strain rate of .0067 inches/inch/minute. The as-cured specimens were tested without an environmental chamber. The moisture-conditioned specimens tested at room temperature and above were tested using the humidity enclosure shown in Figure A25. This chamber consists of a glass outer shell with a hole at the center of its span for insertion of a temperature monitoring thermocouple. Inside the tube, a wire coil was wrapped first with absorbent paper and then with cheesecloth. The ends were sealed with soft rubber glued in place with Eastman 910 adhesive. A small slit was cut in each end so that the specimen could be placed in the chamber. Prior to test, distilled water was squirted into the chamber with a syringe to saturate the paper and cheesecloth. After test, the chamber would visually be examined to make sure that the paper and cloth were still wet.

The measured data obtained are presented in Figures A37 through A40 of the Appendix.

For ease of intercomparison, reduced curves of each of the four adhesive systems is replotted as shown in Figure 24. Each reduced curve encompasses (σ_f vs ϵ_f) data points for all environmental testing conditions and represents an "average" behavior of that adhesive system. Thus, the region between the reduced curve and the origin $\sigma_f = 0$ and $\epsilon_f = 0$, for each material represents the failure free region. Keeping in mind that this is derived from limited test conditions, e.g., one strain rate, nevertheless, the characteristics desirable for such a representation can be stated. Note that a reduced curve is roughly made up of a vertical and horizontal boundary representing a strain and a stress limit, respectively. From a design point of view, it is desirable to have both limits as far removed from the origin as possible. Furthermore, since adhesive bonds are not likely to be used for extensive periods of time under extreme conditions of either stress or strain, it is more desirable to have the boundary removed as far as possible from the origin. Therefore, with these two criteria in mind, it would not seem difficult to establish acceptance criteria for certain bonding applications of the four adhesive systems.

While it should be remembered that these data result from somewhat preliminary screening tests, they give some indication of material toughness: the larger the failure strain at a given failure stress value, the larger is the energy expenditure to adhesive fracture.

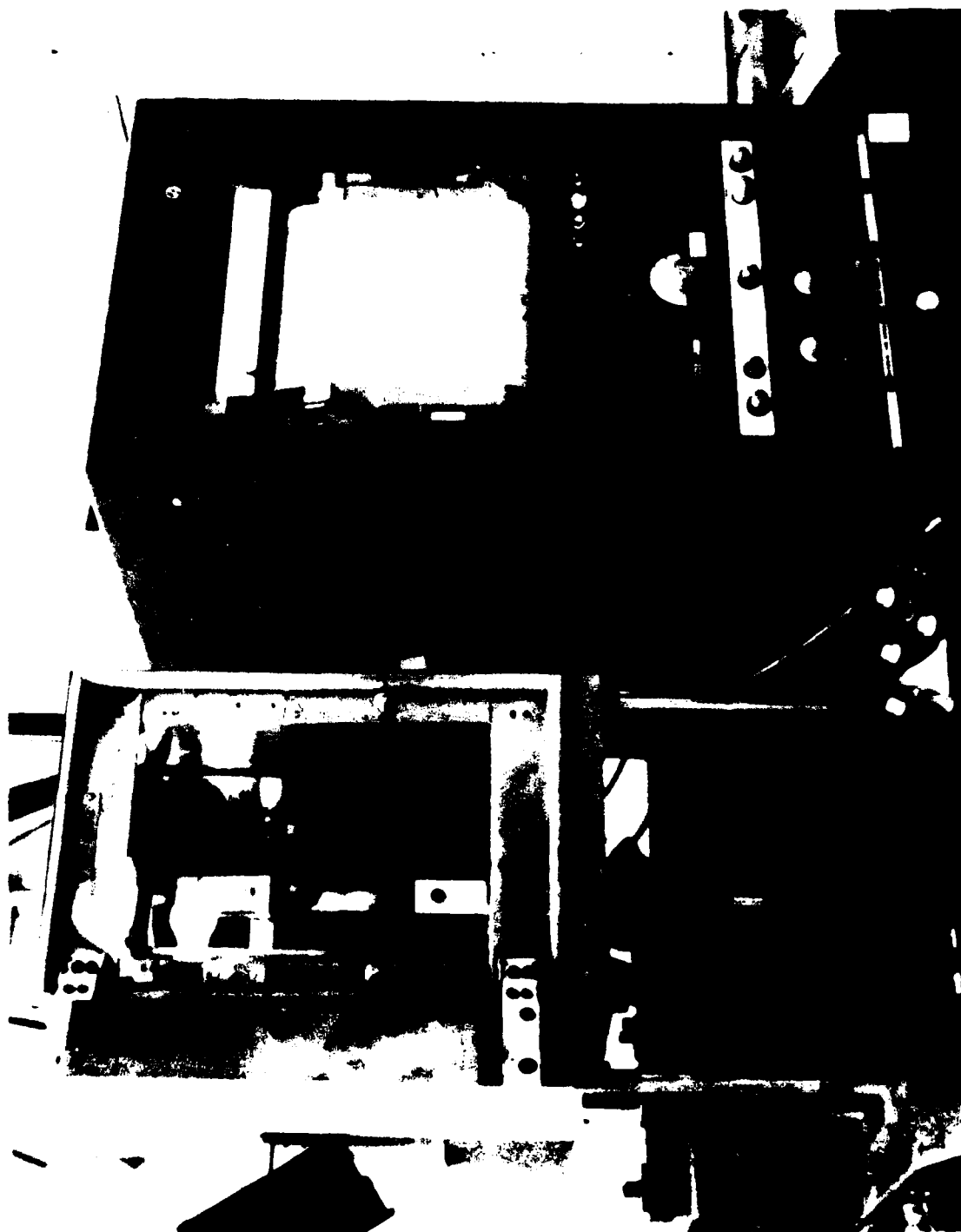


Figure 23 Experimental Set Up for Fracture Energy & Smith Plot Measurements

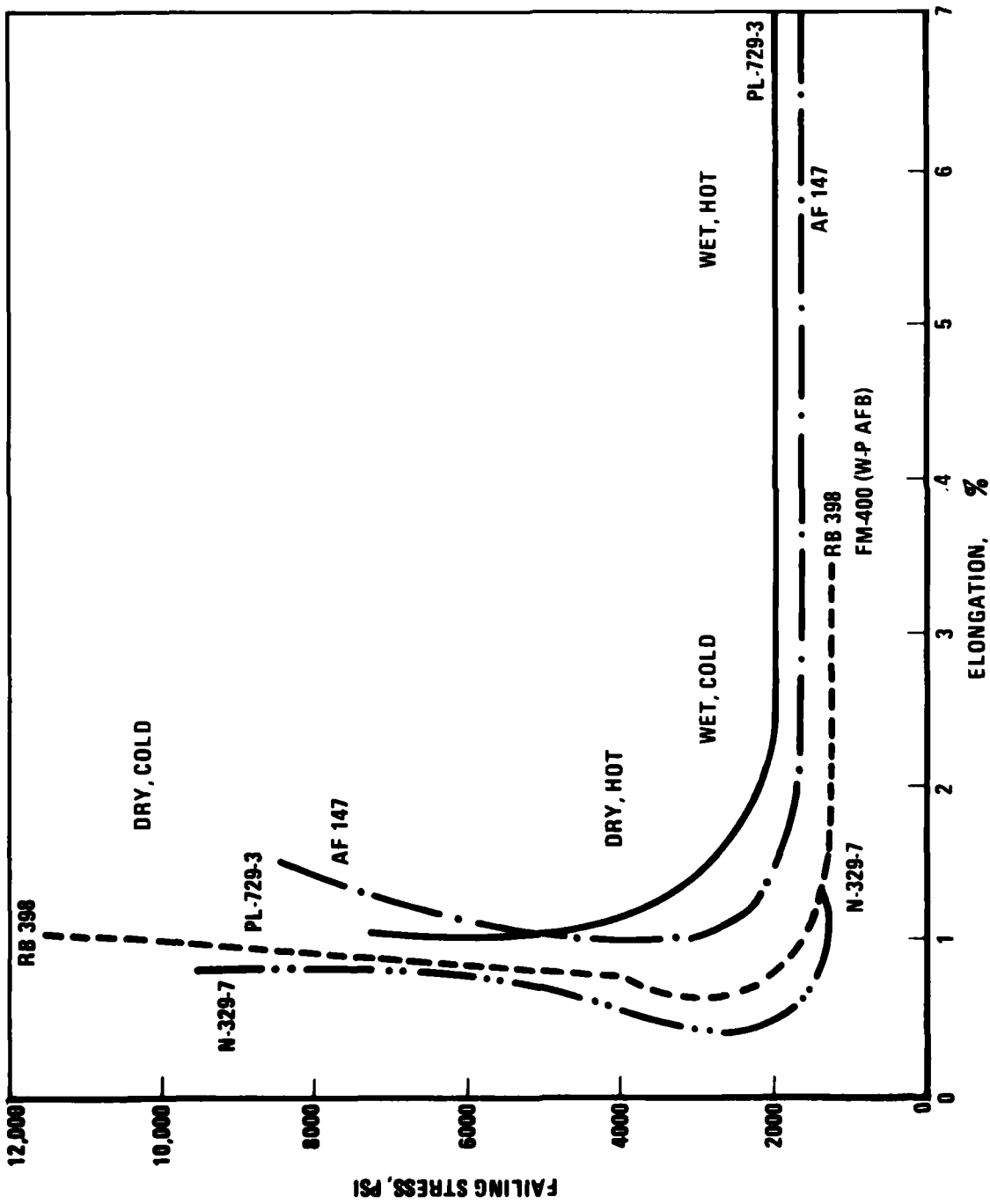


Figure 24 Smith Plot Envelopes for 350°F - Cure Adhesives

3.4 Fracture Properties

Failure of a bonded joint occurs due to cracking at the adhesive/adherend interface or within the adhesive itself as will be discussed later. There are some inherent qualities of any material which determine how fast a crack grows for a given geometry, load, and environment. These qualities will be referred to as the material's fracture properties. One property is the ability to resist final, catastrophic failure. It will be referred to as the fracture toughness. Another property, termed here the crack growth rate, $\frac{da}{dN}$, is the increment of crack growth occurring for a single cycle of fatigue loading. As stated, this is not solely a property of the material but also of the associated loading and geometry, including crack length. For purposes of discussion it will be assumed that the curve relating crack growth per cycle, $\frac{da}{dN}$, to the applied stress intensity factor range, ΔK , is a good measure of this property.

Fatigue crack growth occurring within the adhesive layer is probably controlled by the fracture properties found for the neat adhesive. Factors such as temperature or moisture content, which affect the mechanical response properties of the neat adhesive, probably affect the fracture properties as well. It is now well known that the mechanical response of FM-73M adhesive is time dependent. It is not surprising, then, that the apparent crack growth rate should possibly depend on the frequency of loading. Also, the fracture toughness can be expected to depend on strain rate.

In a bonded joint there must be an adhesive/adherend interface. Fatigue crack growth occurring along the interface surely depends on the adherend and surface preparations as well as on the properties of the adhesive itself. Thus, "interface properties" may be thought of as existing similar to the material properties of a single medium. All of the discussion above for material properties may apply to interface properties as well and variations in interface fracture properties may be important.

3.4.1 Specimen Design and Precracking

Center-notched tensile coupons of 4-ply FM-73M with integrally bonded Al end takes described in Section II and shown in Figure 4 were used for the fracture energy measurements.

The specimens for the crack growth measurements were pre-cracked to a $2a$ value of 0.30 inches. From a starting chevron notch length of 0.20 inches, the crack was grown at three successively lower load levels, with the last 0.05 inch growth increment being made at the lowest load level. The first load was 175 pounds, the second was 140 pounds, and the third was 112 pounds. The last load level produced crack growth rates of between 0.2 and 0.4 μ inches per cycle.

Specimens for the stress intensity measurements were pre-cracked to a $2a$ value of 0.5 inches yielding a $2a/W$ ratio of 0.25. The $2a$ of the chevron starter notch measured between 0.25 and 0.30 inches. The crack was started and grown to a $2a$ value of 0.4 inches using a maximum load of 150 pounds. The next two growth increments were 0.05 inches, with maximum cyclic loads being 125 pounds and 100 pounds. The final 0.050 inches of crack growth required sinusoidal loading of between 8,540 and 21,300 total number of cycles, N . This corresponds to a da/dN rate of between 1.1 and 3 μ inches per cycle.

All the precracking was done using a sinusoidal wave form with a stress ratio of $R = 0.1$ and a cyclic rate of 7 Hertz. To measure the crack length, a mylar scale graduated in 0.010-inch increments was glued above the crack path on each specimen. The crack length was then monitored with a 10X microscope with a vertical crosshair reticle. By aligning the crack tip with the crosshair, the crack length was read using the mylar scale.

3.4.2 Stress Intensity Measurements

The stress intensity measurements, including pre-cracking on the fracture energy specimens, were performed in the test frame with the temperature chamber shown in Figure 23.

Instrumentation for the test consisted of an X-Y recorder which plots the load applied by the Instron test machine versus the output from an induction deflection measuring unit which measured compliance over a two inch span. The use of the compliance gage was discontinued in favor of the Instron chart which provided a load versus time recording. This recording could also be correlated with cross head movement. This also allowed the use of an environmental chamber which would encompass the entire specimen.

Monotonic load levels ranging from 50 pounds up to relatively high values of 350 pounds were used in the energy release rate measurements. A motor driven 35 mm camera with two one-inch extension tubes and a 105 mm lens was used to photograph the crack during testing.

Photographs were taken at the rate of two frames per second for specimens tested using the 0.5 inches per minute cross head movement rate. At the slower cross head movements, pictures were taken at selected intervals and the Instron chart was marked to indicate where each exposure was made. This made it possible to correlate frame number with load. Following development of the films, the crack length was measured on each frame using a 10x microscope and a vertical cross hair to match the physical crack tips with the mylar scale attached to the specimen. This crack data was then tabulated with corresponding load and time data for use in subsequent stress intensity and crack propagation rate calculations. Figures A41, A42, and A43 of the Appendix show selected frames from dry and moisture conditioned specimens tested at room temperature and 140°F at various strain rates. As shown in the figures, the crack growth behavior was good for all the dry specimens and for the moisture conditioned specimens tested at room temperature. The moisture conditioned specimens tested at 140°F show excessive plasticity. No attempt was made to correct for the effect this plasticity had on the width of thickness of the specimens in the crack path because of experimental difficulties, including specimen distortion.

The equation used for calculating stress intensity, K, of the center-notched flaw is the well-known secant equation (Ref. 41):

$$K = \frac{F}{B} (\pi a)^{\frac{1}{2}} \cdot \left(\sec \frac{\pi a}{w} \right)^{\frac{1}{2}} \quad (2)$$

where K = stress intensity psi. in^{1/2},
 F = load in pounds
 B = thickness (inches)
 2a = physical crack length (inches)
 w = specimen width (inches)

Crack length, a, versus time, t, data were plotted for each of the environmental conditions selected in the test plan and the best smooth curve fitted to each data set. A typical data curve fit is shown in Figure 25. The rest of the data curve fits are shown in the Appendix, Figures A44 through A59. Tangents were then constructed to these curve fits at the experimentally determine crack lengths and the slopes calculated to yield the corresponding crack growth rate values, da/dt.

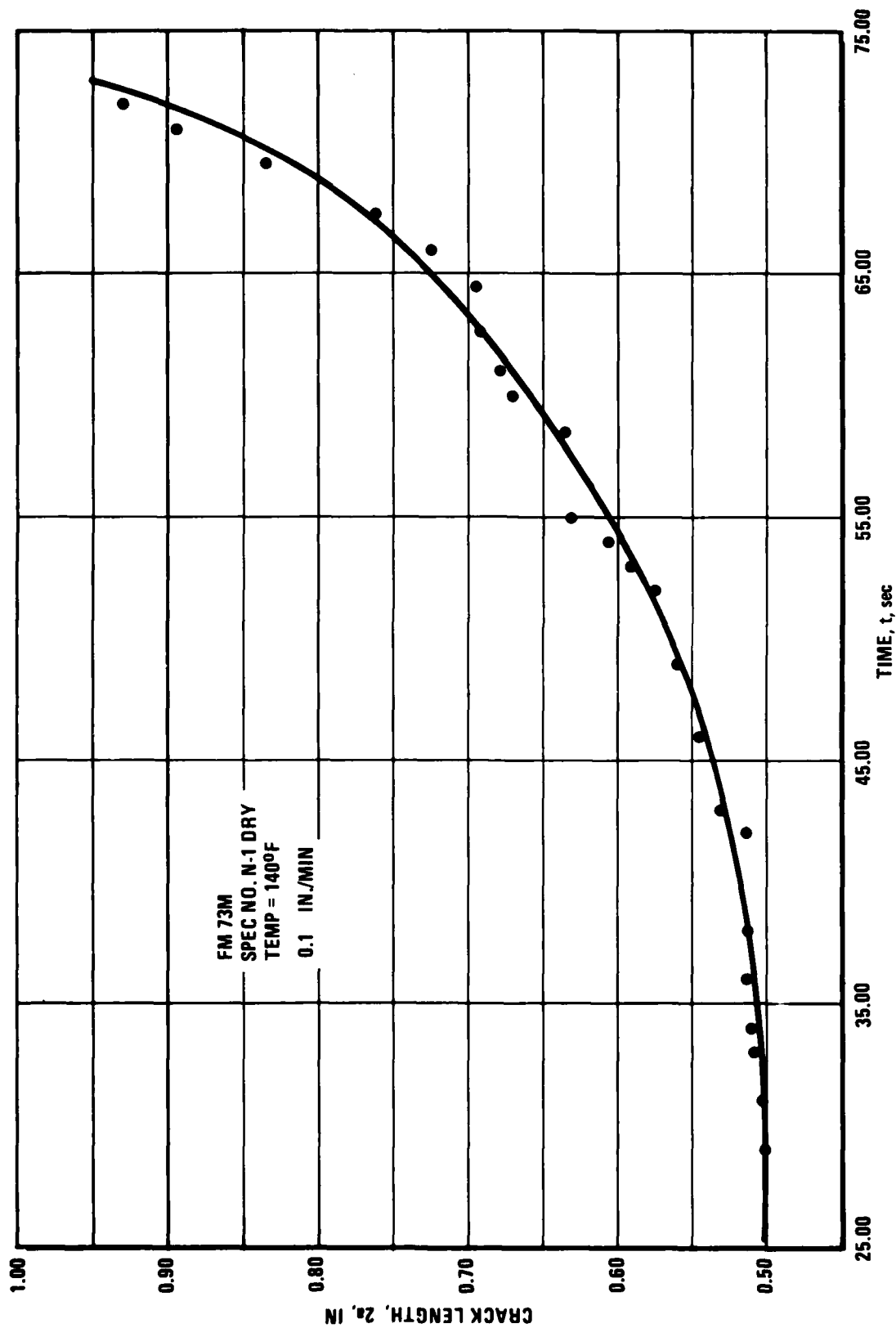


Figure 25 Crack Growth in Dry FM-73M at 140°F

Log-log plots of these crack growth rates, da/dt , versus the corresponding previously calculated stress intensities, K , were then plotted as shown in Figures 26, 27 and 28 for three categories of test conditions, viz., Series I, ($R=0.1$, Dry), Series II, (Ambient, Wet), and Series III (140°F , Dry). For each of these three series a best fit log-log slope was constructed as indicated by the straight lines in Figures 26, 27, and 28 respectively. The individual three slopes are practically identical so that a simple shift of Series I and II data along the crack rate axis yields the line shifts shown in Figure 29. Thus it can be concluded that the crack propagation rates under monotonically increasing stress intensity (constant displacement rate) follow the same log-log straight line behavior within a factor of da/dt equal to \pm one decade.

3.4.3 Cyclic Crack Growth Rate Measurements

The cyclic crack growth rate measurements, da/dN , were conducted using a sinusoidal wave form with a stress ratio, R , of 0.05 at frequencies of 10Hz and 0.1 Hz for the four different environmental combinations shown in the experimental outline in Figure A60. The initial frequency of 10 Hz was used on all specimens until a crack growth rate in the range of 25 μ inches/cycle was achieved. On the moisture conditioned specimen tested at 140°F , no data was obtained at 0.1 Hz as failure occurred before the change over growth rate was reached. The frequency was then changed to 0.1 Hz keeping the same sinusoidal load amplitude. The moisture-conditioned specimens were tested in a humid environment rather than being completely immersed as previously discussed. The sinusoidal stress intensities, ΔK , at the corresponding crack lengths were calculated using the secant equation. The computer plots of da/dN vs. ΔK , for the test conditions cited in Figure A60 are shown in Figures 30 through 33. The combined shifted ambient and 140°F data of Figures 30 and 31 are shown in Figure 34(a). The combined shifted "wet" data of Figures 32 and 33 are replotted in Figure 34(b).

Examination of Figure 34(a) dry data shown that the dry da/dN ambient and 140°F curve should (perhaps) shift with cycling (a_T). There is no common slope indicating possibly that at high temperatures plasticity or similar non-linear effects are occurring. Neglecting the points at 140°F in brackets in Figure 34(a), the remaining ones shift with those at room temperature without accounting for the temperature difference. A possible explanation is that thermal acceleration is counteracted by increased non-linear plasticity-like dissipation processes.

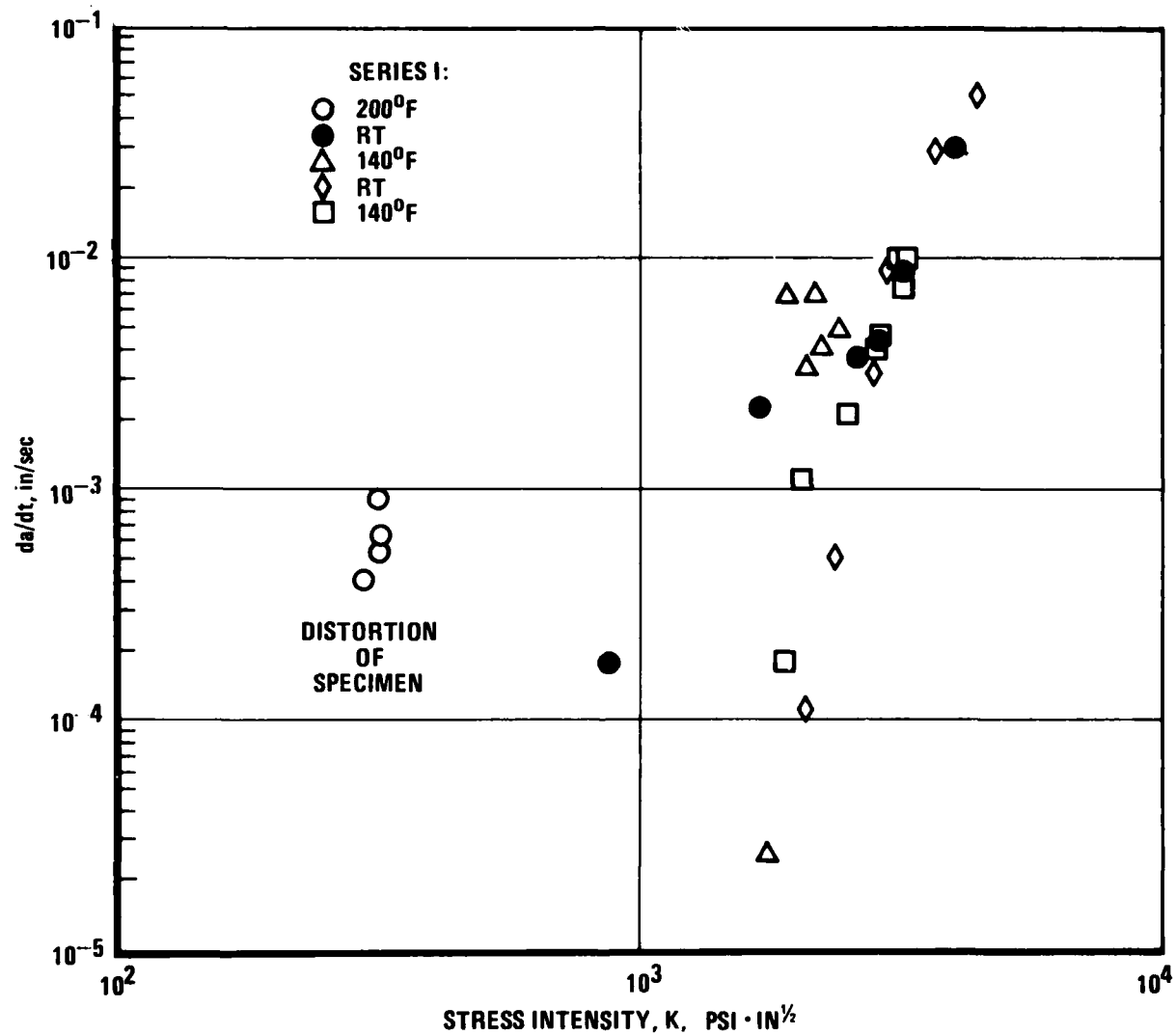


Figure 26 Crack Growth Rate vs Stress Intensity, FM-73M, Series I

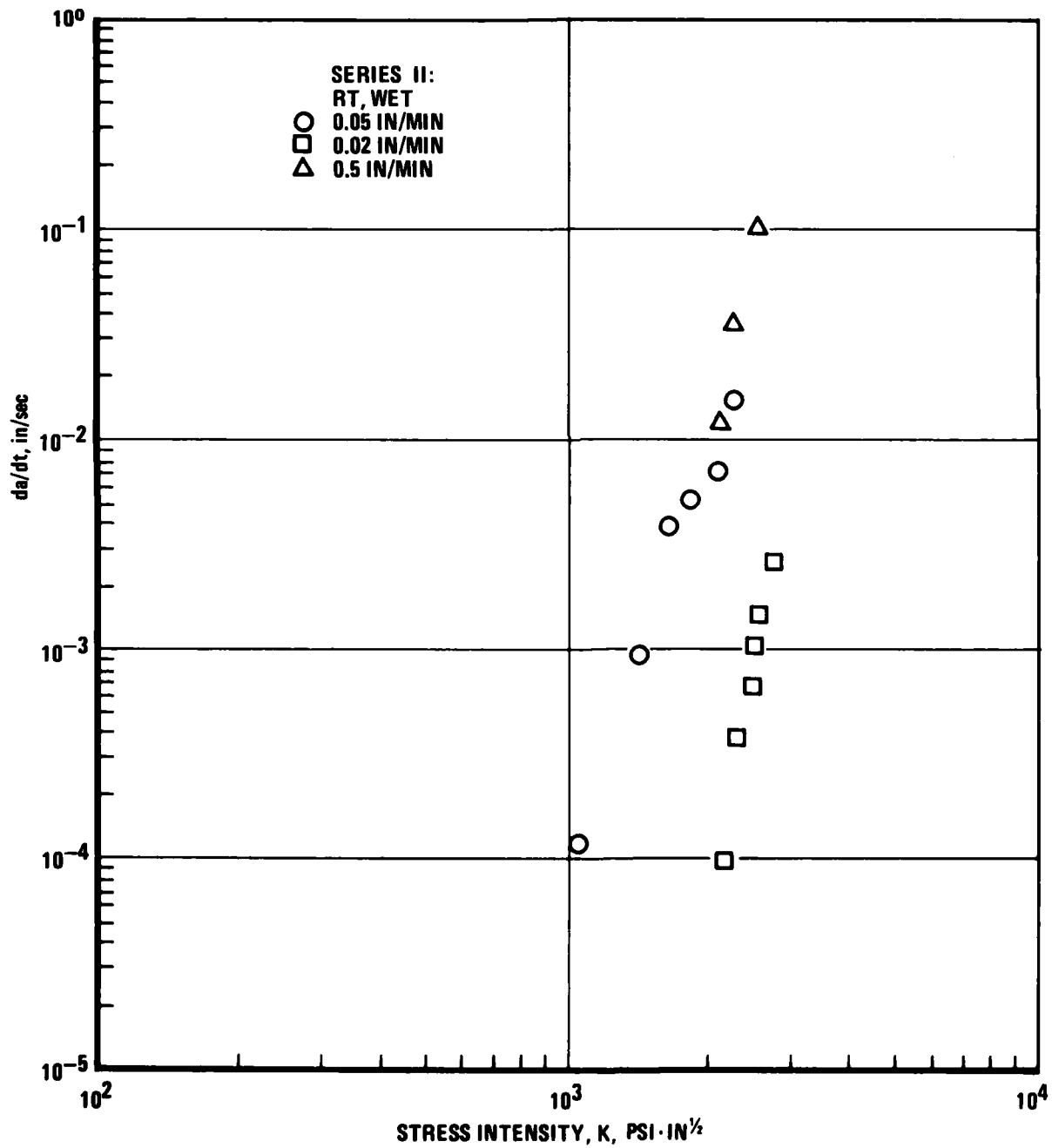


Figure 27 Crack Growth Rate vs Stress Intensity in FM-73M, Series II

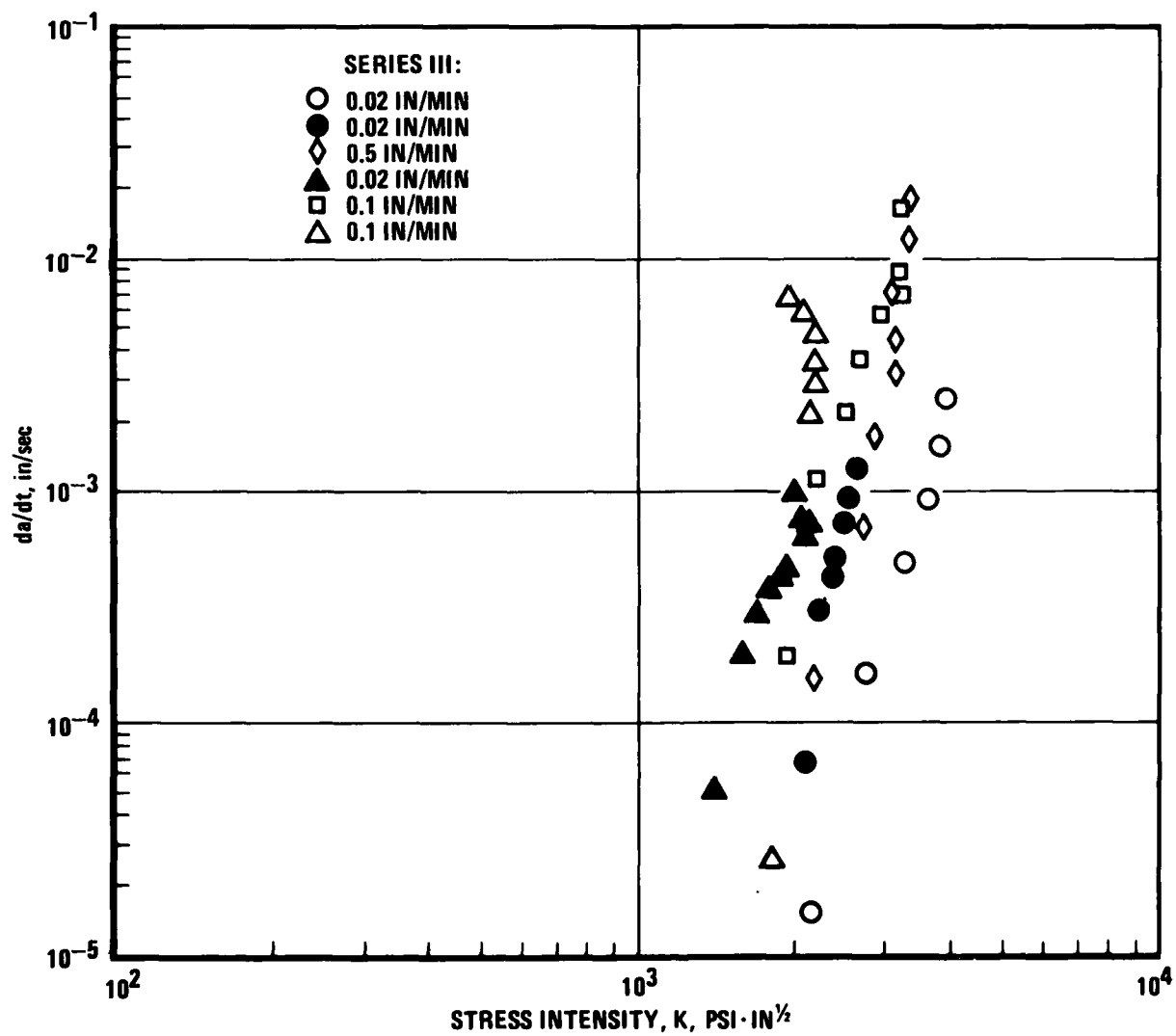


Figure 28 Crack Growth Rate vs. Stress Intensity, FM-73M, Series III

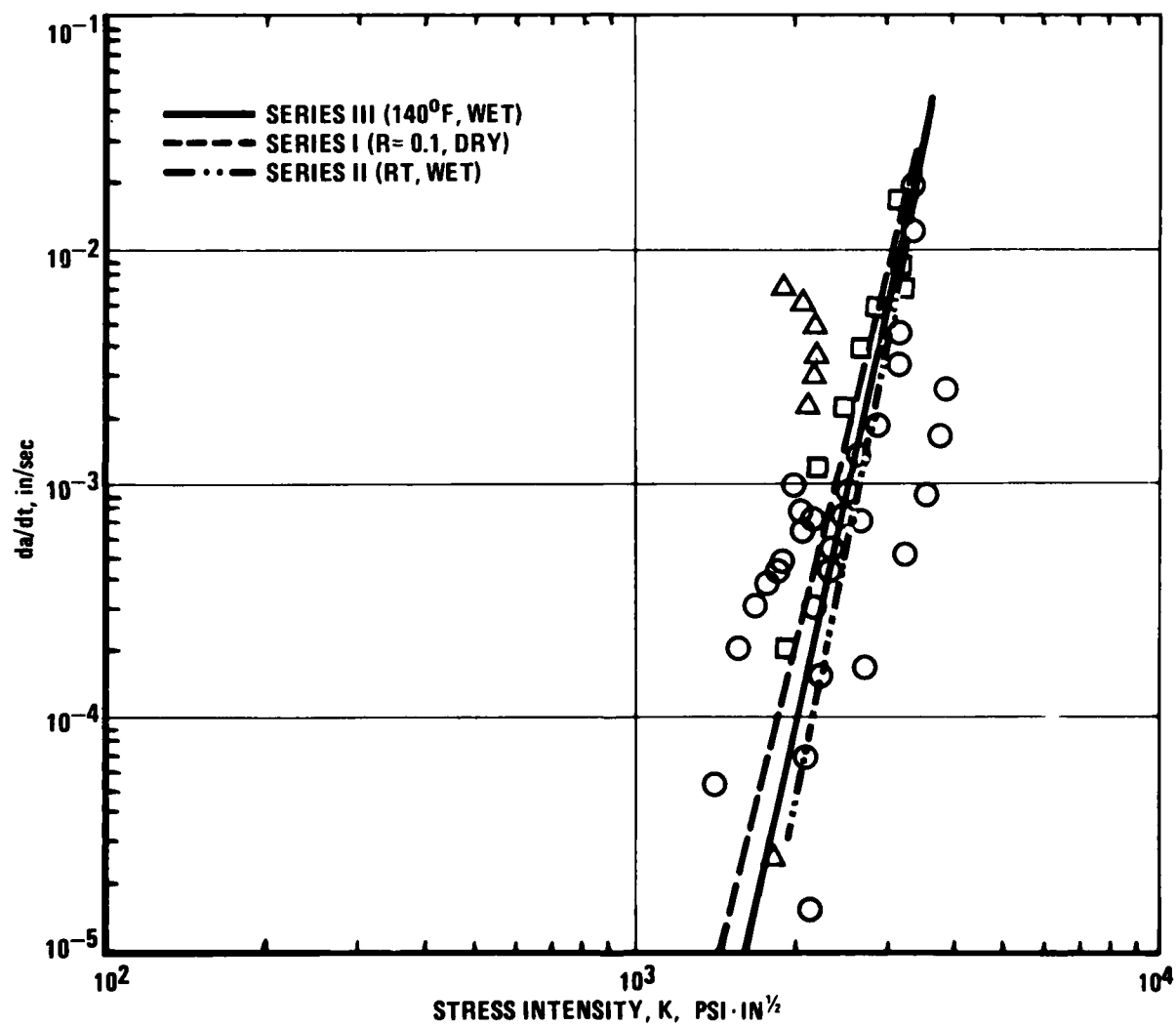


Figure 29 Crack Growth Rate vs Stress Intensity, FM-73M, Various Environmental Conditions (Shifted in da/dt)

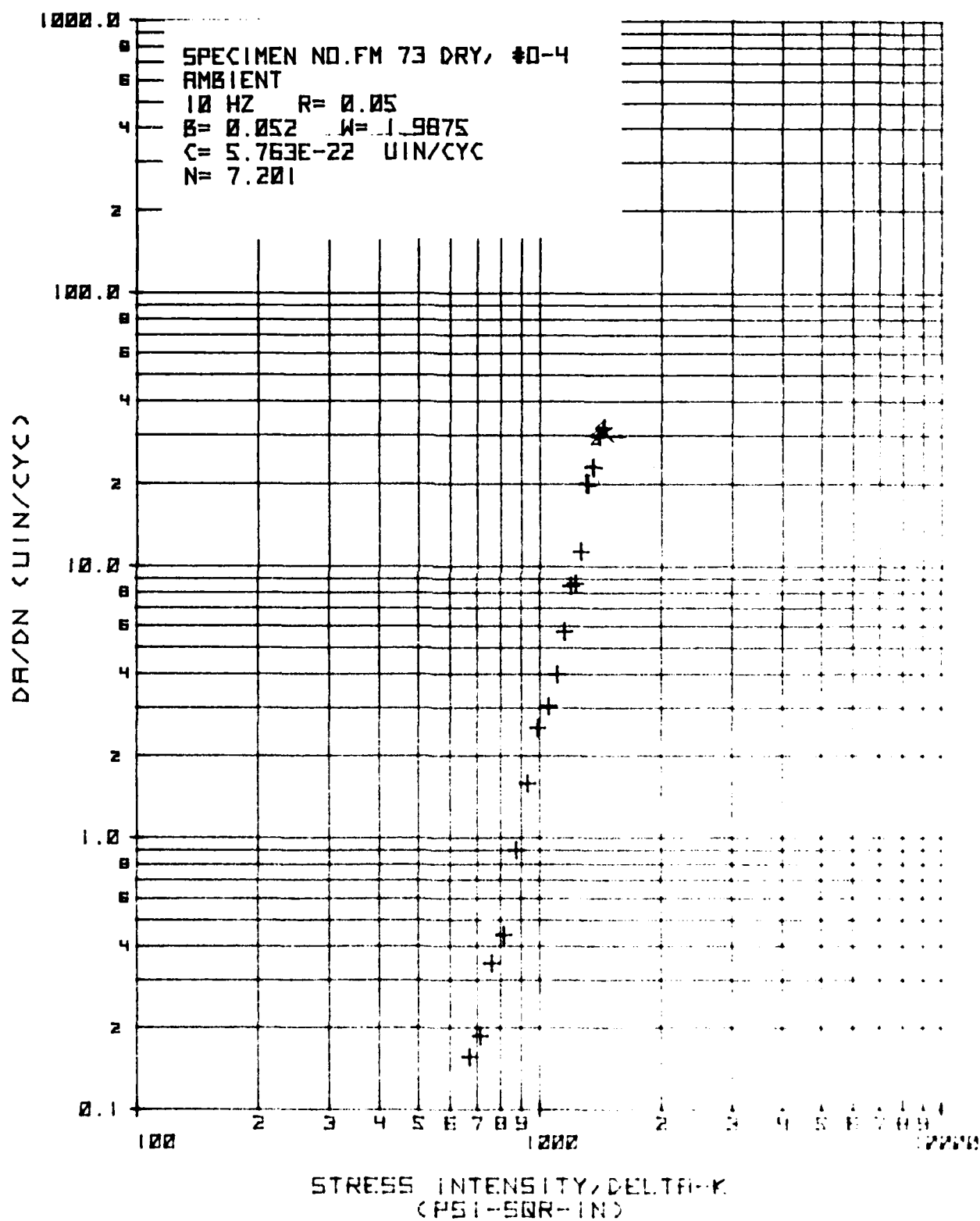


Figure 30 Cyclic Crack Growth Rate Dependence on Stress Intensity for Dry FM-73M at 75°F

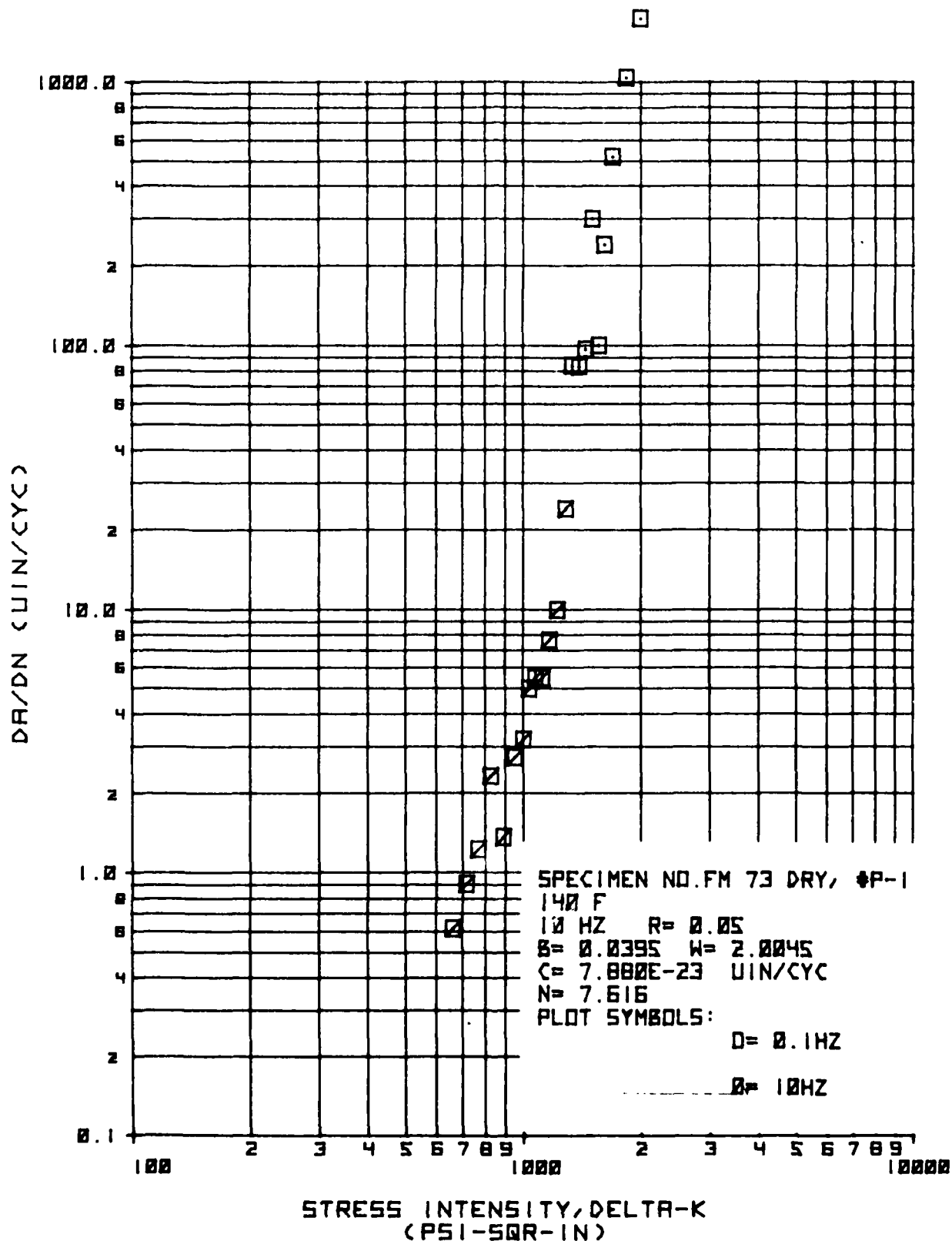


Figure 31 Cyclic Crack Growth Rate Dependence on Stress Intensity for Dry FM-73M at 140°F

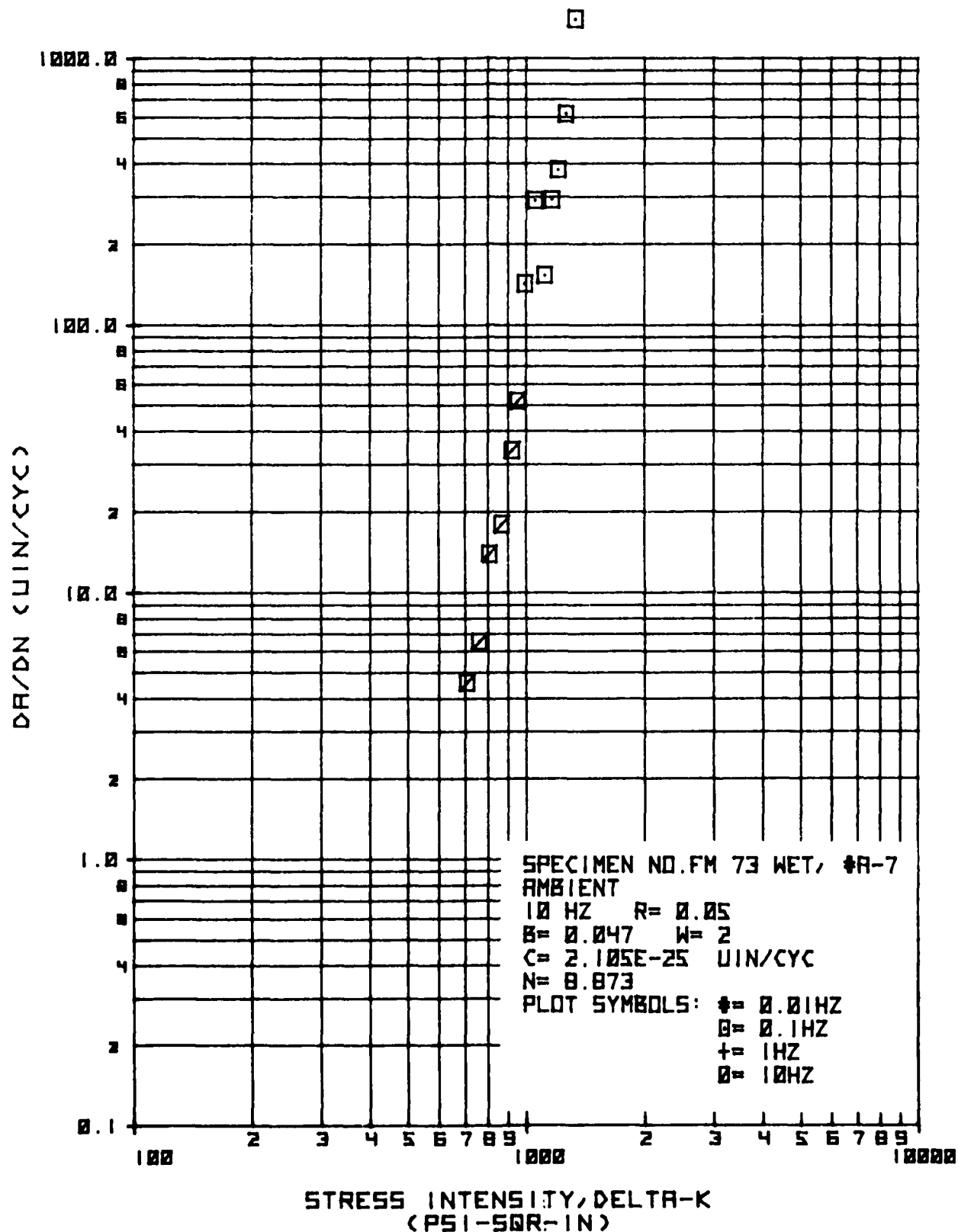


Figure 32 Cyclic Crack Growth Rate Dependence on Stress Intensity for Wet FM-73M at 75°F

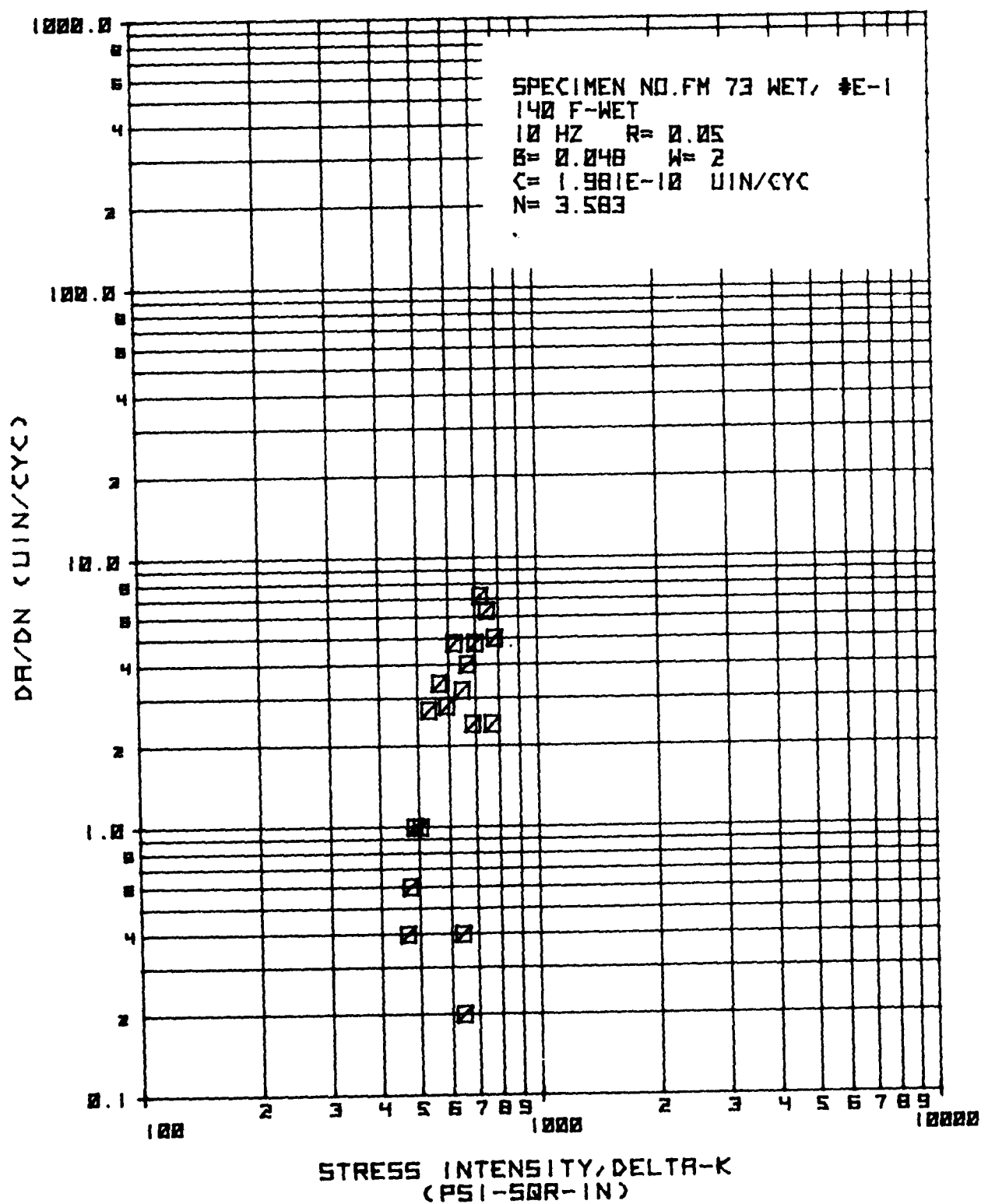


Figure 33 Cyclic Crack Growth Rate Dependence on Stress Intensity for Wet FM-73M at 104°F

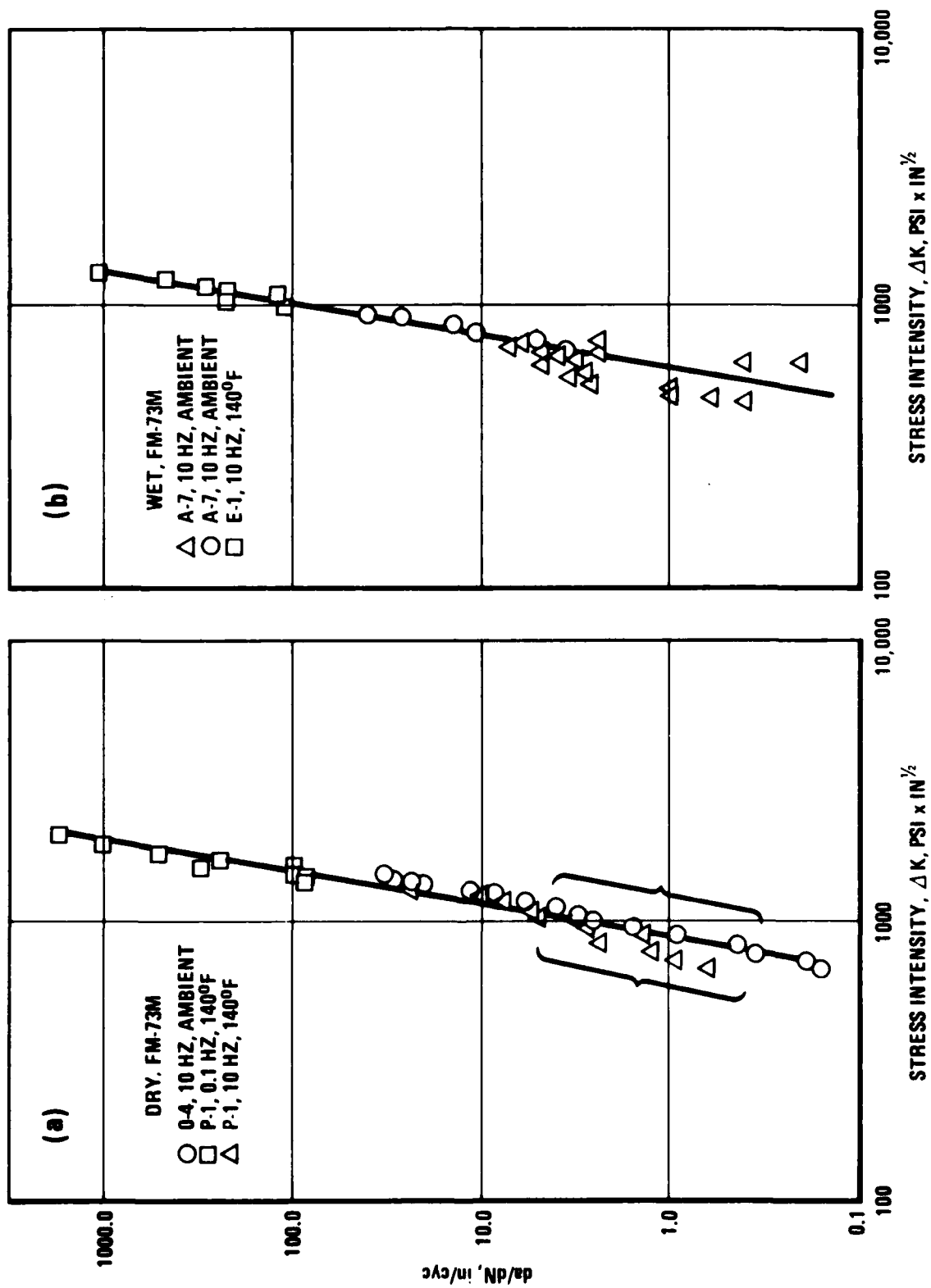


Figure 34 Cyclic Crack Growth Rate vs Stress Intensity (Shifted Master Curves)

Examination of Figure 34(b) wet data shows that the same seems to be true for both the ambient and 140°F data. However the wet data shifts by 2 decades with respect to the dry, indicating that similar mechanisms are operative, except faster in the plasticized (wet) material. Furthermore, there seems to be very little, if any, "frequency effect", which is surprising. Compared to bonded joints, this is not so.

3.5 Fatigue Testing of Neat Adhesives

Dynamic tests composed of sine wave stressing were performed to determine the velocity of the time-temperature transformations imposed on the creep tests and the ability to predict viscoelastic behavior in other loading histories.

A fixture adapted to a servo hydraulic testing machine was used to apply a 0-100 lb. amplitude sine wave to the 4-ply laminated adhesive specimens. The loading fixture shown in Figure A61, is set up on the test table of a two-inch ram MTS machine. The loads were applied by the ram below the table and were read from the double-key hole load cell below the specimen. The load cell, calibrated for 100 pounds full scale, provided the feedback signal to the servo amplifier and the load output to an X-Y recorder. A function generator, capable of both sine and square wave outputs, delivered the command signal to the servo system.

Deflection measurements were taken with an induction proximity gage with a range of 0.100 inches and linear to 0.5%. Long term stability of this induction gage was determined to be very good with no measurable drift recorded in a two hour period in a system capable of resolving 10 microinches of movement. The output voltages of the load and deflection measuring systems were fed to an X-Y recorder to which an automatic presettable pen down control was attached to record load-deflection response at predetermined intervals.

Typical load-deflection, (F vs δ) curves for FM-73M dry and wet adhesive materials are shown in Figs. 35 and A62, respectively. Comparison of these experimental histories with the corresponding MARC predictions are presented in Section IV.

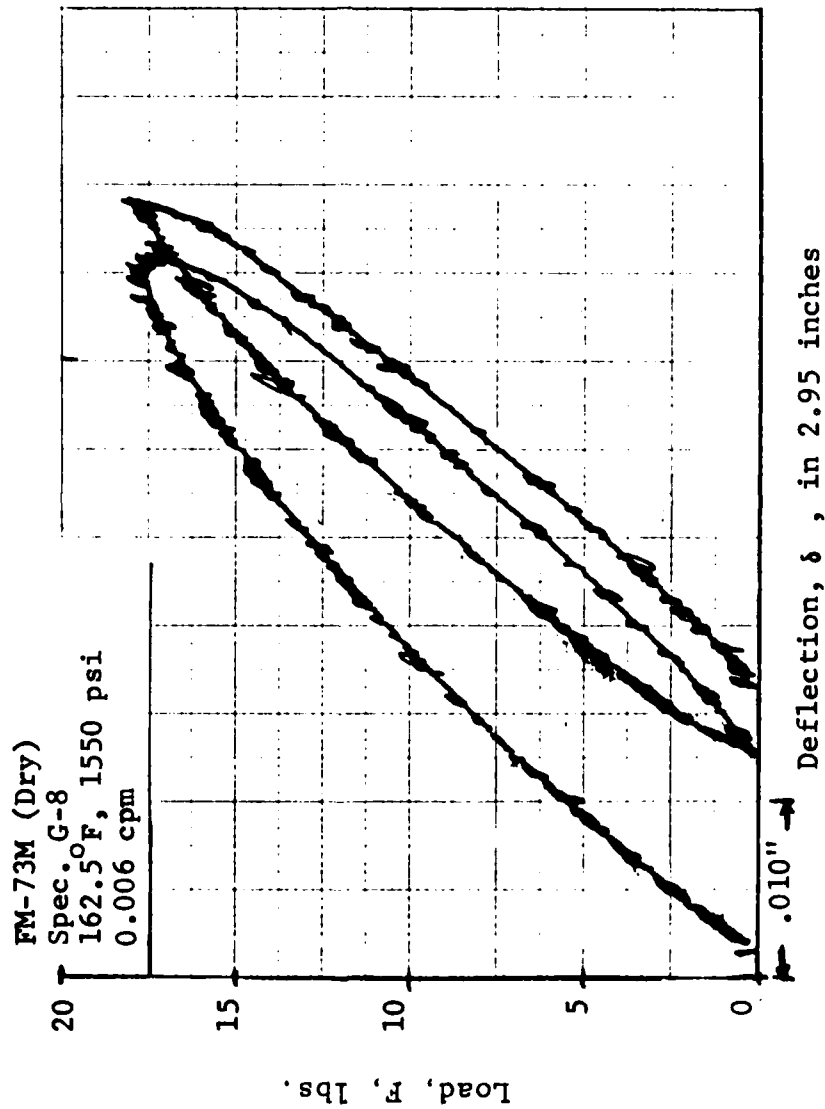


Figure 35 Load-Deflection History of Dry FM-73M Coupon, First Two Cycles of Loading and Unloading, Low Frequency

SECTION IV

STRESS ANALYSIS

4.1 Finite Element Technique

In the study of fatigue properties of joints, we wish to be able to calculate the normal (peel) and shear stresses in the adhesive interlayer and their distribution throughout the adhesive thickness. Since we wish to explore the effects of moisture ingress, cure, cooling, and cyclic loading on the stress distributions, we have chosen to use a finite element stress analysis. These effects would be very difficult to account for by a classical mechanics approach such as developed by Goland and Reissner (Ref. 28) and by Hart-Smith (Ref. 29). It is only with a flexible, numerical procedure, such as a sophisticated finite-element digital computer program, that these real-life effects can be conveniently analyzed.

The application of advanced finite-element techniques to an adhesively bonded joint not only results in a realistic stress analysis but also accommodates spatial variations in material properties which may be encountered in association with temperature and moisture gradients or with local damage. Utilization of incremental loading with finite-element techniques provides the opportunity to explore possible non-linear viscoelastic behavior of the adhesive.

From the numerous finite element programs available, we have chosen to use MARC. It is a general-purpose program designed for elastic/generalized plastic (with creep) analysis of structures and is capable of handling large deformations.

In view of the time-dependent mechanical properties measured for the neat adhesive, a simple viscoelastic stress analysis using MARC is attempted with its adhesive material behavior approximated using a Kelvin model in a series with a Maxwell spring. This material representation, although recognized to be somewhat inadequate, was conducted in order to guide the interpretation of the experimental results. The originators of the MARC program have subsequently provided a generalized Kelvin (Prony series) model representation of linear viscoelastic behavior. Although this new model has not been applied to the adhesive joint, it should be useful in later explorations.

First, in order to become acquainted with the capabilities of the MARC program, some initial problems were run using the simpler, less expensive elastic analysis procedure. This also permitted studying gross features of the spatial stress distribution in the adhesive interlayer.

4.2 Elastic Analysis

In this section we consider some problems of bonded joint geometry in the context of linear elastic and small deformation theory. It is recognized, of course, that viscoelastic behavior should be accounted for. However, as a first attempt in understanding and computationally experimenting with stress and strain fields in bonded joints, it seems appropriate to exploit the readily available (and much less expensive) elastic finite element techniques. We shall deal primarily with new problem areas, mainly stresses resulting from (a) mechanical forces with special attention being paid to the high corner stresses (corner singularity), (b) cure shrinkage and cool down from cure, (c) moisture infusion where the time dependent moisture infusion into the elastically modeled material is accounted for, and (d) prediction of the stiffness of the bonded joint.

4.2.1 Corner Singularity

It has been clear from the beginning of the Fatigue Behavior program that the greatest uncertainty exists in connection with the singularities arising from corners. Since experiments have shown that cracks or debonds tend to initiate in the high stress region in the corner of the slot cut of the model joint, it is important to resolve the character of the singularity. Although no amount of economically acceptable mesh refinement can accurately predict the strength of the singularity, the stress intensification created by the slot cut corner is present in varying degrees in nearly all of the elastic finite element analysis performed. These finite element analyses encompassed geometric modifications of the bonded joint as well as varying degrees of mesh refinement. The significant results of these studies will be summarized in the following discussion.

The effects of the geometry of the slot cut on the stress distribution in the adhesive interlayer were determined using a constant strain finite element model of the bonded joint. Two geometric modifications were examined: 1) variation of the slot cut depth and 2) variation of the slot cut width.

For the slot cut width analysis, a coarse grid model was developed which had one layer of constant strain elements representing the adhesive layer. This model was used to calculate the boundary displacements corresponding to a 1000 lb load which were then applied to a more detailed model that included only that portion of the bonded joint near the saw cut. The results of this portion of the study (Ref. 30) showed that no significant difference exists in the stress distribution between a bonded joint with a 1/16" versus a 1/8" slot cut width.

However, the study of the effect of slot cut depth showed the necessity for uniformly cut specimens. Two cases were examined using the 1/8" mill cut specimen:

1. Specimens with a cut completely through the upper adherend and the adhesive, and slightly into the lower adherend.
2. Specimens with a cut completely through the upper adherend but not into the adhesive layer.

In Case 1, a cut into the lower adherend of 13 1/3 mils was simulated by removing a portion of the adherend elements. This analysis showed a significant change in the peak stresses in the adhesive layer with a reduction in magnitude of 30 to 40% from the unmodified model joint. The stiffness of the bonded joint also decreased by 14% which is very important when predicting the behavior of the model joint.

In Case 2, three layers of elements were added to the model so that the adhesive layer would be continuous across the slot cut. This analysis showed the model joint stiffness to be unaffected by this modification. In general the adhesive stresses decreased since the continuous adhesive layer provided an additional means of load transfer. However, the maximum adhesive stresses did increase and relocated at the bottom edge of the cut.

These two studies showed the basic effects resulting from various slot cut widths and depths. However, the stress distribution in the region near the slot cut was of limited detail due to the use of constant strain elements and the coarseness of the mesh. Hence, a study was conducted to define the elastic stress variation through the adhesive thickness and investigate the merits of different amounts of mesh refinement.

Three different grids (Ref. 23) were designed in this stage of the analysis with the distinguishing feature being the number of layers of adhesive elements (one, two, and four) in the overlap region adjacent to the slot cut. Isoparametric plane strain elements with a parabolic displacement function (linear strain) were used to model half of the bonded joints. Antisymmetry boundary conditions were imposed at the center of the joint using the TYING function available in MARC. An elastic analysis was performed with each grid using adhesive properties representative of FM-73M dry at room temperature.

Typical peel and shear stress distributions at the center of the bondline are shown in Figures 36 & 37. Although the basic stress distribution is nearly identical in all three models, significant differences appear in the region near the slot cut. Both the peel stress and shear stress are found to decrease in this region of the fine grid model. Also, the shear stress approaches zero as it should since the free face at the cut can have no net shear stress.

Contour plots of the bond normal stress and shear stress are shown in Figures 38 and 39, respectively, for the fine grid model. This model clearly shows that a significant variation in the stresses exists near the slot. The presence of the corner singularity can be seen at the lower corner of the cut where large stress gradient exists. These large stresses, created by the bending in the cut section of the aluminum adherends, is of considerable importance in predicting the strength and life of the bonded joint.

4.2.2 Moisture Absorption Stresses

The MARC program was used in an elastic analysis to predict the stresses in the bonded joint resulting from the expansion of the adhesive caused by moisture absorption. In order to calculate these stresses, a coefficient of expansion had to be determined which could then be input into the MARC finite element program as the coefficient of thermal expansion. Thus, with a suitable temperature distribution, the desired free strain in the adhesive could be created.

In order to determine the coefficient of expansion, several FM-73M specimens were exposed to a 100% RH, 60°C environment for 46 days. During this period, the weight, length and width were measured at 0, 1, 3, 7, 29, and 46 days. Although the specimen

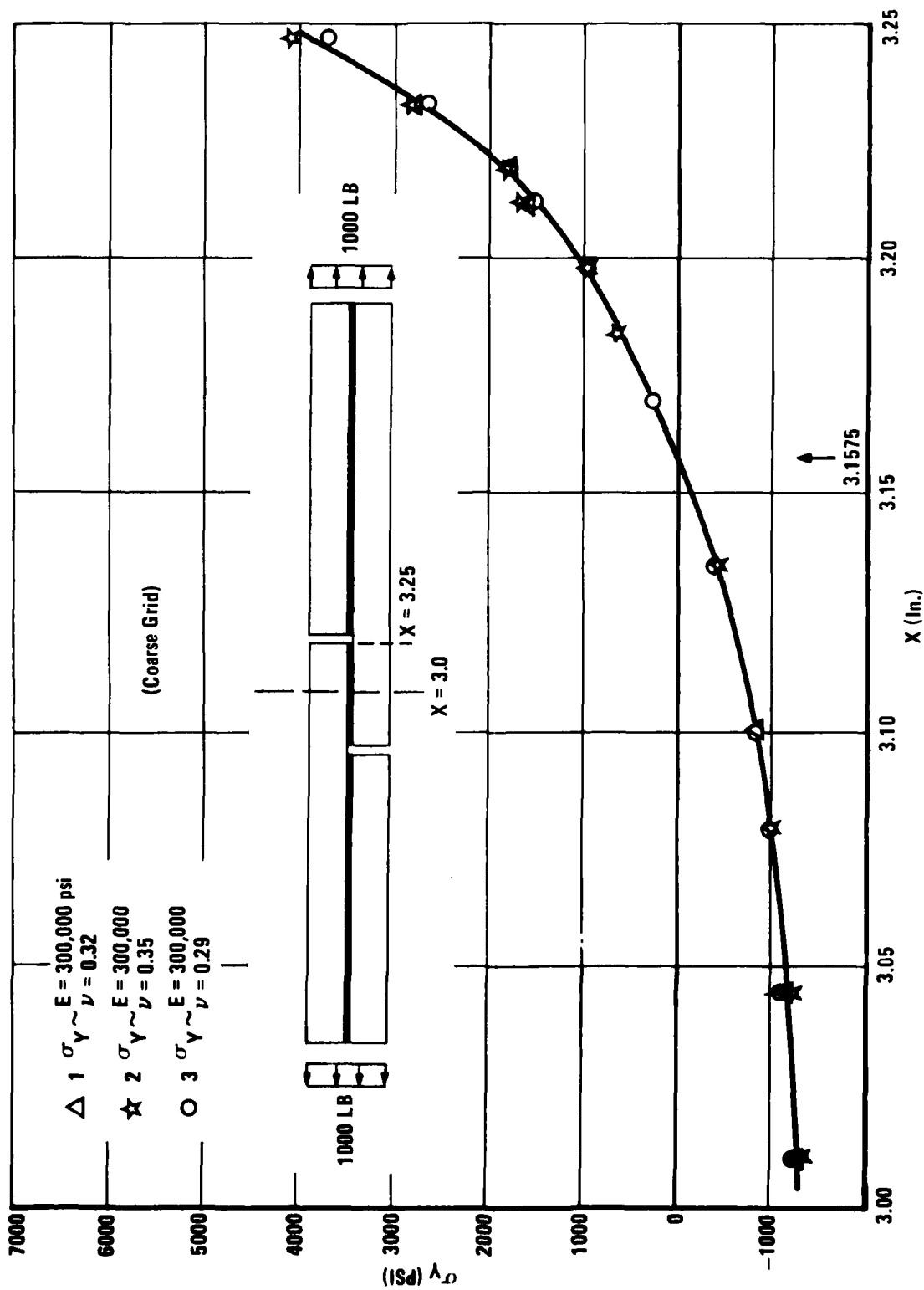


Figure 36 Peel Stress In Center of Adhesive: Poisson's Ratio Sensitivity

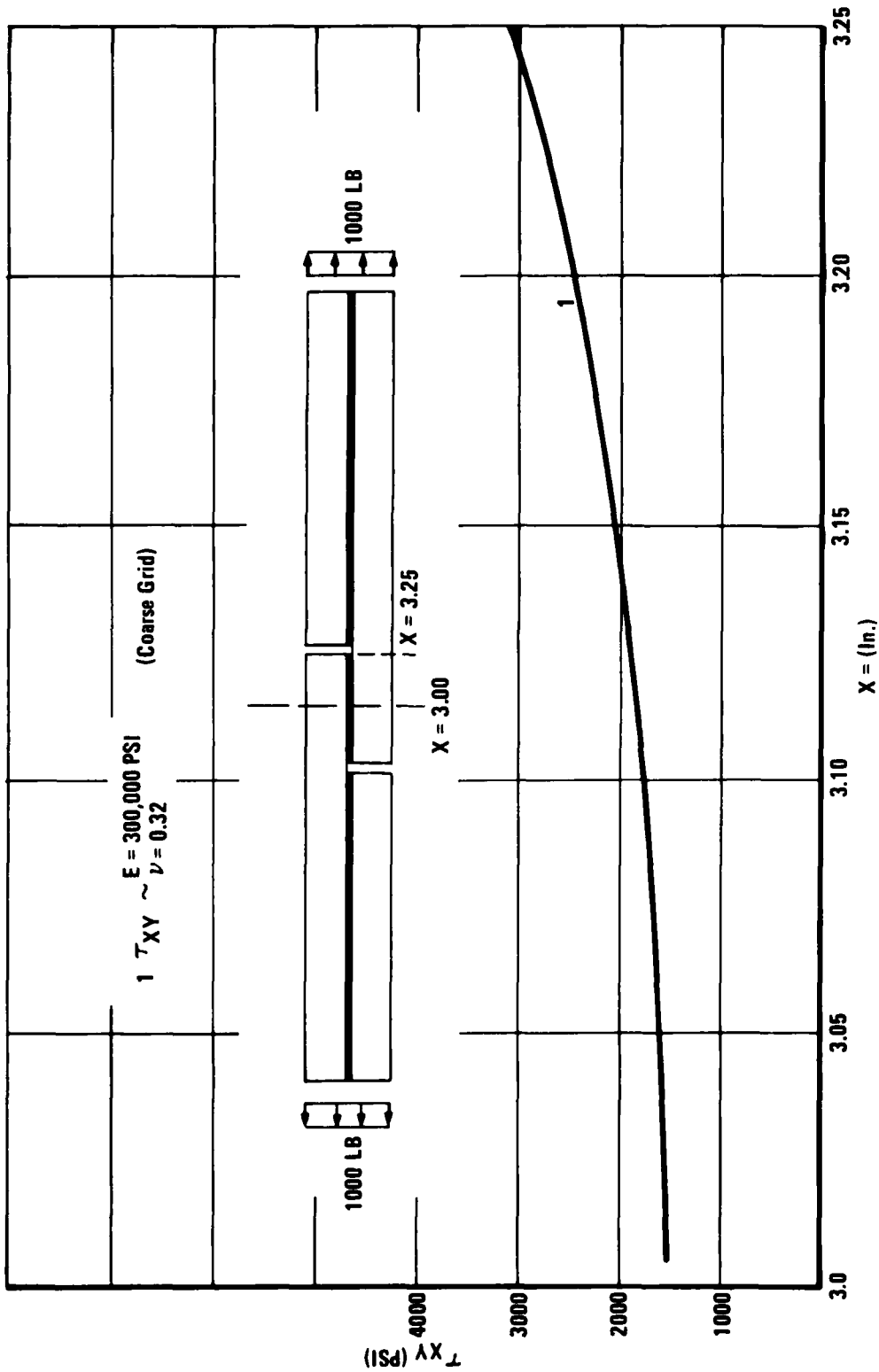


Figure 37 Shear Stress in Center of Adhesive: Poisson's Ratio Sensitivity

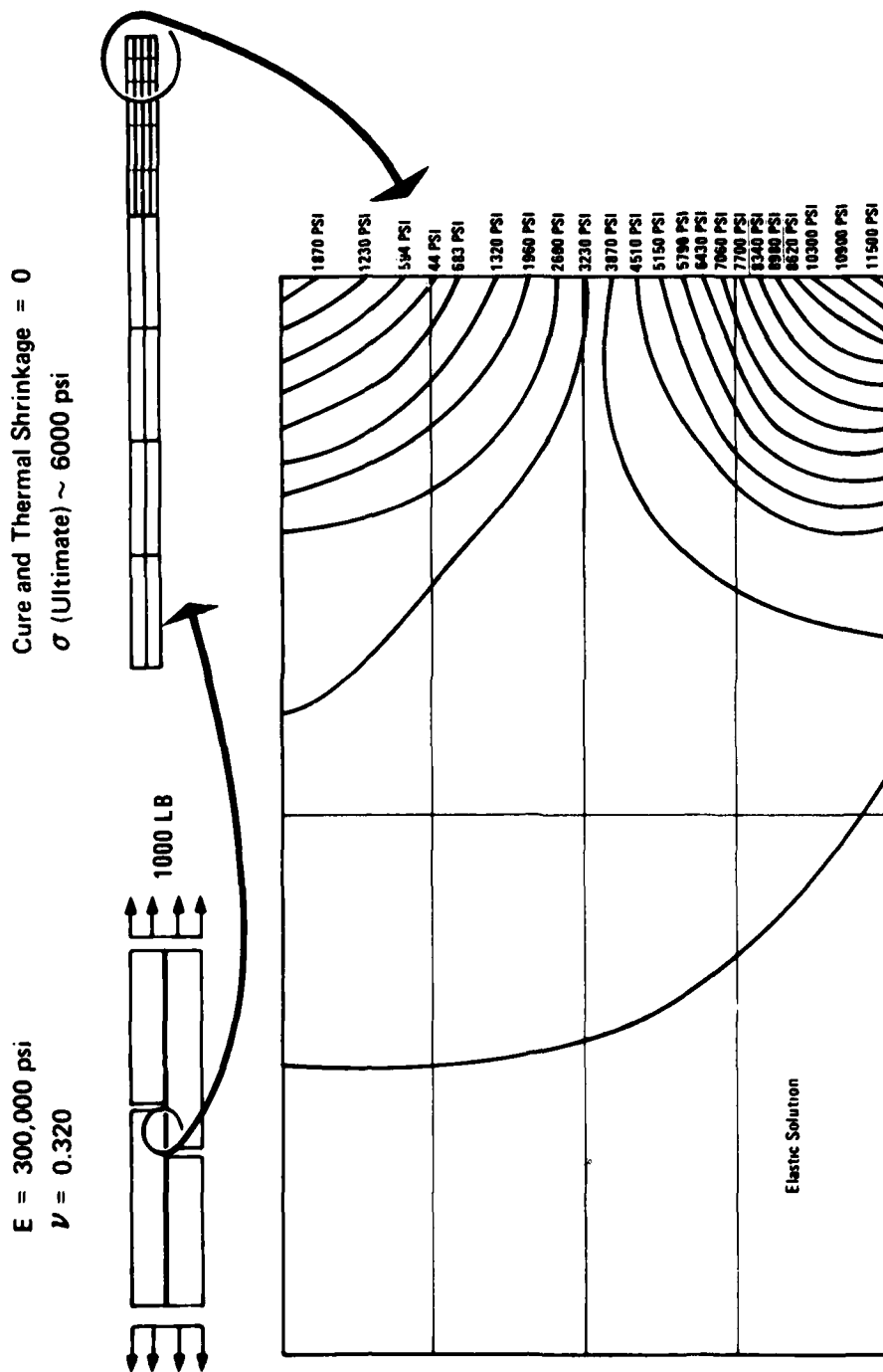


Figure 38 MARC Calculated Peel Stress Distribution in FM-73M Interlayer

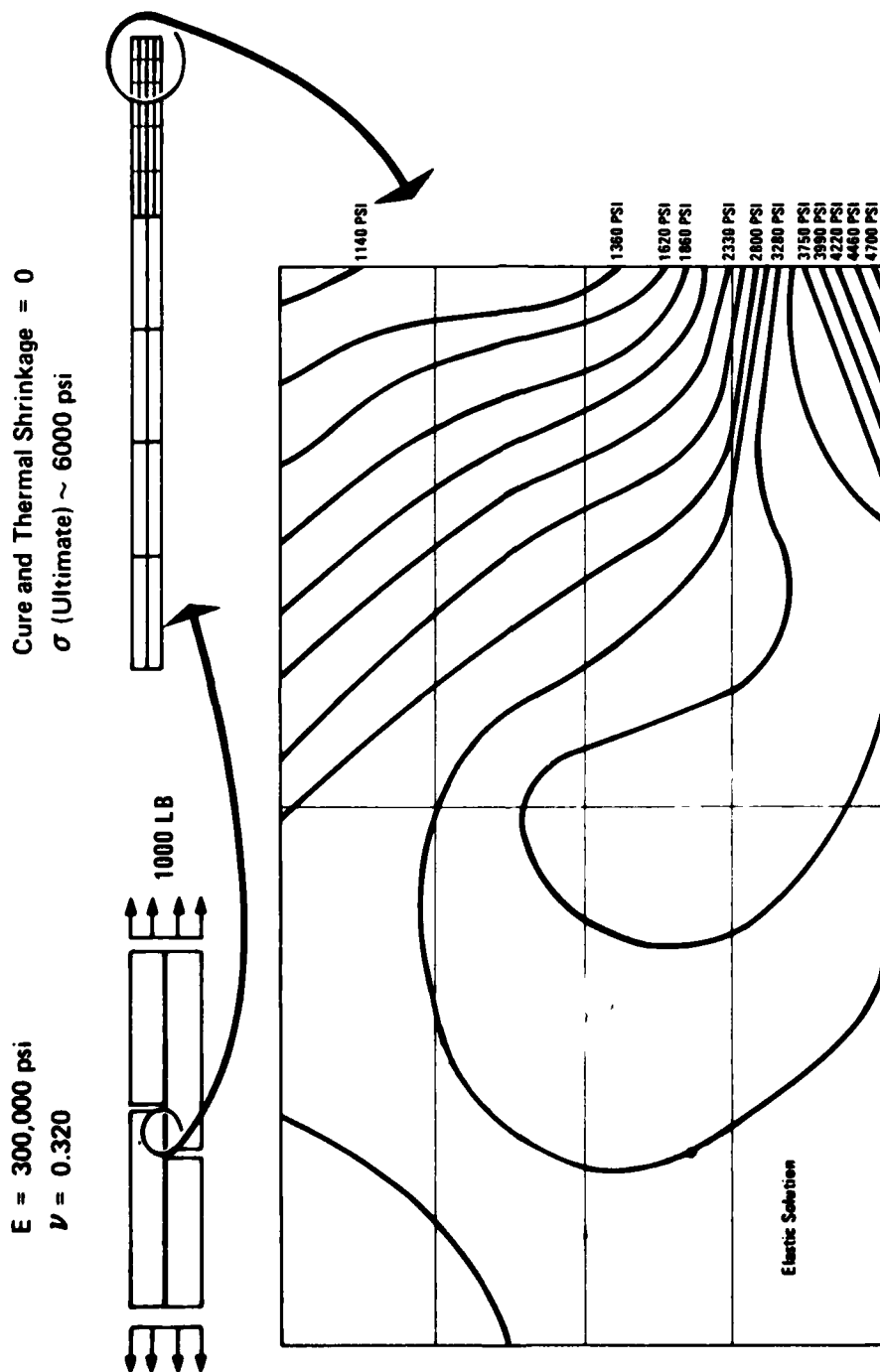


Figure 39 MARC Calculated Shear Stress Distribution in FM-73M Interlayer

reaches an equilibrium moisture concentration very quickly, the data taken at 1, 3, and 7 days was nonequilibrium data; and hence a predicted value of the change in length had to be calculated. This was done in the following manner.

Based on the dimensions of the specimen (1.0"x 0.5"x 35 mils thick) diffusion through the thickness dominates, and it is reasonable to assume a one dimensional diffusion problem. Hence, the modified Fickian equation presented in Reference 18 could be used to calculate the variation of the moisture content through the thickness. There are two parameters in this equation which had to be obtained before it could be applied, viz., the diffusion coefficient and the moisture saturation value. Since the weight gain recorded represented the total change, the one dimensional moisture diffusion equation was integrated through the thickness and the parameters were then determined from the experimental data by a least squares curve fit. The equilibrium saturation value P_e was calculated to be 2.06% and the diffusion coefficient, D , was 6.3×10^{-5} in.²/day. A plot of the fitted curve and experimental data (Fig. 40) shows good agreement.

The calculation of the predicted change in dimensions for the coupons with non-equilibrium moisture concentration was performed by modeling the thickness of the specimen with 10 rectangular finite elements and applying a moisture distribution for 1, 3, and 7 days (calculated with the modified Fickian equation) as a temperature variation through the thickness. Since a value of 1.0 was assumed for the coefficient of expansion, the coefficient of expansion for the non-equilibrium data taken at 1, 3, and 7 days was determined by a simple ratio of the experimental value with the corresponding value of $\Delta l/l$.

The coefficient of expansion based on width and length changes of the FM-73M coupons at various points in time is shown in Figure 41. The average value of the coefficient of expansion is calculated to be .0018 in./in. per 1% increase in weight with a standard deviation of .0016. Note that the coefficient calculated for the non-equilibrium data shows good agreement with the data taken when the coupon is saturated. This supports the validity of the procedure used to determine the coefficient at 1, 3, and 7 days.

The coefficient of expansion of .0018 in/in per 1% increase in weight was input in the MARC program to determine the elastic stresses in the adhesive layer due to moisture absorption. It should be noted that the moisture tends to accelerate the viscoelastic effects of the adhesive in the bonded joint. This effect

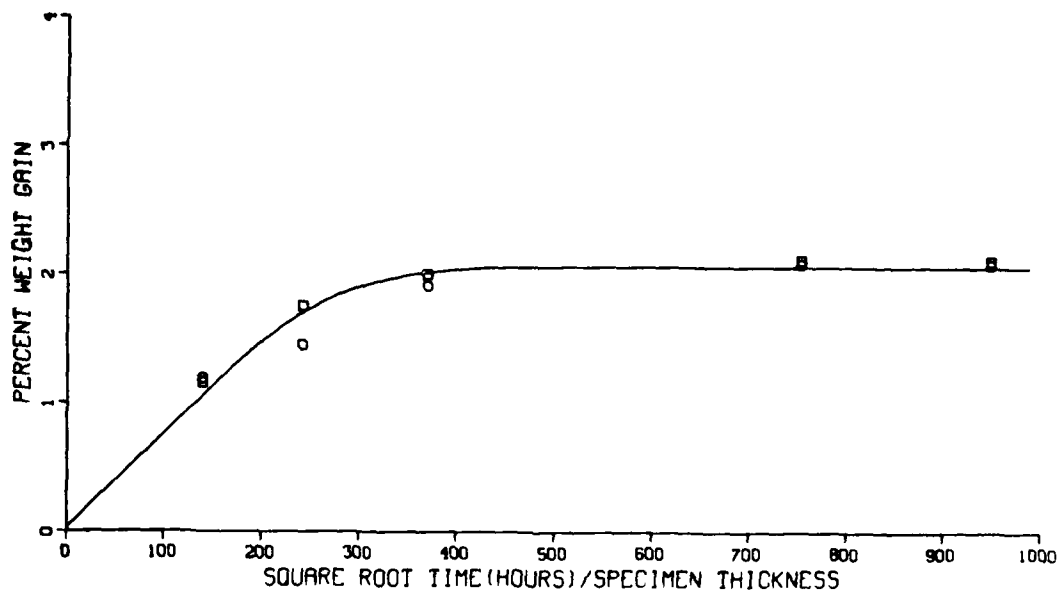


Figure 40 Moisture Uptake by FM-73M at 60°C and 100% RH

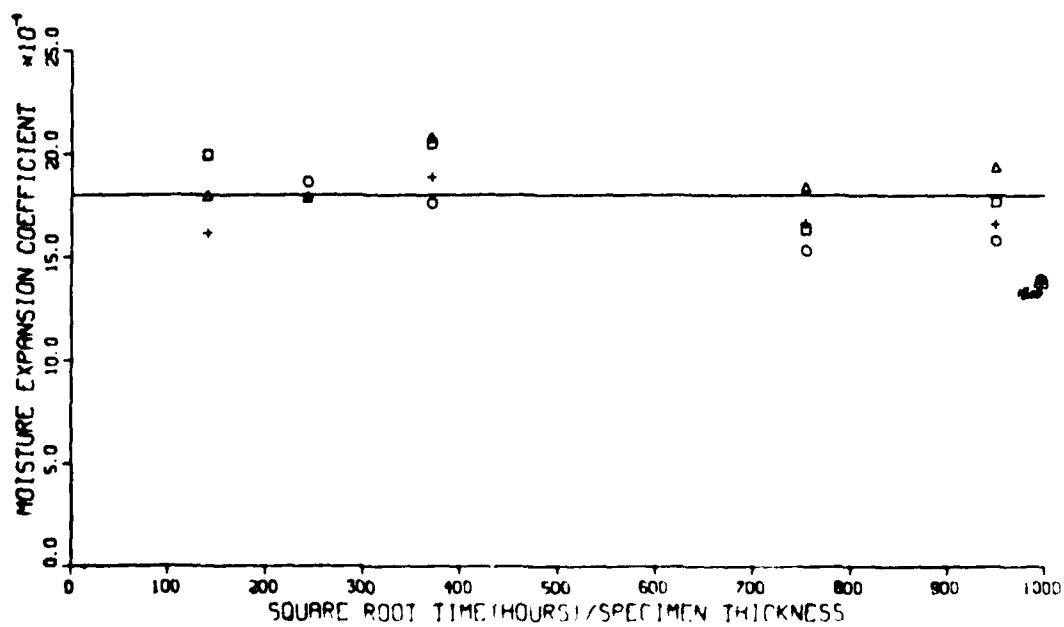


Figure 41 Moisture Expansion Coefficient vs Time for FM-73M

was neglected for the present study since the primary purpose is to gain insight into the effect of moisture infusion on the stresses in the adhesive interlayer. In the particular case of the bonded joint, the sides of the model were taped so that moisture could only be absorbed through the ends of the adhesive overlap. Since the bondline was thin, the moisture variation was assumed to be constant through the thickness but was allowed to vary along the overlap as determined by the modified Fickian equation.

The stress variations corresponding to 3, 7, 29, 100, and 350 days of moisture conditioning were determined in an elastic analysis using the coarse grid model. The shear stress and bond normal stress distribution at 1/10" from the aluminum adherend are shown in Figures 42 and 43, respectively. It must be emphasized that the time variation of the stresses is created by the changing moisture distribution and not by changes in the adhesive properties. The inset plots show that the stresses tend to peak within 3 to 5 days of conditioning. However, the tensile stresses in the center of the overlap region continue to increase until about 30 days when sufficient moisture has diffused to the center of the overlap to relax the stresses. At the end of one year, the adhesive is nearly saturated and the bond normal stresses have dropped to nearly zero. However, the adhesive shear stresses generally remain uniform except near the edge of the overlap where there is a slight peaking. The uniformity of the shear stresses is due to the fact that the change in swelling along the length of the overlap is readily balanced by the aluminum adherends.

In order to examine the stresses more closely, the fine grid model was analyzed with a moisture distribution corresponding to 3 days. Figures 44 and 45 show the variation of the shear and bond normal stresses, respectively, through the adhesive layer. These plots show that the effect of the corner singularity is to create a fairly strong stress gradient at the overlap edge.

4.2.3 Cure Shrinkage

In order to determine the total residual stress distribution in the adhesive joint prior to any loading, the curing process must be analyzed. As the adhesive stiffens, a certain amount of contraction occurs in the adhesive. An additional contraction is created as the model joint is lowered from the cure temperature to the test temperature. The stresses created by this shrinkage

Adhesive Shear Stress Distribution

Moisture Absorption

Elastic Analysis

E Adhesive = 131290 psi

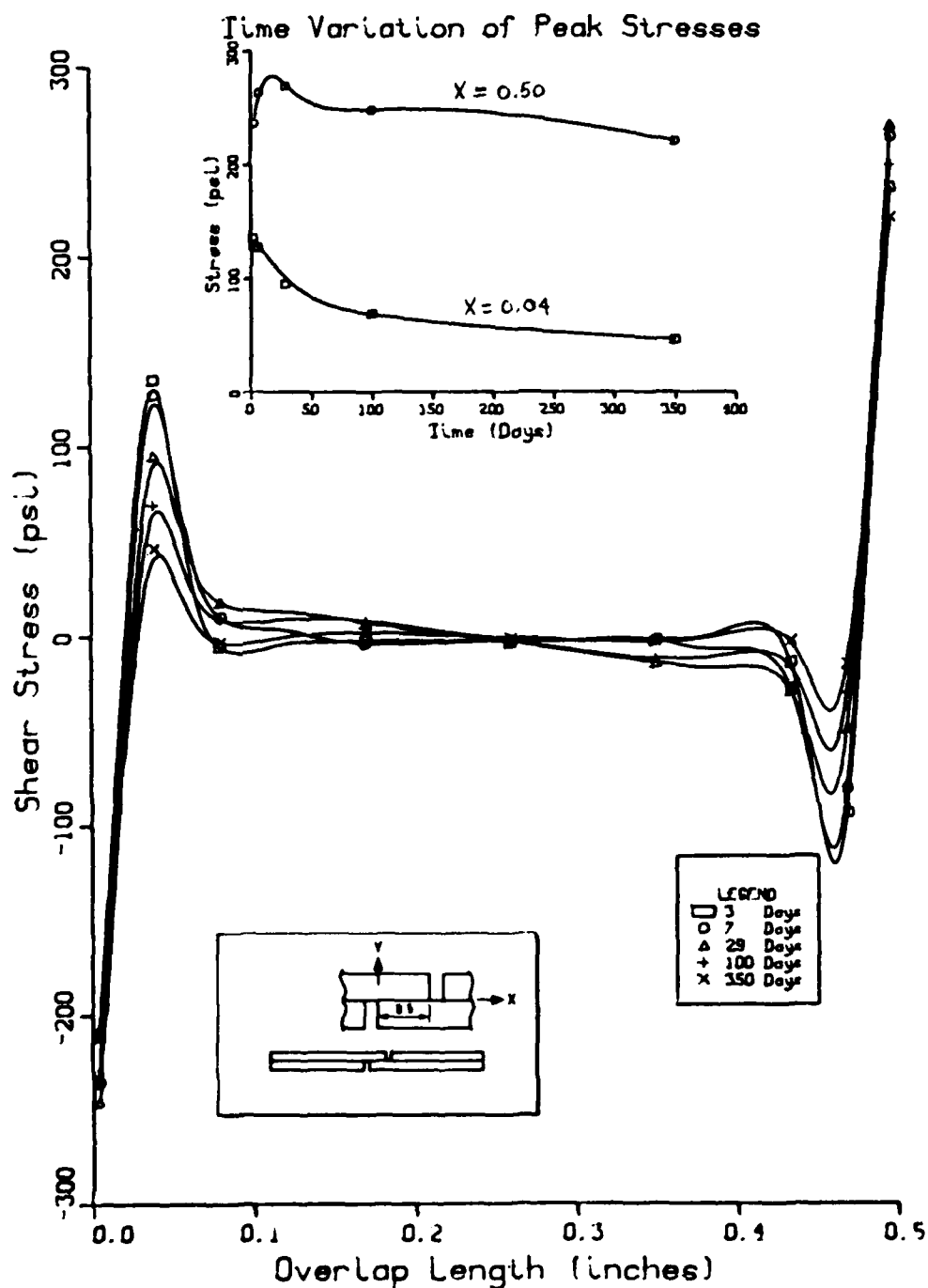


Figure 42 Adhesive Shear Stresses in Adhesive Overlap of Bonded Joint Resulting from Moisture Infusion

Bond Normal Stress Distribution

Moisture Absorption
Elastic Analysis
E Adhesive = 131290 psi

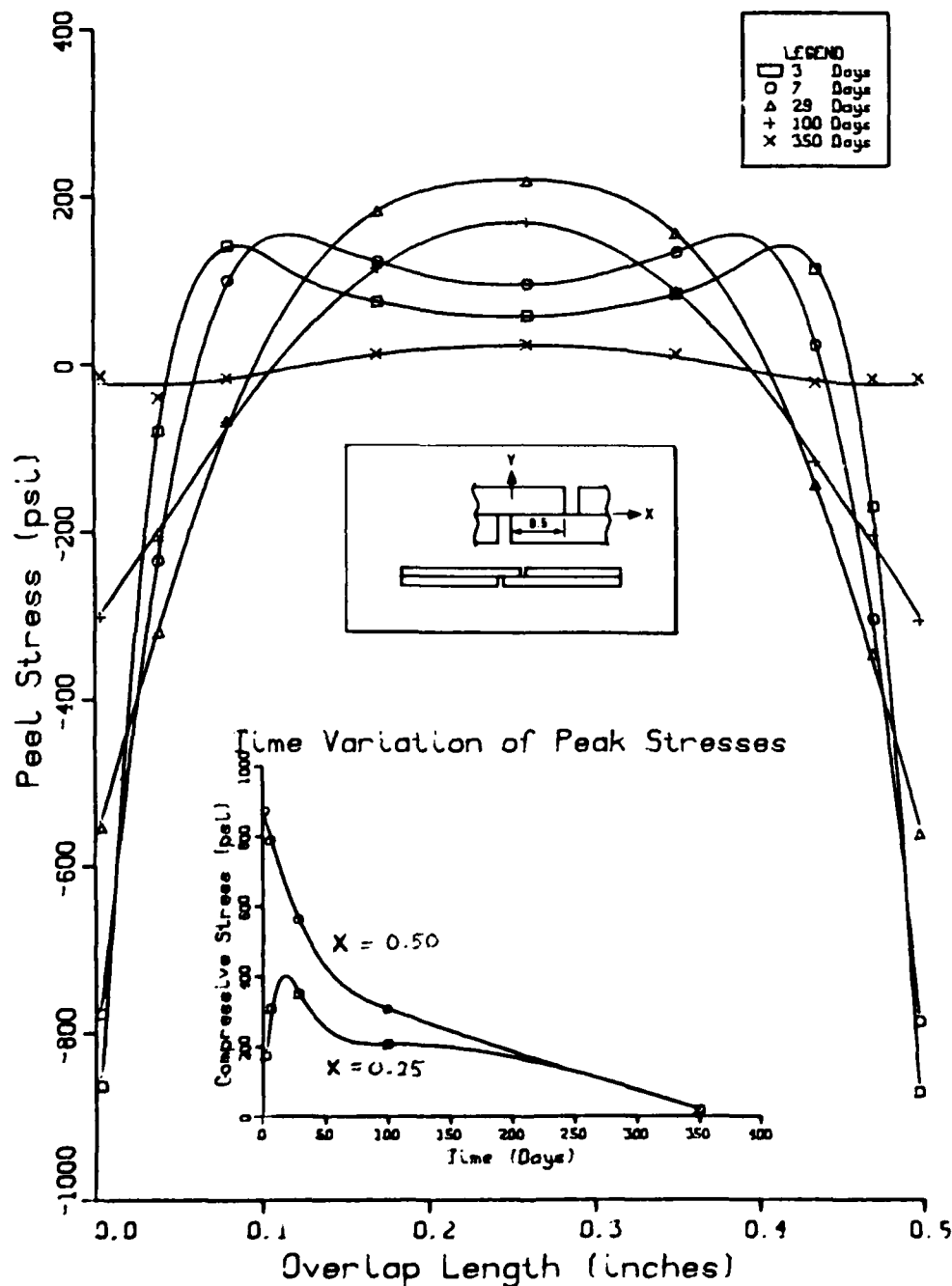


Figure 43 Bond Normal Stresses in Adhesive Overlap of Bonded Joint Resulting From Moisture Infusion

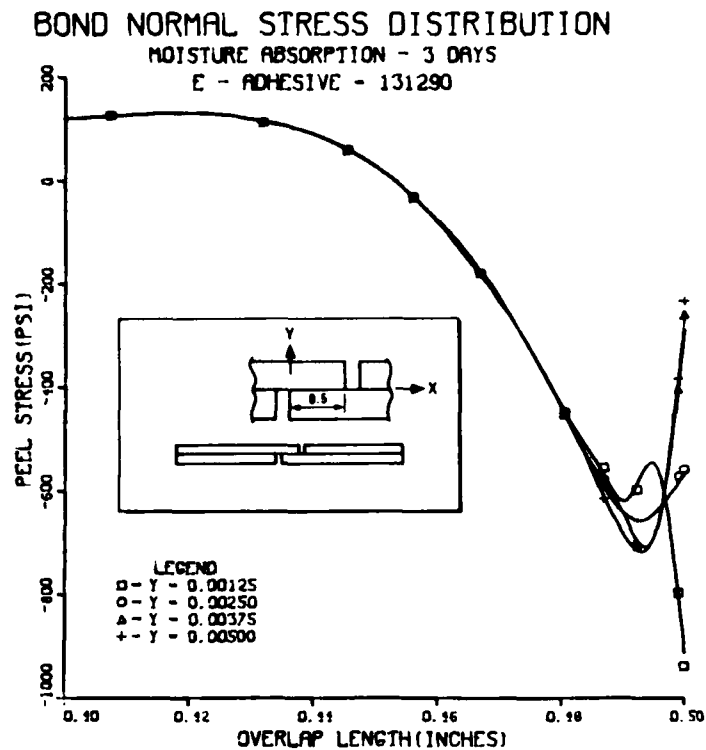


Figure 44 Bond Normal Stresses at Edge of adhesive Overlap Corresponding to 3 Days of Moisture Conditioning

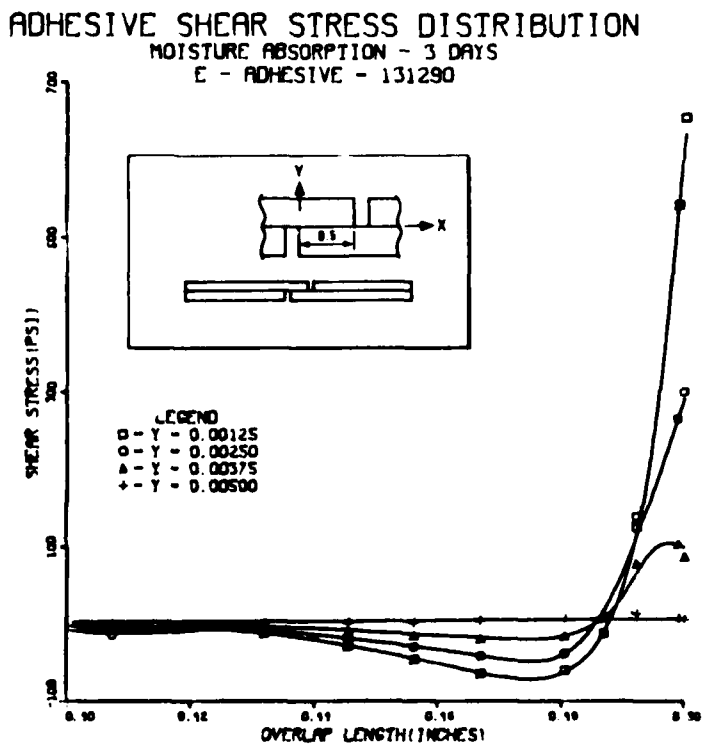


Figure 45 Shear Stress Variation at Edge of Adhesive Overlap Corresponding to 3 Days of Moisture Conditioning

were calculated in an elastic analysis using MARC. Although viscoelastic effects were not considered during this analysis (including temperature dependence of adhesive properties), the analysis does give an idea of the magnitude of the stresses created by the curing process.

In order to calculate the cure shrinkage stresses, the adhesive had to be characterized with regard to the shrinkage created during the curing process. This was accomplished by curing a 3" x 4" specimen and recording the change in length. This change in length divided by the uncured length gives the free strain which results during the curing process. The value which was determined for FM-73M was 0.025 inches/inch.

In addition to the shrinkage created by curing, there is a 0.009 in/in shrinkage created by lowering the specimen from the cure temperature (250°F) to the test temperature (70°F). An expansion coefficient and temperature were input in the MARC analysis so that the total free strain of -0.034 inches/inch was created.

The value of the stresses calculated by the MARC program reach a peak of 6600 psi in the center of the overlap, which is very close to the tensile strength of the FM-73M at room temperature (7000 psi). The stress calculated by MARC is close to the value one would calculate using the elastic relations for plane stress. If a value of E of 131,290 psi is used, the calculated stress is 6565 psi.

The plots of the bond normal and shear stress shown in Figures 46 and 47, respectively, show that there is a significant variation of the stress through the adhesive layer near the edge of the overlap. However, the stresses do approach a constant value at a short distance away from the slot cut.

4.2.4 Combination of Moisture Absorption with Cure Shrinkage Stresses

A consideration of the superposition of the stresses created by cure shrinkage and moisture absorption shows that the effect of the expansion caused by the moisture is relatively small compared to the shrinkage created during curing. For long-time static equilibrium, there are three free strains that must be combined: 1) that due to cure shrinkage, 2) that due to cooling of the test specimen from 250°F to 70°F, and, 3) that due to the expansion of the adhesive caused by moisture. The values of

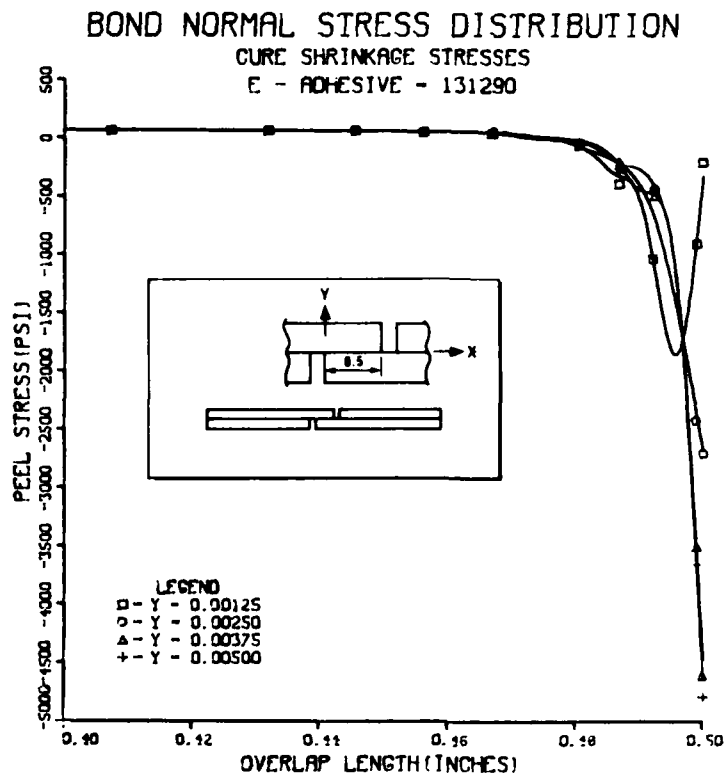


Figure 46 Bond Normal Stress Variation at Edge of Adhesive Overlap Created by Cure Shrinkage

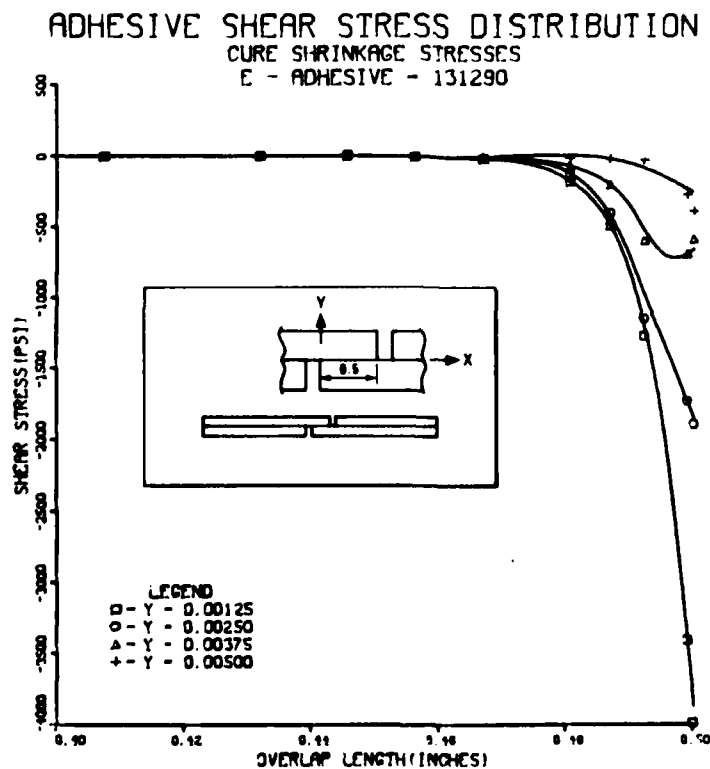


Figure 47 Shear Stress Variation at Edge of Adhesive Overlap Created by Cure Shrinkage

these strains are .025, .009, and -.004, respectively, creating a total free strain of .030 inches/inch. Note that the effect of a saturated adhesive is to reduce the free strain by only 12%. Thus, the most significant residual stresses are created by the curing process.

In addition to long-term static equilibrium, there are transient stresses created by the diffusion of moisture into the adhesive bondline. Figures 48 and 49 show the bond normal and shear stress distribution, respectively, at 1/10 of thickness of the bondline from the adhesive adherend interface. The stresses are shown for the shrinkage created by the curing process and the swelling created by the moisture expansion at one and three days.

It can be seen that neither the bond normal nor shear stresses would be significantly affected by a superposition of cure shrinkage and moisture effects. However, near the edge of the overlap there is a peak in the bond normal stress created by the cure shrinkage which would increase by 50% if superposed with the stresses created by moisture ingress. Similar behavior is shown by the adhesive shear stresses near the edge of the overlap except that the moisture stresses would only cause a slight decrease in the magnitude of the shear stresses. These results indicate that the stresses created by cure shrinkage (as compared to moisture ingress) are of significant importance when considering residual stresses in the bonded joint.

4.2.5 Prediction of Joint Stiffness

An examination of the load deflection response obtained during fatigue cycling of the bonded joint reveals that a gradual decrease in stiffness occurs. This is evidenced by the diminishing slope of the load versus deflection plots. This behavior was initially associated with either a reduction in overlap area created by interfacial cracks (debonding) or an actual change in the material properties which occurred after extended periods of fatigue cycling. In order to determine the sensitivity of the stiffness of

AD-A087 280

GENERAL DYNAMICS CORP FORT WORTH TX FORT WORTH DIV
FATIGUE BEHAVIOR OF ADHESIVELY BONDED JOINTS. VOLUME 1.(U)
APR 80 J ROMANKO, W G KNAUSS

F/G 11/1

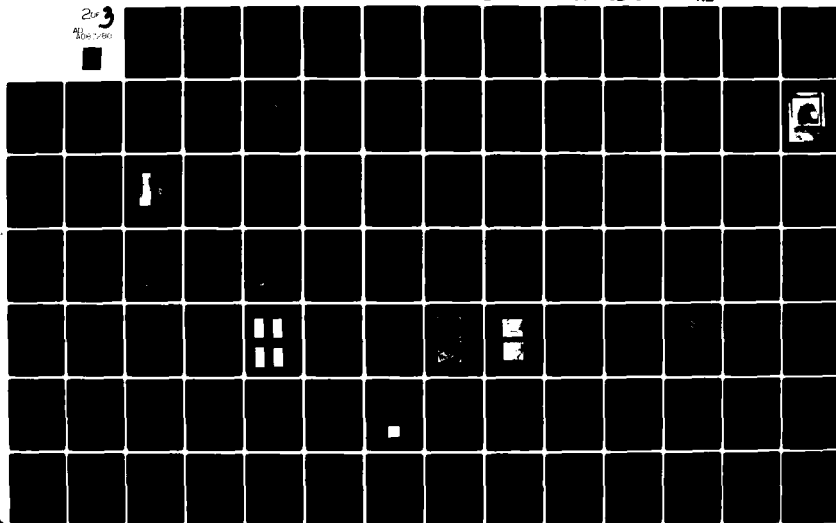
F33615-76-C-5220

UNCLASSIFIED

AFWAL-TR-80-4037-VOL-1

NL

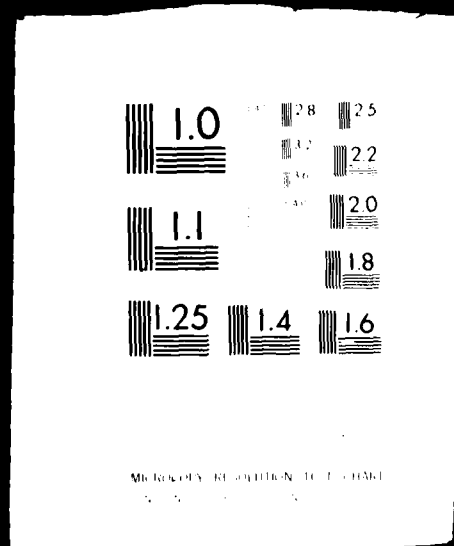
203
11/1/80



55111L

2 OF 3

AD
A087280



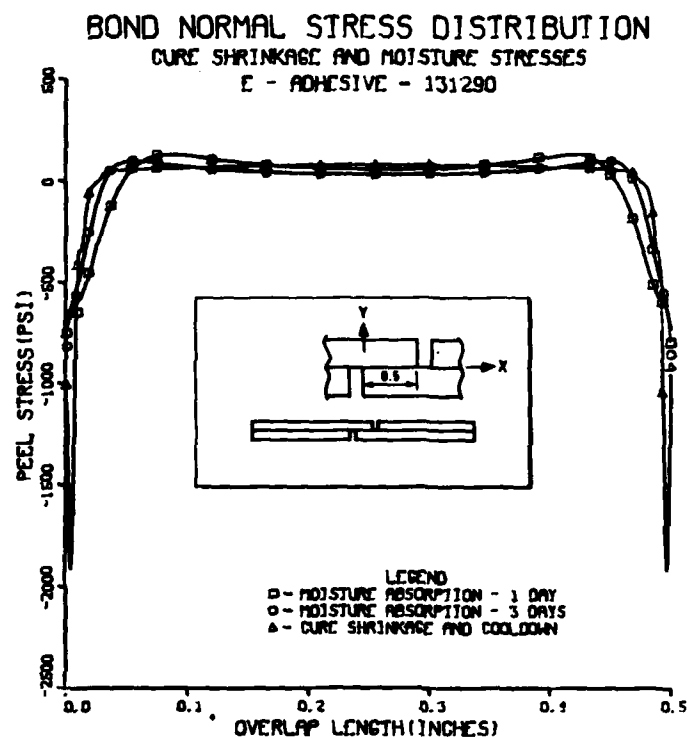


Figure 48 Bond Normal Stresses Corresponding to 1 and 3 Days of Moisture Conditioning and Cure Shrinkage

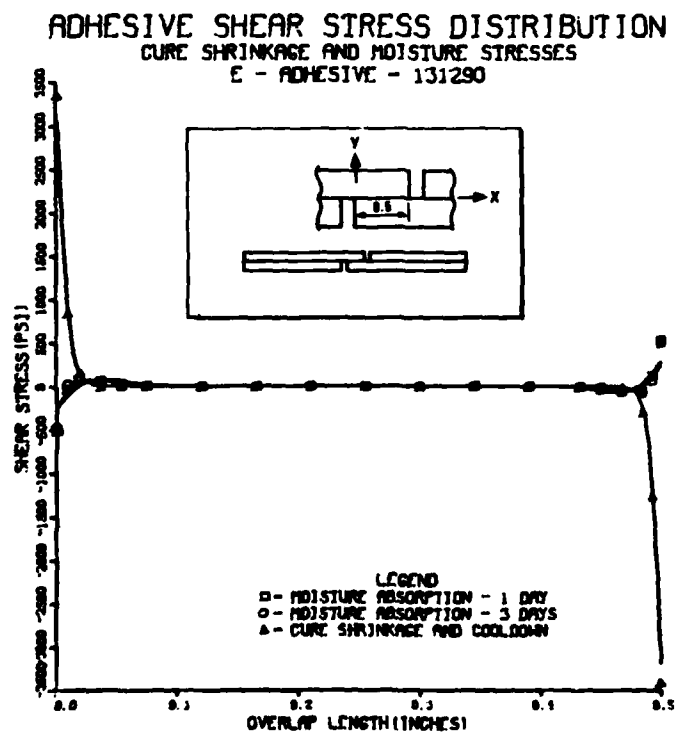


Figure 49 Adhesive Shear Stresses Corresponding to 1 and 3 Days of Moisture Conditioning and Cure Shrinkage

the bonded joint to these two changes, a series of finite element analyses was performed. The results of this study were essential in arriving at the conclusion (discussed in Section 6.5) that the observed loss of stiffness is due to interfacial cracks. The following discussion presents the method used to determine the sensitivity of the joint stiffness to debonds and adhesive modulus variations.

For this study, the fine grid MARC model, which has four layers of linear strain elements representing the adhesive, was selected. A uniform load of 214.3 lbs was applied to the ends of the joint, and interfacial cracks of 0.013, 0.04, 0.10, and 0.16 were selectively added to the model. These cracks or debonds were assumed to initiate at the high stress region in the corner of the slot cut as observed in experiments. Since an antisymmetric math model was used, the analyses actually included two cracks, one at each corner of the adhesive overlap. The load tends to both open and shear the crack (Mode I and II, respectively), and thus no modeling inconsistency was created by the attempted overlapping of grid work.

In addition to cracks of various lengths, three values of the adhesive modulus were considered: 131,290, 112,161, and 105,032 psi. These values were used in various combinations with the previous crack lengths in an elastic analysis. The joint stiffness was calculated for each run by ratioing the load and the change in displacement at the slot cut. This displacement corresponds closely to that measured by the clip compliance gage.

A plot of the calculated joint stiffness versus debond length is shown in Figure 50. The stiffness is found to decrease in a nearly linear fashion up to a length of 0.1" (20% of the overlap). At this point, the stiffness begins to fall off more rapidly. The sensitivity of the model joint to adhesive modulus variations is also seen in Figures 51 & 52. A 20% change in the adhesive modulus results in only a 6% decrease in the stiffness of the bonded joint. This indicates that the stiffness of the bonded joint is not particularly sensitive to adhesive modulus variations because a substantial portion of the clip gage displacement is due to deformations of the aluminum adherends.

Plots of the peel and shear stresses shown in Figures 51 and 52 show that the presence of the crack sharply reduces the high peel stress near the slot cut. This results from the fact that the crack prevents significant load transfer in that region. As expected, the average shear stress increased to compensate for the decreased area of the overlap.

DEBOND EFFECT ON JOINT STIFFNESS FINE GRID MODEL APPLIED LOAD - 214.3 LBS

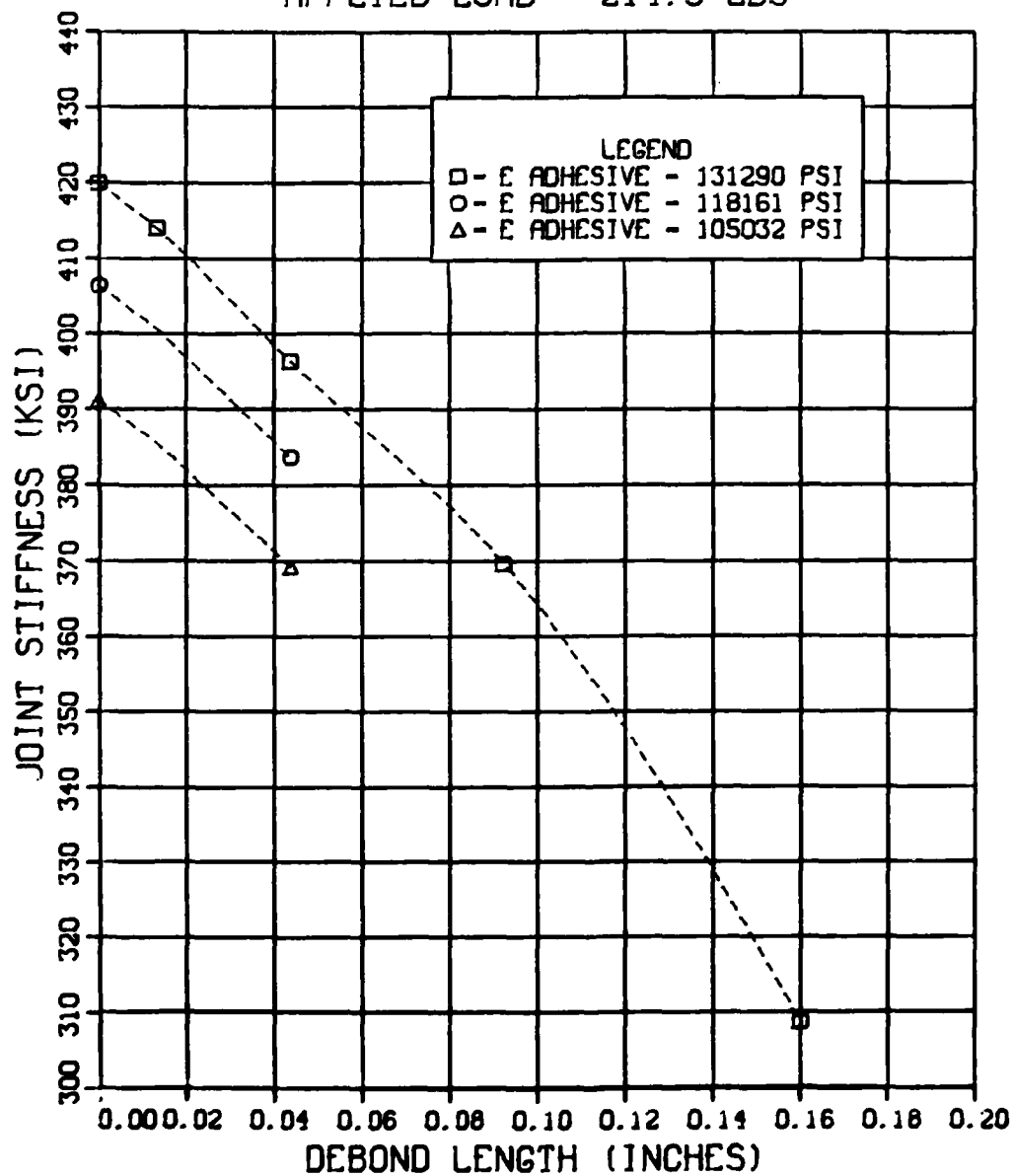


Figure 50 Dependence of Model Joint Stiffness on Interfacial Crack Length and Adhesive Modulus

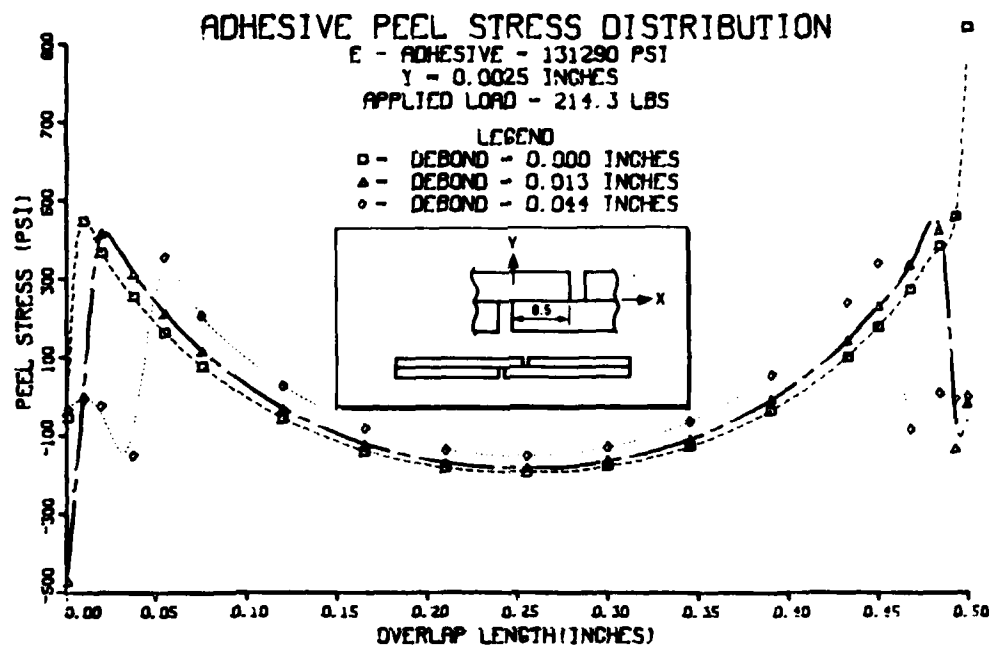


Figure 51 Effect of Interfacial Cracks on Adhesive Peel Stress

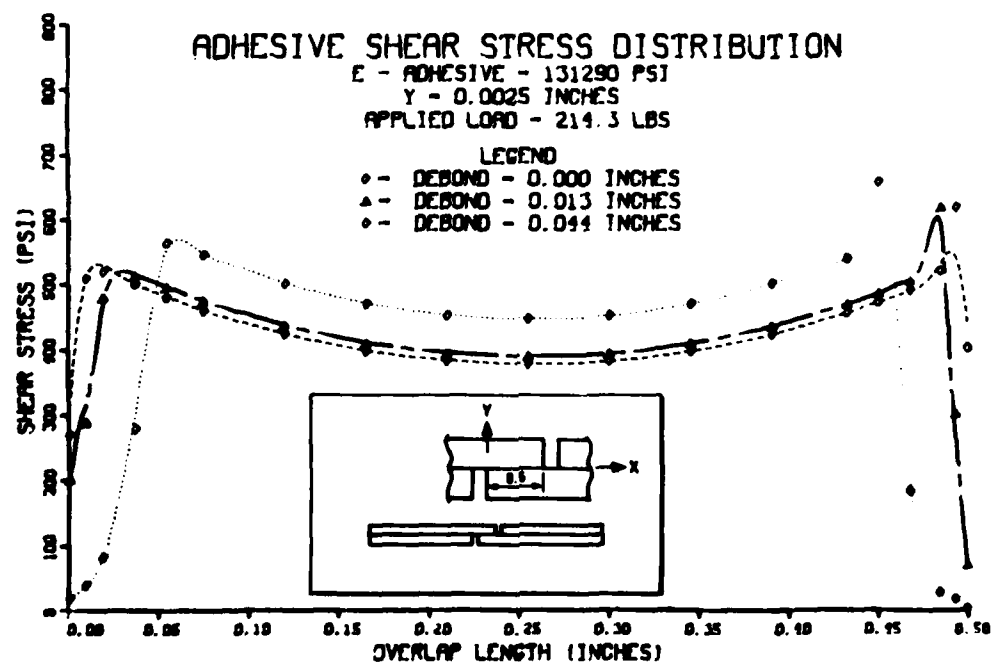


Figure 52 Effect of Interfacial Cracks on Adhesive Shear Stress

The variation of the adhesive modulus as discussed in this section caused only a slight decrease in the peak stresses as the modulus was decreased. Over the majority of the overlap, the stresses did not change more than 1%. The behavior of the peel and shear stresses could be predicted based on the effect of rigid adherends on the stress distribution as discussed in Section 4.3.3.

4.3 Viscoelastic Analysis

Predicting the stress strain distribution in the adhesive layer during cyclic loading of the bonded joint was one of the primary goals of the stress analysis task of this program. Recognizing the complexity of this problem, an attempt was made to acquire an analytical method that would provide the greatest versatility in finite element analysis. The MARC finite element program was selected because of its ability to solve problems that involve large deflections, inelastic behavior, and some viscoelastic analysis. The application of finite element techniques allows realistic stress analysis of the bonded joint since point by point material variations may be introduced into the adhesive layer as occur in the adhesive under influence of a moist environment.

The application of a sophisticated finite element program, such as MARC, requires a substantial amount of time be expended to become familiar with its capabilities and confidence in its use. Hence, many test problems were run before a viscoelastic analysis of the model joint was attempted. The following sections document those results that pertain directly to the MARC viscoelastic analysis of neat specimens and the model joint including: 1) the viscoelastic material characterization of FM-73M, 2) creep compliance and cyclic response of the model joint, 3) effect of rigid versus non-rigid adherends on the stress distribution of the model joint, and 4) effects of material nonlinearities on model joint response.

4.3.1 Viscoelastic Characterization of FM-73M

Examination of the load deflection plots obtained from the fatigue tests shows that an elastic or inelastic analysis would be inappropriate. The behavior of the model joint must be attributed to the viscoelastic properties of the adhesive. Subsequent tests have indicated the likelihood of nonlinear viscoelastic

behavior but no viable constitutive relations have been developed for the adhesive. Thus it was assumed that under low load levels, the adhesive, FM-73M, behaved as a linear viscoelastic material.

The latest release of the MARC program allows the definition of a viscoelastic material model through a Prony series. However, this feature was not available during the Fatigue Behavior Program so a three parameter solid material model had to be adopted. Although a Maxwell element in series with a Voigt element was allowed in the MARC code, both were predicated on the assumption of an incompressible material which is not valid for FM-73M. Program modifications were made to remove the incompressibility from the Voigt element but the Maxwell element could not be modified. Thus the three parameter material model was used for the viscoelastic analysis.

To define the three parameters in the viscoelastic material model, it was necessary to relate the physical adhesive material response to that predicted by the material model. This was accomplished by making a least squares fit of experimental compliance data to the analytical solution of the differential equation which describes the material model.

As a check on the material model obtained in this manner, FM-73M adhesive was characterized for the dry condition at 72°C. This characterization was compared to information on the shear creep compliance of the neat-neat adhesive at 72°C obtained from recent experiments conducted at the California Institute of Technology (Ref. 31). By multiplying the shear creep data times the factor $1/2(1 + \nu)$, the equivalent tensile creep compliance, $D(t)$, was calculated. This data is shown plotted in Figures 53 & 54 along with the data collected in the Fatigue Behavior program. The GALCIT data is stiffer elastically and shows less time dependence than the corresponding Fatigue Behavior program data. Although the GALCIT data was obtained from tests on an adhesive without a scrim layer, it was not expected that this would result in a significant difference from the data obtained on the scrimmed adhesive in the Fatigue Behavior program.

Since a considerable discrepancy existed between the two sets of data, it was decided to characterize the adhesive based on the response of the neat specimen to cyclic loading. Four different coupons were cycled and a least squares fit of the experimental data was made to the analytical solution. Plots of a portion of this data and the corresponding analytical predictions are shown in Figures 55, 56, & 57. The predicted response

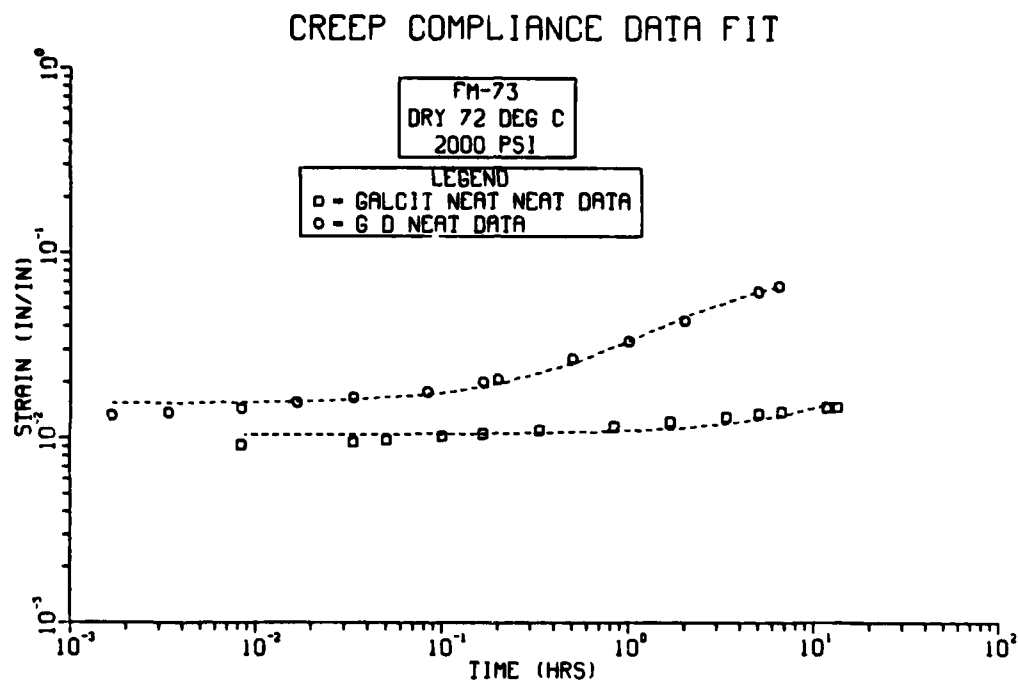


Figure 53 FM-73M Tensile Creep Compliance Data Fit

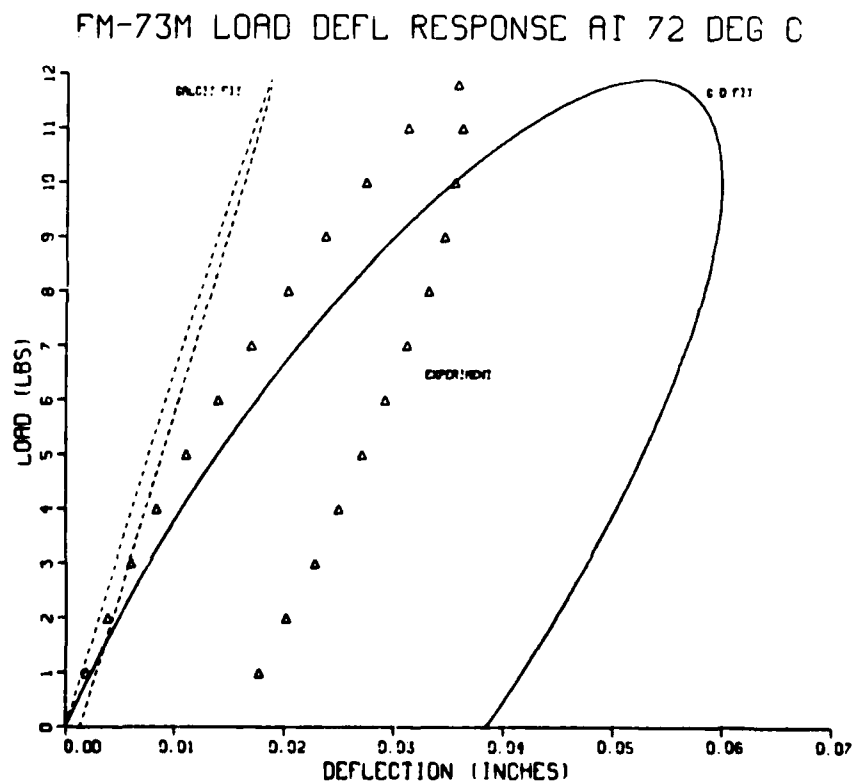


Figure 54 Comparison of Analytical and Experimental FM-73M Neat Load-Deflection Responses

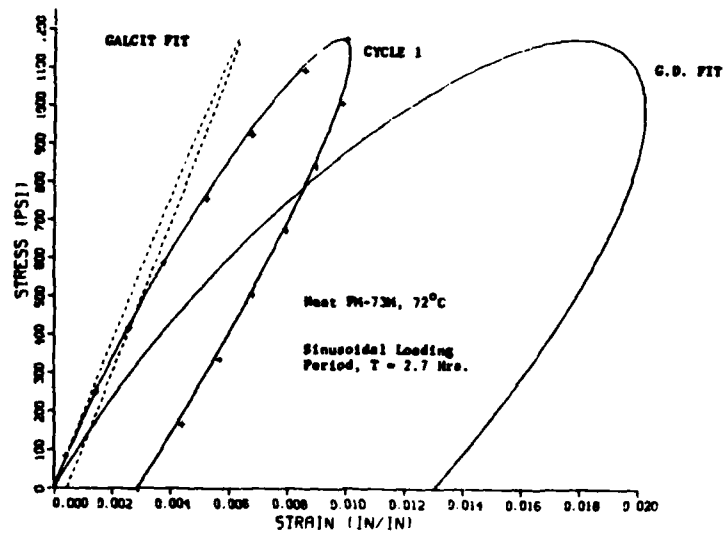


Figure 55 Comparison of Analytical and Experimental Load-Deflection Responses (Cycle 1)

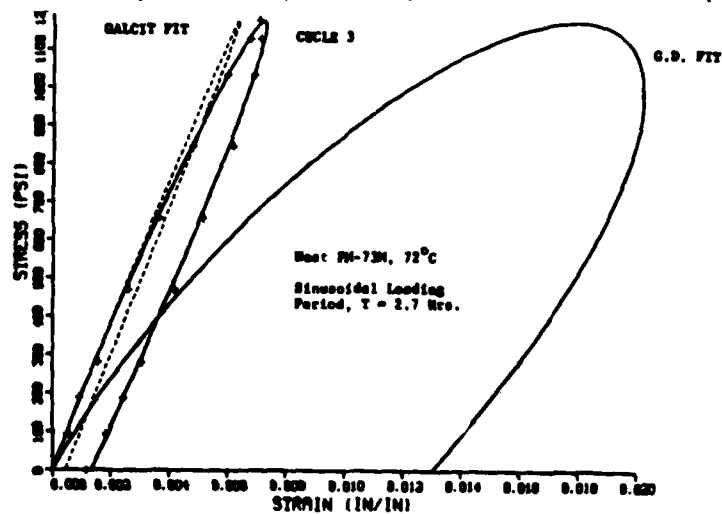


Figure 57 Comparison of Analytical and Experimental Load-Deflection Responses (Cycle 3)

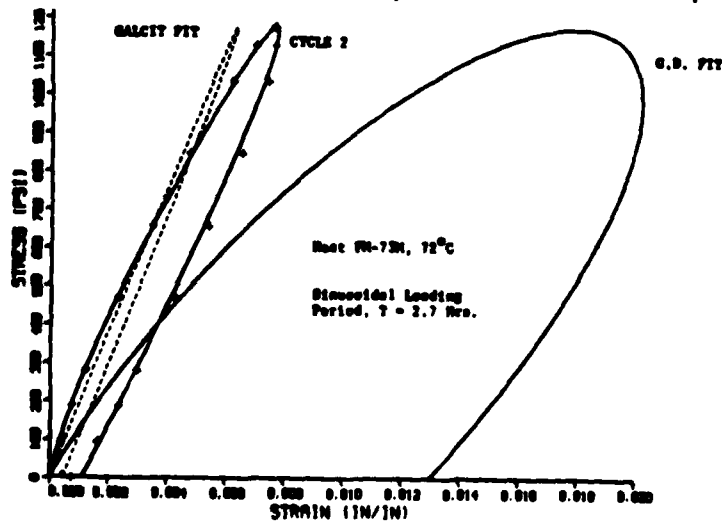


Figure 58 Comparison of Analytical and Experimental Load-Deflection Responses (Cycle 2)

based on the analytical solution for the GALCIT and Fatigue Behavior program creep data are also shown.

Significant differences can be seen in the response of the coupons between the first (Fig. 55) and second (Fig. 56) cycles. The adhesive is stiffer and shows less time dependence during the second cycle. This apparent change in the mechanical properties of the adhesive is present even after the coupons were allowed to relax overnight and then cycled again. (Fig. 57). This behavior is attributed to a "shakedown" phenomenon caused by a residual stress state created during the curing of the adhesive. (See also Section 5.4.2). Thus, mechanical properties obtained from tests of the virgin adhesive will not represent the properties of the adhesive material as required for a viscoelastic analysis of the model joint. The properties determined from creep compliance tests and sinusoidal testing on virgin material will only be valid to the extent that the residual stresses on the two specimens are the same. Even so, the "shakedown" effect requires that a new model be obtained for subsequent cycles.

The analytical creep compliance response based on the three parameters derived from the cyclic test specimen is shown in Figures 58, 59, and 60. The plots also show creep compliance data taken in the Fatigue Behavior program and supplemental data obtained from the Cal Tech program. As expected from a review of the sinusoidal load deflection diagrams, the creep compliance of the model before "shakedown" falls between the creep compliance data fits. However, after "shakedown" (1st cycle after overnight relaxation), the adhesive creep compliance was found to closely resemble that generated in the Cal Tech program. In fact, the creep compliance predicted from the cyclic test data provides a better fit of the Cal Tech program data than the least squares fit of the data.

This is the result of the application of the very limited three parameter solid viscoelastic model to data which spans more than two decades in time. Since all of the data was weighted equally in the least squares fit, some accuracy was given up in the early time decades to fit the data at later times. Hence, the least squares objective function effectively forces the compliance at earlier times to remain nearly constant. However, it is in the early time decades that a significant portion of the creep occurs and thus the analytical prediction tends to be too time independent. This has been confirmed by fitting the GALCIT data over a time period of only two decades resulting in a significant increase in the time dependence and a predicted stress strain plot under a cyclic load closely resembling the data generated by the Fatigue Behavior program.

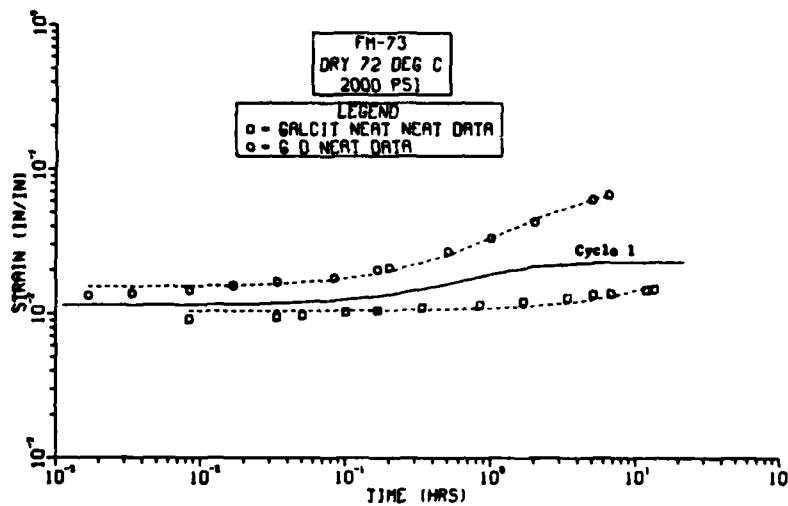


Figure 58 Comparison of FM-73M Analytical and Experimental Creep Compliance (Cycle 1)

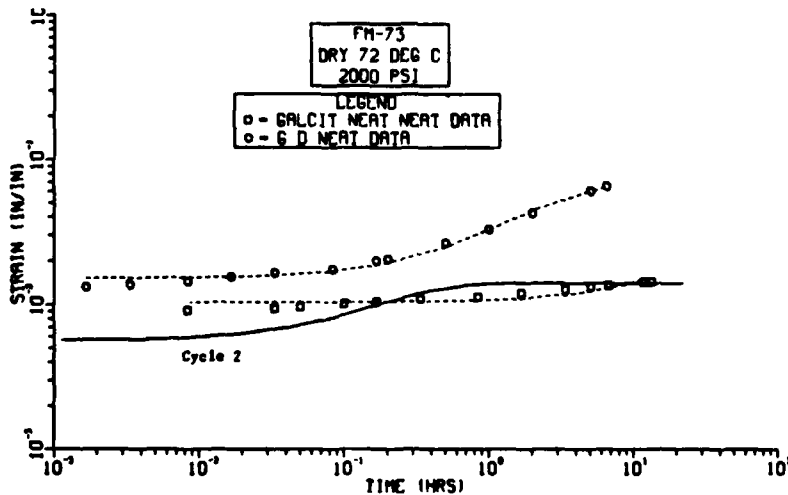


Figure 59 Comparison of FM-73M Analytical and Experimental Creep Compliance (Cycle 2)

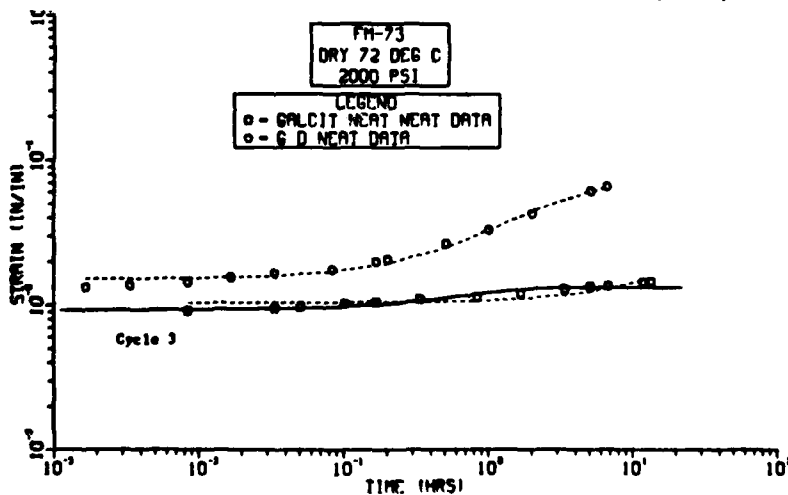


Figure 60 Comparison of FM-73M Analytical and Experimental Creep Compliance (Cycle 3)

In addition to characterizing FM-73M through tests of neat specimens, it was also characterized by backing the parameters out of test data obtained during cyclic testing of the model joint. The material properties required to predict the response of two bonded joints were determined by using the coarse grid MARC finite element model in a viscoelastic analysis. The thickness of the bondline in the finite element model was adjusted so that it matched that of the corresponding test article and a sinusoidal load of proper magnitude was applied. The three parameters in the material model were then varied until a good agreement was obtained between the experimental data and the predicted response.

Plots of the experimental data and predicted response is shown in Figures 61 and 62. Both joints show good agreement between the experimental and predicted response. However, 52A11 seems to be too soft elastically. If the parameters determined from the bonded joints are used to predict the tensile creep compliance of FM-73M, it is found to closely match the experimental data for FM-73M dry at 72°C (Fig. 63). This fact lends support to the feeling that the bulk properties of the adhesive do not change when used in the model joint.

4.3.2 Viscoelastic Analysis of Model Joint

In anticipation of a viscoelastic analysis of the bonded joint, a study was performed to determine how sensitive the stresses in the adhesive interlayer are to variations in Poisson's ratio, ν . This was considered necessary since the formulation of the viscoelastic problem could be simplified if Poisson's ratio was assumed to be constant. Also, if the elastic stress distribution was not very sensitive to moderate variations of Poisson's ratio, an assumed constant value could be used even if some time variation were present.

Elastic solutions were performed using the coarse grid model (one layer of elements representing the adhesive) while the value of Poisson's ratio was varied between 0.29 and 0.35. A plot of the peel stress and shear stress at the center of the adhesive is shown in Figures 36 and 37, respectively. The shear stresses show no observable variation and the variation in peel stresses is, at most, 6%.

EXPERIMENTAL RESPONSE VS MARC PREDICTED

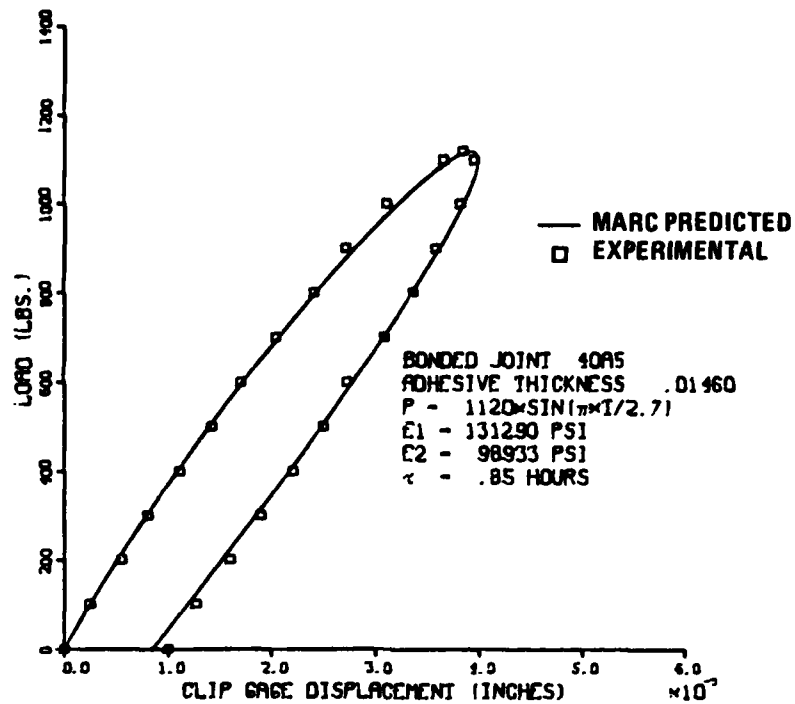


Figure 61 Comparison of Experimental and Predicted Resonse of Bonded Joint 40A5

EXPERIMENTAL RESPONSE VS MARC PREDICTED

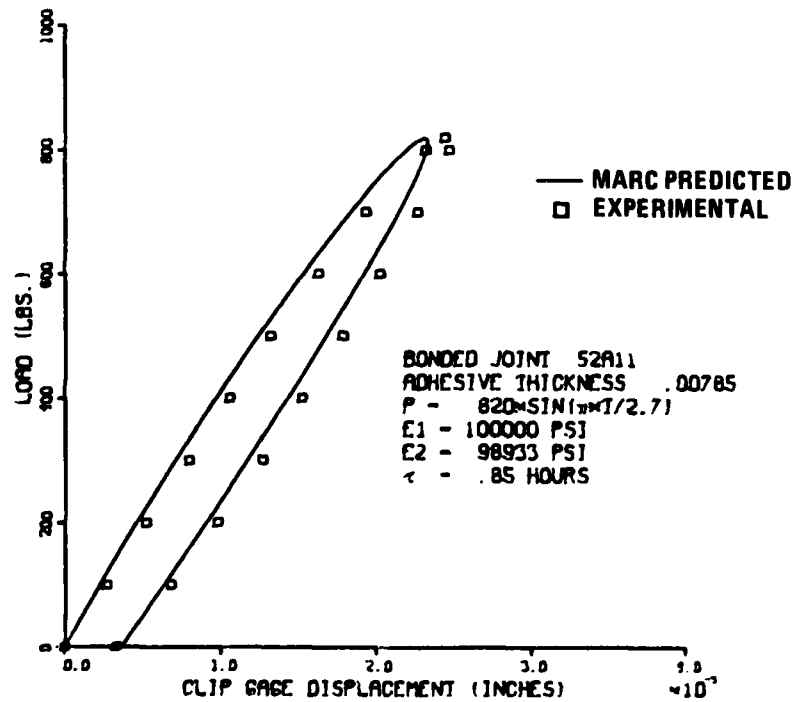


Figure 62 Comparison of Experimental and Predicted Response of Bonded Joint 52A11

CREEP COMPLIANCE DATA FIT

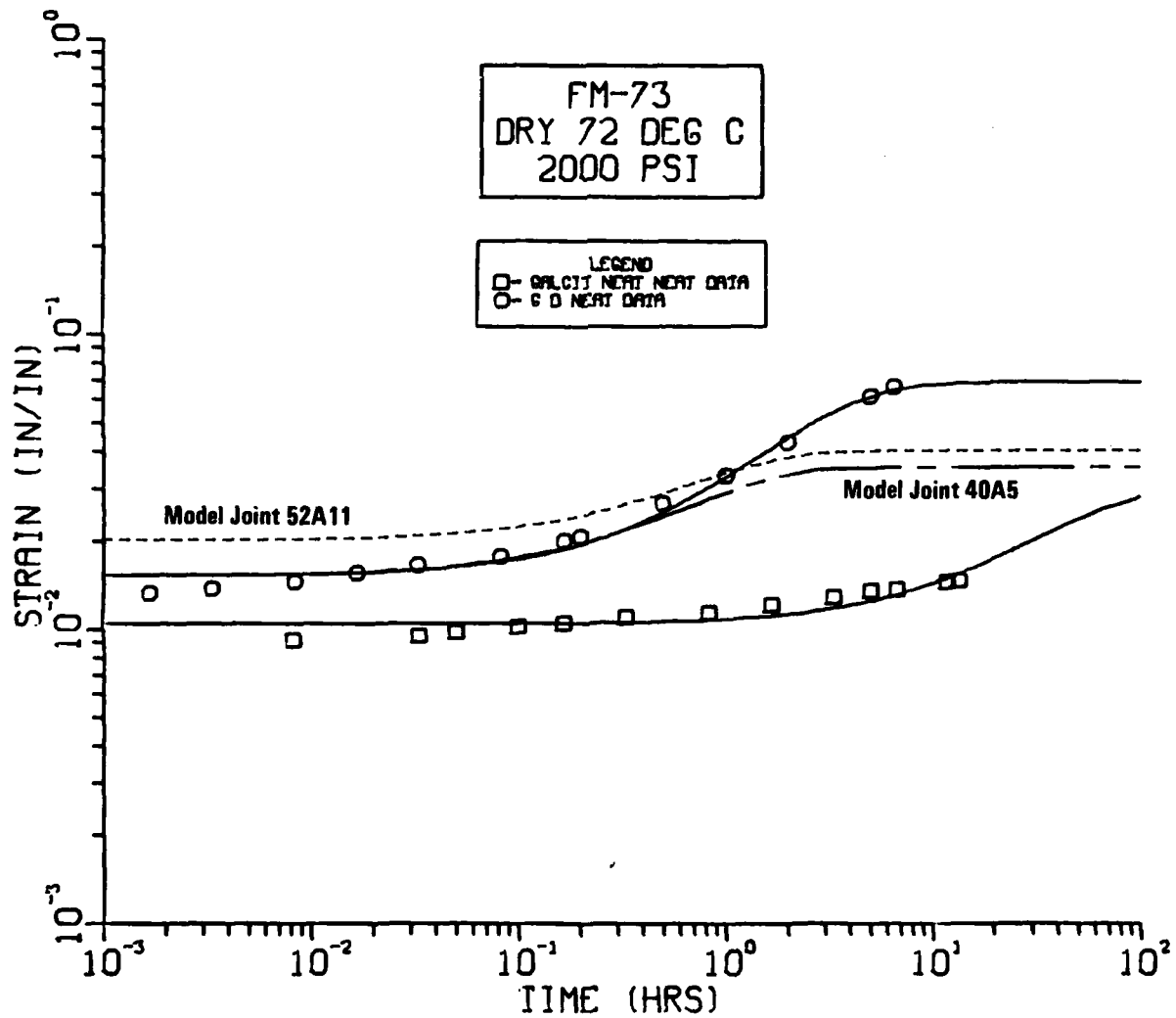


Figure 63 Comparison of Experimental Creep Compliance Data and Predicted Creep Compliance Based on Model Joint Data

In order to more accurately assess the impact of variations of Poisson's ratio on the stress distribution, the fine grid model was analyzed with $\nu = 0.24$ and $\nu = 0.32$. The peel and shear stress contour plots were superposed for these two analyses and are shown in Figures 64 and 65, respectively. Minor changes in the stresses are present as would be expected from altering the material properties, but the basic trend in stress distribution remains intact. This fact was sufficient to allow the assumption of a constant Poisson's ratio for use in the formulation of the viscoelastic analysis.

Since comparisons of the elastic stress distribution observed in the fine grid and coarse grid models showed excellent agreement, the latter was selected for the viscoelastic analysis. The viscoelastic properties of the adhesive interlayer, represented by a single layer of elements, were defined using the standard 3-parameter solid material model as discussed in Section 4.3.1. The properties selected were similar to FM-73M dry at 72°C.

The most important effect observed in the viscoelastic analysis of the model joint was the redistribution of stresses which results from the fact that the adherends are not rigid. Under cyclic loading with a period of 2.7 hours, the MARC results showed that the adhesive stresses were relaxing faster than the stresses caused by the applied load are increasing (Figs. 66 and 67). However, near the corner, this effect is reversed. The stress gradient is high in that region and the stress induced from the increase in the applied load exceeds the stress decrease caused by relaxation that occurs. This results in a net increase in stress. After unloading, the MARC program predicts a residual stress state exists in which the peel stress shows compression at the slot cuts and tension in between. The shear stresses show a similar reversal of sign at the slot cuts (Fig. 67).

Similar results were obtained when the creep compliance of the bonded joint was predicted. Plots of the adhesive bond normal and shear stresses are shown in Figures 68 and 69, respectively. The shear stresses in the ends of the overlap region and all the peel stresses relax with time resulting in a stress redistribution.

Attempts to compare the experimental creep compliance of the bonded joint with the predicted response was complicated by the fact that the model joints tested had bondlines of varying thicknesses and the same loads were not used on all of the joints. Thus, two assumptions were made: the clip gage displacement is proportional to, 1) the adhesive thickness and, 2) the applied load. These two assumptions are based on the response of a model joint

$E = 300,000 \text{ psi}$

Cure and Thermal Shrinkage = 0
 σ (Ultimate) ~ 6000 psi

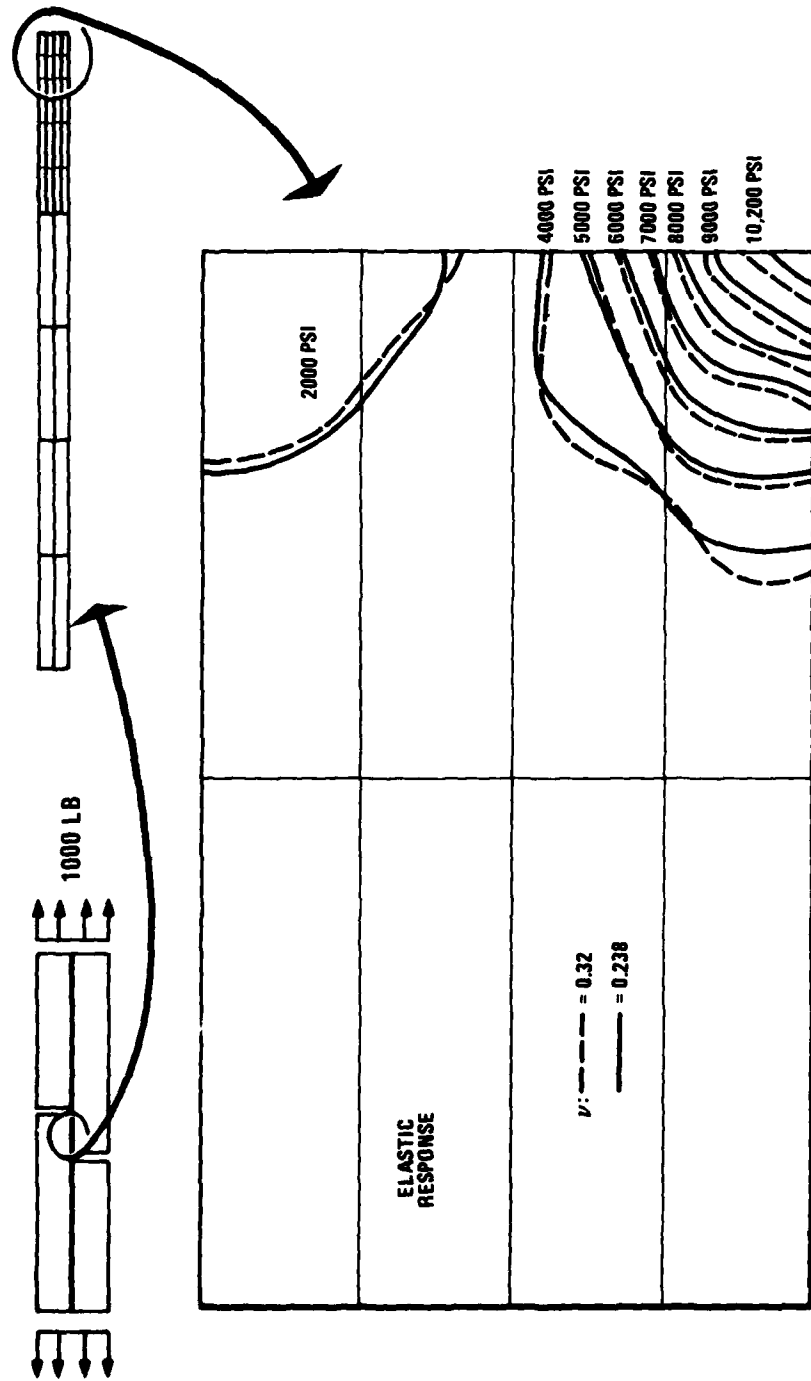


Figure 64 Poisson's Ratio Sensitivity: Peel Stress Contours

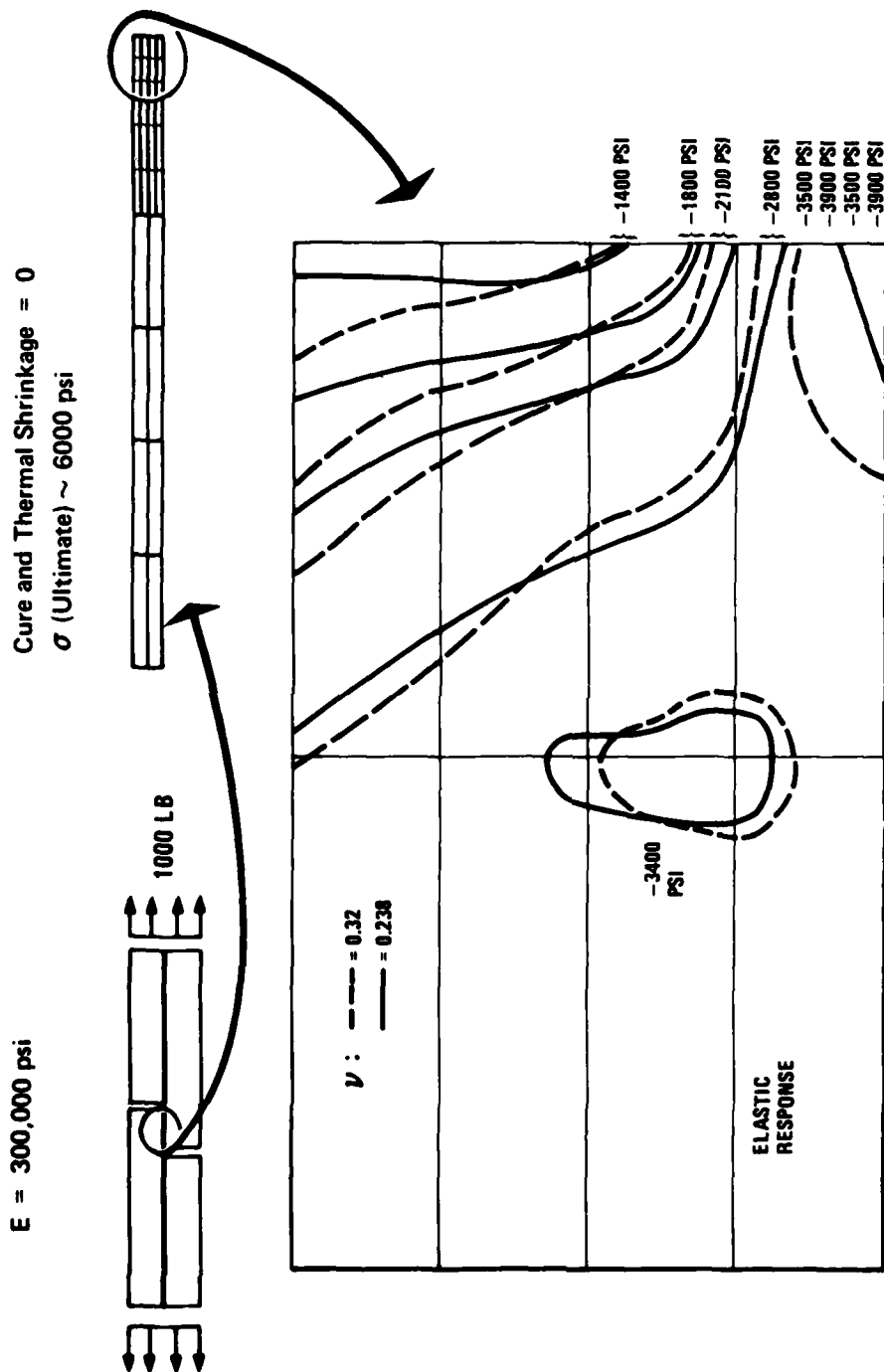


Figure 65 Poisson's Ratio Sensitivity: Shear Stress Contours

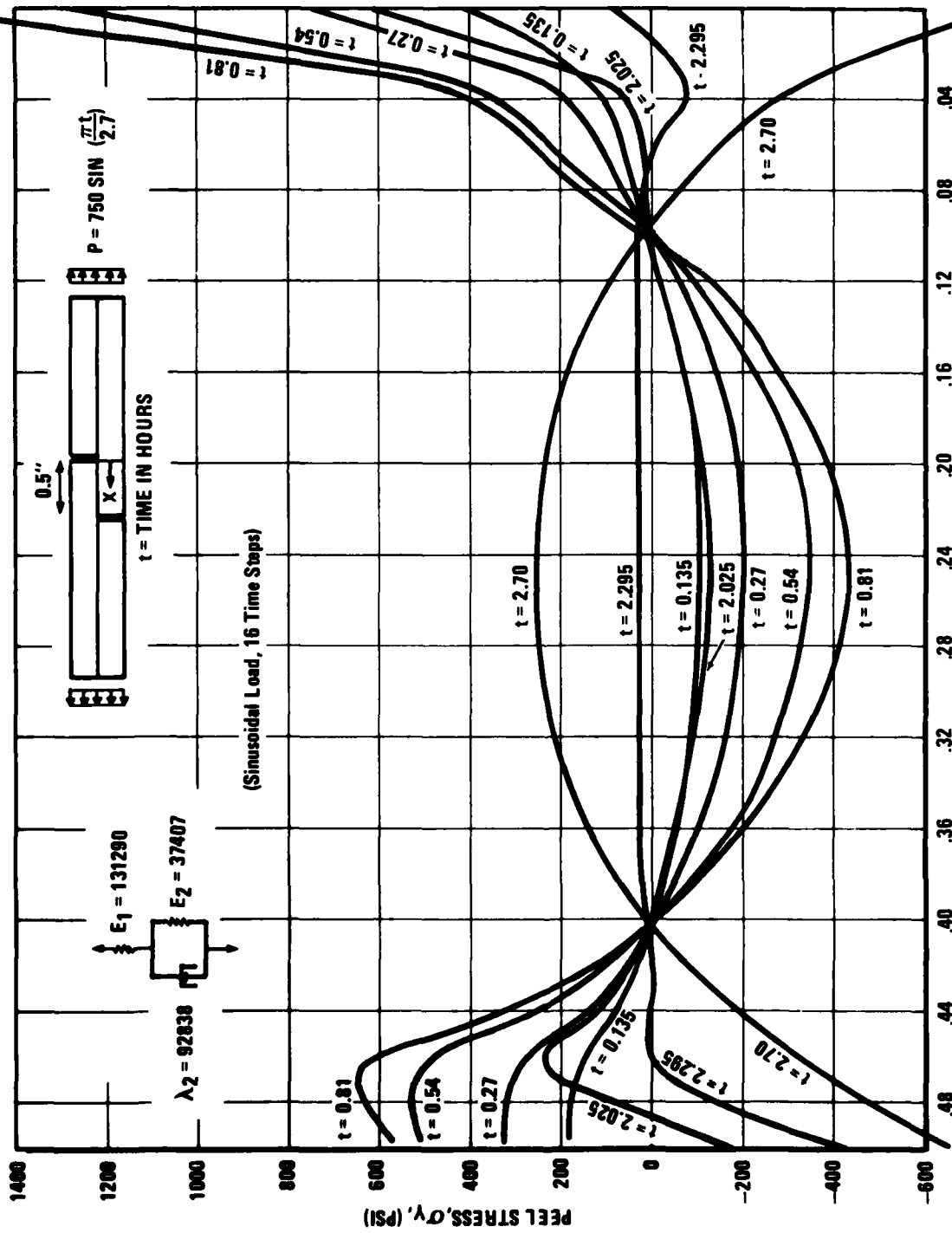


Figure 66 Peel Stress Distributions Along Adhesive-Adherend Interface (Sinusoidal Load)

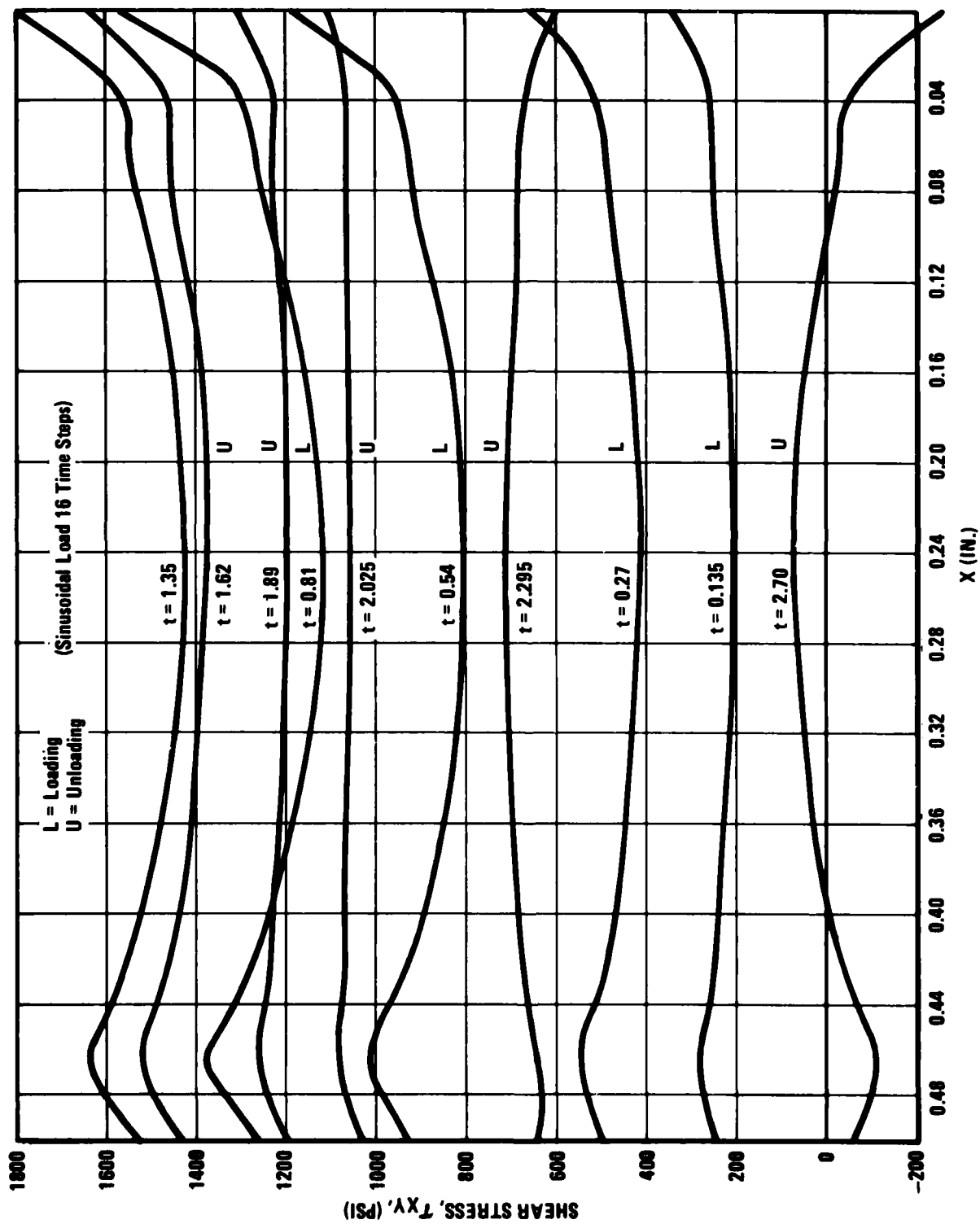


Figure 67 Shear Stress Distributions Along Adhesive-Adherend Interface (Sinusoidal Load)

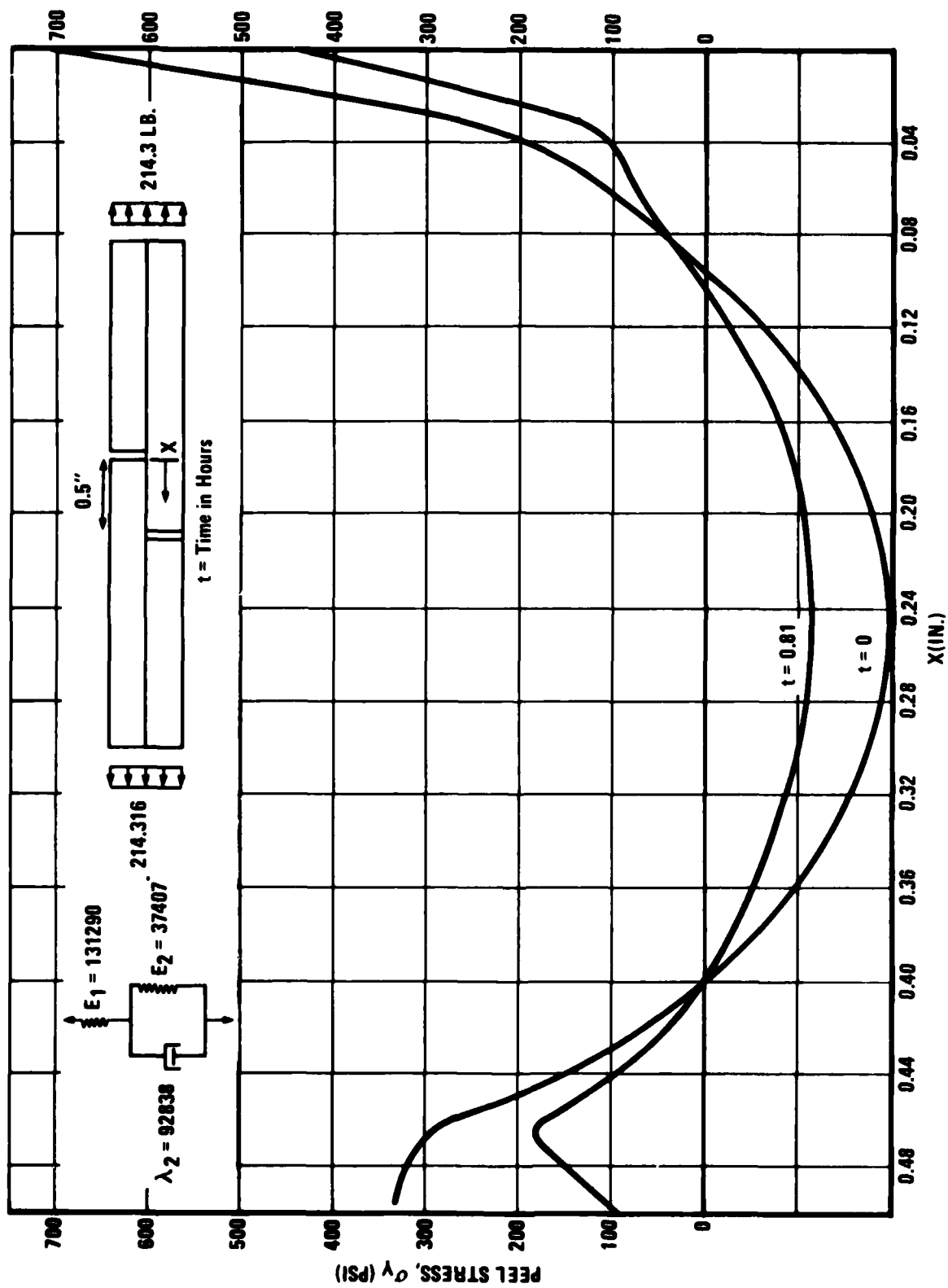


Figure 68 Peel Stress Distributions Along Adhesive-Adherend Interface (Constant Load)

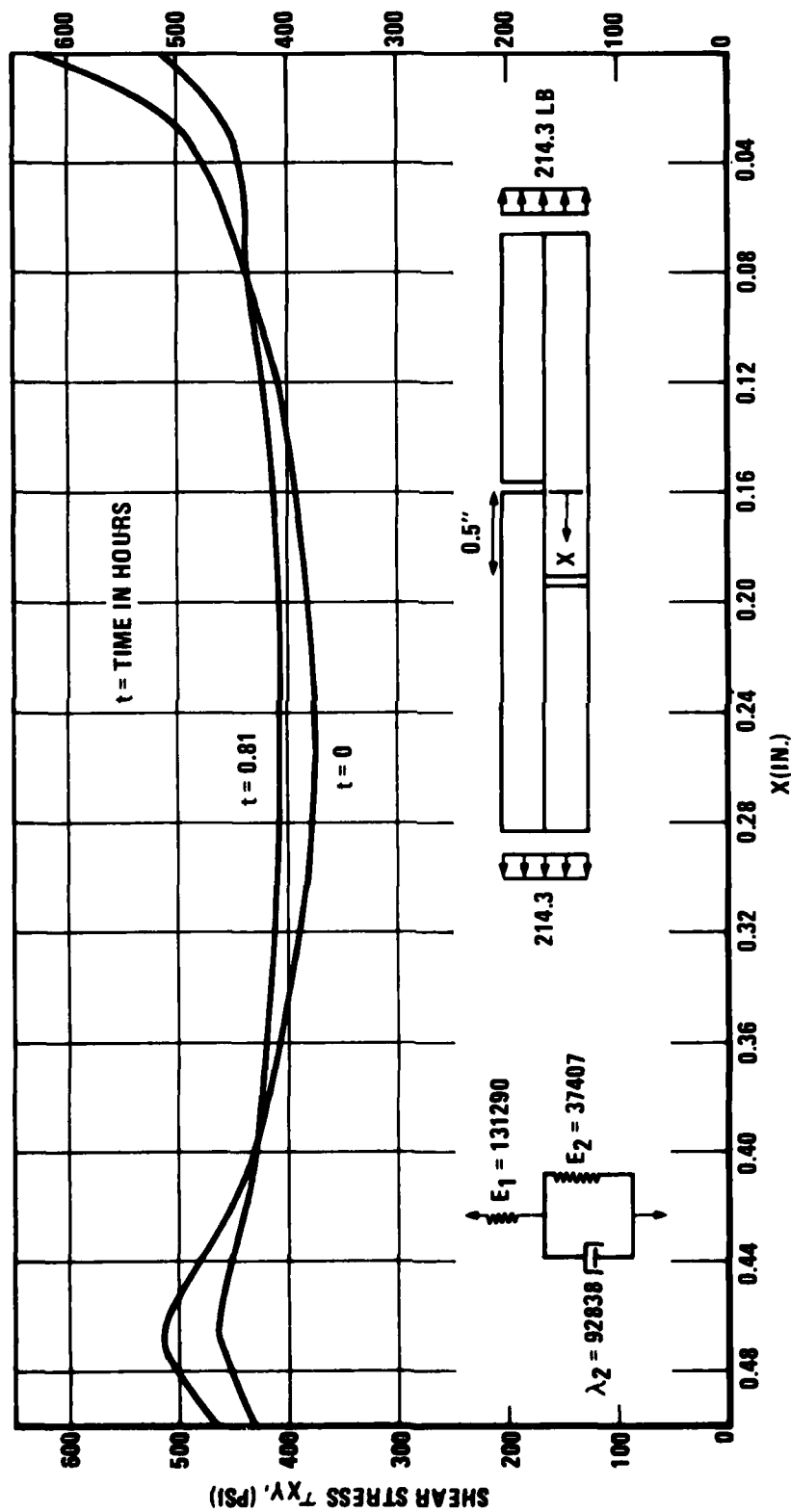


Figure 69 Shear Stress Distributions Along Adhesive-Adherend Interface (Constant Load)

with rigid adherends and a linear viscoelastic adhesive. As pointed out in Section 4.3.3, the fact that the adherends are not rigid resulting in stress redistribution and hence these assumptions were not completely valid.

After ratioing the loads and thicknesses to those used in the MARC analysis, it was found that the bonded joint was stiffer than predicted by MARC. Also, the creep rate was significantly higher in the first few minutes of loading. Although it is probable that some of the problems which arise in predicting the response of the model joint are due to nonlinear effects, it appears that the major obstacle is the limited three parameter material model. In the early period of the loading, the 3-parameter model has very little creep and thus the MARC program cannot predict the response with any accuracy. However, the Prony series expansion available in the latest release of MARC should allow better description of the viscoelastic properties of the adhesive.

It is expected that a more elaborate material model will allow a more accurate prediction of the response of the model joint. This is suggested by the fact that since the model joint is not very sensitive to the adhesive elastic modulus, the inability to accurately predict the time dependent response of the joint must be due to the time dependent capability of the present material model; in this case, the single Voigt element (spring and dashpot in parallel). The least squares data fit used in determining the constants for the three parameter material model tends to average out the time dependence of the material during the earlier time interval where a significant amount of creep occurs. Hence, the MARC program could not predict the response of the model joint very accurately.

4.3.3 Rigid Versus Non-Rigid Adherends

In the course of predicting the stress distribution in the adhesive interlayer during the viscoelastic analysis of the model joint, it was observed that there was a redistribution of stresses. This behavior contradicted the results expected if the adherends were perfectly rigid as developed in Appendix A of Vol. II. In this analysis, the stress distribution in the adhesive interlayer of a model joint with rigid adherends is considered. The two dimensional boundary value problem is formulated with a constant Poisson's ratio and a time dependent Young's modulus. The analysis shows that under constant load, there is a time independent stress distribution, and there are time-dependent creep displace-

ments. However, this is possible only because Poisson's ratio is assumed constant and because the displacements could be prescribed, a priori, on the rigid boundaries. Since in the analysis performed the adherend modulus was 78 times larger than the adhesive modulus, it was assumed that the MARC solution would yield an adhesive stress distribution that was independent of time and load. Such was not the case. Two reasons were considered for the stress redistribution: 1) the MARC solution scheme was inconsistent, and 2) the adherends were not rigid.

To isolate the cause, the MARC viscoelastic code was checked in the analysis of a simple problem whose solution is well documented. The problem selected was the bending of a beam under a uniform load. This stress boundary value problem, found in Reference 32, has an elastic solution in which the stresses are independent of the material properties and the displacements are inversely proportional to the modulus of elasticity. Therefore, the viscoelastic solution had to yield time independent stresses and time dependent displacement which were always proportional to the elastic solution. This was the result obtained from the MARC finite element analysis.

With the MARC solution scheme verified attention was focussed on the effect of adherend stiffness on the elastic stress distribution. The adhesive stress distribution was used as an indication of how rigid the adherends were. Elastic analyses were performed with an adherend modulus of 10^7 psi, 10^8 psi and rigid adherends. The bond normal stresses and adhesive shear stresses are shown in Figures 70 and 71, respectively. The analysis indicates that as the stiffness of the adherends increases, the bond normal stresses approach zero except for the peaking at each end of the overlap. The shear stresses also approach the average of 428.6 psi while dropping to zero at the free surface on the end. These results indicate that the stresses are significantly sensitive to the increased adherend modulus.

Since the elastic stress distributions in the model joint are decisively different from those obtained in a joint with completely rigid adherends, it seems reasonable to expect the viscoelastic solutions to reflect the same behavior. Thus, it was concluded, that although the model joint consists of stiff adherends, the adherends are not stiff enough to result in a stress distribution comparable to that expected if the adherends were perfectly rigid. In particular, the viscoelastic response of the model joint results in a redistribution of the stresses.

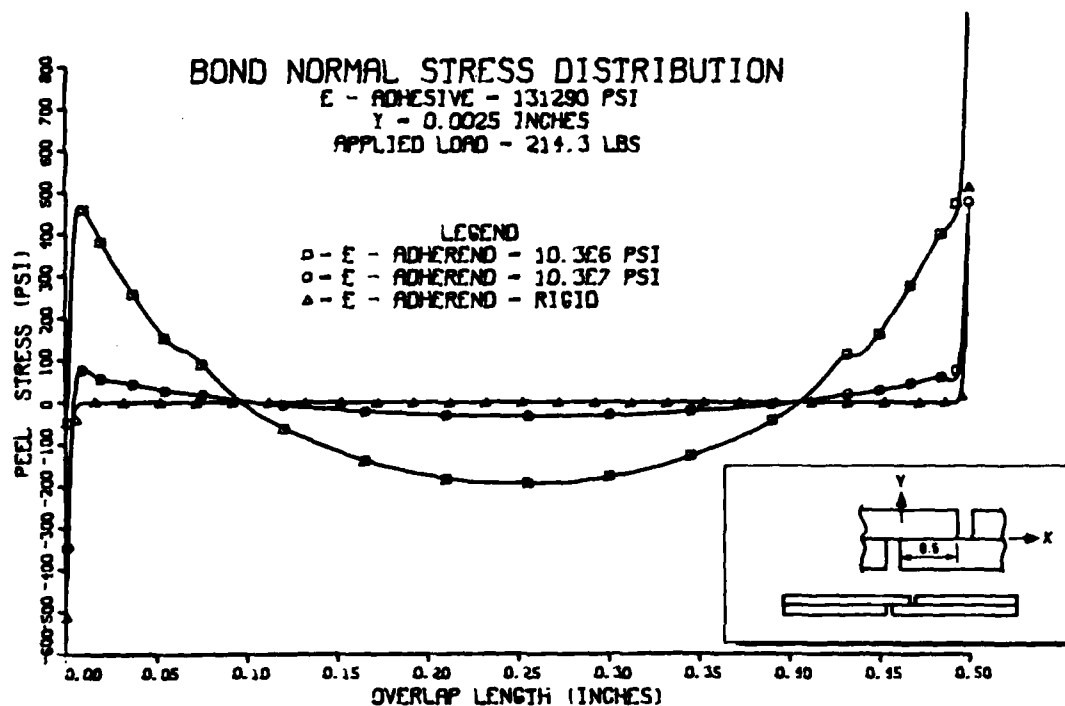


Figure 70 Effect of Adherend Stiffness on Bond Normal Stress Distribution

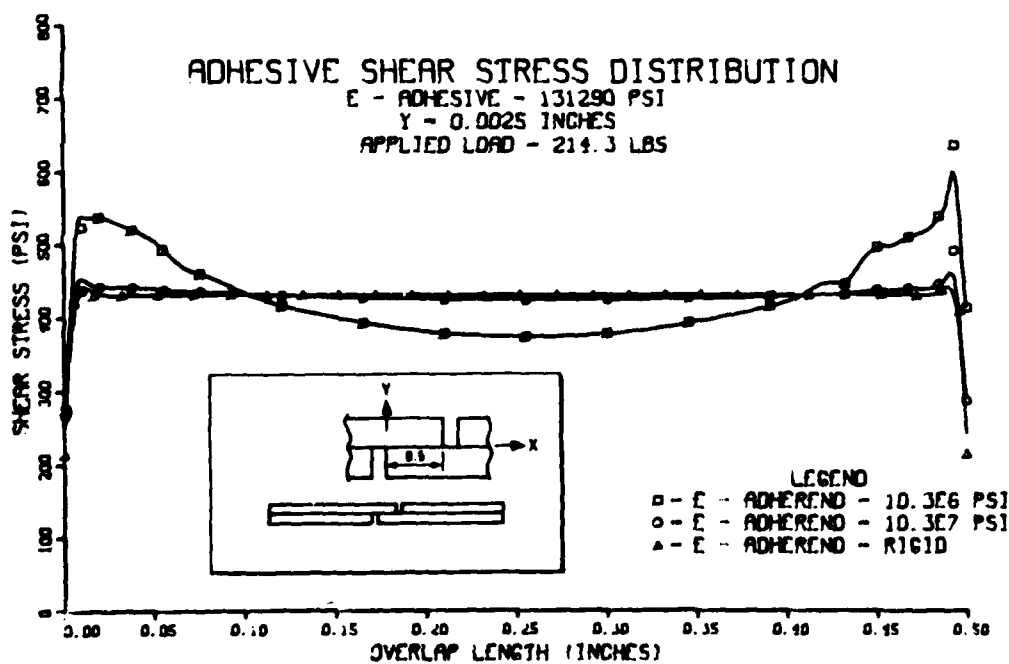


Figure 71 Effect of Adherend Stiffness on Adhesive Shear Stress Distribution

4.3.4 Effects of Material Nonlinearities

As discussed previously, the adhesive used in this study (FM-73M) was considered to act as a linear viscoelastic material at low load levels. However, the adhesive characterization measurements made during the Fatigue Behavior program have indicated possible nonlinear viscoelastic response. These nonlinear effects, in combination with the limited material model available at the time of this program, prevent one from confidently predicting the response of the model joint using MARC. The incorporation of the Prony series into the MARC code will provide a considerable increase in the analytical power available for characterization of the adhesive and the response of the model joint. However, the inclusion of nonlinear effects creates a significant increase in the cost required to predict the response of the bonded joint using finite element analysis. Hence, it appears likely that a specialized viscoelastic code that is more efficient will be required to cost effectively investigate nonlinear effects.

In addition to an improved and efficient viscoelastic code, the equipment available for experimental measurement must have sufficient resolution to allow subtle changes in adhesive response to be observed. Higher loads than desirable were often applied to neat specimens and model joints so that displacements could be measured with some accuracy. However, these increased load levels were not in the best interest of a linear viscoelastic analysis.

SECTION V

CYCLIC TESTING OF BONDED JOINTS

5.1 Fatigue Testing Equipment

Tension-tension fatigue testing of environmentally conditioned model joints was conducted at a stress ratio, R , of 0.1 in the AMETEK servo-hydraulic fatigue test machine (Fig. A63) on the 3000 pound full scale range. Displacement of the model joint was measured by means of a strain-gage compliance gage, clipped to grooves milled into the slots. Load-displacement (F vs δ) curves were recorded on a HP Model 7004B X-Y plotter. From these curves it is possible to monitor the change in the "effective modulus" (slope) as well as the area of the hysteresis loop of each individual cycle to evaluate the effects of temperature, moisture level, loading waveform, frequency, and stress level on fatigue characteristics of the adhesive interlayer of the bonded joint.

Testing temperatures of -65°F to $+140^{\circ}\text{F}$ for FM-73M joints were obtained through the use of special environmental chambers surrounding the region between the clevises of the fatigue machine. The low temperature environment was obtained by blowing vaporized liquid nitrogen into a polystyrofoam enclosure surrounding the region between the loading fixtures.

Two thermocouples were used to monitor and control temperatures; one to monitor temperature inside the milled slot of the bonded joint specimen, and the other in the chamber enclosure to activate the temperature controller valve. The compliance gage used to measure displacements was wrapped in thermal insulation to reduce the effects of temperature fluctuation on the sensitive component strain gages. Temperature was controlled to $\pm 3^{\circ}\text{F}$.

The elevated temperature tests were conducted in the test chamber shown in Figure 72. Temperature was maintained to $\pm 3^{\circ}\text{F}$ by means of a recirculating fan and a Honeywell proportional temperature controller regulating the electrical resistance heat.

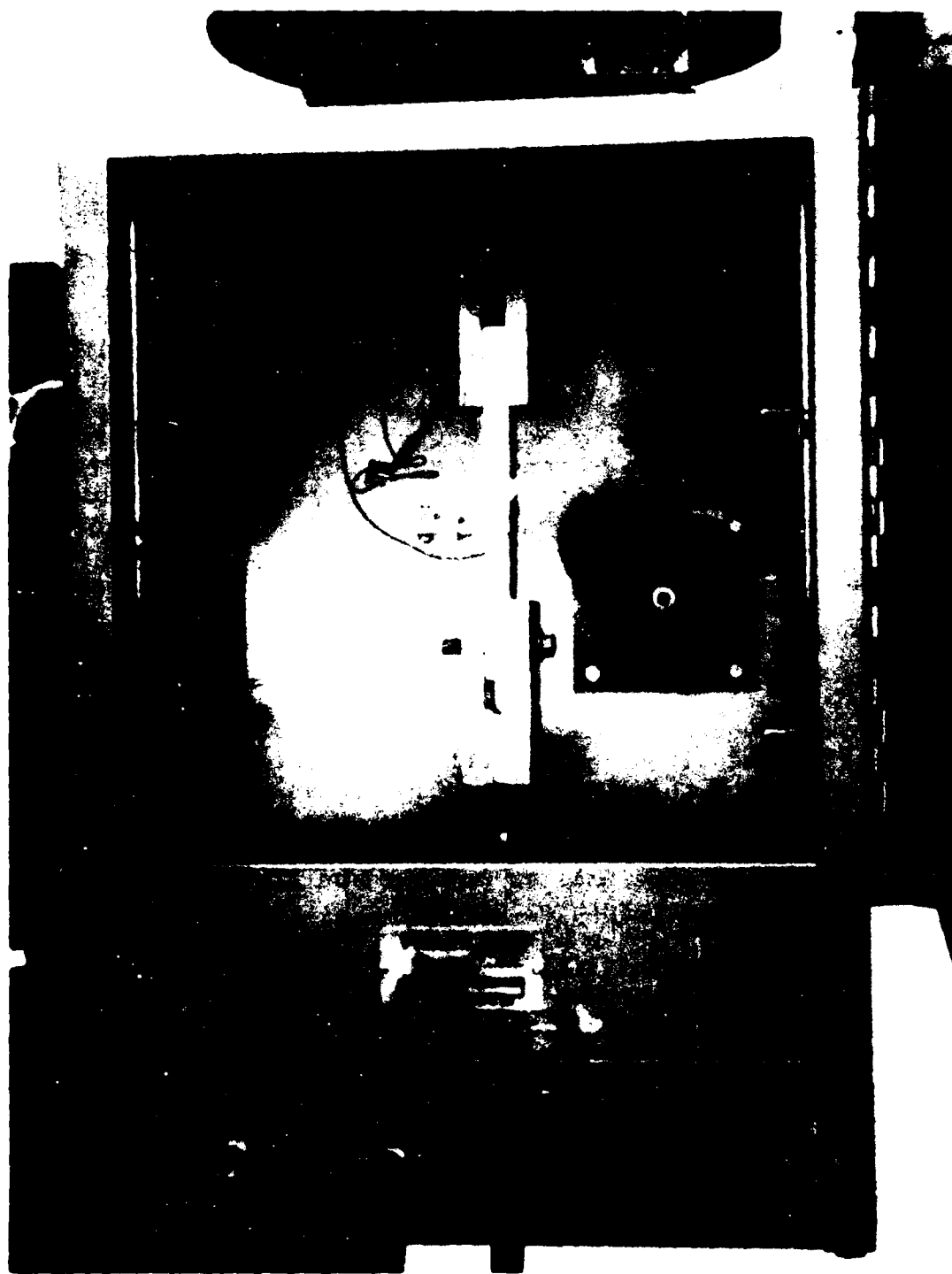


Figure 72 High Temperature Chamber for Fatigue Testing of Model Joints

5.2 Monitoring of Loads and Deformation Measurement

One of the key elements of the Fatigue Behavior program is the accurate measurement of the model joint test specimen response to the load imposed under the different temperature/moisture environments and relating this to the adhesive characteristics.

The model thick adherend joint is instrumented to measure and record the mechanical response of the model adhesive joint during cyclic loading. The following measurements are desirable: compliance of the joint in shear, tensile and bending strain in adherend adjacent to the joint; and dimensional changes of the joint in the thickness direction.

There are at least two main types of extensometers that could be used to measure deformation in the model joint. Vought Corporation Advanced Technology Center's program on "Rigorous Property Measurements of Adhesively Bonded Joints" (Contract F33615-76-C-5205) (Ref. 2) evaluated at least two extensometer techniques, the linear variable differential transformer or LVDT concept and the air gap capacitor concept, for both the static and cyclic loading cases.

Accurate measurement of the adhesive deformation is impossible unless one can attach a measurement device at the adhesive bondline. Such a system, based on the LVDT principle and using a three point pick-up on each side of the specimen in the proximity of the adhesive-adherend interface has been proposed by Krieger of American Cyanamid for measurement of deflections under static and cyclic loading cases (Ref. 33).

An air gap capacitor device has also been evaluated by Renton of Vought Corporation and has recently been checked out for use on thick-adherend single lap shear joint specimens for both the static and cyclic loading cases (Ref. 3).

The environmental effects (temperature, humidity), the long term stability, and the dynamic response of these two systems are somewhat as yet undetermined although Renton has recently checked out the capacitor device for fatigue experiments (Ref. 3). The standard clip compliance gage was used to obtain the deformation measurements in the Fatigue Behavior program which was well underway before Renton's work was completed. The strain of the joint in shear is measured with a clip compliance gage similar to that

commonly used in crack opening displacement studies. It is placed in the retaining rail grooves (See Fig. 73). This gage provides a direct measurement of the shear displacement response of the adhesive by the tensile loading imposed on the adherends. It also provides a method for recording the hysteresis and permanent set of the joint. This gage provides the information of a "zero-gage-length extensometer" (Ref. 34) but is more resistant to the testing environments and thus provides more reliable information.

A comparison of this compliance gage measurement of load-deflection history to the response predicted by the MARC finite element stress analysis program indicates the success achieved in predicting the displacements of a model joint. As seen in Figure 74, the predicted opening of the saw cut under load agrees well with the experimental data. This agreement indicates that the finite element analysis has correctly calculated the stresses in the bondline and related the stress-strain distribution to a measurable quantity.

5.3 Fatigue Testing Matrix

Of particular interest in cyclic testing of model joints is determining the fundamental mechanisms of fatigue in structural adhesive joints. As such, the emphasis, therefore, is on fundamentals. An assessment of fatigue mechanisms and failure modes in metal-to-metal joints was made over a range of loads and environmental conditions experienced by modern high performance aircraft. The fatigue loading was, for the most part, constant amplitude in order that the results might be integrated with those of the other programs with the intent of eventually deriving a form of "cumulative damage" model, or for developing a methodology for accurately predicting service life and for establishing criteria for accelerated testing of bonded joints and structures.

The model joint test program consisted of various matrices of static, creep, and fatigue tests under combinations of environments intended to isolate and determine the individual and combined effects of load level, load rate, frequency, duration, temperature, and moisture content. The matrix for the constant amplitude fatigue tests of the model joints is shown in Table I . The test program was specifically structured to identify failure mechanisms and changes in mechanisms.

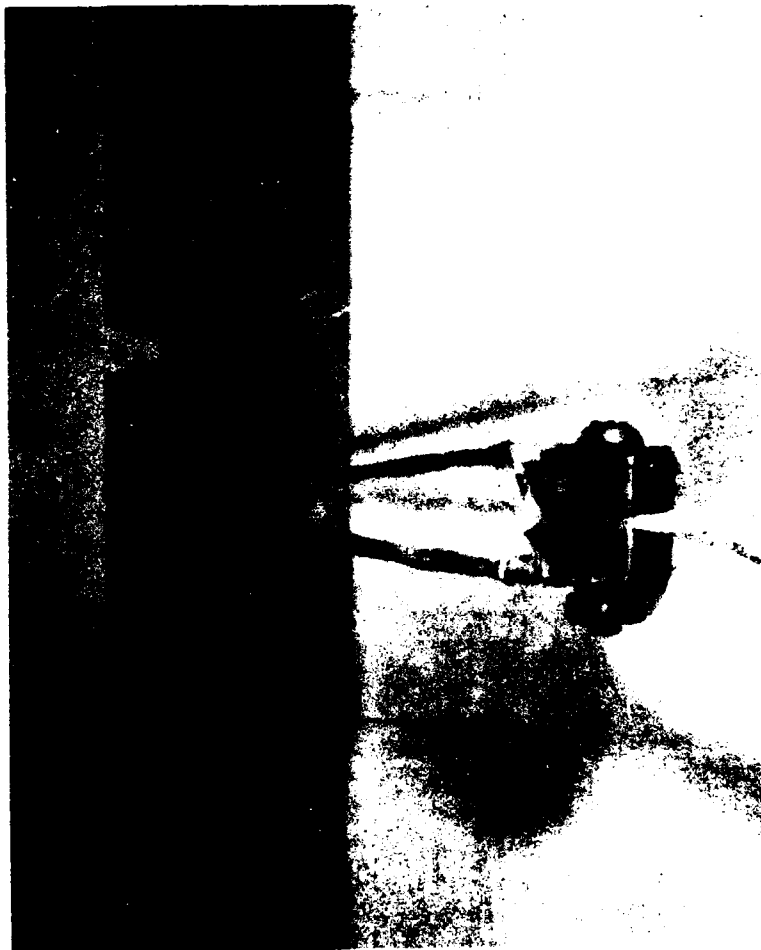
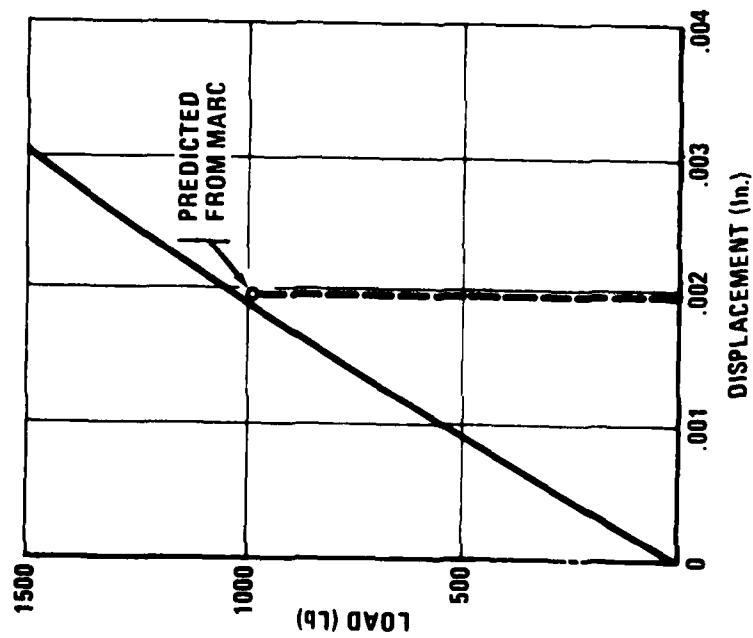


Figure 73 Instrumented Model Joint

EXPERIMENTAL LOAD-DISPLACEMENT



PREDICTED LOAD-DISPLACEMENT

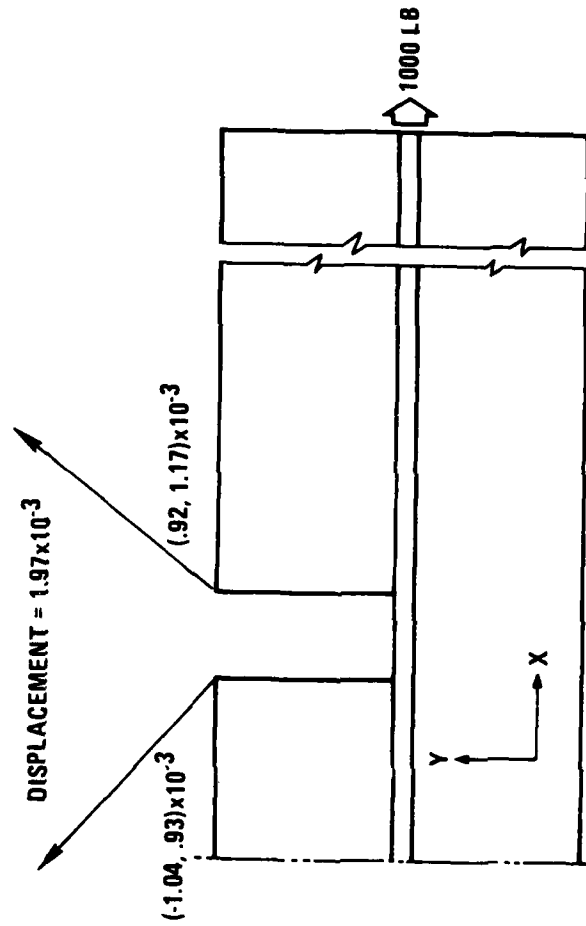


Figure 74 Comparison of Measured and MARC Predicted Joint Displacements

Table MODEL JOINT CONSTANT - AMPLITUDE FATIGUE CYCLING MATRIX

T ₁ (-55°C)		T ₂ (RT)			T ₃ (+60°C)		
DRY	M ₁	M ₂	DRY	M ₁	M ₂	DRY	M ₁ M ₂
10 ⁻²	10 ⁻⁴		10 ⁻⁴	10 ⁻⁴			10 ⁻⁴
	10 ⁻² ~A ₁		10 ⁻² ~A ₁	10 ⁻² ~A ₁			10 ⁻² ~A ₁
	10 ⁻² ~A ₂	10 ⁻²	10 ⁻² ~A ₂	10 ⁻² ~A ₂	10 ⁻²	10 ⁻²	10 ⁻² ~A ₂
	10 ⁻² ~□		10 ⁻² ~□	10 ⁻² ~□			10 ⁻² ~□
30	3	3	3	3	3	30	3
	30		30	30		30	30

NOTES:

3 Specimens Per Condition

10⁻⁴, 10⁻², 3, 30 are Cyclic Frequencies in Hertz

~□ are Loading Waveforms

~A₁, ~A₂ are Different Constant Amplitude Sinusoids

All Loads are Sinusoidal Unless Otherwise Indicated

Based on the Static Creep Results on Adhesive Material with Primary Emphasis on the More Severe Conditions

5.4 Fatigue Testing Results

Tables 2 and 3 summarize most of the cyclic testing conducted in this program, listing the pertinent environmental and loading conditions for the individual model joint specimens, with remarks on the condition of the specimens after test completion (not necessarily to failure).

Typical load-deflection (F vs δ) histories for dry and moisture-conditioned model joints for a number of environmental and loading conditions are shown in Figures 75, 76, and 77.

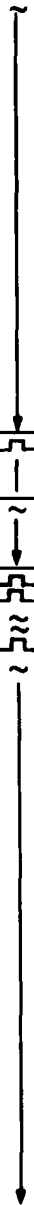
There are several important, general features of the response (output) histories of the model joints (see, e.g., Ref. 35): First, there is progressive deformation with load cycling, somewhat akin to creep. Second, there are hysteresis loops showing that part of the deformation is recoverable. Last, the slopes of the curves (joint stiffness) decrease with load cycling. These effects are more pronounced for the wet specimens than for the dry.

Referring to the schematic in Figure 78 representing the output response history for a sinusoidal, tension-tension input loading function, the following measurements were extracted, where possible, from the experimental data: the "effective" modulus or stiffness at cycle N , K_N , ($N=0, 1, N_f$) given by $\tan \theta_N$, the slope of the major axis of the hysteresis loop (assumed to be an ellipse); the energy dissipated as heat in the N th cycle given by the area of the loop, $A_N = \pi ab$, where a and b are the semi-major, and semi-minor axes, respectively, of the "ellipse", and the steady creep at cycle N given by the displacement, δ_N .

During the course of data reduction, it was determined that changes in these parameters between the N th cycle and the first measurable cycle, viz., P_N/P_{initial} , where P is I , A or δ , were generally more meaningful than the corresponding "absolute" components. Accordingly, the succeeding section in this report deals primarily with these ratios, including the stiffness ratios, the area ratios and the displacement ratios.

During data reduction in the manner described above, it was discovered that the first few (one, two or three) cycles of any output response history were usually complicated by "shakedown" effects associated with physical aging of the adhesive (see Section 5.4.2) which were not representative of the material response properties required as input parameters for the stress analysis.

Table 2 TEST HISTORIES OF DRY FM-73M MODEL JOINTS UNDER CYCLIC LOADING

Joint number	Temp. °F	Freq. Hz	Wave-form	Maximum stress psi	Cycles to fail	Type of failure
47A-6	78	0.017		4500	1	C
Rerun	78	0.017		4200	44	C
46A-8	78	0.017		4100	128	C
37A-9	78	0.017		4200	122	C
37A-10	78	0.017		4200	141	C
37A-11	78	0.017		4200	220	NF
Rerun	78	0.017		4400	200	NF
Rerun	78	0.017		4600	101	NF
Rerun	78	0.017		4800	8	C
31A-4	78	0.017		4600	1000	NF
Rerun	78	0.017		4800	114	C
31A-5	78	0.017		4800	450	C
52A-7	-65	0.017		4800	200	NF
Rerun	-65	0.017		5000	200	NF
Rerun	-65	0.017		5200	100	NF
Rerun	-65	0.017		5400	100	NF
Rerun	-65	0.017		5600	100	NF
Rerun	-65	0.017		5800	100	NF
Rerun	-65	0.017		6000	80	NF
Rerun	-65	0.017		8000	5	C
54A-6	-65	0.017		7200	98	C
52A-8	-65	1.		7200	346	C
52A-9	-65	0.17		7200	75	C
49A-8	-65	1.		6000	5719	C/A
49A-9	-65	0.17		6000	2434	C
37A-8	78	0.17		4800	39	C
8C-8	78	1.		4800	2871	C/A
8C-9	-65	0.17		7200	20	C/A
8C-10	-65	0.17		6000	960	C/A
33A-4	+140	0.17		4800	2	C
33A-5	+140	0.17		4000	81	C
45A-10	+140	0.017		4000	39	C
C9-4	+140	1.		4000	319	C
29A-12	+140	1.		4000	70	C
29A-11	+140	0.17		4000	13	C
9C3	RT	1.		4800	2119	C/A
3C12	RT	0.017		4800	51	C
3C8	RT	0.017		4800	5	C
*3C10	RT	1.		4000	24,182	A/C
3C9	RT	0.17		4800	273	C
3C11	RT	0.17		4000	8410	NF
	RT	0.8		----	20,537	A
12C7	RT	0.17/8		4000	3415	NF
					19,669	NF
					27,795	A
*12C10	RT	1.		4000	15,000	NF
*12C11	RT	1.		4000	3010	NF
					10,000	NF
*12C12	RT	1.		4000	20,000	NF
41A3	RT	1.		4000	17,369	A
41A10	RT	1.		4000	512	NF
					6,840	NF
					12,352	NF
6C5	RT	0.0001		3090	1	NF
49A11	162°F	0.0001		1950	2	NF
8C12	RT	1		2000		
				2000	40,1210	
8C13	RT	1		3000	164,410	A
8C11	140°F	1		1000		
	140°F	1		----	61,500	NF
13C7	140°F	1		3000	91,750	A
13C9	140°F	1		2000	551,780	NF
13C8	140°F	1		4000	1477	NF
13C10	RT	0.017		----	11,805	NF
1C9	RT	1.		4000	10,000	NF
1C8	RT	1.		4000	10,000	NF
4C13	RT	1		4000	14,170	F
4C12	RT	1		4000	12,600	F
4C11	RT	1		4000	15,001	F
4C10	RT	1		4000	11,550	F
4C9	RT	1		4000	13,990	F

* denotes series of specimens subsequently adherend-etched for optical analysis of adhesive interlayer

A - Adhesive C - Cohesive F - Failure NF - No Failure

Table 3 TEST HISTORIES OF WET FM-73M MODEL JOINTS UNDER CYCLIC LOADING

Joint number	Time mo	Temp °F	Freq. Hz	Wave-form	Maximum stress psi	Number of cycles	Type of failure
42A-4	5.5	78	0.017	~	4200	3	C
29A-6	5.5	78	0.017		4000	10	C
C1-5	6.5	-65	0.017		6000	21	C
C1-1	6.5	-65	0.17		6000	150	C
C1-3	6.5	-65	1.0		6000	1099	C
10C5		140°F	1		3000		PMF
41A1		140°F	1		3000		PMF
41A2		140°F	1		2400		PMF
10C2	9.0	140°F	1		2000	10,060	C
43A1	9.0	140°F	1		2000	5,000	NF
54A2	9.0	140°F	1		2000	10,000	NF
43A2	9.0	140°F	1		2000	240	
54A1	9.0	140°F	1		2000	590	
42A2	9.0	140°F	1		2000	3,590	
41A10	9.0	140°F	1		2000		
42A1	9.0	140°F	0.0001		1950	2	NF
52A5	9.0	RT	1		2000	347,000	
8C3	9.0	RT	0.017		3000	11,805	NF
52A2	9.0	RT	1		3000	10,000	NF
52A4	9.0	RT	1		3000	1,760	NF
52A3	9.0	RT	1		3000	2,020 lb	Static
30A2		RT	1		3600	440	C
30A7		RT	1		3200	16,680	A
*30A8		RT	1		3000	25,710	A
30A8	13.0	RT	1		3000	27,498	
*3C5	13.0	RT	1		3000	20,000	NF
3C6	13.0	RT	1		3000	12,350	A
7C3	13.0	RT	1	↓	3000	13,340	A
*3C3	13.0	RT	1		3000	10,000	A
*1C2	13.0	RT	1		3000	15,000	A
18C1	20.0	RT	1		3000	2,800	C
18C2	20.0	RT	1		3000	1,368	C
16C5	20.0	RT	1		3000	739	C
16C3	20.0	RT	1		3000	900	NF
17C6	20.0	RT	1		3000	600	NF
16C6	20.0	RT	1		3000	300	NF
4C4	20.0	140°F	1		2000	91	C
4C5	20.0	140°F	1		2000	24	C
14C6	20.0	140°F	1		2000		C
14C4	20.0	140°F	1		2000	50	NF
14C2	20.0	140°F	1		2000	100	NF
14C1	20.0	140°F	1		2000	314	C
17C4	20.0	140°F	0.017		2000	83	C
17C5	20.0	RT	0.017		2000	1493	NF
17C2	20.0	RT	0.017		3000	108	C
4C6	28.0	RT	1		2400	3,440	
16C2	28.0	RT	1		2400	1,480	
4C7	28.0	RT	1		2400	8,660	
13C6	28.0	RT	1		2000	1,910lb	Static
16C1	28.0	RT	1		2400	1,775lb	Static
17C3	28.0	RT	1		2000	480,930	NF

* denotes series of specimens subsequently adherend-etched for optical analysis of adhesive interlayer

A = Adhesive C = Cohesive F = Failure NF = No Failure PMF = Premature failure

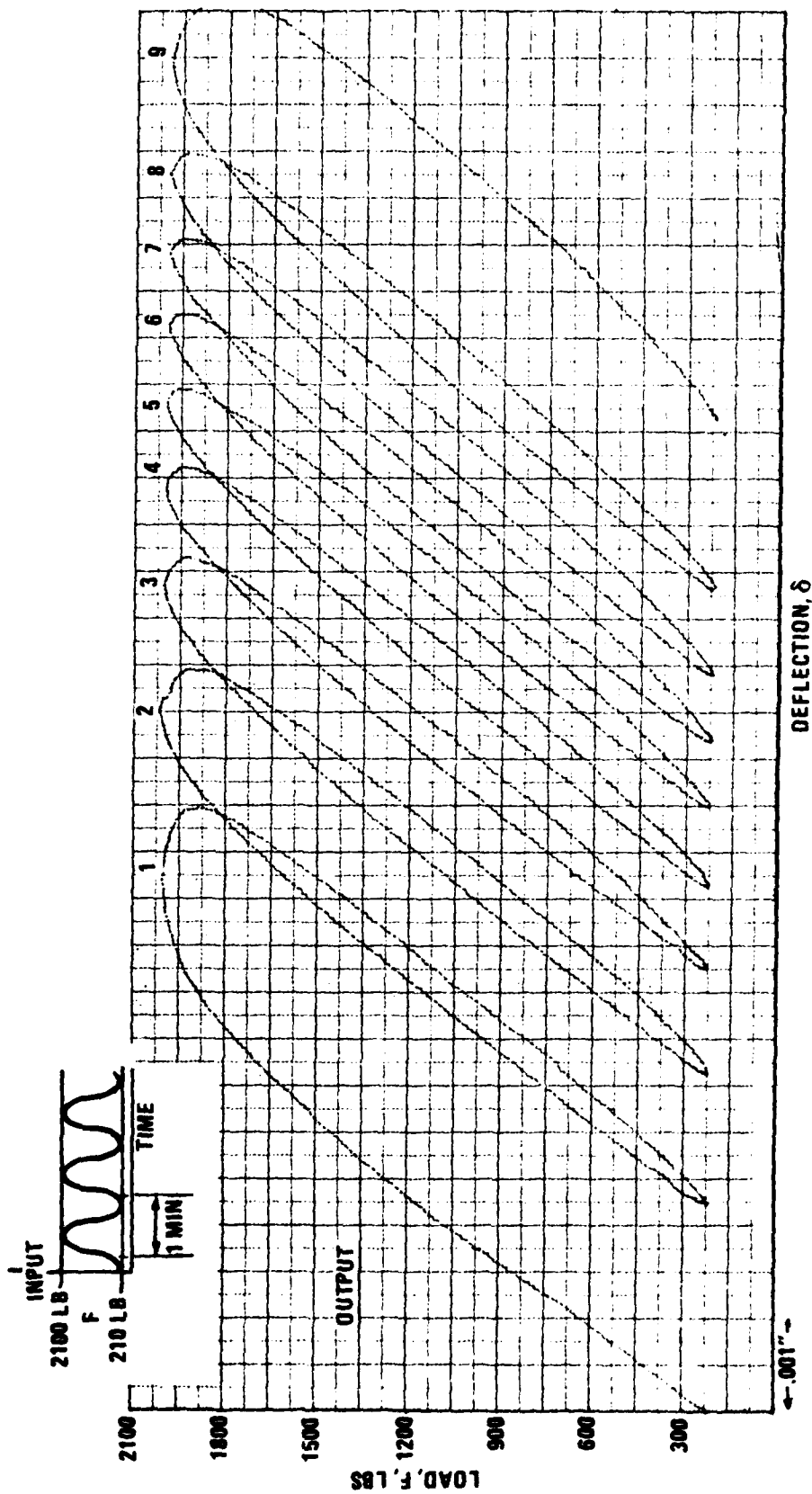


Figure 75 Load-Deflection History of Wet FM-73M Model Joint (Sine Wave Loading)

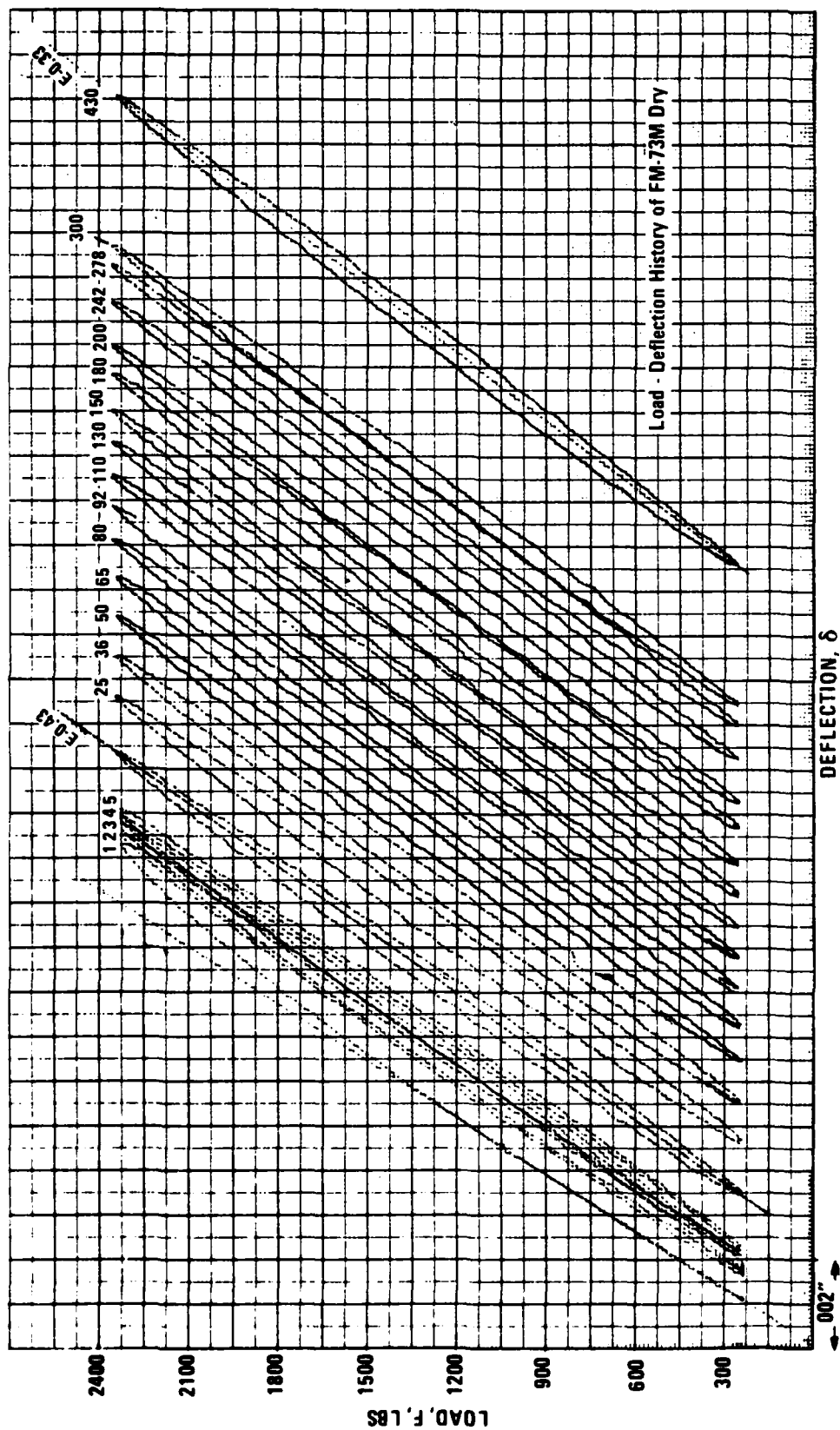


Figure 76 Load-Deflection History of Dry FM-73M Model Joint (Sine Wave Loading)

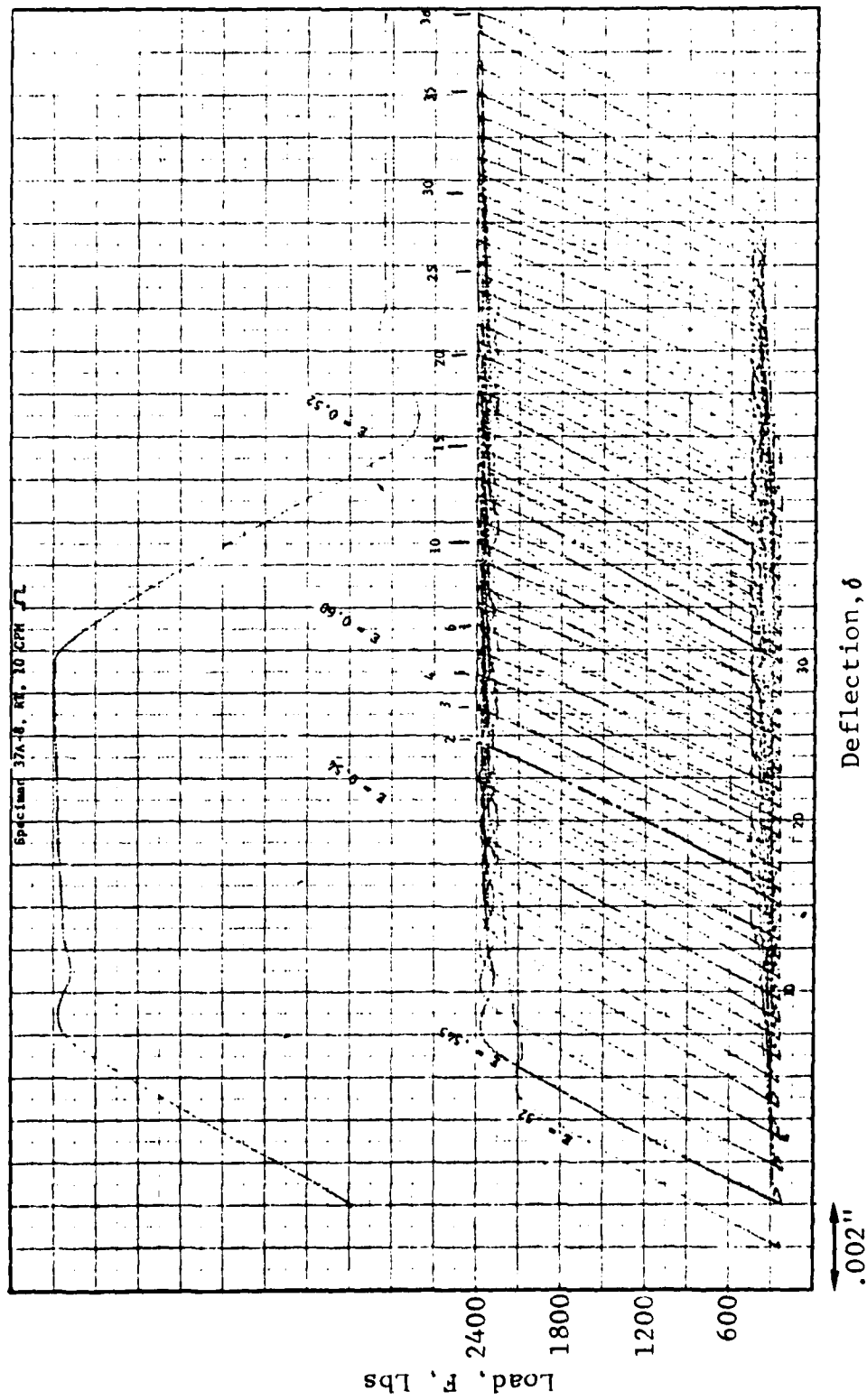


Figure 77 Load-Deflection History of Dry FM-73M Model Joint (Square Wave Loading)

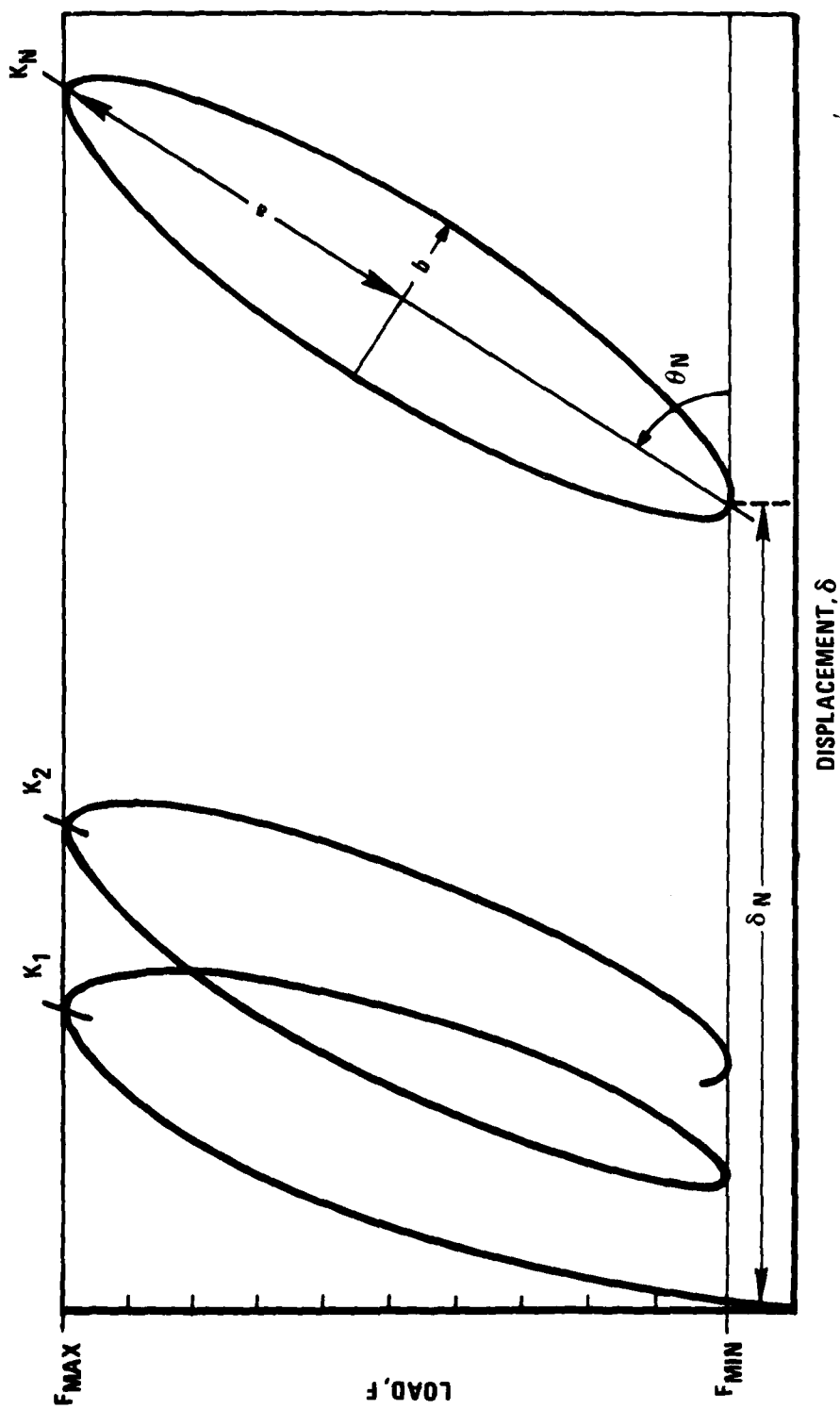


Figure 78 Load-Deflection Hysteresis Loop Elements

Thus, the first "measurable" cycle was used as the initial cycle in the data reduction of the aforementioned ratios rather than the chronological first cycle.

5.4.1 Data Reduction and Deductions

5.4.1.1 Joint Stiffness Ratios, K_N/K_i

For the dry and wet FM-73M model joints tabulated in Tables 2 and 3 the stiffness ratios K_N/K_i were measured (as described above) at sufficient number of N-values to establish its functional dependence on the various environmental parameters, including specimen condition (dry, various degrees of moisture conditioning) load level, frequency of cycling, and temperature. Some of the more important observations and conclusions are presented herein as "bullet" statements:

- o There is a marked variability of number of cycles to failure for identical conditions of about a factor 3 or 5 in many cases.
- o There is a trend in the failed joint data showing that the total time under load is more important than the number of cycles, N, and that the loading wave shape (sinusoidal, square wave) makes little difference within variability limits of the data. Three such examples are cited in Table 4 where within each case, failure occurred after the same total time at load within variability of the data.
- o From the dry and wet series of four sacrificed joints, it will be shown in Section 6.5 that the effective joint stiffness ratio depends mostly on (interfacial) crack advance (see Fig. 98). We thus establish the fact that the joint stiffness ratio, K_N/K_i , after shakedown is a good measure of crack advance.
- o The rate of stiffness change with number of cycles, N, indicates crack growth rate. For example, from data plotted in Figure 79 , the dry and 9-months wet joints exhibit significantly different crack growth rates, with the dry joint showing essentially zero growth rate and the corresponding wet joint showing a strong growth rate dependence. The growth rates may vary statistically, but the slope rates would reflect this variation.

Table 4 TIME UNDER LOAD DATA FOR SELECTED FM-73M MODEL JOINTS

Pre-test exposure condition	Waveform	Temperature °F	Maximum Stress psi	Cycles To Failure	Frequency hz	Time Under Load Sec
Wet 9 months	~	-65	6000	21	0.017	235
			6000	150	0.017	882
			6000	1099	0.017	1099
Dry	⌏	140	4000	70	1.0	70
				30	0.017	76
Dry	~	RT	4800	51	0.017	1647 avg.
				5	0.017	
				273	0.017	

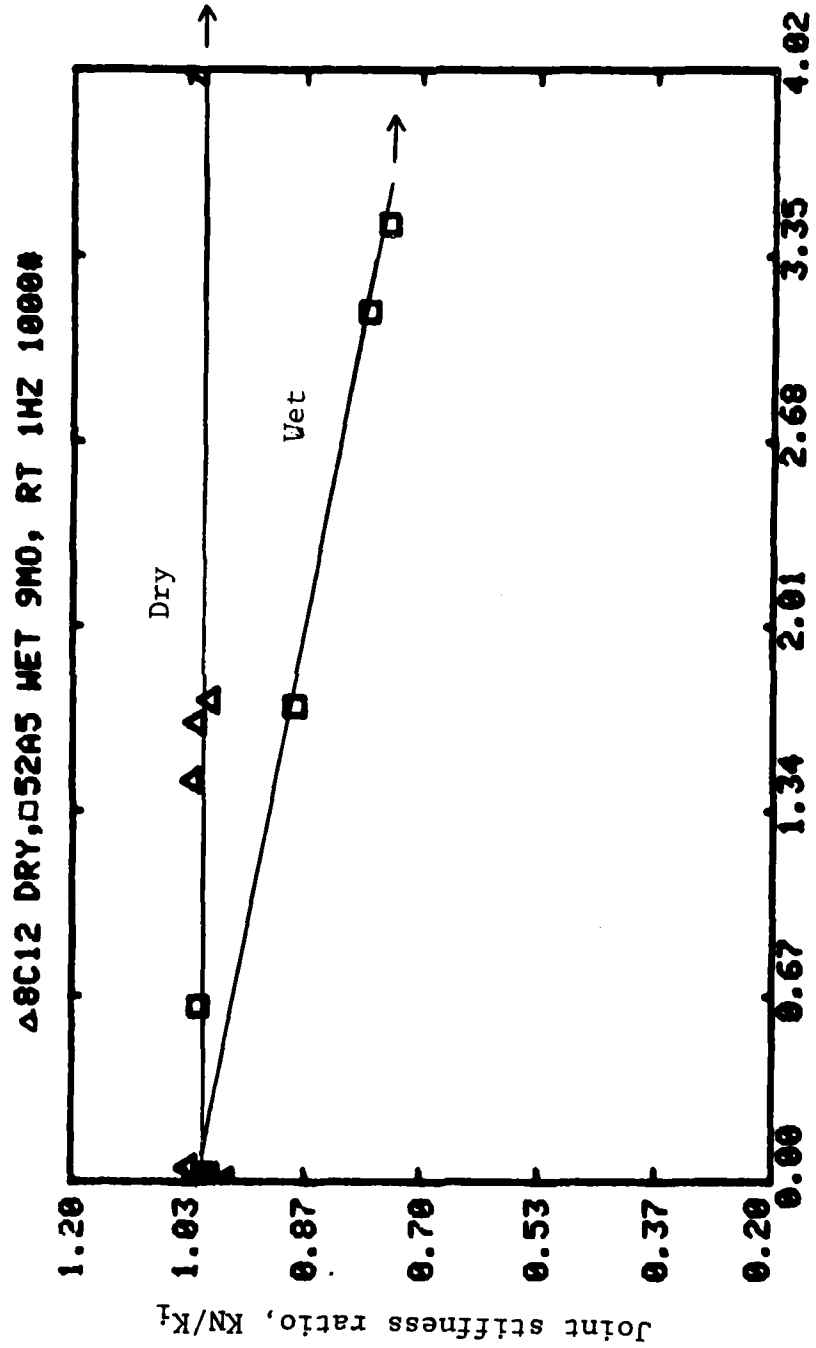


Figure 79 Joint Stiffness Ratio vs Number of Cycles for Dry and Wet FM-73M Model Joints

o A consequence of this is that for a constant load, failure of the joint should result if the joint stiffness ratio has dropped by a given amount, the latter depending on the applied load. For example, for the data plotted in Figures 80 and 81, if the joint stiffness ratio decreases to approximately 84%, failure results as indicated by the vertical arrow (\downarrow) after the data point under consideration. Those joints that did not achieve this decrease in stiffness ratio did not fail. This is indicated by the horizontal arrow (\rightarrow) after the data point under consideration.

o There does not seem to be a large difference in this (joint failure) level as a function of water content, as is observed from a comparison of Figures 80 and 81.

o One of the problems in this joint testing effort concerns the small range of loads used. If (too) high loads are used, there is rapid joint failure in the predominantly shakedown phase (see Section 5.4.2), and if (too) low loads are used, it takes an inordinately long time to complete each test in a reasonable period of time, especially under the conditions of the extensive range of parameters in the test matrix (see Tables 2 & 3). The crack growth rate is a high power of the stress intensity and hence load level.

o The effect of temperature on joint stiffness ratio is displayed in Figure 82 comparing (9 months) wet joints at two temperatures, viz., 140°F and 75°F, other conditions remaining constant. In general, increasing the temperature decreases the joint stiffness ratio and joint life-time as seen in Figure 82, a replot of Figure 83 with additional data on semilog scale.

o The effect of moisture content on joint stiffness ratio is shown in Figure 84 comparing data sets for dry, 9 months-13 months- and 20 months-moisture conditioned joints all tested at 1Hz and 75°F. Within variability of the data, increasing the moisture content decreases the joint stiffness ratio, and subsequently joint life time.

From Figure 98, it is not unreasonable to conclude that, within experimental error, the observed stiffness changes in the experimental load-deflection histories can be accounted for as due almost entirely to interface crack propagation or debond length.

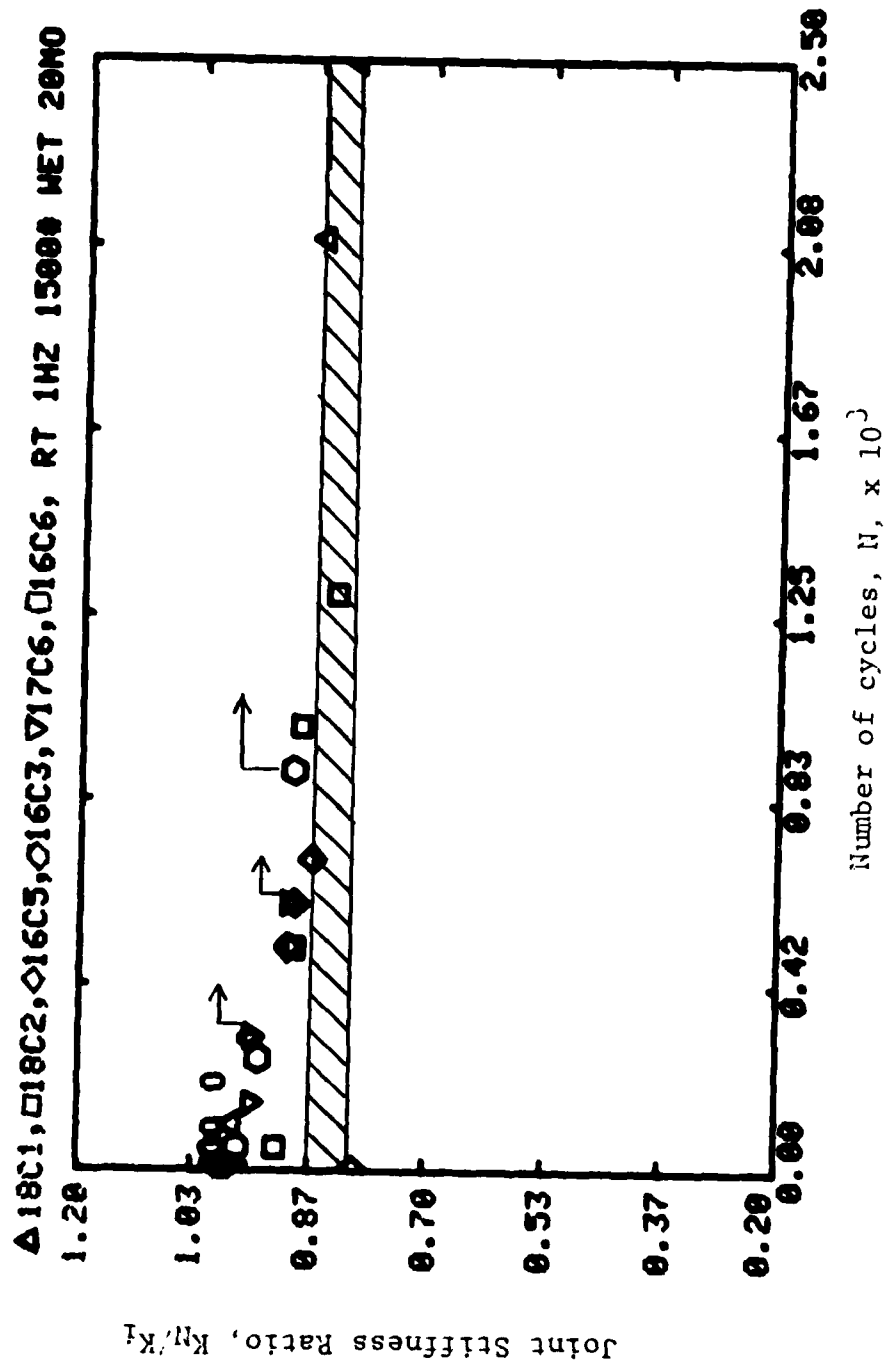
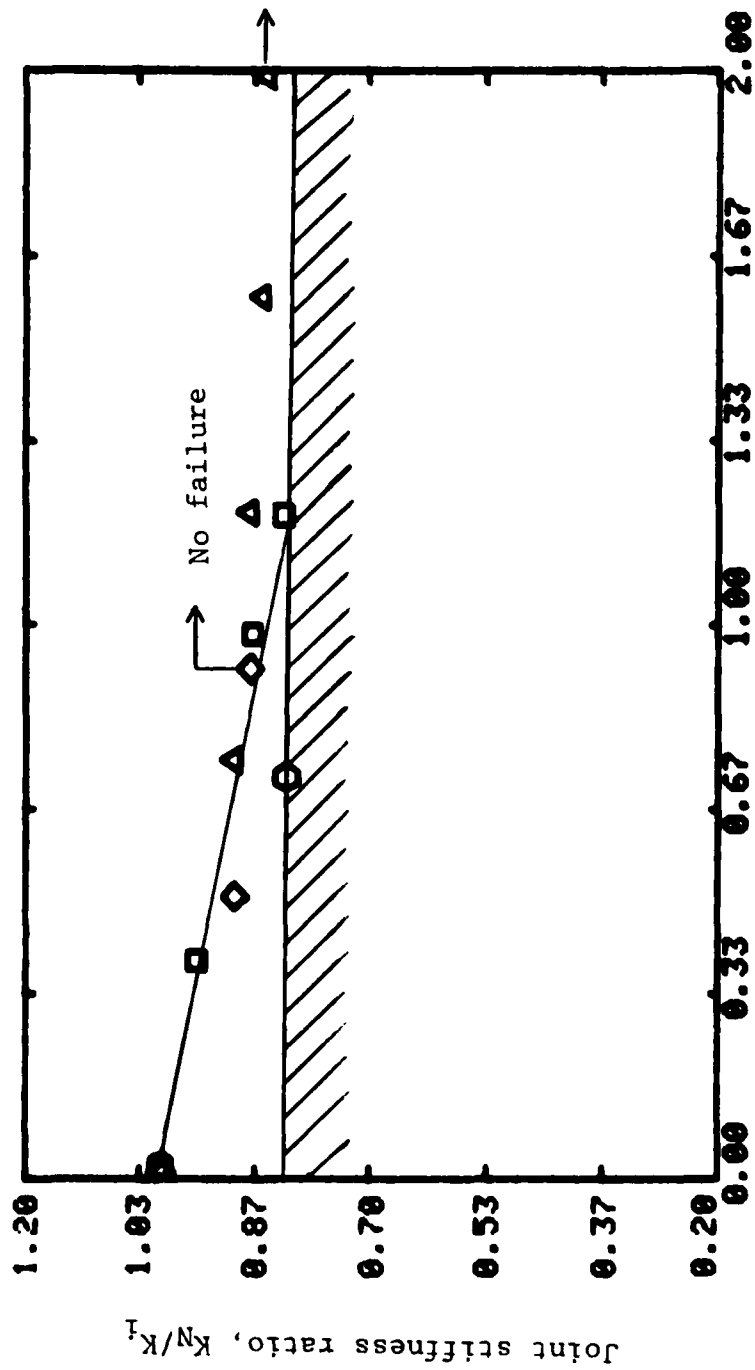


Figure 80 Joint Stiffness Ratio vs Number of Cycles for Wet FM-73M Model Joints

Δ3C5, □3C6, ◇3C3, ○1C1, RT 1HZ 15000 HET



Number of cycles, $N, \times 10^4$.

Figure 81 Joint Stiffness Ratio vs Number of Cycles for Wet FM-73M Model Joints (2)

Δ10C2, □43A1, ◇54A2, ○43A2, ▽54A1, □42A2, TEMP=140°F, FREQ=1HZ, MAX LOAD=1000, WET9

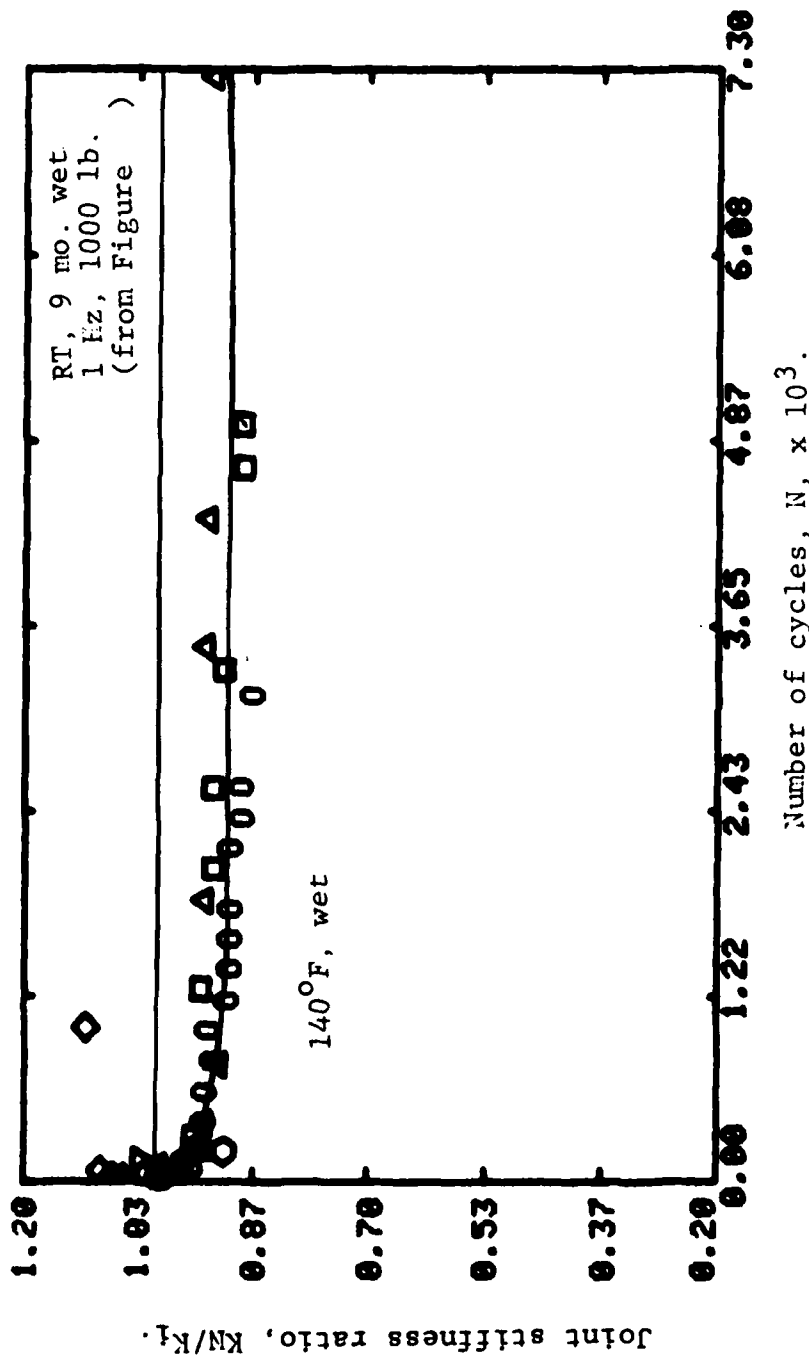


Figure 82 Joint Stiffness Ratio vs Number of Cycles for Wet FM-73M Model Joints (3)

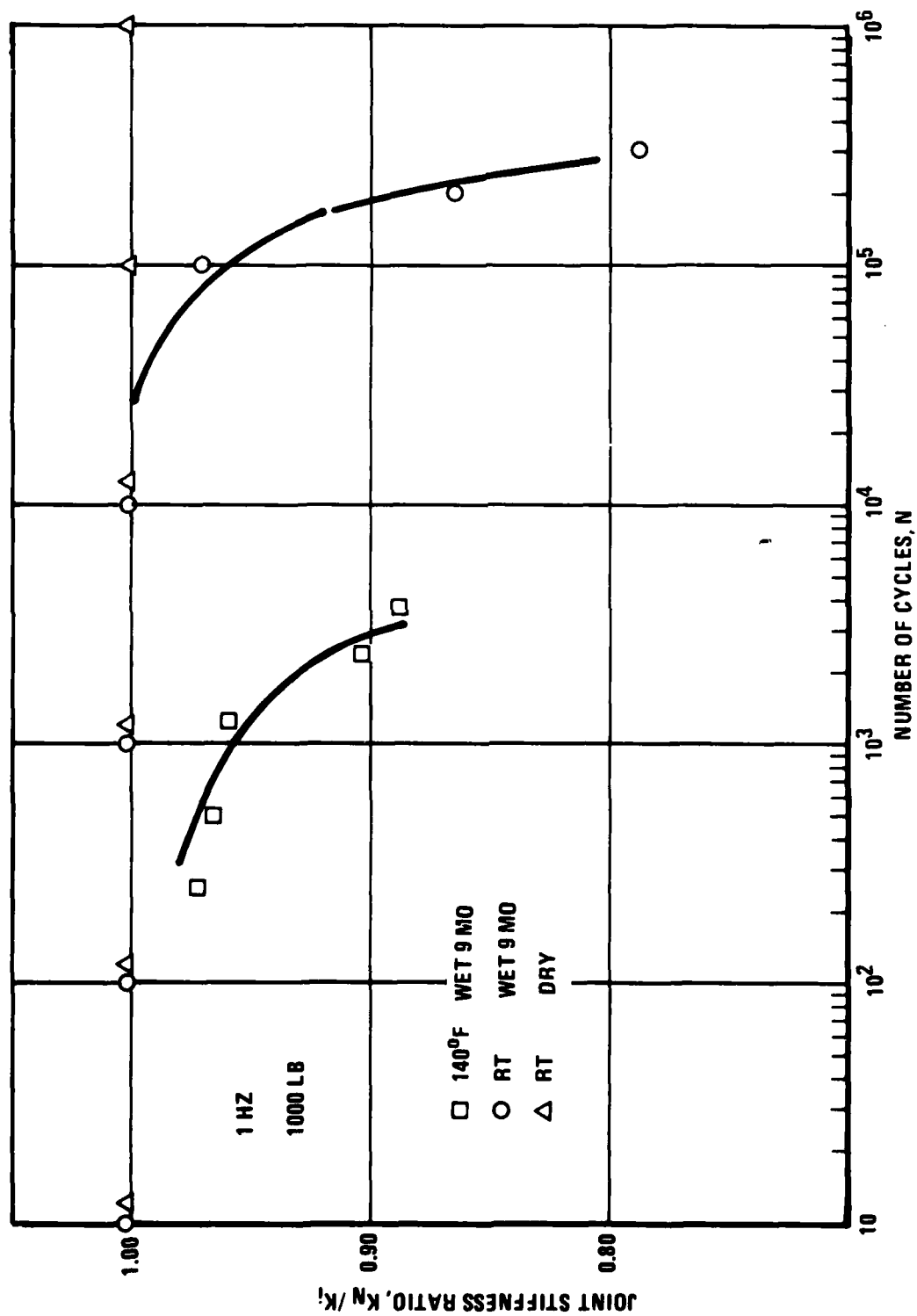


Figure 83 Joint Stiffness Ratios vs Number of Cycles for Various Temperatures and Moisture Conditions (4)

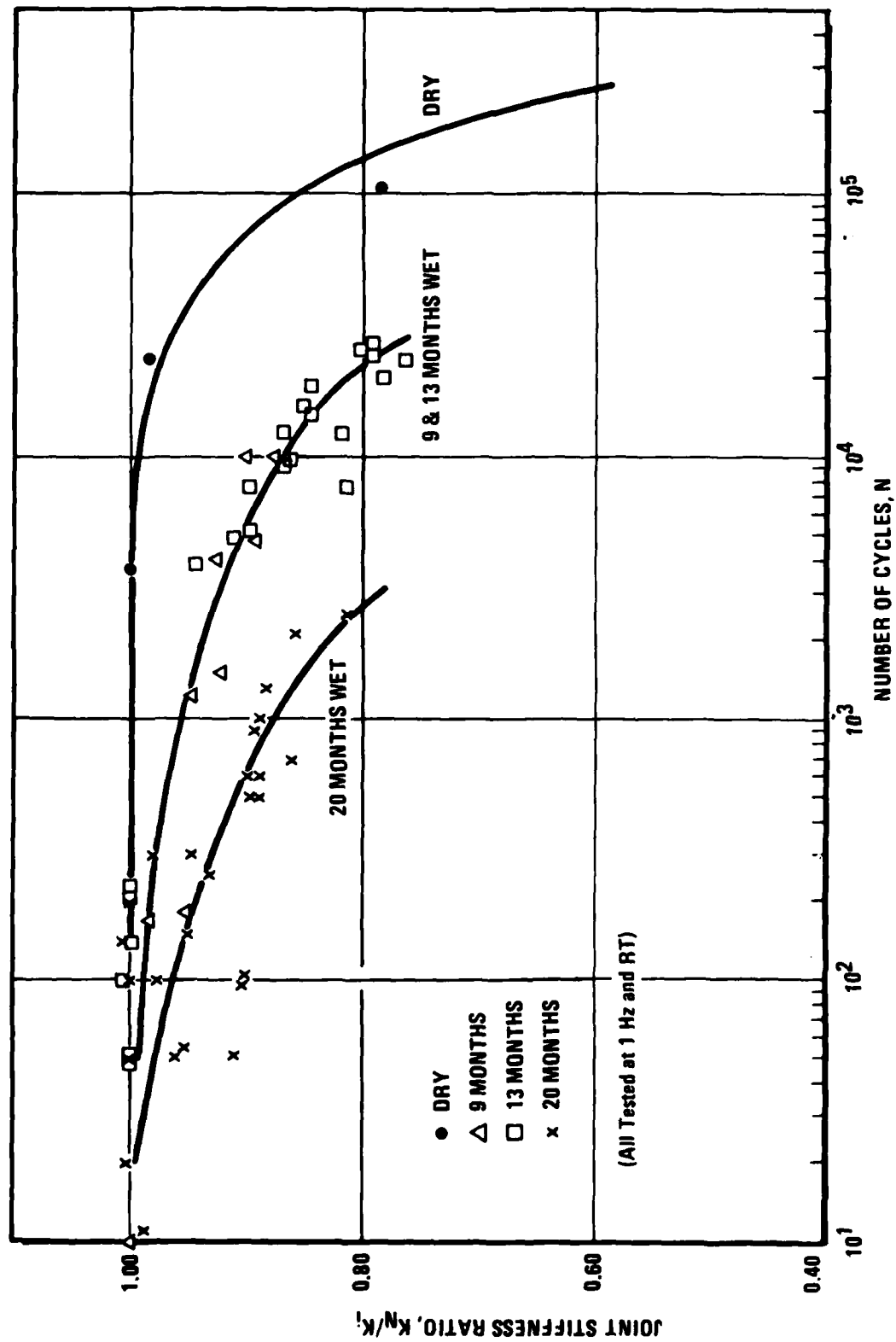


Figure 84 Joint Stiffness Ratios vs Number of Cycles for Different Moisture Conditions

- o The effective joint stiffness ratio decreases with decreasing (maximum) load level as shown in a typical example (Fig. 85) of 9-months conditioned wet joints tested at 1Hz at 75°F.
- o In general, it is observed that increased load level, temperature and moisture content all shorten joint lifetime; and the effect of frequency is reflected in the total time the joint is under load.
- o Use is made of estimates of stress intensity at joint failure for a number of representative testing conditions. These are based on the assumption that a crack length, a , can be estimated from the stiffness ratio at failure assuming that the corresponding stiffness ratio is ostensibly due to interface crack propagation as is shown in Section 6.5 for the case of the sacrificial dry and wet joints after post-test examination of the adhesive interlayer after adherend removal by acid etching. Such a calculation is shown in Figure 97 for a particular joint condition, viz., dry joint tested at 1 Hz at 75°F under 1500 lb. max. From Figure 86, failure after 164,410 cycles corresponds to a stiffness ratio of 70%, which in turn corresponds to a crack length of 0.17 inches. The corresponding predicted stress intensity is $F \cdot a^{\frac{1}{2}}$ which for this case is 618 psi. in. ^{$\frac{1}{2}$}

A plot of load, F , versus crack length, a , predicted in this manner for a number of joint testing conditions both for failed and unfailed joints is presented in Figure 87. (The unfailed points are labelled with a horizontal arrow thus " \longrightarrow ". The solid line is drawn in for comparison purposes and represents the relation, $F \sim a^{-\frac{1}{2}}$, which is characteristic of the fracture behavior of metals. It is of interest to note that the unfailed points lie below this $F \sim a^{-\frac{1}{2}}$ line. On the basis of the experimental data points plotted in Figure 87, the function form for the model joints is approximately given by the relation $F \sim a^{-0.35}$.

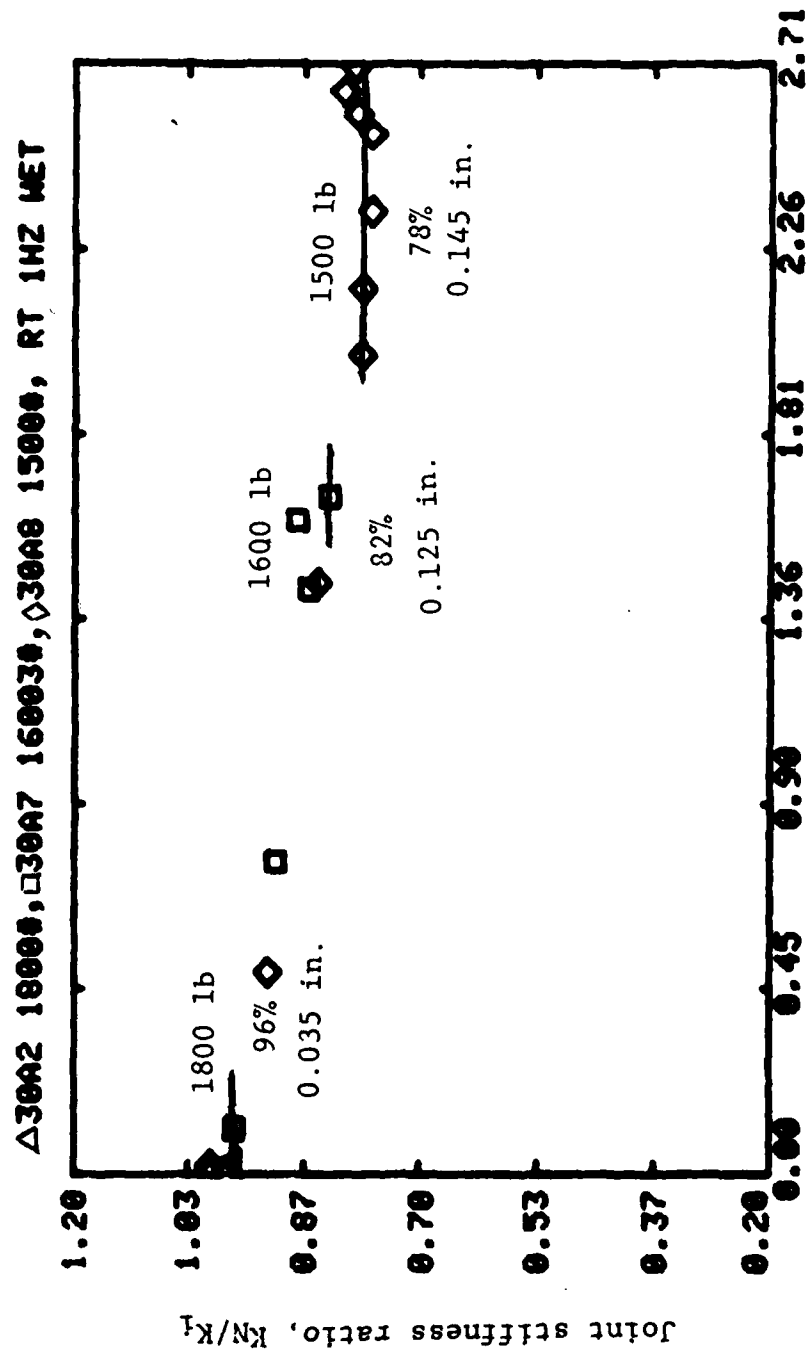
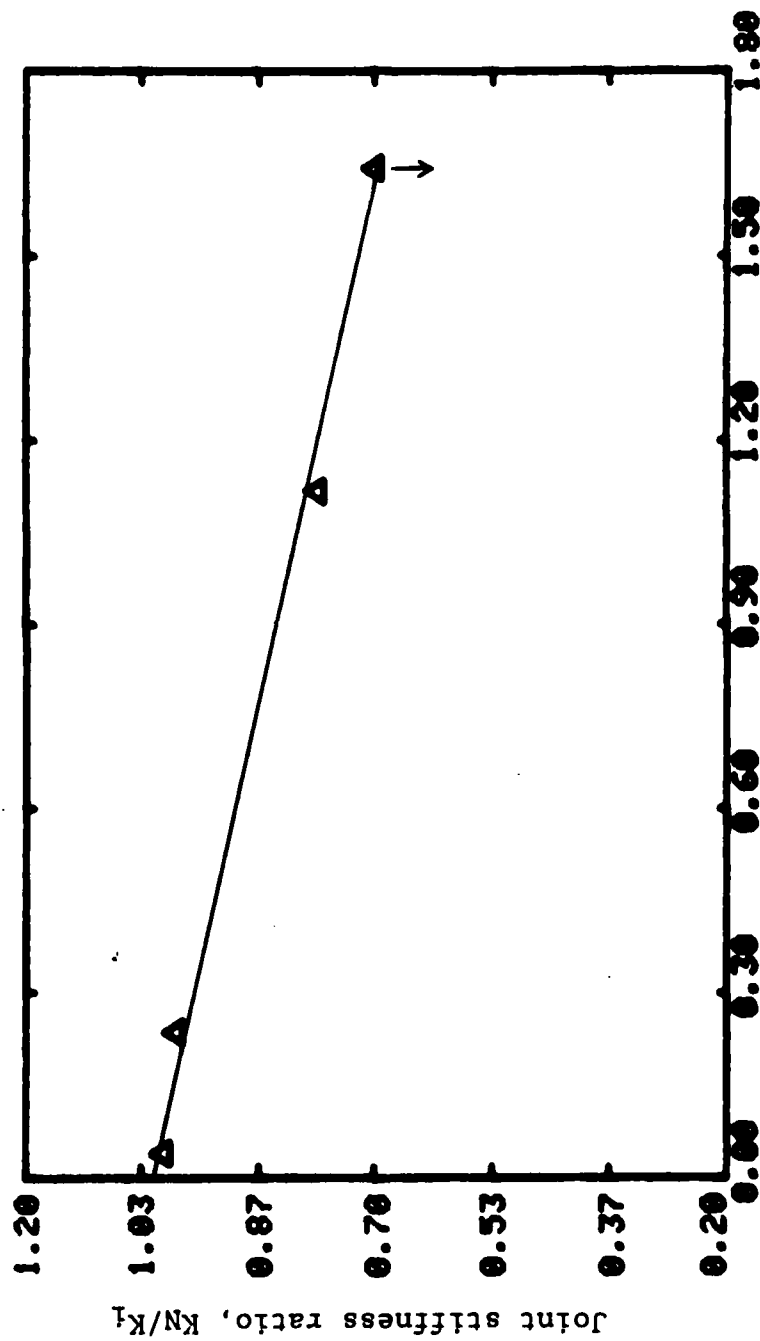


Figure 85 Joint Stiffness Ratio vs Number of Cycles for Wet FM-73M Model Joints (4)

Δ8C13 1HZ 15000 DRY RT 164410ADH/COH



Number of cycles, $N, \times 10^5$.

Figure 86 Joint Stiffness Ratio vs Number of Cycles for Dry FM-73M Model Joint

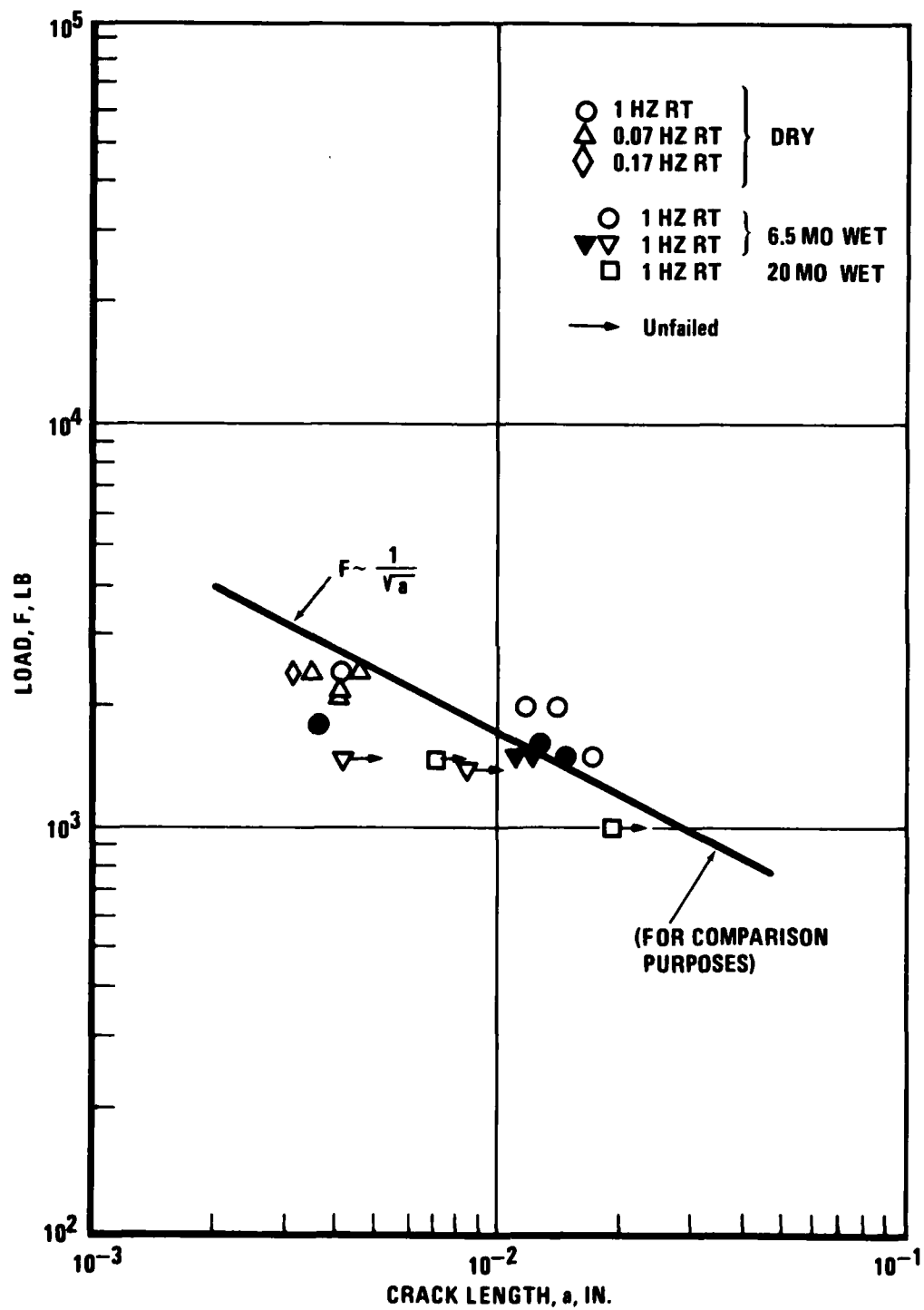


Figure 87 Load vs Inferred Crack Length for Various Test Conditions

5.4.1.2 Hysteresis Energy Dissipation Ratios, A_N/A_i

For the dry and wet FM-73M model joints tabulated in Tables 2 and 3, the energy dissipation ratios, measured by the corresponding hysteresis loop area ratios, were calculated to establish the functional dependence, if possible, on the various environmental parameters. The following generalizations are made on the basis of analysis of these measurements:

- Both area ratio decreases and area ratio increases up to approximately 40% were observed, with increases occurring in approximately two-thirds of the cases. No clear relationships could be established from this data. This may not be too surprising since the energy dissipated in the fracture process is too small a portion of the energy measured and the variability of data is somewhat high as mentioned earlier.
- Since the area of an individual hysteresis loop may be of the order of 10% of the energy required for crack propagation and the temperature at the crack tip is not really known, it is not clear at this time on how to interpret the area data even if the variability in data could be reduced. Possibly measurements of the temperature in the crack tip area with a thermographic camera might be helpful in interpreting this data.

5.4.1.3 Creep Ratio Measurements, δ_N/δ_i

For the dry and wet FM-73M model joints tabulated in Tables 2 and 3, the ratio of steady state creep, δ_N/δ_i , were obtained. Figure 88 represents the steady creep rate (δ vs N) on which the cyclic deformations must be superposed. We note that data on specimens identified at 1, 2, and 3 have reasonably close creep rates. These correspond to the sacrificial unfailed specimens at 10K, 15K, and 20K cycles discussed in Section 6.3.

Specimen 4 had twice the creep rate and failed at 27.1K cycles with a crack length larger than any of 1, 2, and 3. While a part of the increase in the average creep rate can be accounted for (10-20%) by a larger crack growth rate, this is not enough to account for that great a difference. We are, therefore, led to conclude that material variability should account for the balance.

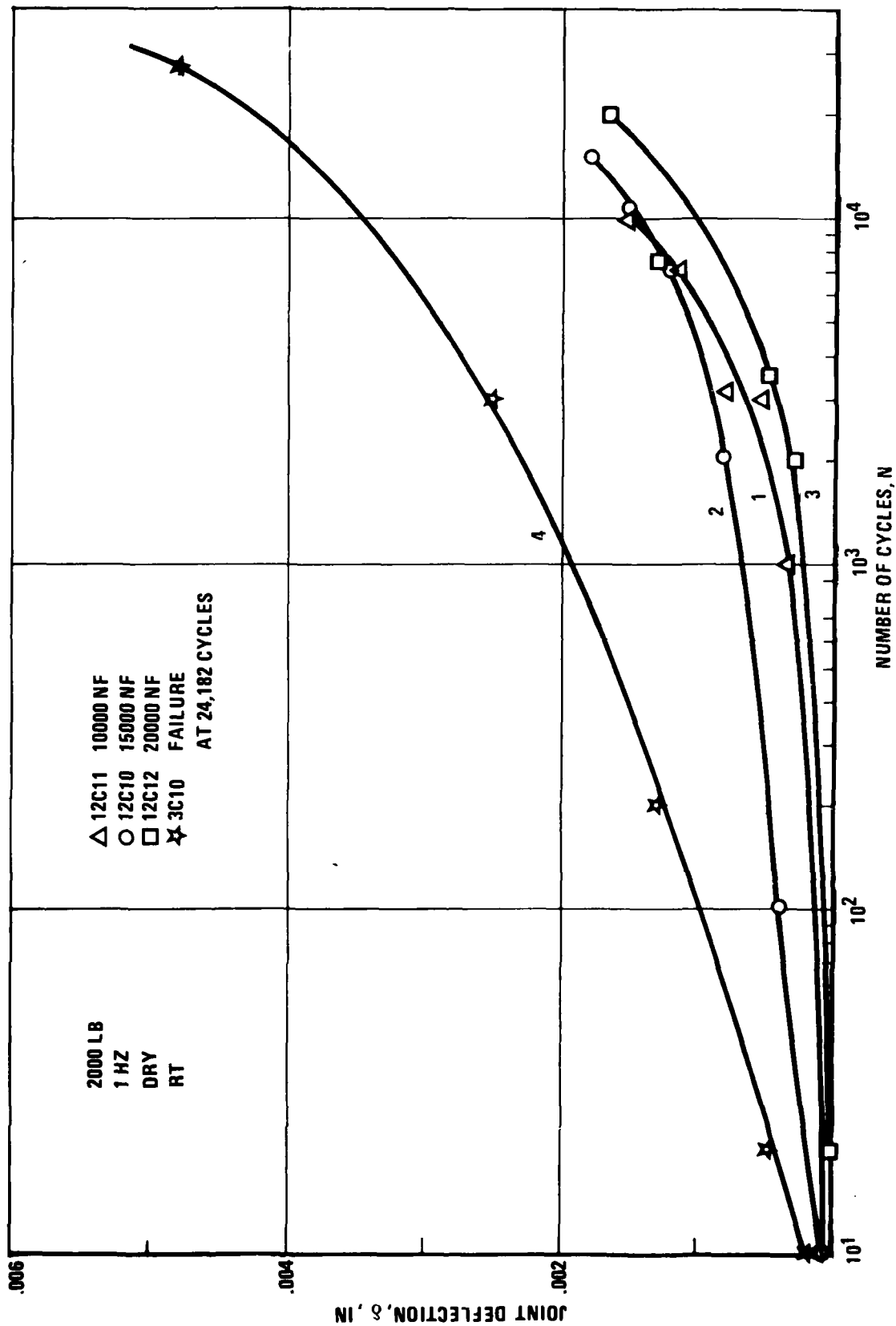


Figure 88 Deflection vs Number of Cycles for Adherend Etched Joints

5.4.1.4 Effect of Stress Level on Creep Rate

It has been determined that different stress levels produce different time responses in the compliance of the model joint, as measured by the joint displacement, δ , per unit bond-line thickness, per unit stress level, τ , as shown in Figure 89. Within repeatability (variability) of the data, the joint compliance curves are shiftable through a stress dependent shift factor, ϕ_τ , as shown in Figure 90. This indicates that at sufficiently high stress levels, the viscoelastic response of the model joint depends on the stress level which is a typical characteristic of one type of nonlinear viscoelastic behavior of the adhesive.

5.4.2 Material Shakedown

- The phenomenon of material shakedown is observed in load-deflect characteristics of the model joint and of neat coupons of the adhesive, and in measurements of thermal expansion coefficient, α_T , (cyclic Tg measurements), and possibly in moisture swelling studies.
- Physical aging takes place in these materials which manifests itself in changed response on repeated "exercising" thereof. (Ref. 36).
- We see evidence of this in repeated cyclic loading (not superposed creep on cyclic load) in that the first two or three cycles give rise to measurably different response characteristics. This difference is invariably such that the area contained in the corresponding hysteresis loop finally decreases to a more or less steady value. We consider that it is very well possible that this arises from a compacting of the molecule structure of the adhesive material from the configuration into which it was originally cured.

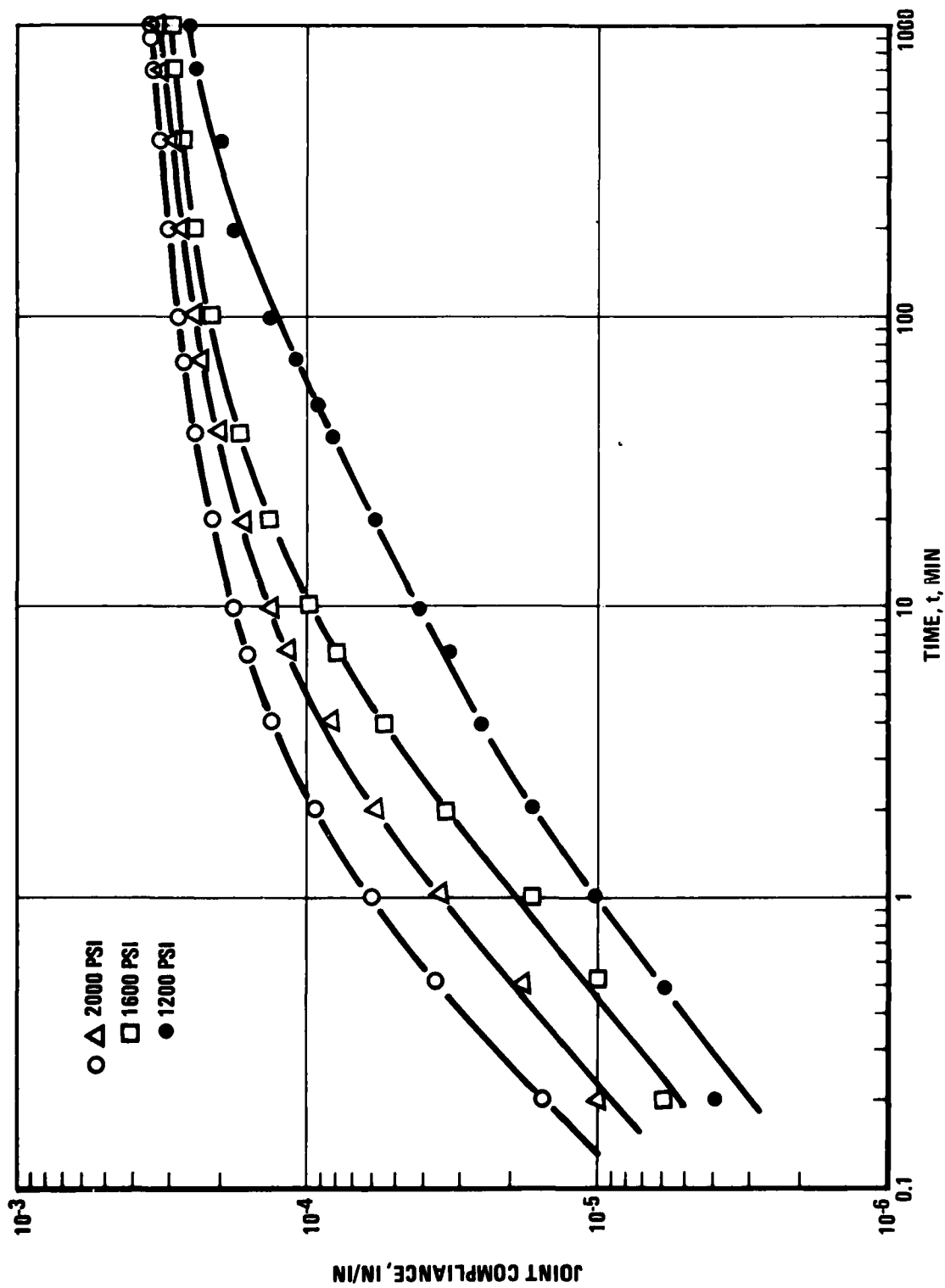


Figure 89 Effect of Stress Level on Joint Compliance

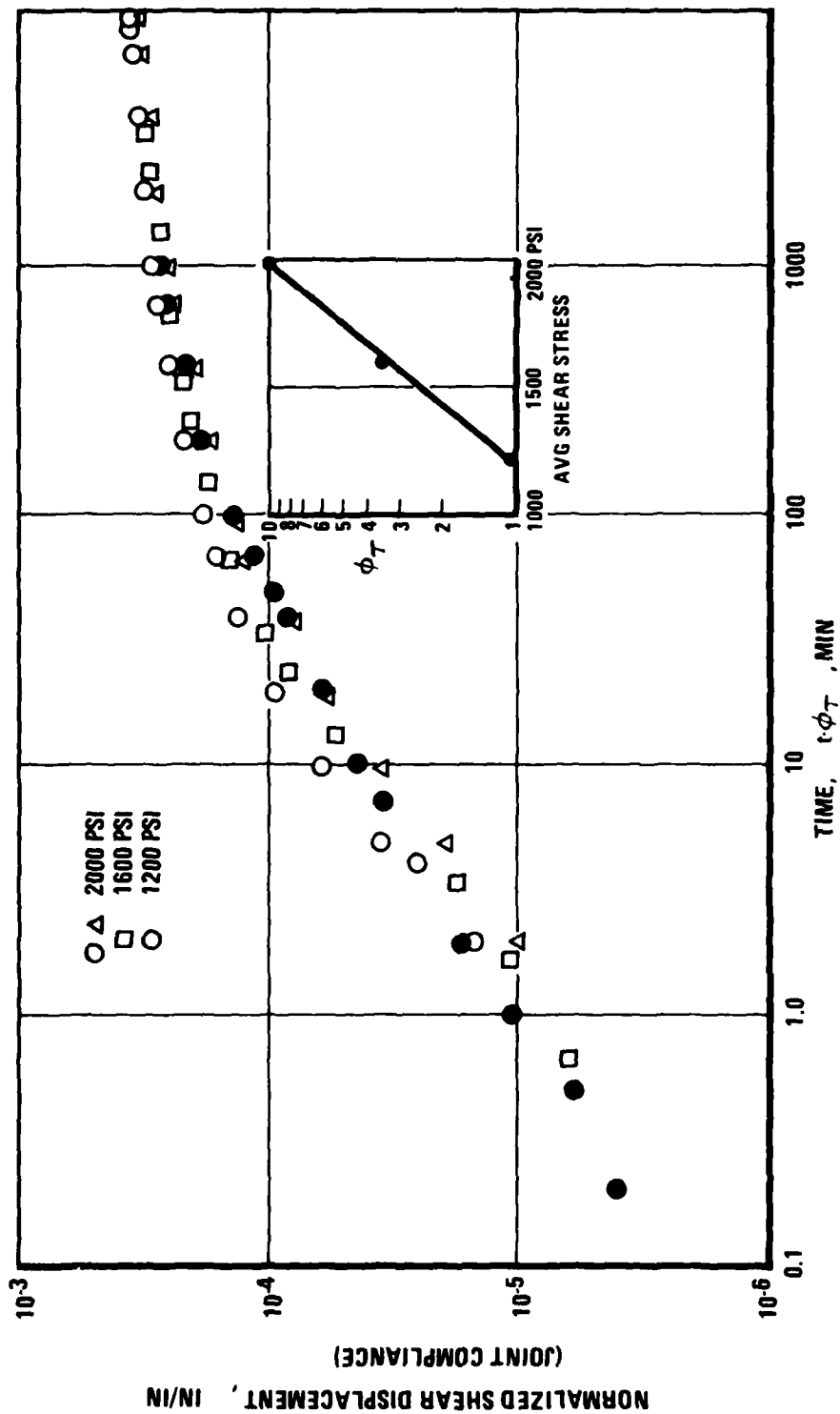


Figure 90 Master Curve Shifting of Joint Compliance with Stress Level

SECTION VI

POST-TEST EXAMINATION

6.1 Optical and SEM Analysis of Failed Joints

One of the more direct techniques of studying fatigue failure mechanisms in bonded joints is the use of the optical microscope and the scanning electron microscope (SEM) to interrogate the nature and topography of the failed joint surfaces. (e.g., Refs. 36 to 39).

The different techniques of viewing with the optical microscope, including dark field illumination, bright field illumination and viewing in transmitted light, are used to advantage in studying fatigue degradation in bonded joints.

Photomicrographs were obtained with a JEOL Model JSM-35 Scanning Electron Microscope operating at 20 kv. The specimens of failed surfaces were carefully cut with a wafering saw to approximately $1 \times 1 \text{ cm}^2$ and fastened to SEM mounting pegs with adhesive-coated, conductive copper tape. To enhance conductivity, a thin ($\sim 200\text{\AA}$) film of Au/Pd alloy was vacuum evaporated onto the samples. Photomicrographs were generally taken with the samples inclined at some specified angle to the incident electron beam, usually about 20° .

The SEM was used in the normal mode - secondary electron (emissive) - for which uniform illumination permits viewing into holes and crevices, and in the backscattered electron (reflective) mode which is analogous to oblique illumination and especially useful for topography studies.

Optical studies of failed surfaces of FM-73M model joints, both dry and those conditioned to approximately 9 months at 150°F and 100% (condensing) R.H., show two quite similar general features of failure, but with some important differences.

One general feature consists of an apparent primarily adhesive failure zone emanating from the high stress region of the overlap, the so-called load-transfer edge, (see for example, Fig. 91). This "adhesively failed" region is variously referred to as the "slow crack growth" region or the "fatigue-failed" zone and because of edge effects arising from the finite one-inch width of the overlap, it takes on a fingernail appearance

as shown. The "missing" material in the top portion of Figure 91 constitutes the "slow failed zone" on the other not shown (mate) adherend.

The second general feature of the failed joint surface consists of the primarily cohesive failure zone between the aforementioned two symmetric slow failed regions. This "cohesively-failed" zone is also referred to as the "fast crack" zone or the "statically failed" region, and occurs in the scrim plane midway between the two adherends (labelled CC¹ in Fig. 91).

The above-described two distinct features of FM-73M bonded joint failed surfaces are much more pronounced in the dry joint than in the wet joint. In the wet specimens, the "slow growth" zone, although still discernible, generally appears interspersed with small cohesive failure regions, and extends over only a much shorter distance from the high stress edge, (See Fig. 91)

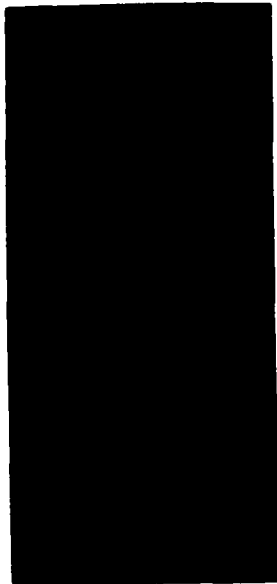
The second feature of the wet failed joint surface, viz., the cohesively failed zone, extends over a correspondingly larger area than for the dry specimen, but also reveals some adhesive failure regions which dot the primarily cohesive failure region. This same topography is observed in dry specimens fatigued at low frequency (0.17 Hz) and at high temperature (140°F).

As the stress level is reduced, the size of the interfacial delamination region increases. Correspondingly, the number of cycles to failure increases with decreasing load, as expected. The "slow crack growth" region also decreases with decreasing frequency of cycling. For example, the low frequency failures (at 0.17 Hz) exhibit only a very small "slow crack growth" region, with the failed surfaces appearing to fail almost entirely in the cohesive mode.

The above observations are in accord with those of another study on model joints by Marceau et al. (Ref. 7) which discusses two fracture modes observed for slow and fast cycling as depicted in Figure 93.

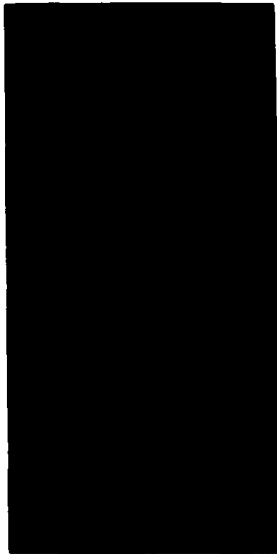
SEM examination of the fatigue fractured zone of the FM-73M adhesive shows a mixture of adhesive-delamination and cohesive failure occurring in the fatigue-cracked zone. The statically failed region consists of a cohesive matrix failure with tearing away from the randomly-oriented reinforcing Dacron

a.



Specimen 33A-4, Dry
+140°F, 4800 psi,
Sinusoidal, 0.17 Hz,
(portions of both fractures),
cohesive failure after 2
cycles.

b.



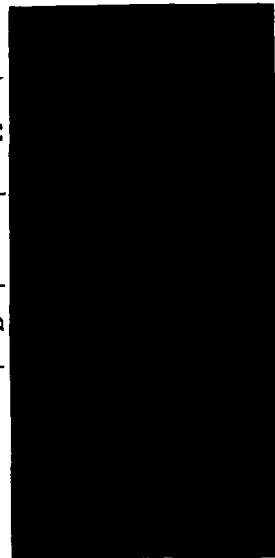
Specimen 29A-6, Wet
RT, 4000 psi, Sinusoidal
0.17 Hz, 10 cycles,
cohesive failure after
10 cycles.

c.



Specimen 8C-8, Dry
RT, 4800 psi, square
Fatigue Zone is adhesive,
interface failure. Static
portion is cohesive.

d.



Specimen 3C-10, Dry
1 Hz, 24,182 cycles.
Same fracture topography as
specimen 8C-8. Mag. 3.8X

Figure 91 Appearance of Fracture Surfaces of Fatigue-Failed FM-73M Model Joints,
Different Testing Conditions

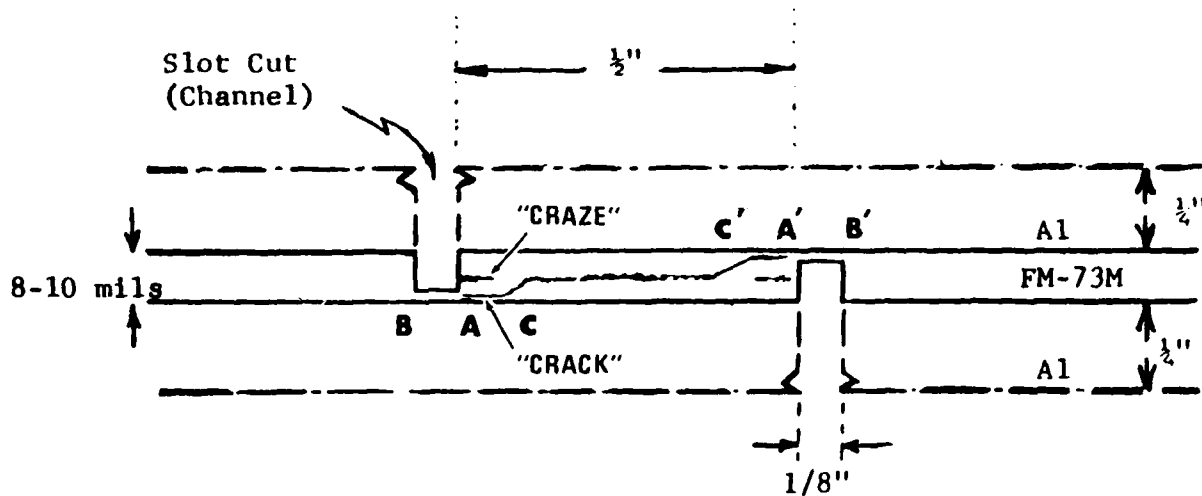


Figure 92 Crack and Craze Loci in FM-73M Model Joint Interlayer

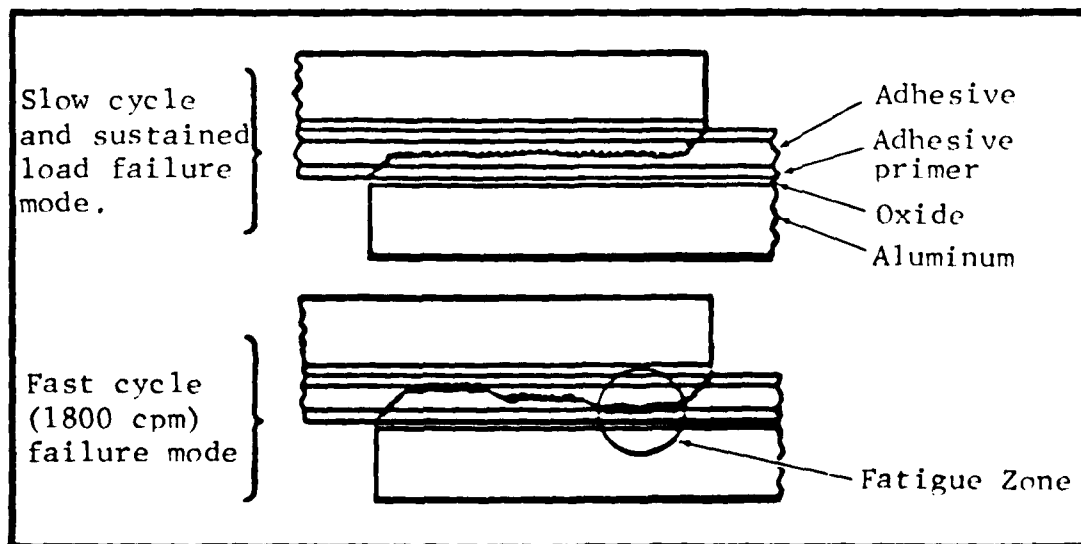


Figure 93 Failure Mode Characteristics of Model Joints

fibers. There is a difference in the texture of the interfacial failure in the slow (fatigue) and fast (static) crack growth zones as shown in Figures 94a and 94b. The texture of the fast crack zone shows a large portion of tear failures which progress into the interior of the adhesive thickness.

Extremely high magnification (10,000X) SEM examination of the slow crack growth surface (Fig. 113a) does not reveal any of the fatigue striations commonly found in metal fractures. This is also noted by Sutton (Ref. 40). However, it is possible that the thin sputtered-gold coating, vacuum-deposited uniformly on the non-conducting adhesive surface during sample preparation for SEM analysis, does not highlight fatigue striations in the same manner as does chromium-shadowing used in transmission electron microscopy. Thus fatigue striations may be present but another technique would have to be used to display them.

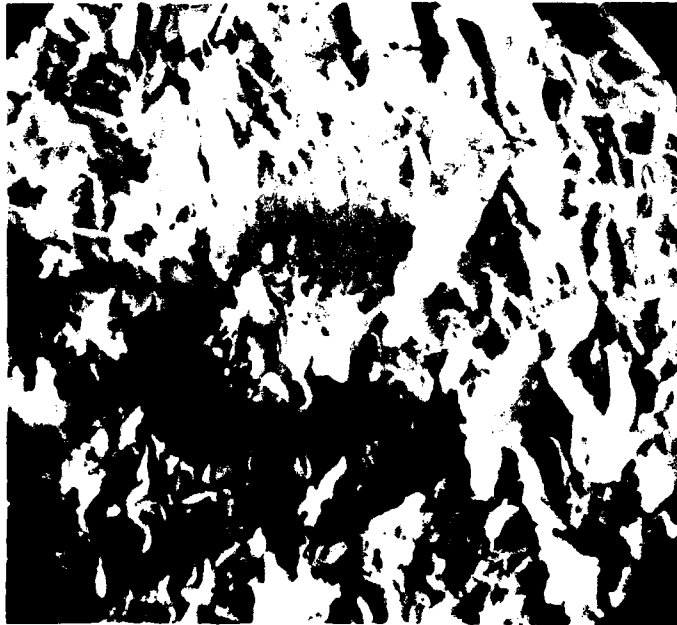
SEM analysis of the matrix material surrounding the reinforcing fibers in the cohesively failed region (Fig. 113b) show many small nucleating dimples on the matrix surface and tear ridges adjacent to the Dacron^R fibers.

6.2 Direct Measurement of Crack Growth

Attempts to monitor adhesive-delamination crack growth optically while fatigue testing, as in da/dN measurements for metals, proved unsuccessful, even with a 45X Gaertner creep microscope. Since the bondline is loaded primarily in shear, the crack opens up very little, and it is difficult to discern the crack tip from the junction of the adhesive and adherend. Use of red penetrant dye-check to accentuate the fatigue crack with cycling also proved unsuccessful; the penetrant bled along the glue line resulting in erroneous readings.

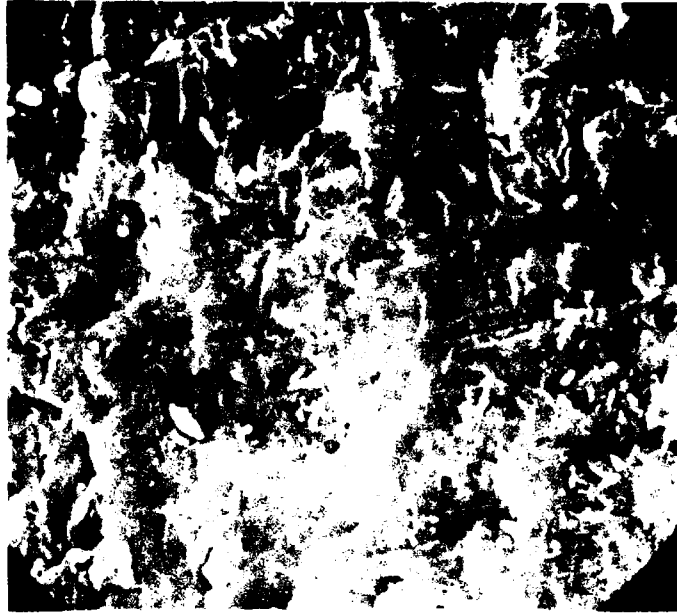
6.3 Optical Analysis of Adhesive Interlayers After Adherend Removal by Etching

A relatively simple technique of studying fatigue damage mechanisms in the adhesive interlayer of bonded joints involves removal of the adherends after fatigue cycling as follows: a series of initially "identical" bonded joint specimens are cycled to progressively larger total number of cycles, including failure. The bonded joints are subsequently sacrificed to remove



Mag. 1000X

a. Rapid Fatigue Crack Growth Zone



Mag. 1000X

b. Slow Fatigue Crack Growth Zone

Figure 94 Scanning Electron Micrographs of Fatigue-Failed FM-73M Model Joint 3C-10, I



a. Zone of Slow Fatigue Crack Growth.
Typical Fatigue Striations are not
Evident.



b. Note Nucleating Failure
Dimples on Adhesive
Failure Surface.

Figure 95 SEM Photomicrographs of Failed Surface of FM-73M Model Joint

intact the corresponding adhesive interlayers. This is accomplished by removal of the aluminum by concentrated (12N) hydrochloric acid in the overlap area, leaving bare the corresponding adhesive interlayer. The intact adhesive interlayer contains a permanent record of the progressive fatigue damage sustained during joint cycling and can be examined afterwards by suitable analysis techniques to extract information on the operative fatigue degradation mechanisms.

This technique is especially valuable in studies involving translucent adhesives, such as FM-73M, which can readily be interrogated optically by transmission microscopy to elucidate on damage features on both the exposed surfaces and at various depths within the volume of the interlayer.

The adherend etching technique reveals internal "crazing" within the volume of the delamination zone along the scrim plane initiating at the high stress edge. These internal cracks are not necessarily continuous, with some isolated cracks forming in advance of the coalesced internal crack front (see, for example, Fig. 91).

SEM examination of the interfacial delamination zone above the zone of internal crazing in the dry joint does not reveal any evidence of fracture topography directly relatable to the random internal cracking occurring below it.

6.4 Effect of Cycling Duration and Humidity

By sacrificing a number of joints in a series of fatigue experiments maintaining constant conditions but varying the number of cycles, N , the progression of the internal damage initiating from the high stress edges of the overlap can be permanently recorded and studied. In fact, the condition of the internal damaged region just before failure can be estimated from observation of the portion of the interlayer on the adjacent side of the slot to the failed region which is subjected to similar stresses.

A distinction is made here between the adhesive-delamination zone, (pronounced in the dry specimens and characterized as the fingernail feature herein and by Marceau et al. (Ref. 7). and the internal cracking phenomenon in the matte scrim plane within the interlayer volume (quantified herein as the internal damage zone). Both originate at the edge of the joint and proceed toward the center of the overlap, but apparently

at different rates depending on whether the joint is wet or dry. In the dry joint, the two dimensions appear about the same, but the fingernail feature is much smaller than the internal damage zone in corresponding wet joints. The reasons for this are as yet unknown.

Analysis by transmission microscopy of adhesive interlayers from "identical" dry and wet FM-73M model joints cycled at 1 Hz at 75°C to N values of 10,000, 15,000, and 20,000 cycles and to failure show the extent of internal damage as testing progresses (Fig. A64 through A67 show the results for the "dry" series).

Measurements of the advancing internal damage length, with error bars are plotted in Figure 96 against the respective N values for these two series of sacrificed joints. The corresponding fitted curves have shapes similar to da/dN behavior observed for fatigue crack propagation in metals. As expected, the damage is larger for the wet joint than for the dry joint at the same N value.

6.5 Discussion/Deduction

A comparison is now made of the joint stiffness predicted by the stress analysis (see Section 4.2.5) with that measured from the load-deflection ($F-\delta$) curves for each set of the aforementioned four dry and wet sacrificial joints. The comparison involves the ratio, K_N/K_i of joint stiffness at the last cycle (just prior to adherend etching) and the "initial" cycle of loading.

From the measured load-deflection ($F-\delta$) histories of the (sacrificed) joints, the effective stiffness at any cycle of loading is the slope of the major axis of the (approximately) elliptical hysteresis loop. Thus, the appropriate stiffness ratio after the Nth cycle is simply the ratio of the slope of the major axis of the Nth loop to that of the initial loop. Such an analysis of the experimental load-deflection curves for one case of (sacrificed) model joint (viz., $N=20$ K cycles, wet joint) is shown in Figure 97. Plots with estimated error bars of these stiffness ratios and the corresponding crack lengths for the complete sets of four measurements for each of the dry and wet joints are shown in Figure 96. Table V provides the measured (after adherend etching) delamination or debond length and stiffness ratios. A replot of the ratios obtained from the MARC-predicted stiffness analysis through four selected crack lengths is shown as the solid curve in Figure

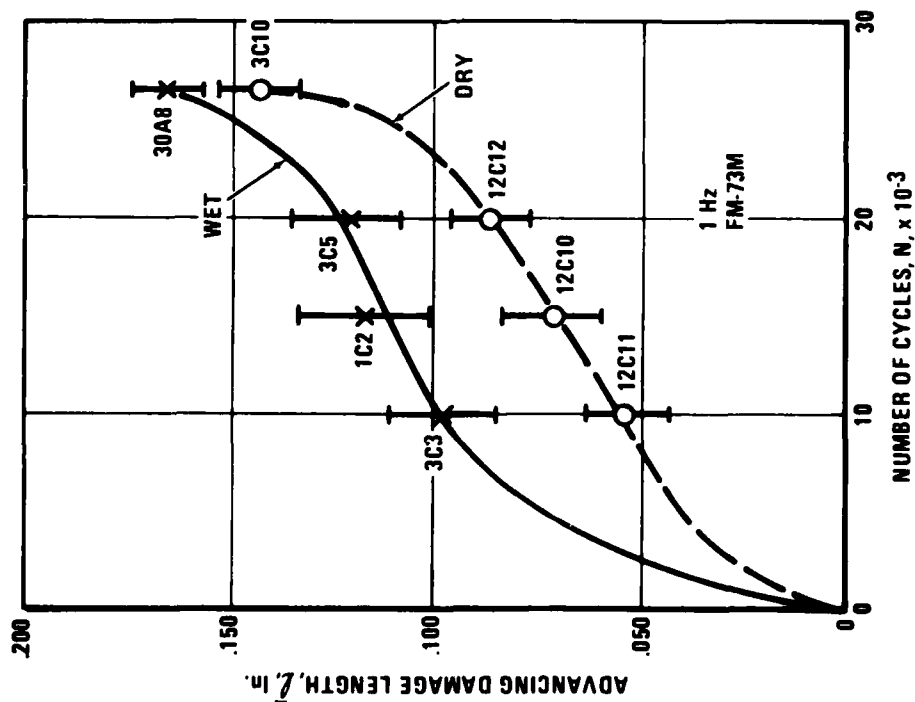


Figure 96 Dependence of Debond Length on Number of Cycles for Sacrificial Dry and Wet Model Joints

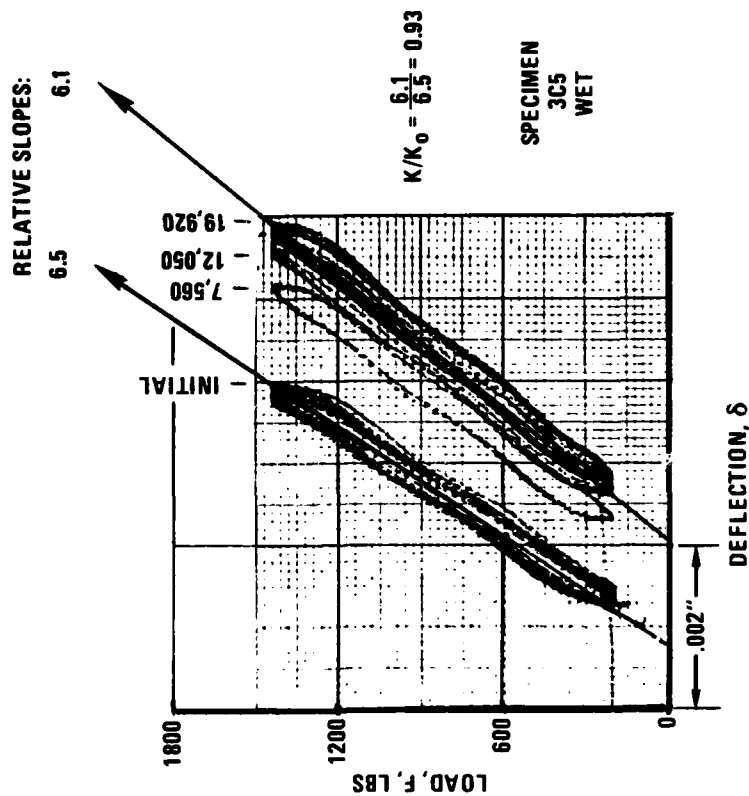


Figure 97 Load-Deflection History, Wet Model Joint, 3C5

Table 5 SUMMARY OF DELAMINATION LENGTH & JOINT STIFFNESS RATIO MEASUREMENTS

NUMBER OF CYCLES, N	DRY JOINTS			WET JOINTS		
	SPEC No.	AVE DEBOND LENGTH, $\bar{l}_{in.}$	K/K _o	SPEC No.	AVE DEBOND LENGTH, $\bar{l}_{in.}$	K/K _o
10,000	12C11	0.051	$\frac{4.3}{5.6} = 0.92 \pm 10\%$	3C3	0.098	$\frac{5.5}{6.2} = 0.89 \pm 10\%$
15,000	12C10	0.071	$\frac{5.2}{6.2} = 0.85$	1C2	0.118 ⁻	$\frac{4.5}{5.1} = 0.88$
20,000	12C12	0.087	$\frac{5.2}{6.5} = 0.80$	3C5	0.118 ⁺	$\frac{6.1}{6.5} = 0.93$
24,182 (Dry)	3C10	0.142	$\frac{5.2}{5.9} = 0.88$	30A8	0.165	$\frac{5.2}{6.7} = 0.78$
27,498 (Wet)						

From Figure 98, it is not unreasonable to conclude that, within experimental error, the observed stiffness changes in the experimental load-deflection histories can be accounted for as due almost entirely to interface crack propagation or debond length.

6.6 Stiffness of Center-Cracked Test Specimen

A comparison was made of the normalized stiffness ratios versus crack length derived experimentally and analytically for a FM-73M center-notched fracture energy specimen (see Fig.

3). A sinusoidal load with stress ratio, R , of 0.05 was applied to the specimen, the crack length was read after the completion of each cycle and the corresponding load-displacement (F vs. δ) history was recorded on the X-Y plotter. Such a typical history is shown in Figure 99. The effective stiffness (as measured by the slope of the semi-major axis) was determined for each cycle and then normalized with respect to the slope of the first cycle to yield the stiffness ratios, K_N/K_i , plotted as the sixteen experimental points in Figure 100.

The stiffness of this fracture energy specimen geometry was then calculated as a function of crack length, $2a$, using the relationship for the center-notched geometry derived in Reference 41. Referring to Figure 3, the stiffness, K , of this fracture energy specimen is, by definition,

$$K = F / \Delta_{\text{total}}, \quad (3)$$

where F = applied load and Δ_{total} = total displacement.

For displacements at points far removed from the center ($h/b > 3$) and taking into account the presence of a center crack, the total displacement, Δ_{total} , is the sum of the displacement of the crack and the displacement of the specimen without a crack and is given by:

$$\begin{aligned} \Delta_{\text{total}} &= \Delta_{\text{crack}} + \Delta_{\text{no crack}} \\ &= \frac{4\sigma a}{E} V_2(a/b) + \frac{\sigma}{E} 2h, \end{aligned} \quad (4)$$

where σ = stress, a = half crack length, E = Young's modulus, h = gage length, b = half width, and $V_2(a/b) = 1.071 + 0.250(a/b) - .357(a/b)^2 + .121(a/b)^3 - .047(a/b)^4 + .008(a/b)^5 - 1.071(b/a) \ln(1-a/b)$.

Substituting Equ. (4) into Equ. (3) and rearranging yields

$$K = AE \left[4aV_2(a/b) + 2h \right]^{-1}. \quad (5)$$

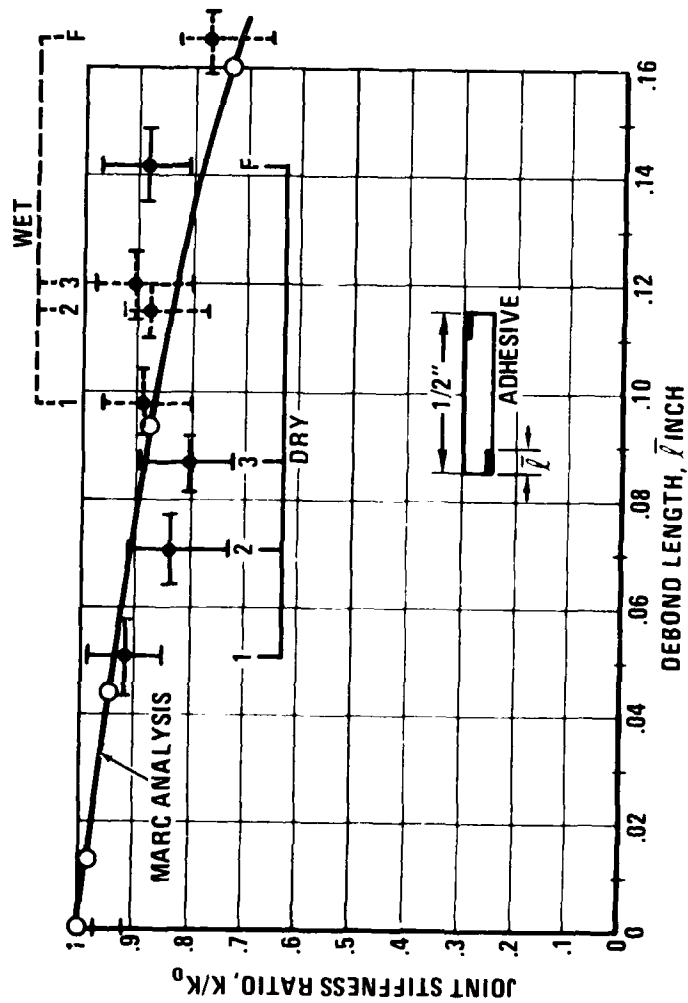


Figure 98 MARC Predicted and Experimental Joint Stiffness Ratios vs Debond Length

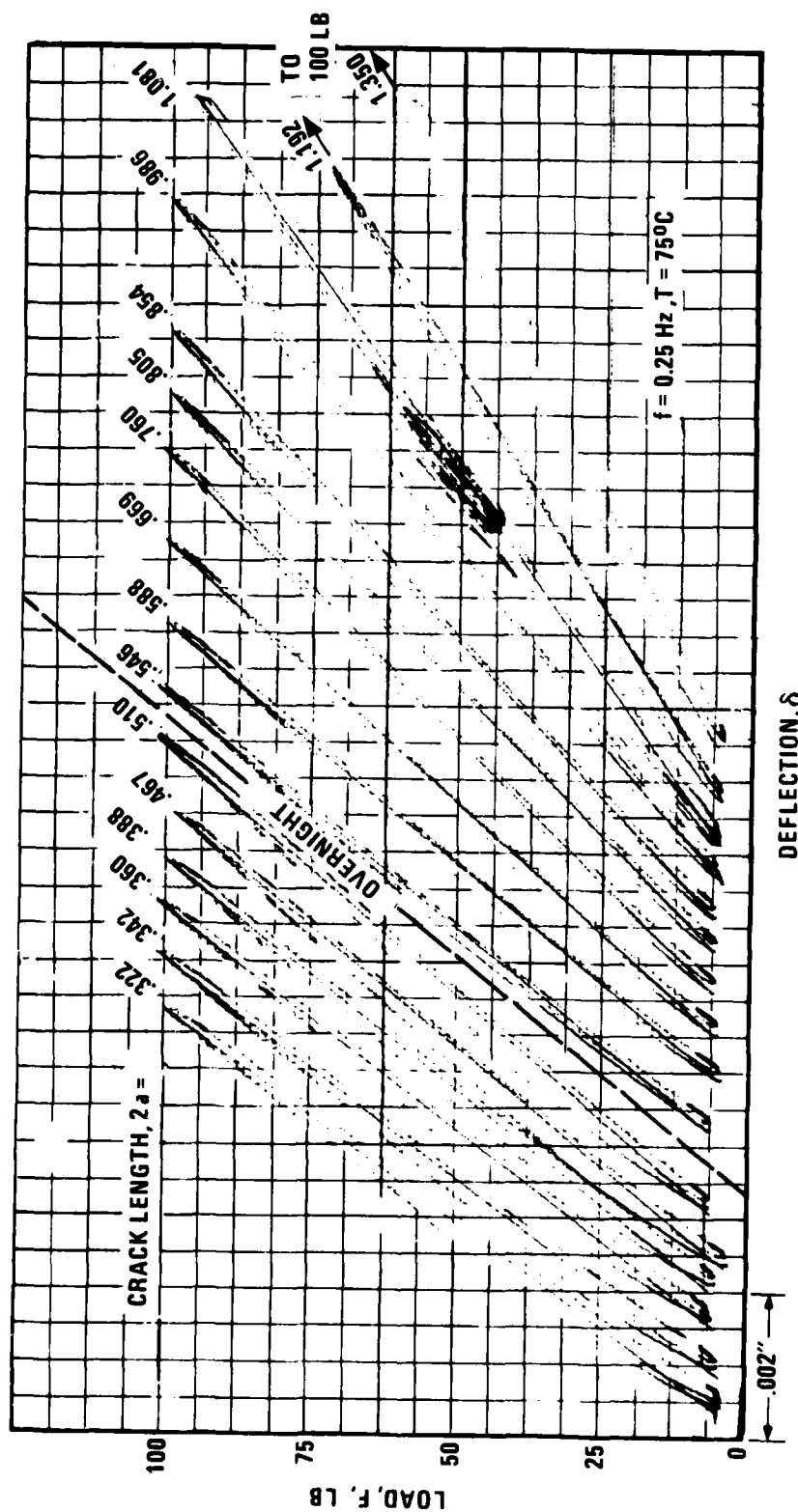


Figure 99 Load-Deflection History of Dry FM-73M Fracture - Energy Specimen

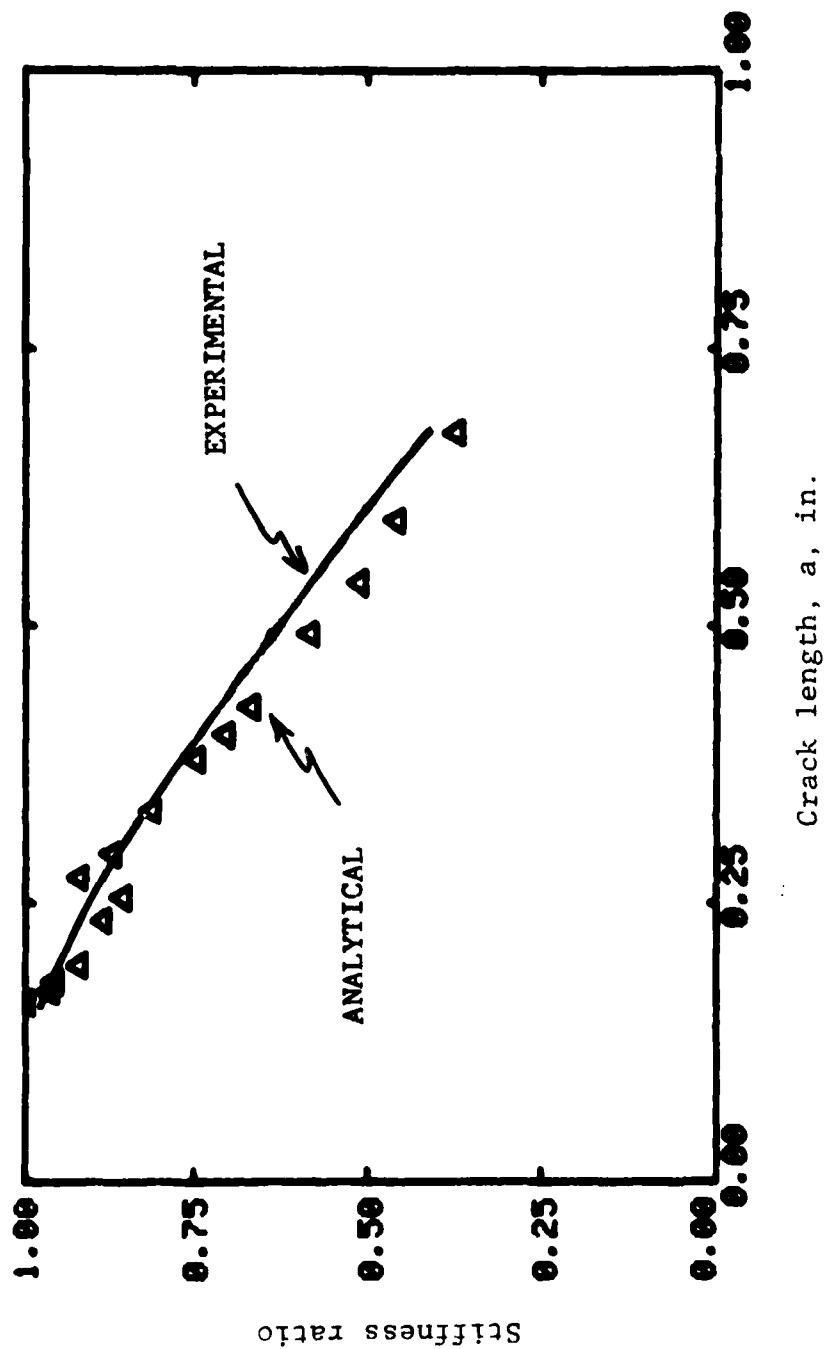


Figure 100 Comparison of Experimental and Analytical Stiffness Ratios for Fracture Energy Specimen

Normalizing these values at various crack lengths to the stiffness at zero crack length gives the "calculated" smooth curve shown in Figure 100. A comparison of the measured and calculated stiffness ratios shows good agreement, again supporting the conclusion reached in the case of the model joint geometry that within experimental error, the stiffness ratio changes can be accounted for entirely by crack propagation.

6.7 XPS Surface Analysis of Failed Joints

Detailed physical and chemical surface characterization of failed adhesively bonded joints, guided by qualitative fracture mechanics theory, constitutes a semi-empirical method to elucidate adhesive bonding phenomena, including failure modes and mechanisms (see for example, Refs. 36 and 37). Inherent flaws, interfacial separation, viscoelastic and plastic responses, and crazing and crack propagation are the main factors governing overall bond strength and behavior. Surface analyses, by SEM and XPS (also known as ESCA or Electron Spectroscopy for Chemical Analysis) provide an estimate of the nature and extent of each mechanism.

In an XPS spectrometer, a source of high energy X-rays in the range of a few keV is used to excite inner-shell electrons of sample atoms in a high vacuum. Each inner-shell electron has a binding energy unambiguously defining its specific parent atom in a molecule. The XPS spectrometer measures the kinetic energy, E_{kin} , of the ejected electrons and produces a spectral plot of the electron intensities at binding energies in the 0 to 1 keV range by subtracting E_{kin} from the energy of the incident X-ray photons, $h\nu$. Qualitative identification of the atoms associated with observed binding energies is obtained from tables listing the multiple binding energies for each atom. In addition to the elemental composition of the sample, the XPS spectra show chemical shifts, giving the chemical state of the atoms and molecular structure information.

A modest program of surface analysis of failed model joints was initiated at Spectro Chemical Research Laboratory (SCRL), Houston, TX, and at Materials Laboratory, LTV Aerospace Corp., Dallas, TX, using in each case a Model 548 XPS system by Physical Electronics Industries.

The failed surfaces of the wet and dry model joints of FM-73M were carefully sectioned into two pieces each of approximate size $\frac{1}{2}$ " x $\frac{1}{2}$ " using a precision microwafering saw. The adhesive interlayers obtained after adherend etching and the neat adhesive specimens were carefully sectioned to the above-mentioned mounting size. All specimens were mounted in

the twelve-place carousel sample holder with a gold reference standard.

Figs. 101, A68, A69, and A70 show only some of the original $N(E)$ vs. Binding Energy traces obtained for these surfaces. All XPS spectra display the ever-present O_{1s} , N_{1s} , and C_{1s} peaks characteristic of epoxy resins (see also Ref. 23), among others. The appearance of the Si peaks in the dry, neat FM-73M (Fig. 101) is unexplained at this time.

The XPS spectra of the FM-73M adhesive interlayer, Fig. A69 and A70, shows some interesting details. Both the unspattered and spattered spectra display Cl peaks, probably due to the HCl etchant. In addition, the spattered adhesive interlayer spectrum (Fig. A70) shows Al peaks, which upon high resolution are identified with the oxide of aluminum, rather than to metallic aluminum itself. This is tentatively attributed to a portion of the oxide layer produced on the Al adherend during the phosphoric acid anodize. Evidently, some of this oxide remained on the adhesive interlayer after the adherend etching process. Its absence in the unspattered interlayer spectrum (Fig. A69) is probably due to a contaminant overlayer on the interlayer surface.

6.8 Chemical Aging in Moisture-Conditioned FM-73M Adhesive Interlayers

The XPS surface analysis technique was used to study possible chemical aging effects occurring in moisture-conditioned FM-73M adhesive interlayers between glass adherends used for monitoring moisture ingress in bonded joints.

Three different adhesive conditions were examined: the straw-colored dry FM-73M interlayer (control specimen), the straw-colored central portion of the wet (21-month conditioned) FM-73M interlayer, and the much darker-(almost brown) colored edge portions of the same wet FM-73M interlayer. These are identified in Fig. 102 and on the corresponding XPS spectra titles as "dry", "wet central", and "wet edge", respectively.

For each of the above-mentioned three different adhesive conditions, the following XPS spectra were recorded: the normal, broad band, $N(E)$ vs. Binding Energy, spectrum over 1 kv $E_B = 0$ for three cases, viz., adhesive surface "as is" after removal of the glass adherends, and then after two Argon ion sputtering sessions resulting in removal of approximately 800 Å per 10 minute-session. In addition, a number of high resolution (i.e.,

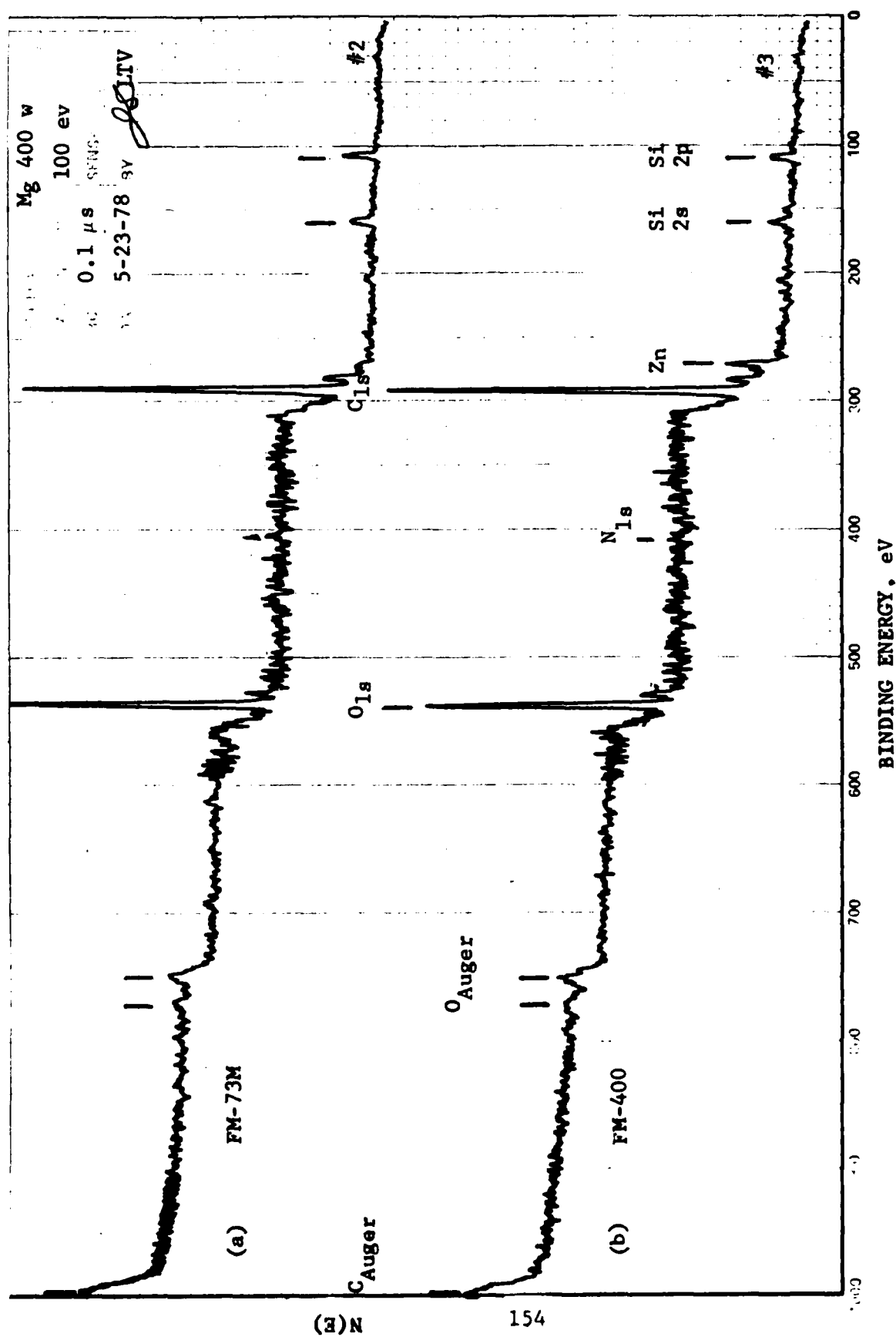
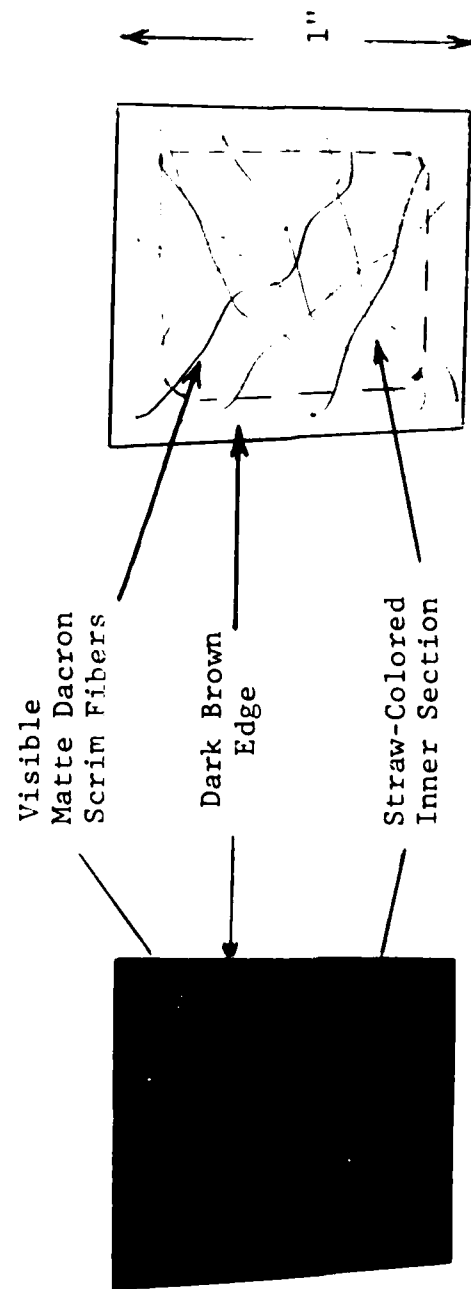


Figure 101 XPS Spectra of Dry Neat FM-73M and FM-400 Adhesives



(a) Transmission Photograph

(b) Schematic

Figure 102 Adhesive Interlayer Between Glass Plates Conditioned for 24 Months at 150°F/100% Condensing Humidity

narrow band) spectra were recorded in the vicinity of the O_{1s} and C_{1s} regions for chemical binding details.

All the broad band XPS spectra display the ever-present O_{1s} , C_{1s} , lines characteristic of epoxy resins (see also Ref. 23), among others.

The high resolution (narrow-band) spectra (Figs. 103 and A71) for the three conditions show a progressive chemical shift of the same magnitude of the O_{1s} and C_{1s} peaks all in the same direction towards higher binding energies, in going from the dry, to wet central, to wet edge conditions. This implies a chemical change involving the O-C group.

Sputtering of the surface layers of all three conditions of specimens does not reveal any additional information about the state of the exposed surfaces. The appearances of Si, Sn, Al, and Mg peaks in the region $E_B \sim 260$ eV in the spectra of the sputtered interlayers (see, for example, Fig. A72) is a result of the higher count rate used in accumulating the data. These peaks are probably also present in the unsputtered spectra taken at lower count rate. All of these peaks, with the possible exception of the Sn peak, may be attributable to the filler material used in the formulation of the adhesive tape. The Sn peak may possibly be due to tin laurate commonly used as an accelerator in the curing process.

On the basis of the chemical shifts observed in high resolution XPS data reported above, it may be concluded that the chemical state of the three different conditions of the adhesive interlayer, viz., the dry, the wet central and the wet edge, are all different. The precise nature of this chemical change is as yet unexplained.

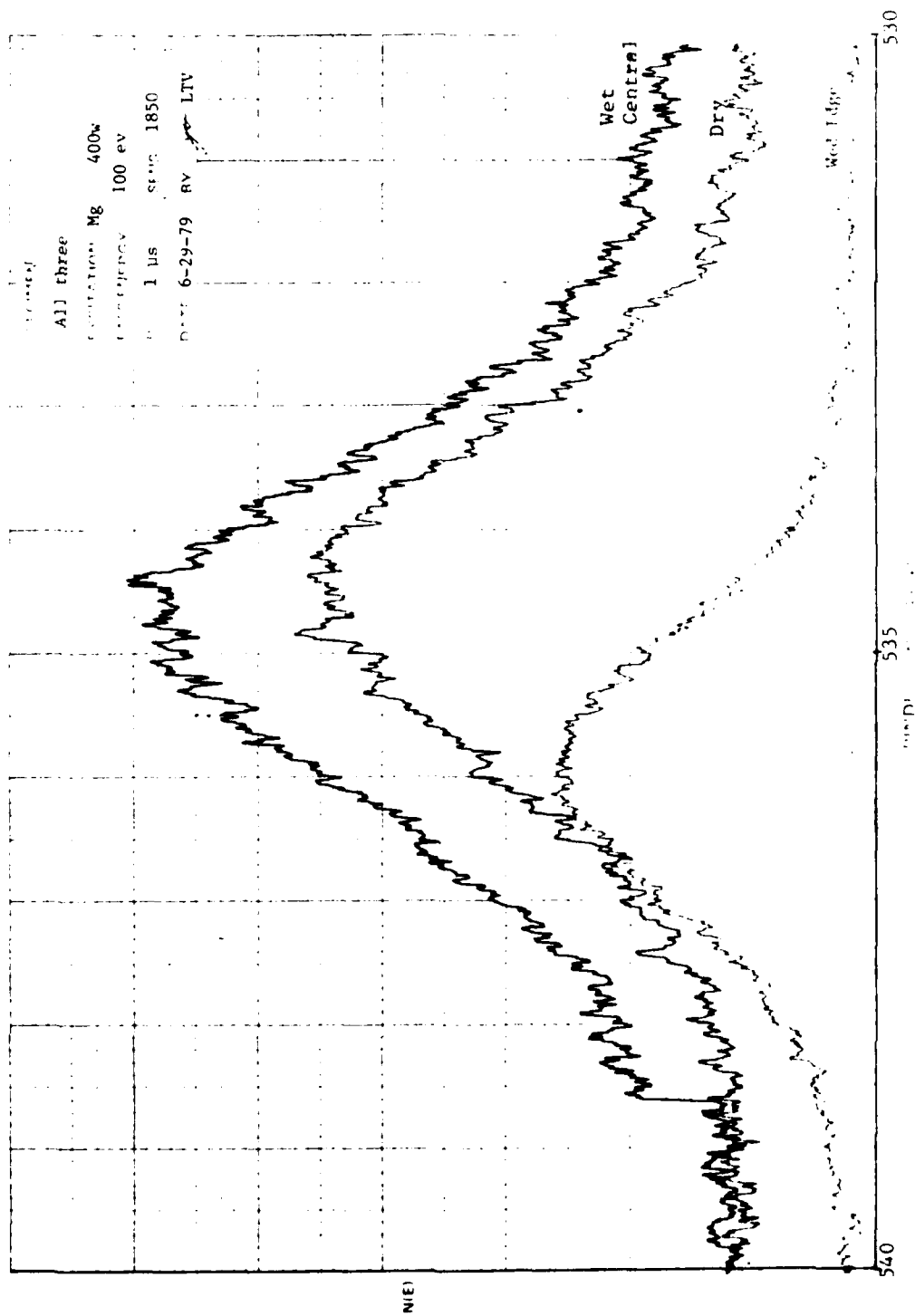


Figure 103 High Resolution XPS Spectra: O_{1s} Peak for Different FM-73M Adhesive Conditions

SECTION VII

MODEL DEVELOPMENT

The most widely accepted theory of adhesive joint strength states that whatever is the cause of interfacial adhesion, the strength of an adhesive joint is determined by the mechanical properties of the constituent materials of the joint and by the local stresses set up in the joint by the applied loads, whatever their origins may be. (Ref. 42).

7.1 BULK EFFECTS

Stresses set up in the adhesive interlayer may arise from a number of different mechanisms: from the adhesive curing kinetics and resultant adhesive shrinkage; from expansion and contraction of the adhesive interlayer due to moisture absorption and desorption, respectively; from temperature differentials between the metal adherends and the predominantly dielectric adhesive; from chemical reactions that could occur between moisture (absorbed in the adhesive) and the filler material, e.g., with Al powder, commonly used in adhesives, especially at high temperatures; from swelling in water of resins containing imbedded crystals of various ionic and non-ionic substances (see, for example, Ref. 43); and from temperature excursions in the adhesive occurring during fatigue cycling. On the basis of the foregoing, it is apparent that two important general considerations must be accounted for in studying fatigue degradation in adhesively bonded joints. First, the rheological properties of the adhesive material, per se, must be delineated as a function of the important ambient environmental parameters, including temperature, relative humidity, and cyclic loading. Second, the distribution of stress in a bonded joint must be computed and analyzed in conjunction with the ambient environments in order to predict the onset of joint failure.

One of the difficulties in determining moisture degradation of adhesively bonded joints arises from geometry effects. Only a small portion, namely the ends and sides, of the adhesive material of a joint is exposed directly to moisture which diffuses into the interior of the adhesive only very slowly. Even after exposure to moisture over a fairly long period of time, only a relatively thin outer portion of adhesive is plasticized which might even inhibit further moisture ingression. Another complicating factor is the parabolic stress distribution

along the lap length in, for example, lap-shear specimens upon plane stress loading as predicted by the well-known Goland and Reissner relation (Ref. 28). This gives rise to the most severe stresses at the ends of the joint so that the center portion of the adhesive contributes very little to the total load carrying capacity of the joint. Unless these high stresses are relieved, e.g., by plastic deformation, local brittle fracture of the adhesive can occur. A crack once started at the joint end propagates rapidly and can result in brittle failure of the entire joint at a relatively low average stress level, below the strength of the adhesive, unless plastic or viscoelastic response to these shearing stresses are available. On the other hand, if such response to shearing stress is too efficient, the joint will fail at a relatively low load level from the accumulated shearing deformation itself.

7.2 Interfacial Effects

In discussing the importance of the rheological properties of the bulk adhesive interlayer in determining fatigue degradation mechanisms, mention should also be made of the role of interfacial effects. Certainly in the "static" loading experiments of Gledhill and Kinloch (Ref. 44) the data strongly suggest that the loss in joint strength of a mild steel butt joint cemented with a simple epoxy after immersion in water results from the adverse affect of water on the interface, or interphase, rather than on the bulk properties of the adhesive. Their experiments involved strength measurements of butt joints and of the bulk "neat" adhesive itself over a large range of moisture uptake (up to 2500 hour immersion time), and over a wide range of temperatures (up to and exceeding the glass transition temperature, T_g , of the adhesive).

Pre-failure and post-failure analysis of the surfaces were conducted by electron probe microanalysis, X-ray diffraction and by scanning electron microscopy for identification of chemical corrosion products and for locus of failure details. Their studies show that water ingress in a joint results in an absorbed water layer at the interface which changes the interfacial thermodynamic work of adhesion from a positive value to a negative value ("spontaneous debonding") and this provides the driving force for the displacement of the adhesive on the metal oxide surface resulting in joint strength degradation. Their data indicates that if a joint is subjected to a humid environment, there is a progressive encroachment into the joint of this debonded interface

which has the effect of progressively reducing the joint strength and also of progressively changing the locus of failure from cohesive within the dry adhesive region to interfacial between the "wet" adhesive areas and the substrate. The rate of this debonding is controlled by the availability of water at the interface which is governed by the diffusion of water (with activation energy 32kJ/mole) through the adhesive. The rate of interfacial debonding is greatly increased above T_g and possible chemical degradation of the adhesive occurs at this high temperature. Corrosion is also shown to occur in the debonded substrate region as the initial ferric oxide (Fe_2O_3) is converted to magnetic iron oxide (Fe_3O_4) in the presence of water.

A works of adhesion model has been developed at General Dynamics to predict the relative environmental stability of an adhesively bonded system in any liquid, including water, and in air. This is described in detail in Ref. 45. Defined in the three-phase model are: a locus (straight line) of effective bond coordinates in the wettability diagram on which the bond stability is unchanged; regions on either side thereof where the interfacial bond is more stable and less stable upon water immersion; a locus (circle) encompassing the adhesive bond coordinates within which the liquid immersant will cause spontaneous debonding of the joint. This model predicts environmental stability criteria described by a current fracture mechanics model of moisture stability of adhesively bonded systems (see, for example, Ref. 46) and additional criteria.

In another study involving the application of a combination of static stress and solvolysis to tapered double cantilever beam (TDCB) specimens containing a precrack, it is shown experimentally that true interfacial failure is possible (Ref. 47). Furthermore, the authors show that while rapid cracking of the epoxide bond of the TDCB specimen results in center of bond failure, slow crack extension in a humid environment, or liquid water, can take place at the interface.

Whereas this interfacial effect may be operative in the static loading case in the predominantly Mode I loading examples of the butt joint and stress-solvolytic cracking study cited above, it is not possible to generalize its importance in the cyclic loading case in the predominantly Mode II loading example of the model lap shear joint.

Two excellent review articles on various aspects of environmental failure of structural adhesive joints are presented by Wake (Ref. 48) and Kinloch (Ref. 49).

7.3 Fatigue Degradation Mechanisms

Adhesives fail in fatigue. They do so, in analogy with more well-studied metals, because of a cycle-by-cycle accumulation of damage resulting from repeated non-elastic strain. This strain can further be influenced by frequency of loading, temperature, humidity and time (viscoelastic) effects. After a sufficient number of stress (strain) applications numerous micro-cracks form, grow incrementally and eventually propagate in an unstable manner, resulting in specimen failure.

The results of other studies in bonded joint behavior are surveyed for comparison in the current program: for example, the damage mechanisms proposed by Sutton (Ref. 40) for an epoxy are not unlike those found for our adhesives. Photomicrographs of the fatigue fracture surface in Sutton's adhesive tensile coupons reveal no observable striations, but show a rough hackle whose features are roughly one or two orders of magnitude larger than the average growth per cycle. The rough surface hackle is also characteristic of failed surfaces of FM-73M observed in the current program. In addition, the presence of cleavage-like or branch cracking mechanisms (river marking) in failed epoxy recorded by Sutton and others have been observed in the fatigue behavior program.

The two different fracture modes observed by Marceau et al. (Ref. 7), the one type in fast cyclic tests (30 cps) and the other type in the slower cyclic rate tests and in the sustained load tests, have also been observed in the Fatigue Behavior program. In the former case, a fingernail fatigue type pattern initiates in the bondline at the load transfer edges, then slowly propagates adhesively towards the center up the overlap with fatigue cycling, after which the failure mode changes and ultimate fracture occurs cohesively and instantaneously over the remainder of the joint. In the latter case (slow cyclic and static tests), the fracture is virtually entirely in the center of the bond in the cohesive mode. Figure 7 shows the two fracture modes observed for fast and slow cycling by Marceau et al. Figure 7 herein shows schematically the fracture mode for fast cycling. The observed failure modes in FM-73M model joints as a function of various environmental conditioning and testing parameters are summarized as follows. A main feature of damage in the interlayer is the initiation of small internal cracks around the individual matte scrim fibers, initiating at the high stress edge of the overlap. With fatigue cycling, more fibers become the centers of these small internal cracks which coalesce

to form larger internal cracks propagating into the center of the joint along the matte scrim plane, thus weakening the joint. The following different situations occur.

7.3.1 Dry FM-73M Joint, Room Temperature Case

In addition to the scrim plane cracking phenomenon occurring during fatigue cycling, the high peel (and shear) stresses at the corner singularity edge initiate a primarily adhesive delamination which propagates along the adhesive-adherend interface, probably along the aluminum oxide-primer interphase, giving the fingernail feature described earlier. As this interface cracking progresses along with the competing cracking in the scrim plane, a change in mode to cohesive failure along the scrim plane finally occurs probably due to weakening of the joint by the crazing in the scrim plane.

This interfacial delamination increases with decreasing fatigue load level and increases with increasing fatigue frequency. In the low frequency limit, i.e., the static loading case, this interfacial delamination is almost non-existent so that static cohesive failure along practically the entire scrim plane occurs.

7.3.2 Wet FM-73M Joint, and High Temperature Case

The moisture-conditioned FM-73M adhesive interlayer is plasticized to a high degree with even the central section of the overlap at approximately 80% of saturation after 9 months (See Fig. 104). It is even possible that moisture has ingressed along the matte scrim fiber-modified epoxy resin interface sufficiently to weaken the structure along and close to the high stress edge (cf., Wicks wicking phenomenon (Ref. 48)). Thus no matter what the environmental testing parameters are, the joint fails almost entirely in the cohesive mode along the plasticized fiber-resin plane. That this wicking phenomenon is occurring is supported by the following observation.

Removal of the adhesive interlayer by the adherend etching technique of a 21-month moisture conditioned specimen reveals optical opacity of the fiber-epoxy interface similar to that observed by Wake (Ref. 48) signifying a refractive index change arising from moisture ingression at this interface. At this moisture level, the specimen is almost completely saturated (see, e.g., Fig. 104).

The failure mode for the hot dry model joint is cohesive in the scrim plane. This is attributed to weakening of the scrim-epoxy interfaces due to the difference in thermal expansion and thermal conductivities of these two materials under cyclic loading.

Table 6 summarizes the relative importance of the environmental factors for the model joint determined in this program.

Table 6 SUMMARY OF SEVERITY OF ENVIRONMENTAL CONDITIONS ON MODEL JOINTS

FEATURE ENVIRONMENT	FAILURE SURFACE APPEARANCE	CORNER DEBOND TO MIDPLANE FAILURE	CRACK (DEBOND) GROWTH RATE ACCELERATION	EFFECT OF SCRIM
DRY - WET	PERMANENT CHEMICAL CHANGE WITH MOISTURE	++	+++	WICKING WITH WATER
TEMPERATURE	0	++	?	
LOAD LEVEL	0	++	?	
CYCLIC FREQUENCY	0	0+	?	
Monotonic vs. Cyclic	0	?	$t_f < 3$ hrs. ++	
Sine Wave vs. Square Wave	0	0		

+++ large effect
 + little effect
 0 no effect

SECTION VIII

CONCLUSIONS & RECOMMENDATIONS

Many similarities are being noted between neat adhesive and bonded joint fatigue behavior; e.g., displaying lower stiffness at high temperature and load-deflection hysteresis losses varying with temperature, moisture and loading frequency, and wave shape. The bonded joints have their own non-uniform stress distributions and, since the first approximation analyses have assumed linear behavior, care must be exercised in making "correlations" at this time. The adherend etched joints reveal "crazed" and/or "cracked" regions that verify the approximate analytical stress distributions, and these damaged regions precede and accompany the contiguous cracks. The measured joint compliance change is due for the most part to crazing and crack growth which constitutes irreversible damage. Certainly one major mechanism of fatigue damage is crack growth whose growth rate is sensitive to temperature, moisture, loading frequency and wave shape.

Specific conclusions and recommendations concerning the individual tasks in this program are summarized below:

Specimen Fabrication

- Procedures for the fabrication of model joints with (250°F-cure) FM-73M and (350°F-cure) FM-400 in large numbers suitable for environmental testing have been developed, aided by NDE techniques, including neutron radiography and ultrasonic spectroscopy.
- Procedures for the fabrication of large quantities of neat adhesive coupons for time-dependent response property measurements, and failure (fracture) property measurements (material characterization) for the aforementioned adhesive systems have been developed.

Material Characterization

- FM-73M and FM-400 adhesives display time and temperature dependent behavior.
- FM-73M absorbs water, in an anomalous manner, with 4% saturation at 60°C (140°F) and 12% saturation at 100°C (212°F).

- Moisture plasticizes FM-73M (e.g., lowers T_g by 40°F) with less than 30% neat strength reduction.
- Moisture plasticizes FM-400 (e.g., lowers T_g by 80°F) and degrades the neat strength (i.e., 64% lower at 75°F , and in bonded joints, $F_f = 440 \text{ lb.}$ at 310°F , 100% RH (15 cycles at 1 Hz)).
- FM-400 is especially sensitive to water and we have tested four other 350°F -cure systems for a high temperature replacement material for FM-400 and we think we can make a reasonably good selection on the basis of material characterization tests on the corresponding neat adhesive materials.

It is recommended that additional measurements of creep compliance of neat (with scrim) FM-73M, and of "neat-neat" (without scrim) FM-73M, be conducted to provide more accurate (response property) inputs to the finite element stress analysis and to deduce the effects (if any) of the scrim, per se, in the joint failure modes.

- A suitable optical holographic interferometry technique has been developed to measure the time (in)dependence of the Poisson function for dry FM-73M at 75°C over a 30-day period.

It is recommended that measurements of Poisson's ratio be extended to cover other temperatures of interest, e.g., 140°F , and for the "wet" adhesives, and to the 350°F -cure adhesive systems.

- The fracture properties of neat, dry and wet FM-73M have been measured at selected temperatures (75°F and 140°F) and frequencies (10Hz and 0.1Hz), including crack propagation rates with time (under monotonic loading), and with cycle (under cyclic (haversine) loading), yielding corresponding crack rate, (da/dt) , vs. stress intensity, (K) , and crack growth with cycle, (da/dN) , vs. sinusoidal stress intensity, (ΔK) .
- The shifted crack propagation rates under monotonically increasing intensity show the same log-log straight line behavior for the different loading and environmental combinations within a factor of \pm one decade in da/dt .
- The shifted da/dN vs. ΔK curves for the different loading and environmental combinations show no common slope indicating possibly that at high temperatures, plasticity or similar nonlinear effects are occurring.

- Now that adequate testing procedures have been optimized for these measurements, it is recommended that the tests be extended over wider temperature and frequency ranges.
- The fairly extensive material characterization tests on four candidate replacement adhesives for FM-400, viz., AF 147, PL 729-3, N 329-7 and RB 398, show that neither of the latter four adhesive systems display material property characteristics which can be considered decided improvements over those of FM-400 for high temperature application .
- The four candidate 350°F-cure materials have comparable log-log creep compliance slopes in the temperature-reduced time range tested. The low compliance materials, N329-7 and RB-398, appear on the Smith plots with relatively low elongation, while the more compliant materials, PL729-3 and AF-147, seem to exhibit some measure of ductile-like behavior leading to a tougher failure characteristic. However, the less compliant materials might also achieve high elongations provided they are tested under higher temperatures and/or for longer periods of time.

It is recommended that a new generation of 350°F-cure adhesive systems, based on chemistry different from the current modified epoxy used, be sought.

- Material characterization measurements must be accurate if statements about the fracture processes in bonded joints are to be made. Also, a better knowledge of sources of specimen-to-specimen variability and its control is required.
- Although we did not pay specific attention to the effect of primer in this program, it appears that some of the unexplained behavior of the model joint may be associated with our lack of knowledge of the primer role and the viscoelastic (response) and failure properties thereof.
- Practically all our measurements required material "shakedown" indicating that the manufacturing process was such as to foster physical aging.
- Stresses induced by cure shrinkage are large in combination with thermally induced stresses on cool down and are of the same order of magnitude as tensile failure stress.
- Stress relief induced by moisture ingress and heating does not appear to be sufficient to nearly offset effects due to cure shrinkage.

Stress Analysis

- The finite element MARC stress analysis procedure applied to the model joint shows that bonded joints have their own stress distributions which are non-uniform with normal (peel) and shear stresses varying by orders of magnitude throughout the thickness of the bondline.

It is recommended that "thickness-averaged" stress analyses procedures of bonded structures commonly used by structural engineers cannot be considered representative of good design procedures and should be abandoned.

- The finite element MARC analyses performed confirm the presence of the corner singularity at the overlap edge of the bonded joint. The large stresses created by this singularity provide a natural site for debonds or interfacial cracks to initiate and propagate and this is in fact found to be the case.
- The aluminum adherends of the model joint are not stiff enough to be considered "rigid" as shown by the redistribution of stresses in the adhesive layer during a viscoelastic analysis of the model joint.
- The finite element analyses show a significant stress variation through the adhesive thickness near the edge of the overlap. This behavior dies out rapidly.
- The response of the model joint (i.e., displacement) is not very sensitive to changes in the adhesive modulus. A substantial portion of the displacement is due to bending of the aluminum adherends.
- The 3-parameter material model used in the viscoelastic analyses is too limited to allow accurate prediction to be made of the model joint response.

It is recommended that the revised MARC code, with the more general Prony series, be used in the future to provide much improved results in stress analysis of bonded structures.

- The nonlinear response of the adhesive material is an important consideration when predicting the response of the model joint. Cost effective analysis of bonded joints including nonlinear viscoelastic materials will most likely require specialized codes.

- The stresses based on elastic analysis resulting from cure shrinkage and cool down of 6600 psi are very close to the room temperature allowable of FM-73M of 7000 psi.
- Viscoelastic stress analysis is possible and feasible provided deformation (response) properties are measured accurately and a suitable computer code (finite element) accepting general viscoelastic properties is made available (e.g., Prony computer program as a starter).
- Even using thick adherends was not sufficient to justify the assumption that the adherends can be treated as infinitely stiff in comparison to the adhesive. As a consequence, the stress distribution in a joint will vary with time, even under constant (creep) load.

Bonded Joint Testing

- The use of the standard clip compliance gage to measure the load-deflection response characteristics of the model joint has proved suitable for most of the environmental ranges of (mechanical) loading frequency, temperature and humidity, except for the high temperature range (310°F for FM-400).
- Changes in these response characteristics have been shown to yield detailed information on the damage processes occurring in the adhesive interlayer as a function of the various loading and environmental parameters.
- Changes in the stiffness of the joint, as measured by the average slope of the load-deflection curves are directly related to the initiation and propagation of the interface crack from the high stress edge.
- The same results are obtained for center-hole-notched neat adhesive coupons of FM-73M.
- Many similarities have been noted between neat and bonded joint behavior, e.g.,
 - (a) lower stiffness at higher temperature,
 - (b) hysteresis losses varying with temperature and frequency,
 - (c) strength reduction with moisture in FM-400.
- It is even suggested that bonded joint response and fracture properties may be predictable on the basis of the response and fracture properties of the adhesive material itself, provided an accurate stress analysis of the joint (interlayer) is effected

with a suitable finite element procedure, such as the MARC with the Prony series modification.

- Variability in the load-deflection data of the joint of the order of a factor of 3 or 5 in many cases, e.g., in the number of cycles to failure for identical conditions, precludes the development of specific quantitative relationships involving combinations of the various loading and environmental parameters.

It is recommended that the number of replicate samples for any set of conditions be increased at least three-fold for statistical significance.

- The total time under load is more important than the number of cycles, N , and the loading wave shape (sinusoidal, square wave) makes little difference within variability limits of the data.
- Changes in the effective joint stiffness ratio depends mostly on (interfacial) crack advance thus establishing that the joint stiffness ratio, K_N/K_1 , after shakedown is a good measure of the crack advance.
- The rate of stiffness change with number of cycles, N , indicates crack growth rate, with wet joints showing a stronger growth rate dependence than the corresponding dry joints.
- Failure of the joint results when the joint stiffness ratio decreases by a given amount, the latter depending on the applied load. Joints that do not achieve this decrease in stiffness ratio do not fail and there does not seem to be a large difference in this (joint failure) level as a function of water content.
- The effective joint stiffness ratio decreases with decreasing (maximum) load level.
- Increased load level, temperature and moisture content all decrease the joint stiffness ratio and shorten joint lifetime; and the effect of frequency is reflected in the total time the joint is under load.
- In joint testing a small range of loads was used. Too high loads would lead to rapid joint failure in the predominantly shakedown phase and too low loads would require an inordinately long time to complete each test in a reasonable period of time, especially under the conditions of the extensive range of parameters in the test matrix. Also, the crack growth rate is a

high power of the stress intensity and hence load level. Because of the toughness of the bonded joints, it was only when unusually high amplitudes and temperatures were used that effects could be measured in reasonable times. Accordingly, the results represent relatively short term, accelerated test conditions.

It is recommended that further studies be considered on the rate of fatigue damage accumulation, and especially on extrapolation of results from these short term over tests, to define equivalent lifetimes expected in the less severe, actual service environments.

Post-Test Examination

- Optical analysis of adhesive interlayers at various fractions of joint lifetime show that in dry, cold model joints failure initiates and propagates as an interface crack from the high stress corner singularity, and is accompanied by a crazed region in the scrim plane, with final bond failure occurring in the cohesive mode in this scrim plane. In the hot and/or wet model joints, failure occurs primarily in the cohesive mode (in the scrim plane), with only a vestige of an initial interface debond apparent.
- The dimensions of the corresponding debond and cohesively-failed zones are dependent on specimen condition (dry, wet), temperature, load level and frequency of cycling.
- The crack and craze zones verify the approximate spatial stress distribution predicted by the stress analysis and these constitute irreversible (permanent) damage.
- The measured joint compliance changes can be reasonably accounted for in terms of the interface crack propagation or debond length (and accompanying scrim plane craze).
- The change in stiffness of the neat (fracture energy) specimen, is also accounted for as due to crack growth.
- A major mechanism of joint fatigue damage is crack growth, and this crack growth rate is sensitive to temperature, moisture, and total time under load, rather than to frequency or wave shape, per se.

It is recommended that microtome techniques with osmium tetroxide staining be used to study the finer details of damage in the craze region in the scrim plane.

- o XPS surface analysis of the adhesive surface of the interface debond indicates that the crack forms in the aluminum oxide interphase region of the joint.
- o High resolution XPS analysis reveals chemical aging in long-term moisture-conditioned FM-73M.

It is recommended that these two effects be studied systematically by XPS techniques to elucidate on the nature of the chemical kinetics involved.

REFERENCES

1. Contract F33615-76-C-5220, "Fatigue Behavior of Adhesively Bonded Joints", sponsored by USAF AFML/MBC Wright-Patterson AFB, Ohio 45433, and conducted by General Dynamics, Fort Worth Division, Fort Worth, Texas, July 1976 - March 1980.
2. Contract F33615-76-C-5205, "Structural Properties of Adhesives", sponsored by USAF AFML/MBC Wright-Patterson AFB, Ohio 45433, and conducted by Vought Corporation, Advanced Technology Center, Inc., Dallas, Texas, May 1976 - May 1978.
3. "Structural Properties of Adhesives", Final Report, Volume I & II, AFML-TR-78-127, prepared for AFML/MBC, W-P AFB, by W. J. Renton, Vought Corporation, Sept. 1978.
4. Schjelderup, H. C., "A Compilation of Mechanical Property Data FM-73, Task 610 and Part of 609", Douglas Aircraft Co., McDonnell Douglas Corp. Data Report No. MDC-J6074, 28 September 1977.
5. Contract F33615-75-C-3016, "Primary Adhesively Bonded Structure Technology (PABST)", sponsored by USAF AFFDL/Wright-Patterson AFB, Ohio 45433, and conducted by Douglas Aircraft Co., McDonnell Douglas Corp., Long Beach, California, March 1975 - December 1978.
6. "PABST General Material Property Data", AFFDL-TR-77-107, prepared for AFFDL, W-P AFB, by Douglas Aircraft Co., Long Beach, California, September 1978.
7. Marceau, J. A., McMillan, J. C., and Scardino, W. M., "Cyclic Testing of Adhesive Bonds", 22nd National SAMPE Symposium, San Diego, Cal., April 26-28, 1977.
8. Althof, W., "The Diffusion of Water Vapor in Humid Air into the Bondlines of Adhesively Bonded Metal Joints", DFVLR-Forschungsbericht 79-06, In German, 1979.
9. Frazier, T. B., "A Computer Assisted Thick Adherend Test to Characterize the Mechanical Properties of Adhesives," SAMPE Tech. Conf. Series, 16, 71-88, 1970.

10. Frazier, T. B., and Lajoie, A. D. "Durability of Adhesive Bonded Joints," Technical Report AFML TR-74-26, March 1974.
11. Boeing Process Specification, BAC 5555, "Phosphoric Acid Anodizing of Aluminum for Structural Bonding", Rev. B, Jan. 28, 1975.
12. Douglas Aircraft Co., McDonnell Douglas Corp., Long Beach, California, "PABST Alert Technical Bulletin", October 31, 1975.
13. Douglas Aircraft Co., McDonnell Douglas Corp., Long Beach, California, "PABST Technical Bulletin No. 1", March 28, 1975.
14. FM 73 Adhesive Film, Data Bulletin BPT 20B, Cyanamid Bloomingdale Aerospace Products, Havre de Grace, Maryland 21078.
15. Chang, F. H., Flynn, P. L., Gordon, D. E., and Bell, J. R., "Determination of Adhesive Bondline Quality by Ultrasonic Techniques", General Dynamics' Fort Worth Division Report ERR-FW-1664, December 1975.
16. Heer, E. and Chen, J. C., "Finite Element Formulation for Linear Thermoviscoelastic Materials", JPL Technical Report 32-1381, June 1, 1969.
17. Quarterly Progress Report No. 3 (1 January to 31 March, 1977), "Fatigue Behavior of Adhesively Bonded Joints", General Dynamics' Fort Worth Division Technical Report, FZM-6658, April, 1977
18. Carter, H. G., and Kibler, K. G., "Rapid Moisture-Characterization of Composites and Possible Screening Applications", J. Comp. Mtls., 10, 1976, 355-370.
19. Heflinger, L. O., Wuerker, R. F., and Spetzler, H., "Thermal Expansion Coefficient Measurement of Diffusely Reflecting Samples by Holographic Interferometry", Rev. Sci. Instr., 44, 1973, 629-633.
20. Jones, R., "Strain Distribution and Elastic-Constant Measurement Using Holographic and Speckle-Pattern Interferometry", J. Strain Anal., 9, 1974, 4-9.

21. Jones, R., and Bijl, D., "A Holographic Interferometric Study of the End Effects Associated with the Four-Point Bending Technique for Measuring Poisson's Ratio", J. Phys. E: Sci. Instr., 7, 1974, 357-358.
22. Fagan, W. F., and Waddell, P., "The Non-Stroboscopic Visualization of Vibrational Patterns by Real-Time/Time Averaged Hologram Interferometry", Proc. Symp. Eng. Appl. Holography, SPIE Publ., 1972.
23. Quarterly Progress Report No. 4 (1 April to 30 June 1979), Fatigue Behavior of Adhesively Bonded Joints, General Dynamics' Fort Worth Division Report FZM-6679, July 1977.
24. Yamaguchi, I., and Saito, H., "Application of Holographic Interferometry to the Measurement of Poisson's Ratio", Jap. J. Appl. Phys. 8, 1969, 768-71.
25. Bijl, D., and Jones, R., "On Tri-Hologram Interferometry and the Measurement of Elastic Anisotropies Using An Adapted Form of Cornu's Technique", Proc. Int. Symp. Holography Applications de l' Holographie (Laboratoire de Physique General et Optique, Universite' de Besanson), 1970.
26. Romanko, John, and Knauss, W. G., "On the Time Dependence of the Poisson's Ratio of a Commercial Adhesive Material", J. Adhesion, 10, 001-009, 1979.
27. Smith, Thor, "Stress-Strain-Time-Temperature Relationships for Polymers", Symposium on Stress-Strain-Time-Temperature Relationships for Materials. Published by the American Society for Testing and Materials, 60-89, 1962.
28. Goland, M., and Reissner, E., "The Stresses in Cemented Joints," J. Appl. Mech. 11, 1944, A17-A27.
29. Hart-Smith, L. C., Adhesive-Bonded Single-Lap Joints, NASA, CR-11236, January 1973.
30. Quarterly Progress Report No. 2 (2 October to 31 December 1976), Fatigue Behavior of Adhesively Bonded Joints, General Dynamics' Fort Worth Division Report FZM-6633, January 1977.

31. Contract AFOSR-F-49620-77-C-0051, "Time Dependent Fracture Processes Relating to Service Life Prediction of Adhesive Joints and Advanced Composites," conducted by W. G. Knauss, California Institute of Technology, Feb. 1, 1978.
32. Timoshenko, S. P., and Goodier, J. N., Theory of Elasticity, 3rd Edition, McGraw-Hill Book Co., Inc., New York. (1970).
33. Krieger, R. B. Jr., "Stiffness Characteristics of Structural Adhesives for Stress Analysis in Hostile Environment", American Cyanamid Company Bloomingdale Plant, Havre de Grace, Maryland, presented at Albuquerque, N. M., SAMPE Meeting, October 1975.
34. McKague, E. L., and Reynolds, J. D., "Gaging and Gripping Methods for Moisture Soaked Composites," General Dynamics' Fort Worth Division Report, ERR-FW-1679, December 1975.
35. Mandel, Jean, Propriétés Mécaniques des Matériaux, Editions Eyrolles, Paris (1978), e.g., p. 28.
36. Struik, L. C. E., Physical Aging in Amorphous Polymers and Other Materials, Elsevier Scientific Publishing Co., New York (1978).
37. Dwight, D. W. , "Surface Analysis and Adhesive Bonding, I. Fluoropolymers", J. Colloid and Interface Sci., 1977.
38. Selby, K. and Miller, L. E., "Fracture Toughness and Mechanical Behavior of an Epoxy Resin," J. Mat. Sci., 10, 12-24, 1975.
39. Dwight, D. W., Counts, M. E., and Wightman, J. P., "Surface Analysis and Adhesive Bonding. II. Polyimides", Recent Advances in Colloid and Surface Science, M. Kerker, editor, Academic Press, 1977.
40. Sutton, S. A., "Fatigue Crack Propagation in an Epoxy Polymer," Engng. Fract. Mech., 6, 587-595 (1974).
41. Tada, H., Paris, P. C., and Irwin, G. R., The Stress Analysis of Cracks Handbook, Del Research Corp., Hellertown, PA (1973)
42. Sharpe, L. H., "The Interphase in Adhesion," Aspects of Adhesion, 7, 139-151, 1973. Transcripta Books (London).

AD-A087 280

GENERAL DYNAMICS CORP FORT WORTH TX FORT WORTH DIV F/G 11/1
FATIGUE BEHAVIOR OF ADHESIVELY BONDED JOINTS. VOLUME 1.(U)
APR 80 J ROMANKO, W G KNAUSS F33615-76-C-5220

UNCLASSIFIED

AFWAL-TR-80-4037-VOL-1

NL

3 OF 3

AD-A087 280



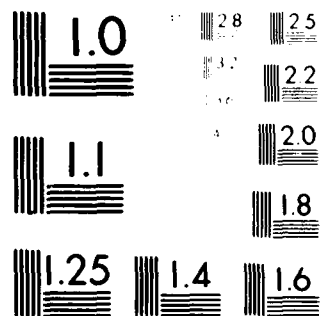
END

DATE

FILED

9-80

DTIC



Microcopy Resolution Test Chart
 National Bureau of Standards

43. Fedors, R. F., "A New Mechanism of Failure in Polymers," Polymer Letters Edition, 12, 81-84, 1974.
44. Gledhill, R. A., and Kinloch, A. J., "Environmental Failure of Structural Adhesive Joints," J. Adhesion, 6, 315-330, 1974.
45. Romanko, J., "Environmental Stability of Adhesively Bonded Systems," General Dynamics' Fort Worth Division Report, ERR-FW-1650, 28 November, 1975.
46. Kaelble, D. H., "A Relationship Between the Fracture Mechanics and Surface Energetics Failure Criteria," J. Appl. Polymer Sci., 18, 1869-1889, 1974.
47. Patrick, R. L., Brown, J. A., Verhoeven, L. E., Ripling, E. J., and Mostovoy, S., "Stress-Solvolytic Failure of an Adhesive Bond," J. Adhesion, 1, 136-141, 1969.
48. Wake, W. C., "Moisture and Adhesion-A Review," Aspects of Adhesion, 7, 232-241, 1973. Transcripta Books (London).
49. Kinloch, A. J., "Environmental Failure of Structural Adhesive Joints - A Literature Survey," ERDE TN 95, August 1973.

